



Technische Universität München
TUM School of Natural Sciences

**A modular concept for enzymatically activatable
caged electrophiles
&
Chemoproteomic analysis of the covalent
ligandability of *Moraxella catarrhalis***

Dissertation

Michael Zollo

München 2023



Technische Universität München
TUM School of Natural Sciences

**A modular concept for enzymatically activatable
caged electrophiles
&
Chemoproteomic analysis of the covalent
ligandability of *Moraxella catarrhalis***

Michael Zollo

Vollständiger Abdruck der von der TUM School of Natural Sciences
der Technischen Universität München zur Erlangung des akademischen Grades
eines

Doktors der Naturwissenschaften (Dr. rer. nat.)

genehmigten Dissertation.

Vorsitz: Prof. Dr. Cathleen Zeymer
Prüfer*innen der Dissertation: 1. Prof. Dr. Stephan A. Sieber
2. Assistant Prof. Dr. Stephan M. Hacker

Die Dissertation wurde am 06.06.2023 bei der Technischen Universität München
eingereicht und durch die TUM School of Natural Sciences am 29.06.2023
angenommen.

Danksagung

Zuerst möchte ich mich bei meinen beiden Doktorvätern, Prof. Dr. Stephan A. Sieber und Dr. Stephan M. Hacker, für die Betreuung meiner Arbeit, für Euer Vertrauen und Eure Unterstützung bedanken.

Prof. Stephan A. Sieber hat den Kontakt zu Dr. Stephan M. Hacker hergestellt und mich auch während meiner Masterarbeit bei fachlichen Fragen und meiner Planung der Dissertation unterstützt. Während meiner Promotion hat er mir die Möglichkeit gegeben weiterhin in seinem Arbeitskreis zu arbeiten, mir alle Freiheiten für meine Forschung gegeben und mich stets bei meinen Projekten begleitet und maßgeblich unterstützt. Ebenfalls beim Schreiben meiner Dissertation und der Publikationen konnte ich immer auf seine fachliche und persönliche Unterstützung zählen.

Dr. Stephan M. Hacker hat mir während meiner Masterarbeit sein Wissen weitergegeben, mich bestmöglich auf die folgende Promotion vorbereitet und mir nicht zuletzt auch ein sehr spannendes Projekt ermöglicht, das auch Teil dieser Dissertation ist. Auf diesem und weiteren Projekten hat er mich immer unterstützt und mir die Freiheiten gegeben, um meine Forschung eigenständig voranzutreiben. Ich bin ihm ebenfalls sehr dankbar dafür, dass die Betreuung auch weiterhin per Remote so nah und intensiv möglich ist, dass er jederzeit erreichbar ist und mir seine Hilfe zu vielen fachlichen Fragen gibt. Vielen Dank ebenfalls für die Hilfe und Unterstützung beim Verfassen meiner Dissertation und meiner Publikationen, sowie bei der komplexen Datenauswertung.

All die Unterstützung und die Freiheiten, die ich von meinen beiden Doktorvätern bekommen habe, sind nicht selbstverständlich und ich weiß dies sehr zu schätzen. Vielen Dank!

Mein Dank gilt auch Prof. Dr. Cathleen Zeymer für den Vorsitz meiner Promotionsprüfung.

Ich möchte mich ebenfalls bei der Studienstiftung des Deutschen Volkes für die Förderung durch ein Promotionsstipendium bedanken. Dieses Stipendium hat mir den direkten Einstieg in meine Promotion ermöglicht und mich auch fast meine gesamte Promotionszeit begleitet. Vor allem Herrn Dr. Antes und Frau Schwarzenberg möchte ich hier stellvertretend danken für Ihre Hilfe bei allen Fragen und für die unkomplizierte weitere Verlängerung meiner Promotionsförderung. Ich bin ebenfalls sehr geehrt und dankbar, dass ich in das neu gegründete Marianne-Plehn-Programm des Elitenetzwerks Bayern und der Studienstiftung des Deutschen Volkes aufgenommen wurde, das mir neben meiner regulären Promotionsförderung zusätzlich eine Anstellung an der Universität ermöglicht hat.

Ich bedanke mich auch für die wunderbare Kooperation mit Dr. Claudia Schmidt und Prof. Dr. Angela Casini, in der wir zusammen die Zielproteine von organischen Goldverbindungen untersucht haben und die Ergebnisse gemeinsam publizieren konnten.

Mein Dank gilt auch an Lisa Lewald mit der ich eine wunderschöne Zeit als Laborkollegin verbracht habe. Das durchgehende Hören von Bayern 1 hat die Zeit im Labor deutlich angenehmer gemacht. Auch Patrick Zanon (Zani) möchte ich danken für all seine Hilfe bei meinen Projekten, für die schöne Zeit im Labor zusammen und für den ganzen Spaß, den man mit ihm haben konnte. Zani hat mich bereits während meiner Masterarbeit und auch während meiner Promotion weiterhin immer bei allen synthetischen, biochemischen und auch privaten Fragen unterstützt. Vielen Dank!

Ich möchte mich auch bei Martin Pfanzelt bedanken. Er hat mich damals als Praktikant dem Arbeitskreis vorgestellt, mir sehr viele synthetische Methoden beigebracht und war immer ein Ansprechpartner für mich. Ebenfalls hat Martin einen Assay entwickelt, den ich zur Bestimmung der enzymatischen Aktivität des SirA-like proteins benutzt habe. Für diese Unterstützung bin ich ihm mehr als dankbar, nach seiner Vorarbeit war der Assay kein Problem mehr. Auch für die netten Gespräche mit ihm und seinen Humor möchte ich mich bedanken, lediglich seinen Auto-Geschmack sollte er vielleicht nochmal überdenken...

Ich möchte mich auch bei Dietrich Mostert, Till Reinhardt, Konstantin Eckel, Alexandra Geißler und Patrick Zanon bedanken für das kritische Lesen dieser Arbeit und für ihre Anmerkungen.

Ich möchte mich auch bei meinen Praktikanten Max Bottlinger, Christopher Dirr, Robert Irle und Victoria Gebler bedanken, die Zusammenarbeit mit euch und eure Betreuung hat mir sehr viel Spaß bereitet und ihr habt mich sehr bei meinen Projekten unterstützt. Auch die wunderschönen Bilder von Chris werde ich vermutlich nicht mehr vergessen. Max ist mittlerweile mein Sitznachbar und sorgt dafür, dass ich stets abgelenkt werde. Für genau diese Ablenkungen und unsere Gespräche möchte ich mich bei ihm bedanken, auch für die super Zusammenarbeit auf unserem besten Gerät, der MSQ.

Ich möchte mich auch bei meinem ehemaligen Sitznachbarn Stuart Ruddell bedanken für die schönen englischen Ausdrücke. Zusammen mit Thomas Gronauer sind legendäre Bilderrätsel daraus entstanden. Josef Braun möchte ich für die lustige Zeit zusammen auf der Konferenz in Nizza danken. Es war immer lustig mit dir, auch wenn du während dieser Zeit leider leicht krank geworden bist. Auch bei allen anderen ehemaligen und aktuellen Kollegen möchte ich mich für die super Zusammenarbeit, für die gegenseitige Unterstützung und für all die lustigen

Momente bedanken. Diese Arbeitsatmosphäre ist nicht selbstverständlich und erleichtert die Zusammenarbeit erheblich. Ich werde vor allem die lauten „sooooo“ Schreie aus allen Ecken sehr vermissen.

Ich möchte auch Mona Wolff, Katja Bäuml, Barbara Seibold und Christina Brumer danken für eure Unterstützung und eure Hilfe, die mir im Labor und der Bürokratie deutlich das Leben erleichtert haben.

Ich möchte mich auch bei meinen Brüdern und vor allem bei meinen Eltern bedanken, die mich seit meiner Schulzeit und während meines gesamten Studiums und der Promotion ständig unterstützt haben, mir den Rücken freigehalten haben und mir gut zugesprochen haben. Vielen Dank für alles! Abschließend möchte ich Ramona danken. Sie begleitet mich schon seit meinem Bachelorstudium und hat mich durchgehend unterstützt, mir Rückhalt gegeben, mich motiviert und war immer für mich da. Ich bin froh jemanden wie sie an meiner Seite zu haben.

Abstract

Bacterial antimicrobial resistance has emerged as a global health crisis that is estimated to have directly caused more than 1.2 million deaths in 2019. Further studies even predict an increase within the next years, if no novel antibiotics are discovered. This thesis establishes two complementary strategies to target antibiotic-resistant bacteria.

The use of highly reactive molecules, that address multiple target proteins simultaneously represents a possibility to decrease the chance of resistance formation since bacteria are most likely not able to mutate multiple proteins at the same time. Nevertheless, as these highly reactive compounds probably also engage many unwanted off-targets in human cells and lead to corresponding side-effects, we developed a modular concept of caged electrophiles based on cysteine-directed bromomethyl ketones that are initially caged as an acetal and are therefore unreactive. After specific activation by bacterial nitroreductases, the highly reactive electrophile is liberated. Following initial proof-of-concept studies and extensive labelling optimizations, we synthesized derivatives with different caging groups to improve the uncaging process. Thereby, we identified a thiophene-based caged electrophile that is activated even in living bacteria with proteome-wide labelling comparable to the respective free bromomethyl ketone. The absence of labelling in a human cell line verified the selective activation in bacteria. Finally, we confirmed the uncaging process and the reactivity with residue-specific chemoproteomics. Due to its modularity, this concept is expected to be transferable to other carbonyl-based electrophiles and other activating enzymes to also target different diseases.

In the second part of this thesis, we studied the emerging Gram-negative pathogen *Moraxella catarrhalis*, which is responsible for many respiratory tract infections. Phenotypic screening identified antibiotically active, cysteine-directed covalent fragments that lack activity against many other tested bacteria indicating the potential use as narrow-spectrum antibiotics. Residue-specific chemoproteomic analysis of the cysteine reactivity in lysate of a β -lactamase-producing *M. catarrhalis* strain demonstrated that the susceptibility could not be attributed to increased cysteine reactivity. We profiled the cysteine ligandability in living *M. catarrhalis* and identified 228 ligandable cysteines in 173 different proteins. Site-specific engagement of cysteines in the essential proteins ThiD, PdxJ and SirA-like protein was demonstrated *in vitro*. We further established a sulfur-carrier protein activity for the poorly characterized SirA-like protein, which was inhibited upon compound binding. Taken together, these results serve as starting points for the development of novel narrow-spectrum antibiotics to selectively target *M. catarrhalis* infections.

Zusammenfassung

Die bakterielle Antibiotikaresistenz hat sich zu einem globalen Gesundheitsproblem entwickelt, das im Jahr 2019 mehr als 1.2 Millionen Todesfälle direkt verursacht hat. Weitere Studien prognostizieren einen deutlichen Anstieg dieser Zahl über die nächsten Jahre, sollten keine neuartigen Antibiotika identifiziert werden. Diese Dissertation beschreibt die Entwicklung zweier komplementärer Strategien zur Bekämpfung antibiotikaresistenter Bakterien.

Der Einsatz hochreaktiver Verbindungen stellt eine Möglichkeit zur Minimierung der Resistenzbildung dar, da Bakterien wahrscheinlich nicht in der Lage sind, mehrere Zielproteine gleichzeitig zu mutieren. Zur Vermeidung von Nebenwirkungen wurde in dieser Arbeit ein modulares Konzept geschützter Elektrophile basierend auf Cystein-reaktiven Brommethylketonen entwickelt. Diese wurden zunächst als unreaktives Acetal geschützt und nach Aktivierung durch bakterielle Nitroreduktasen wieder als reaktives Elektrophil freigesetzt. Zur Optimierung der Freisetzung wurden Derivate mit unterschiedlichen Schutzgruppen synthetisiert. Dabei wurde ein Thiophen-basiertes Derivat identifiziert, das auch in lebenden Bakterien eine zum freien Brommethylketon vergleichbare proteomweite Reaktivität aufweist. Die selektive Aktivierung in Bakterien wurde durch fehlende Reaktivität in menschlichen Zellen bewiesen. Abschließend wurde der Freisetzungsprozess und die Reaktivität durch eine chemoproteomische Methode bestätigt. Aufgrund der Modularität sollte unser Konzept ebenfalls für andere Carbonyl-basierte Elektrophile und Aktivierungsenzyme eingesetzt werden können, um auch weitere Krankheiten zu bekämpfen.

Im zweiten Teil dieser Arbeit wurde das Gram-negative Bakterium *Moraxella catarrhalis* untersucht, das für verschiedene Atemwegsinfektionen verantwortlich ist. Durch phänotypisches Screening wurden antibiotische, Cystein-reaktive kovalente Fragmente identifiziert, die wegen fehlender Aktivität in anderen getesteten Bakterien potenziell als pathogenspezifische Antibiotika eingesetzt werden könnten. Nach chemoproteomischer Analyse im Lysat eines β -Lactamase produzierenden *M. catarrhalis* Stamms konnte die Sensitivität nicht auf eine erhöhte Cystein-Reaktivität zurückgeführt werden. Insgesamt wurden 228 Cysteine in 173 Proteinen in lebenden *M. catarrhalis* als adressierbar identifiziert, wobei die selektive Reaktion mit den essenziellen Proteinen ThiD, PdxJ und SirA-like protein *in vitro* bestätigt wurde. Die zelluläre Funktion des kaum charakterisierten SirA-like protein als Schwefeltransporter und deren Inhibierung wurde in diesem Rahmen bestätigt. Zusammenfassend bilden diese Ergebnisse eine Grundlage für die Entwicklung neuartiger pathogenspezifischer Antibiotika zur Therapie von *M. catarrhalis* Infektionen.

Introductory remarks

Parts of this thesis are based on the following publications:

Chapter II:

M. Zollo, P. R. A. Zanon, S. A. Sieber, S. M. Hacker, Caging Highly Reactive Electrophiles for Selective Enzymatic Activation in Bacteria. *Manuscript in preparation*.

This chapter is additionally a direct continuation of my Master's thesis and some relevant results are therefore included:

M. Zollo, Evaluation of the Antibiotic Potential of Bromomethyl Ketones for the Development of Latent Electrophiles, Master's Thesis, Technical University of Munich, **2019**.

Contributions:

MZ, SAS and SMH planned the project and all experiments. PRAZ initiated the project through the synthesis of the first-generation caged electrophile **CE1** and conducted first proof-of-concept studies. MZ repeated these experiments and conducted all further experiments and data evaluation. MZ and SMH prepared the manuscript for publication with input from all others.

Chapter III:

M. Zollo, M. Pfanzelt, A. P. A. Janssen, S. M. Hacker, *In situ* chemoproteomic profiling identifies new target proteins for narrow-spectrum antibiotics against the Gram-negative human pathogen *Moraxella catarrhalis*. *Manuscript in preparation*.

Contributions:

MZ and SMH planned the project and all experiments. MZ conducted all experiments and data evaluation. MP developed the assay to determine the enzymatic activity of SirA-like protein. APAJ provided figures for the AlphaFold predictions and established procedures for mining of protein data. MZ and SMH prepared the manuscript for publication with input from all others.

Conference presentation:

The following conference presentation includes results from chapters II and III:

M. Zollo, C. Schmidt, P. R. A. Zanon, R. Bonsignore, A. Casini, S. A. Sieber, S. M. Hacker, New Chemoproteomic Technologies and Chemical Modalities for Antibiotic Discovery. *poster presentation and flash talk, EFMC-ISMC, 4th-8th September 2022*, Nice, France.

Publications not highlighted in this thesis:

C. Schmidt,* **M. Zollo**,* R. Bonsignore, A. Casini, S. M. Hacker, Competitive profiling of ligandable cysteines in *Staphylococcus aureus* with an organogold compound. *Chem. Commun.* **2022**, 58, 5526-5529.

P. R. A. Zanon, F. Yu, P. Musacchio, L. Lewald, **M. Zollo**, K. Krauskopf, D. Mrdović, P. Raunft, T. E. Maher, M. Cigler, C. Chang, K. Lang, F. D. Toste, A. I. Nesvizhskii, S. M. Hacker, Profiling the proteome-wide selectivity of diverse electrophiles. **2021**, DOI 10.26434/chemrxiv-2021-w7rss-v2.

* These authors contributed equally to this work

Table of contents

Danksagung	I
Abstract	IV
Zusammenfassung	V
Introductory remarks	VI
Table of contents	VIII
I Theoretical background	1
1 Antibiotic crisis	2
2 Bacterial antimicrobial resistance development.....	4
3 Covalent drugs.....	6
4 Activity-based protein profiling	9
II A modular concept for enzymatically activatable caged electrophiles	16
1 Introduction	17
1.1 Bacterial nitroreductases	18
1.2 Concept of caged electrophiles	20
2 Scope of the project.....	22
3 Results and discussion.....	23
3.1 Synthesis of the first-generation caged electrophile	23
3.2 Proof-of-concept studies	25
3.3 Optimization of labelling conditions.....	27
3.4 Design and synthesis of second-generation caged electrophiles.....	30
3.4.1 Synthesis of improved caging groups	31
3.4.2 Synthesis of caging groups with self-immolative linkers	35
3.4.3 Synthesis of second-generation caged electrophiles	43
3.4.4 Synthesis of a negative control compound.....	46
3.5 Evaluation of the labelling of the second-generation caged electrophiles	48
3.6 Gel-based labelling of the best caged electrophile in bacterial lysate.....	50
3.7 Gel-based labelling of the best caged electrophile in living bacteria.....	51
3.8 Gel-based labelling of the best caged electrophile in living human cells	53
3.9 Chemoproteomic analysis of caged electrophiles in bacterial lysate.....	55
3.10 Chemoproteomic analysis of caged electrophiles in living bacteria	57
4 Conclusion and outlook.....	59

5	Experimental part	62
5.1	Organic synthesis	62
5.1.1	Materials and methods	62
5.1.2	Synthesis of the first-generation caged electrophile	64
5.1.3	Synthesis of improved caging groups	68
5.1.4	Synthesis of caging groups with self-immolative linkers	77
5.1.5	Synthesis of second-generation caged electrophiles	95
5.1.6	Synthesis of a negative control compound.....	101
5.2	Biochemistry	103
5.2.1	Cloning of NfsA and NfsB.....	103
5.2.2	Expression and purification of recombinant NfsA and NfsB	104
5.2.3	Cultivation and lysis of <i>S. aureus</i> SH1000 and HEK293 cells	105
5.2.4	Gel-based labelling experiments in bacterial lysate.....	106
5.2.5	Gel-based labelling experiments in living bacteria	107
5.2.6	Gel-based labelling experiments in living HEK293 cells	108
5.2.7	isoDTB-ABPP experiments in bacterial lysate	109
5.2.8	isoDTB-ABPP experiments in living bacteria	109
5.2.9	MS sample preparation.....	110
5.2.10	Sample analysis by LC-MS/MS.....	111
5.2.11	isoDTB-ABPP data analysis	111
III	Chemoproteomic analysis of the covalent ligandability of <i>Moraxella catarrhalis</i>	117
1	The Gram-negative pathogen <i>Moraxella catarrhalis</i>	118
2	Scope of the project.....	119
3	Results and discussion.....	120
3.1	Antibacterial activity screening.....	120
3.2	Chemoproteomic analysis of cysteine reactivity in <i>M. catarrhalis</i>	123
3.3	Chemoproteomic analysis of cysteine ligandability in <i>M. catarrhalis</i>	126
3.3.1	Optimization and adjustment of the isoDTB-ABPP workflow.....	126
3.3.2	Analysis of cysteine ligandability	129
3.4	Target engagement and verification studies.....	138
4	Conclusion and outlook.....	146
5	Experimental part	150
5.1	Cultivation and lysis of bacterial strains	150
5.2	Determination of MIC values.....	151

5.3	isoDTB-ABPP experiments in lysate to investigate cysteine reactivity	152
5.4	Competitive isoDTB-ABPP experiments in living bacteria	152
5.5	MS sample preparation.....	153
5.6	Sample analysis by LC-MS/MS.....	154
5.7	isoDTB-ABPP data analysis	155
5.8	Cloning	159
5.9	Site-directed mutagenesis.....	160
5.10	Expression and purification of recombinant proteins	161
5.11	Gel-based competitive labelling experiments	162
5.12	Intact protein MS (IPMS) experiments	163
5.13	Activity assay for SirA-like protein	163
IV	Bibliography	165
	Abbreviations	186
	Appendix	192

I Theoretical background

1 Antibiotic crisis

In 1928, *Alexander Fleming* discovered by chance that a *Penicillium* mold strain contaminated a culture plate of *Staphylococci* secreting an antibacterially active substance that led to bacterial lysis. Through further analysis of this observation, he assigned this substance the name penicillin, which is nowadays well-known as one of the first antibiotics.^[1] Together with the discovery of streptomycin in 1943, this set the starting point for the age of antibiotics and, through decreasing numbers of deaths caused by infectious diseases, this was also believed as the starting point of the end for infectious diseases.^[2,3] The following period from 1950 to 1960 marked the golden age of antibiotics where nearly half of the antibiotics that are in clinical use nowadays, e.g. tetracyclines in 1953, cephalosporins in 1953, aminoglycosides in 1957 and vancomycin in 1958, were discovered.^[2,3] However, already in the 1950s first transferable resistance of bacteria to antibiotics was observed.^[2] Even in 1945, in his Nobel Lecture, *Alexander Fleming* warned that it was not difficult to generate antibiotic-resistant bacteria in the laboratory and that resistance formation will most likely also occur inside the human body through underdosing or human misuse of the antibiotic.^[3,4] Nowadays bacterial antimicrobial resistance (AMR) has emerged as a global health crisis gaining more and more public attention by, for example, the World Health Organization (WHO),^[5] the United Kingdom (UK) and European Union (EU)^[3,6,7] and the United States (U.S.).^[8,9] In general, bacterial AMR arises through changes in bacteria that cause the drugs that are usually used for treatment of the bacterial infections to become less effective.^[10] The process of resistance development has been already observed even before the first antibiotics were developed and is a naturally occurring process, but the excessive and inappropriate use of antibiotics, e.g. their availability without prescription, unnecessary prescription and their extensive use in agriculture to prevent infections and promote animal growth rather than treating sick animals, is accelerating the resistance development.^[6,7] Especially in agriculture, there is a reported link between antibiotic usage in animals and resistance formation in humans. This problem is further strengthened through large numbers of animals living in proximity under non-hygienic conditions which easily facilitates the spread of antibiotic-resistant bacteria.^[7]

A review on AMR from the UK in 2014 estimated that worldwide approximately 700,000 people died annually caused by AMR.^[6] In an updated report in 2016, the authors made clear that this even was an underestimate of the situation due to a poor reporting situation and that 200,000 people died from multidrug-resistant tuberculosis alone.^[7] Due to that and based on further projections on AMR development, the authors kept up their previous outlook of up to

10 million deaths annually in the year 2050, if no further action is taken to target AMR.^[6,7] A similar underestimation of AMR could also be observed in the reports from the U.S..^[9] Based on the available data in 2013, it was assessed that annually around 2 million people suffered from an antibiotic-resistant infection and that at least 23,000 people died as a consequence alone in the U.S..^[8] In an updated version of this report in 2019 utilizing more data, it became clear that the situation was completely underestimated with more than 2.6 million antibiotic-resistant infections and with 44,000 deaths in 2013. Even though the number of infections still increased to 2.8 million in 2019 alone in the U.S., the number of deaths decreased to 35,000 people indicating that the taken preventive measurements at least showed some success.^[9] A most recently published review in 2022 further systematically analyzed the global burden of AMR in 2019.^[10] The authors comprehensively estimated that in 2019 more than 1.2 million deaths were directly attributable to AMR. Furthermore, the six leading pathogens *Escherichia coli*, *Staphylococcus aureus*, *Klebsiella pneumoniae*, *Streptococcus pneumoniae*, *Acinetobacter baumannii* and *Pseudomonas aeruginosa* were causing 929,000 deaths directly attributable to AMR, where in addition the methicillin-resistant *S. aureus* (MRSA) represented the most deadly pathogen-drug combination with more than 100,000 deaths annually.^[10] Within this list of leading pathogens, not surprisingly, a large fraction belongs to the so-called ESKAPE (*Enterococcus faecium*, *Staphylococcus aureus*, *Klebsiella pneumoniae*, *Acinetobacter baumannii*, *Pseudomonas aeruginosa* and *Enterobacter* species) pathogens that were already known to be a severe threat to human health.^[11] Already in 2017, the WHO published a priority list of leading pathogens, for which antibiotic development is urgently needed, and assigned the ESKAPE pathogens high to critical priority.^[12] Additionally, a more recent priority list published in the review from the U.S. in 2019 also categorized these pathogens into urgent and serious threats to human health.^[9] Despite the increased attention to this global health crisis and the increasing emergence of antibiotic-resistant bacteria, the development of novel antibacterial agents has slowed down worldwide.^[3,13] Additionally, most of pharmaceutical companies have reduced their research activities in this field due to various reasons and only 20% of drugs against infectious diseases that were in the initial phase of testing in humans got the final approval from the U.S. Food and Drug Administration (FDA).^[9] As a consequence, bacterial resistance formation has exceeded the rate of antibiotic development by far, leading to a gap of approximately 20 years of discovery. Therefore, the discovery of novel classes of antibiotics is a major challenge and has a high priority.^[3,13]

2 Bacterial antimicrobial resistance development

Most of the commonly available antibiotics employ very similar modes-of-action and address only a very limited number of essential pathways and targets in bacteria (Figure 1).^[14]

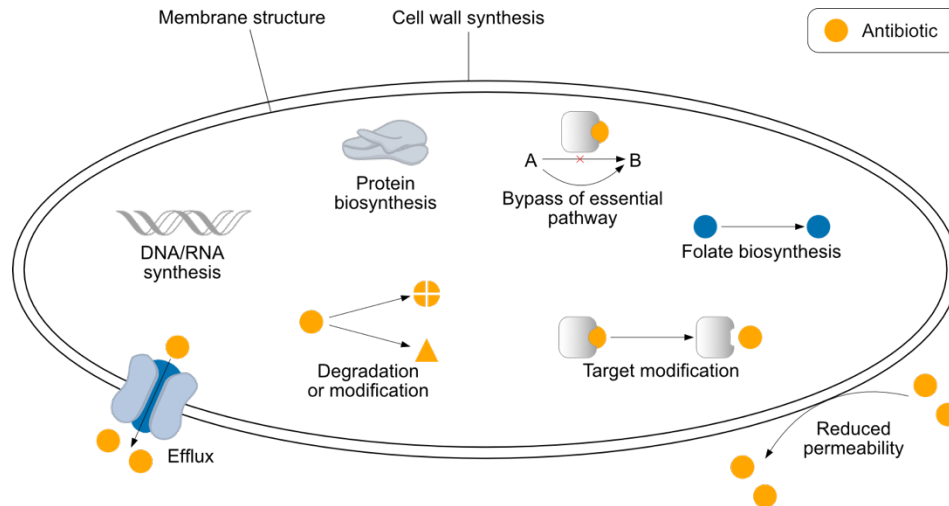


Figure 1: Overview of the most common antibiotic targets in bacteria and mechanisms of bacterial resistance formation. Adapted from *Lakemeyer et al.*^[14]

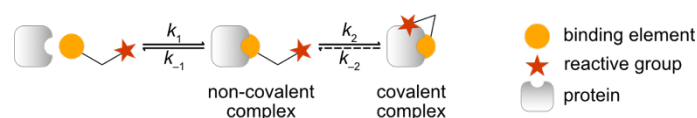
The main targets include the inhibition of the peptidoglycan/cell wall synthesis (*e.g.* β -lactams, glycopeptides), the protein biosynthesis (*e.g.* tetracyclines, chloramphenicol, aminoglycosides), folate and thereby nucleic acid biosynthesis (*e.g.* sulphonamides), RNA polymerase (*e.g.* rifamycins) and DNA gyrase (*e.g.* quinolones) or interference with the membrane integrity (*e.g.* polymyxins).^[14,15] Even though more than 300 essential genes within bacteria were predicted, most of the available antibiotics focus on this limited subset of targets, mainly due to the fact that they were derived from natural product sources that were optimized by evolution towards this small set of targets. As a consequence, multiple resistances within bacteria are developed against this small subset of targets.^[14] Additionally, resistances often occur against a whole class of antibiotics and even against a broad range of structurally and mechanistically unrelated antibiotics.^[16] The resistance formation is a consequence of evolutionary processes of bacteria that respond to the selective pressure during antibiotic treatment that selects for beneficial mutations in their DNA sequences. Bacteria that thereby generated resistance will survive the antibiotic treatment, while all susceptible strains will die, which leads to further propagation of the resistant strains.^[14] Resulting from this, the excessive use and abuse of antibiotics will further promote the evolution of resistant strains.^[3,6,7] The mechanisms of bacterial resistance are well-known and can be divided into different groups (Figure 1).^[14–17] The drug target binding site can be modified in order to promote limited antibiotic interaction and, thereby, resistance formation. As an example, resistance against the

macrolide antibiotic erythromycin is generated by the modification of its binding site on the ribosome through methylation of an adenine residue catalyzed by a family of *N*-methyltransferases.^[16] A β -lactam resistance caused by target modification can be found in MRSA that carry, in contrast to β -lactam susceptible *S. aureus* strains, the *mec* gene. This gene encodes for the penicillin-binding protein 2a (PBP 2a) that in contrast to the other PBPs, that are expressed in methicillin-sensitive strains, only has a very low affinity towards methicillin. PBP 2a can further compensate for the inhibition of the other PBPs and, thereby, render the bacteria resistant. The expression of PBP 2a usually also generates resistance towards the whole class of β -lactam antibiotics.^[16,18] Aminoglycoside resistance can also be attributed to target modification.^[16,19] Furthermore, it was shown that aminoglycoside resistance also arises from the enzymatic modification of the antibiotics through *O*-phosphotransferases, *O*-adenyltransferases and *N*-acetyltransferases, which leads to a reduction in their binding affinities towards their ribosomal targets.^[16,19] The enzymatic degradation of β -lactam antibiotics through β -lactamases that catalyze the hydrolysis of the β -lactam ring system, which renders the antibiotic inactive, is one of the main resistance mechanisms against this class. Especially in Gram-negative bacteria, there is an increasing prevalence of novel β -lactamases that possess a new substrate scope and even lower susceptibility towards β -lactamase inhibitors.^[16,20] Another mode of resistance formation is a reduced permeability of the bacteria, which leads to a reduced uptake of the antibiotic, which can as a consequence not address its intracellular targets. Reduction of uptake is of special concern in Gram-negative bacteria, since they possess an additional outer membrane that functions as permeability barrier. This additional membrane is also one of the explanations for the generally higher resistance of Gram-negative bacteria towards antibiotics in comparison to Gram-positive bacteria that do not have an additional outer membrane.^[14,16,17,21] Besides reduced permeability, resistance can also be induced through the active cellular export of the antibiotics by efflux pumps. This mechanism is typically associated with tetracycline and fluoroquinolone resistance.^[16,17,21,22] These efflux pump systems can be found in both Gram-positive and Gram-negative bacteria, but they reach exceptional efficiency and are of major concern especially in the latter due to their synergistic effects with the additional outer membrane barrier. This comprises that antibiotics that were able to successfully cross the outer membrane are then actively pumped out of the bacterial cell again.^[17,21] In general, efflux pumps and especially so-called multidrug efflux systems can render the bacteria resistant towards multiple different and even structurally unrelated antibiotics. In order to tackle those resistances, new classes of antibiotics with novel modes-of-action are urgently needed.^[14,16,17,21,22]

3 Covalent drugs

In contrast to non-covalent drugs, covalent drugs contain a reactive functional group that facilitates covalent bond formation with their target proteins in order to increase their overall affinity.^[23,24] In the past, the pharmaceutical industry avoided drugs with a covalent mode-of-action mainly due to safety concerns through possible off-target reactions that cause severe side-effects.^[25,26] This reservation resulted from the fact that some reversible drugs were metabolized to chemically reactive intermediates that covalently modified off-target proteins and thereby caused toxicity.^[25–27] As a result, nearly all previously existing drugs with a covalent mode-of-action were not intentionally designed as covalent modifiers, but their mechanism of action was discovered after their development.^[25,26] Aspirin, the oldest covalent drug on the market, was introduced in 1899 and only in 1971, it was elucidated that its anti-inflammatory effects resulted from the covalent acetylation of the active site serine in cyclooxygenase 1, which inhibits prostaglandin synthesis.^[24,28,29] Another example are β -lactam antibiotics that mimic the D-Ala-D-Ala motif of the precursors that are involved in bacterial cell wall biosynthesis. Thereby, they covalently bind to active site serines of PBPs and inhibit the transpeptidase reaction to form crosslinks within the bacterial cell wall, which ultimately leads the cell lysis.^[24,30,31] A large fraction of approved drugs with a covalent mode-of-action were antibiotics (47%) until the 1980s, representing their immense impact on fighting infectious diseases and ultimately also on human health.^[26] In the past decade covalent drugs have seen a resurgence in the pharmaceutical industry and their distinct strengths have been recognized.^[25] Combining non-covalent binding to targets with a carefully fine-tuned covalent reactivity was previously applied for mechanism-based or suicide inhibitors targeting directly catalytically active residues, but current pharmaceutical programs focus on the development of so-called targeted covalent inhibitors (TCIs).^[25,26] TCIs are composed of non-covalent binding motifs that engage the target of interest and of a reactive functional group that facilitates covalent bond formation with non-catalytic and poorly conserved amino acids at the target site.^[25] Covalent inhibitors, in general, have distinct advantages over non-covalent drugs like improved efficiency, opportunity to lower the dosing of the drug, less frequent dosing of the drug and lower probability of resistance formation.^[32–35] Most of these advantages result from prolonged target engagement of covalent and, especially, irreversibly covalent inhibitors, which engage their target permanently until the protein gets degraded and resynthesized.^[32] The extended target engagement is due to the mechanism-of-action that in the first step involves the formation of a non-covalent complex through interactions of the binding motif of the inhibitor with the target protein. This brings the reactive group in close proximity to a specific

nucleophilic amino acid residue within the binding pocket and facilitates the formation of the final covalent complex (Scheme 1).^[23,25,32–34]



Scheme 1: Mechanistic overview of a covalent inhibitor engaging with its target protein.^[23,25,32–34]

The non-covalent complex formation is kinetically defined by the dissociation constant (K_i), which depends on the forward (k_1) and reverse (k_{-1}) rate constants, whereas the covalent bond formation can be described by the rate constants k_2 and k_{-2} , respectively. In the case of irreversible covalent bond formation, k_{-2} will be zero and can be neglected.^[25,34] This leads to a permanent protein inhibition that is in a concentration- and time-dependent manner described solely by K_i and k_2 (often named k_{inact}).^[25,34] Therefore, their properties can be adjusted by either optimizing the non-covalent binding element (K_i) or the reactive group (k_2). In regards to selectivity, care must be taken that there is sufficient non-covalent interaction (K_i) to ensure covalent bond formation with the reactive group, while the potency of the reactive group (k_2) has to be carefully fine-tuned in order to avoid off-target engagement.^[25] Irreversible covalent bond formation also has the inherent advantage of an increased time-of-action, since the target protein remains engaged until degradation, which uncouples the pharmacodynamics from the pharmacokinetics.^[23,25] As a result, fast clearance rates of drugs in this case do not affect efficiency of the covalent inhibitors, but contribute to its selectivity assuming that their non-covalent interaction with off-targets remains short upon clearance and that, within their short half-lives, the inhibitors do not significantly covalently engage any off-targets.^[25] Resulting from these advantages and through the combination of medicinal chemistry and modern bioinformatic approaches, covalent inhibitors gained increasing relevance in modern drug development.^[24–26,36] Still nowadays, the majority of approved covalent drugs are anti-infectives (33%, *e.g.* β -lactam antibiotics), followed by anti-cancer agents (20%, *e.g.* afatinib, ibrutinib, osimertinib), drugs to treat gastrointestinal disorders (15%) and drugs to treat the central nervous system and cardiovascular diseases (15%).^[25,26] Among the antibiotics that react covalently are the aforementioned β -lactam antibiotics,^[30,31] β -lactamase inhibitors (*e.g.* clavulanic acid),^[37] fosfomycin,^[38,39] D-cycloserine^[40,41] and isoniazid (Figure 2).^[42]

Targeted covalent inhibitors are mainly designed to target cysteine side chains within proteins. The cysteine sulfur atom displays the highest nucleophilicity among all natural amino acids and depending on the surrounding pK_a environment it can easily be deprotonated to form the corresponding thiolate anion, which possesses enhanced nucleophilicity. Due to its reactivity,

cysteine also plays crucial roles in many catalytic processes and is, therefore, a prime candidate for inhibitor design. Although the prevalence of cysteines in proteins is quite low (1.9%), especially non-catalytic cysteine residues have emerged as key targets in recent drug development.^[36] As examples, all seven approved TCI kinase inhibitors (*e.g.* afatinib, ibrutinib, osimertinib) that are used for cancer treatments target cysteine residues within their binding site to form a covalent interaction (Figure 2).^[26,36]

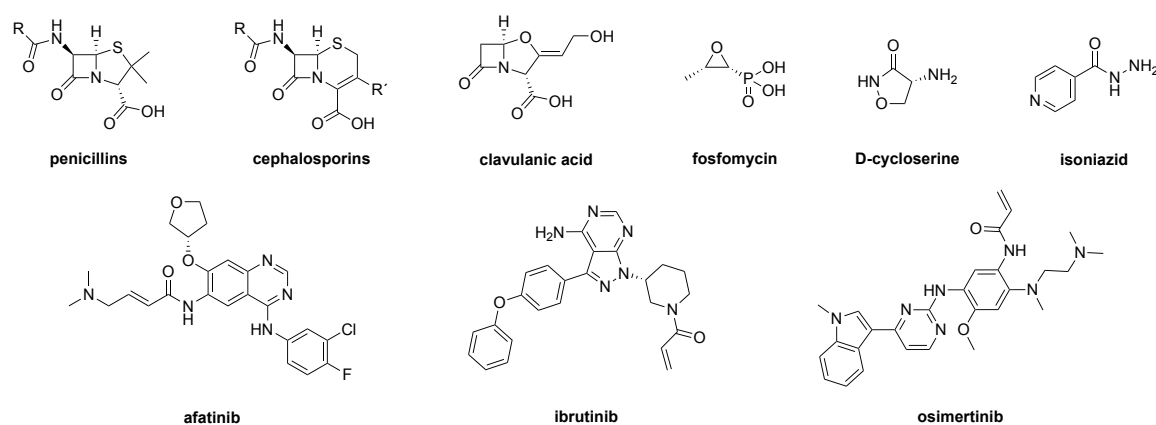


Figure 2: Structures of selected covalent inhibitors discussed in this section including the β -lactam antibiotics penicillins and cephalosporins,^[30,31] the β -lactamase inhibitor clavulanic acid,^[37] fosfomycin,^[38,39] D-cycloserine^[40,41] and isoniazid^[42] as antibiotics and the anti-cancer kinase inhibitors afatinib, ibrutinib and osimertinib.^[26,36]

The most commonly used functional group for cysteine-directed electrophiles are *Michael* acceptors such as α,β -unsaturated amides that are also used in the aforementioned kinase inhibitors. Additional functional groups include epoxides, nitriles, terminal alkynes, α -halomethyl ketones and haloacetamides, which all strongly differ in their overall reactivity.^[36,43] The choice of electrophilic functional group strongly depends on the desired reactivity that should be carefully fine-tuned in order to avoid excessive reactivity and off-target engagement.^[25,36,44] A detailed overview of the reactivity and amino acid selectivity of different functional groups has previously been reported by our group.^[45]

Covalent inhibitors and TCIs can be developed utilizing different strategies, like the already discussed use of non-covalent inhibitors and attaching a reactive functional group at a suitable position to additionally allow covalent bond formation. Nevertheless, this approach comes with the limitations that already pre-existing non-covalent binders are needed and that a nucleophilic amino acid side chain needs to be present in close proximity to the binding site. Recently, the possibility to screen libraries of small covalent fragments gained more attention. The low molecular weight of these fragments enables the identification of novel binding sites beyond substrate pockets, novel modes-of-action, unexpected structures and often yields lead structures

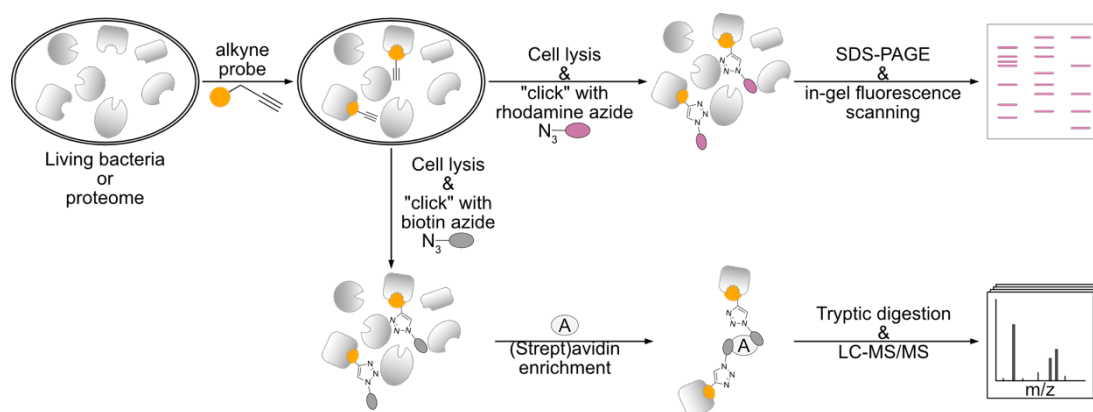
using a smaller library size compared to conventional approaches.^[43,46] Computational approaches, the use of DNA-encoded libraries as well as chemoproteomic approaches and others were also used to identify novel covalent inhibitors.^[43,46–48]

4 Activity-based protein profiling

In drug discovery processes that are based on phenotypic screens of a library of small molecules, one of the major challenges is the identification of the targets of the identified hit compounds and the elucidation of the mode-of-action of the drug.^[49] Proteomic and especially chemoproteomic technologies like activity-based protein profiling (ABPP) have emerged as key technologies to answer these questions.^[49–51] In addition to the target identification of small molecules resulting from phenotypic screens, ABPP can also be used to screen a library of small molecules against a class of only poorly characterized enzymes and, thereby, to identify new lead compounds to target those. Further, ABPP can be utilized to analyze and optimize the selectivity of certain hit compounds, since screenings in complex environments and even in the background of a whole proteome can be accomplished in a highly parallel fashion.^[50,51]

Originally, ABPP was developed to investigate and determine the functional states and activities of a defined subset of proteins and enzymes in complex proteomes and to enable the quantification of the respective functional states. In this approach, activity-based probes (ABPs) are used that covalently target the enzyme active sites of a specific and defined class of enzymes and, thereby, account for the enzyme activity rather than for abundance.^[51–55] ABPs usually consist of three different elements to achieve their function: a reactive group, a linker region and a tag for further downstream analysis of the bound target proteins. The reactive group usually consists of an electrophilic reactive group that modifies nucleophilic amino acids of the targeted class of proteins. *E.g.* fluorophosphonates preferentially react with activated serine residues in serine proteases. Alternatively, a photoreactive group, *e.g.* a diazirine, can be used instead of a constitutively electrophilic functional group to also target proteins that do not possess nucleophilic amino acids within their active sites. These ABPs are initially unreactive but form a highly reactive species upon UV irradiation that forms a covalent bond towards their targets and, thereby, enables the further downstream analysis. The linker region can be composed of structurally simple alkyl chains that only generate a spatial distance between the reactive group and the reporter tag, but they also can contain affinity elements that in addition to the reactive group enhance the selectivity towards the desired enzyme class. Here, *e.g.* peptide linkers mimicking the substrates of proteases can be utilized to selectively target a

specific class of proteases. Additionally, specifically cleavable linkers were developed that will be discussed in the following part. The tag of ABPs allows further downstream analysis of the targeted proteins and can either be an affinity handle like biotin to enable specific enrichment of proteins with (strept)avidin or a fluorophore for fluorescence scanning.^[49,51–57] Since the incorporation of biotin or fluorophore tags directly into ABPs often results in limited cellular uptake and in changes of the physicochemical properties that lead to reduced target binding affinities, a two-step functionalization method is usually used nowadays.^[54,56–59] Here, copper (I)-catalyzed azide-alkyne cycloaddition (CuAAC), that was discovered by *Sharpless*^[60] and *Meldal*,^[61] was adapted for ABPP purposes.^[62,63] This approach resembles the most commonly used biorthogonal reaction in ABPP. Here, relatively small terminal alkyne- and azide-functionalities are introduced into the ABPs and to the suitable reporter molecules for downstream analysis, respectively. The use of these small functionalities instead of relatively large biotin or fluorophore, minimizes structural changes in ABPs and, thereby, usually retains their physicochemical properties, target affinity and permeability. Additionally, higher flexibility is generated through the possibility of a variable functionalization of the labelled proteins with any reporter tag of interest depending on the downstream analysis. The main disadvantage of this approach is the use of toxic copper (I), which can therefore not be used in living cells.^[54,56–59] To circumvent this toxicity issue, alkyne- or azide-functionalized ABPs are incubated with living cells (“*in situ*”) first and after subsequent lysis of the cells, the probe-modified proteins are “clicked” by CuAAC^[60–63] to the reporter tag functionalized with the corresponding counterpart (azide- or alkyne-modification). Although both functionalities are possible on either the ABP or the reporter tag, most commonly the terminal alkyne is attached as tag on the ABPs and the azide-functionality on the reporter molecules, since this combination often resulted in lower background labelling.^[54,56–59] Alternatively to avoid toxic copper (I) and to use the “click” reaction *in situ* and even in living animals (“*in vivo*”), *Bertozzi* and coworkers developed a variant of this biorthogonal ligation that proceeds without the use of copper (I) but is promoted through ring-strain of a cyclooctyne derivatives.^[64–67] After the reporter molecule was clicked to the ABP-labelled proteins, the further ABPP workflow depends on the choice of the selected reporter molecule (Scheme 2).^[49,51,55,57,58]



Scheme 2: Schematic representation of a typical ABPP workflow with an alkyne probe that is modified by CuAAC^[60–63] with rhodamine- or biotin-azide to enable either SDS-PAGE and in-gel fluorescence scanning or (strept)avidin enrichment followed by LC-MS/MS analysis.^[49,51,55,57,58]

Typically, to determine the labelling efficiency of the ABP, to optimize labelling conditions and to rapidly get a first impression of the labelling in general, an analytical ABPP workflow is applied, in which the alkyne probe-labelled proteins are clicked to a fluorophore, *e.g.* rhodamine-azide. After subsequent separation of the sample using sodium dodecyl sulfate polyacrylamide gel electrophoresis (SDS-PAGE), the labelled proteins can be visualized by in-gel fluorescence scanning. In a subsequent experiment with the optimized labelling conditions in hand, a preparative ABPP workflow can be conducted to directly investigate the labelled proteins. For this purpose, the alkyne probe-treated samples are clicked to biotin-azide. The strong binding affinity of biotin to (strept)avidin enables a selective enrichment of the labelled proteins on (strept)avidin-coated beads. The protein disulfide bonds are reduced with 1,4-dithiothreitol (DTT) and free cysteines are alkylated with iodoacetamide (IA). After the digestion of the proteins directly on the beads with trypsin to the respective peptides, the sample is analyzed by tandem mass spectrometry coupled to liquid chromatography (LC-MS/MS). The final data evaluation and identification of modified proteins can be conducted by different software solutions. The identical workflow is also performed with a vehicle/solvent control instead of the ABP to determine the background labelling that is present mainly due to unspecific protein binding to the (strept)avidin beads. Therefore, the final targeted proteins are determined by comparing the non-specific enriched proteins of the vehicle control with the enriched proteins of the ABP treated sample.^[49,51,55,57,58]

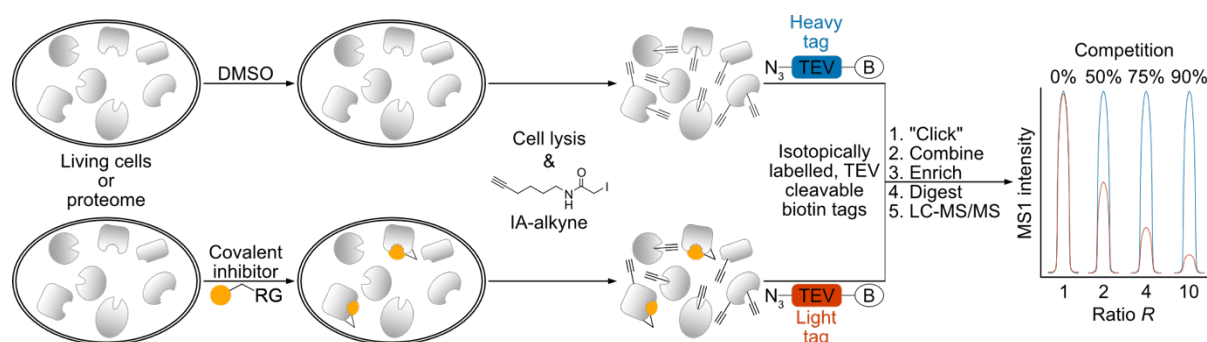
Instead of addressing individual protein classes, it has recently become popular to profile the ligandability of certain types of amino acid residues in the entire proteome based on their inherent reactivity.^[68] Here, the ABPP workflow is usually performed in a competitive mode with broadly reactive alkyne probes that label many residues of a certain type. For this purpose,

different reactive groups targeting specific amino acid residues like cysteines, lysines and serines were developed.^[49,51,55,57,58] A comprehensive study from our group further investigated a large variety of different probes also targeting other amino acid residues.^[45] In the underlying workflow, the compounds of interest can be applied to either cellular lysate (*in vitro*) or to living cells (*in situ*). Simultaneously, another identical sample is prepared that is incubated with a vehicle control instead of the compound. After treatment, the samples are lysed and labelled with a broadly reactive alkyne probe that reacts promiscuously with the amino acid residues of choice. *E.g.* iodoacetamide-alkyne (IA-alkyne) is often used to profile cysteine residues in the whole proteome. The samples are then clicked to the reporter molecules of choice and further analyzed. As a consequence, a decrease in signal intensity of the compound-treated samples in comparison to the vehicle-treated samples indicates that the used probe did not bind to that peptide and, therefore, that the protein binding site was already blocked and engaged by the tested compound. This competitive approach offers several advantages. Firstly, there is no need for often complex probe synthesis of the inhibitor molecules that are investigated and secondly, the inhibitors can be investigated without any structural changes caused by the introduction of an alkyne-handle that possibly could also lead to changes in their biological activity. Additionally, the potential inhibitors are screened against the whole proteome simultaneously and, therefore, not only investigated for their potential to bind different proteins, but also for their selectivity towards the entire proteome.^[49,51,55,57,58]

One important pre-requisite for this method to work is that the interactions can be monitored on a residue-specific basis by detecting and quantifying the peptides modified with the broadly reactive alkyne probe.^[55,57] To achieve this, a concept called tandem orthogonal proteolysis (TOP)-ABPP was developed.^[69,70] In this technology, a reporter molecule was used that was composed of a linker region containing a tobacco etch virus (TEV) protease cleavage site between the biotin tag and the azide-handle. After tryptic digestion, the probe-labelled peptides can be cleaved of the (strept)avidin beads by another digestion with TEV protease. The probe-modified and unmodified peptides can then be analyzed separately by LC-MS/MS, which provides simultaneously information about the engaged proteins in general and about the exact site of labelling.^[55,57,69,70]

Based on this concept, another approach called isotopic tandem orthogonal proteolysis (isoTOP)-ABPP was developed.^[71] In this concept, the reporter molecules with the TEV cleavage site additionally were isotopically labelled as heavy and light tag, respectively, which allowed to study the reactivity of cysteine residues proteome-wide in a quantitative manner.^[71] The isoTOP-ABPP workflow was also applied in a competitive fashion to screen

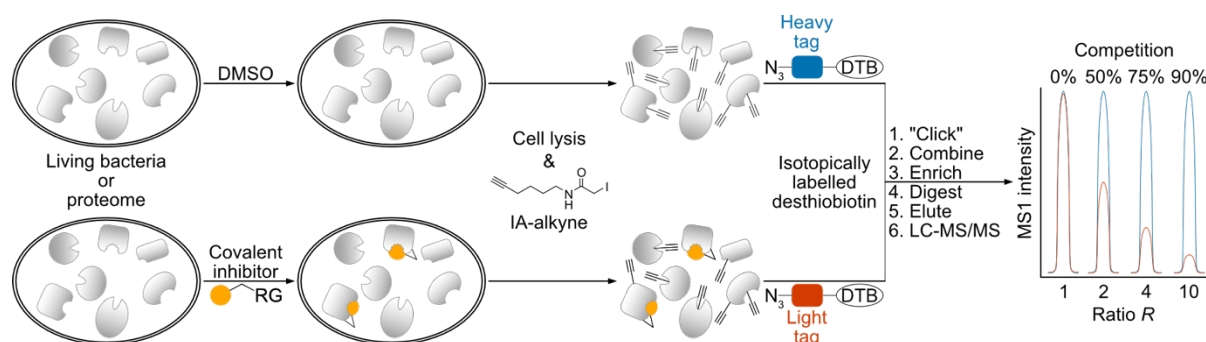
libraries of electrophilic, cysteine-directed fragments in whole proteomes and living cells in order to determine their targeted proteins and to quantitatively investigate the ligandability of cysteine residues within the proteome (Scheme 3).^[68,72,73]



Scheme 3: Schematic representation of the competitive isoTOP-ABPP workflow. Two identical samples of living cells or lysate are incubated with a covalent inhibitor or a solvent control, *e.g.* DMSO, respectively. After cell lysis, the samples are treated with a broadly reactive cysteine probe IA-alkyne and clicked to the heavy- or light-isotopically labelled, TEV cleavable biotin tags, combined, enriched and digested with trypsin and TEV protease. The isotopically labelled pair of probe-labelled peptides are then analyzed by LC-MS/MS which generates the competition ratio R reflecting the difference in MS1 signal intensity between the heavy- (DMSO-treated, blue) and light- (compound-treated, red) labelled peptides and finally the amount of competition.^[68,72–74] B: biotin; RG: reactive group.

Two identical samples of living cells or lysate are incubated with either the covalent inhibitor fragment or with a vehicle control, mostly dimethyl sulfoxide (DMSO), and after cell lysis treated with a broadly-reactive IA-alkyne probe that reacts with cysteine residues. The probe-labelled proteins are then clicked to the heavy- or light-isotopically labelled, TEV cleavable biotin tags, the samples are combined, enriched on (strept)avidin beads and digested on the beads with trypsin and TEV protease. This workflow generates isotopically labelled pairs of probe-labelled peptides that are further analyzed by LC-MS/MS. Finally, a competition ratio R is generated between the MS1 intensities of the heavy- (DMSO-treated) and light- (compound-treated) labelled peptides. Consequently, high R values are obtained, if the same peptide was more strongly quantified in the DMSO-treated sample, which indicates that this cysteine residue was already engaged in the compound-treated sample. This R value, therefore, represents the amount of competition at the cysteine residue.^[68,72,73] The same concept was also applied to assess the proteome-wide reactivity and ligandability of lysine residues by exchanging the cysteine-directed IA-alkyne with a lysine-directed sulfotetrafluorophenyl ester probe (STP-alkyne).^[74]

Adapting this technology, our group developed a residue-specific ABPP workflow that uses isotopically labelled desthiobiotin (isoDTB) azide tags instead of the isotopically labelled TEV cleavable biotin tags and is, therefore, termed isoDTB-ABPP (Scheme 4).^[75]

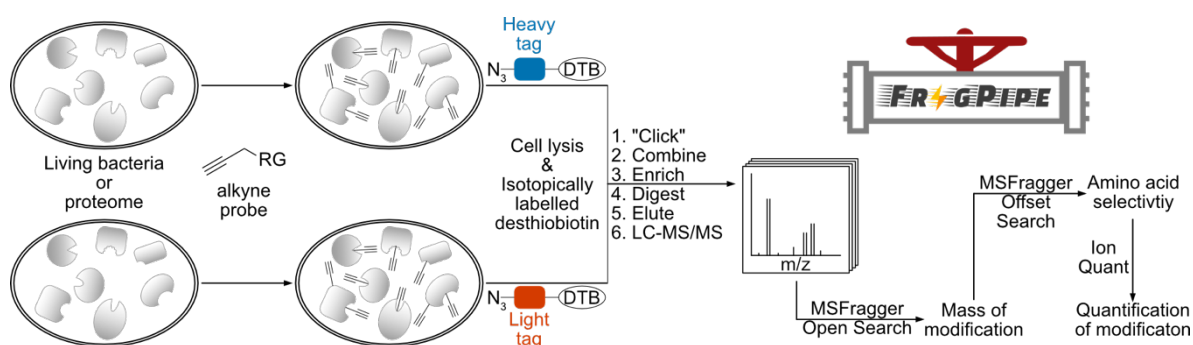


Scheme 4: Schematic representation of the competitive isoDTB-ABPP workflow. Two identical samples of living bacteria or lysate are incubated with a covalent inhibitor or a solvent control, *e.g.* DMSO, respectively. After cell lysis, the samples are treated with a broadly reactive cysteine probe IA-alkyne and clicked to the heavy- or light-isotopically labelled isoDTB tags, combined, enriched, digested with trypsin and eluted from the (strept)avidin beads. The isotopically labelled pair of probe-labelled peptides are then analyzed by LC-MS/MS which generates the competition ratio R reflecting the difference in MS1 signal intensity between the heavy- (DMSO-treated, blue) and light- (compound-treated, red) labelled peptides and finally the amount of competition.^[75] DTB: desthiobiotin; RG: reactive group.

The isoDTB tags do not contain biotin for (strept)avidin enrichment, but instead desthiobiotin that more reversibly binds to (strept)avidin. Consequently, the workflow is identical to the isoTOP-ABPP approach until the tryptic digestion. Afterwards, there is no need for TEV cleavage off the beads, but instead the probe-labelled peptides can be eluted with acetonitrile from the beads and directly analyzed by LC-MS/MS.^[75]

Another study from our group developed a variant of the isoDTB-ABPP workflow^[45] that utilizes the MSFragger-based FragPipe computational platform^[76–84] for data analysis, which enables the investigation of the reactivity and selectivity of diverse electrophilic probes proteome-wide in an unbiased fashion (Scheme 5).^[45] The isoDTB-ABPP workflow is an especially useful technology for this analysis since it enables the specific enrichment of probe-labelled peptides and increases the confidence of peptide assignments due to the isotopic pattern of the isoDTB tags. In this workflow, two identical samples of either living bacteria or lysate are both incubated with a reactive alkyne probe. After cell lysis, one sample is clicked to the heavy- and another sample to the light-labelled isoDTB tags. The samples are combined, enriched on (strept)avidin beads, digested with trypsin, eluted from the beads and analyzed by LC-MS/MS.^[45] The MSFragger Open Search^[76–83] function identifies all masses of

modification that occurred proteome-wide in the samples.^[45] In this way, the modification with the investigated probe will be displayed as a pair of two high-resolution masses reflecting the isotopic pattern of the isoDTB tags. Therefore, the masses of modification resulting from probe treatment can be determined with high confidence.^[45] This pair of masses can further be analyzed with the MSFragger Offset Search^[76,77,79–84] function that identifies the amino acid residues and protein termini, on which the modification occurred proteome-wide and allows to quantify the amino acid selectivity of the tested probe.^[45] The pair of masses of modification and the corresponding amino acid, on which the modification mainly occurred, are then analyzed with the MSFragger Closed Search^[76,77,80–83] and IonQuant^[84] quantification module which finally results in a quantification of the probe-modified peptides.^[45] In summary, the masses of modification, the amino acid selectivity of probes and even the quantification of probe-modified peptides proteome-wide can be analyzed in an unbiased fashion utilizing this variant of the isoDTB-ABPP workflow.^[45]



Scheme 5: Schematic overview of the isoDTB-ABPP workflow^[45] utilizing the MSFragger-based FragPipe computational platform for downstream data analysis.^[76–84] Two identical samples of living bacteria or lysate are incubated with an alkyne probe. After cell lysis, the samples are clicked to the heavy- or light-isotopically labelled isoDTB tags, combined, enriched, digested with trypsin and eluted from the (strept)avidin beads. The isotopically labelled pair of probe-labelled peptides are then analyzed by LC-MS/MS.^[45] The MSFragger Open Search^[76–83] function identifies the masses of modification that occurred proteome-wide after probe treatment.^[45] The pair of masses, reflecting the isotopic pattern of the isoDTB tags and therefore the modification resulting from the probe,^[45] are selected for the MSFragger Offset Search^[76,77,79–84] which identifies the amino acid residues and termini where the modifications occurred and the corresponding amino acid selectivity.^[45] The pair of masses of modification and the amino acid residue, where the modification occurred, are finally analyzed with the MSFragger Closed Search^[76,77,80–83] and IonQuant^[84] quantification module which enables the quantification of the probe-modified peptides.^[45] DTB: desthiobiotin; RG: reactive group.

II A modular concept for enzymatically activatable caged electrophiles

This chapter is based on the following publication:

M. Zollo, P. R. A. Zanon, S. A. Sieber, S. M. Hacker, Caging Highly Reactive Electrophiles for Selective Enzymatic Activation in Bacteria. *Manuscript in preparation*.

This chapter is additionally a direct continuation of my Master's thesis and some relevant results are therefore included:

M. Zollo, Evaluation of the Antibiotic Potential of Bromomethyl Ketones for the Development of Latent Electrophiles, Master's Thesis, Technical University of Munich, **2019**.

Some results of this chapter are further included in the following conference presentation:

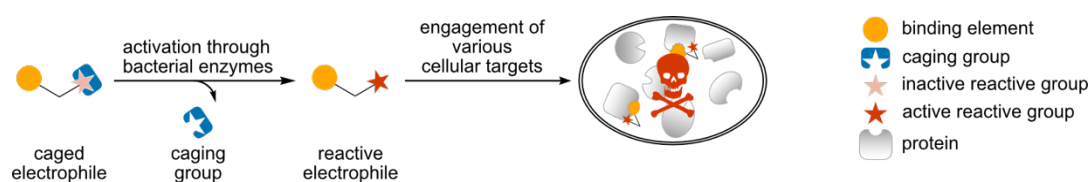
M. Zollo, C. Schmidt, P. R. A. Zanon, R. Bonsignore, A. Casini, S. A. Sieber, S. M. Hacker, New Chemoproteomic Technologies and Chemical Modalities for Antibiotic Discovery. *poster presentation and flash talk, EFMC-ISMIC, 4th-8th September 2022*, Nice, France.

Contributions:

MZ, SAS and SMH planned the project and all experiments. PRAZ initiated the project through the synthesis of the first-generation caged electrophile **CE1** and conducted first proof-of-concept studies. MZ repeated these experiments and conducted all further experiments and data evaluation. MZ and SMH prepared the manuscript for publication with input from all others.

1 Introduction

Drugs are usually developed to engage one single cellular target with high specificity in order to avoid off-targets and side-effects. Nevertheless, these single-target approaches are often not effective in therapy, since complex diseases might use compensatory pathways that are not inhibited by the drug. Additionally, in the case of antibiotics, single-point mutations can render the bacterium resistant towards single-target drugs. One possibility to overcome these limitations is a multi-target approach, where the drugs do not have one single cellular target, but more of them that are either within the same metabolic pathway or completely unrelated.^[85–90] Since it is less probable to develop resistance by single-point mutation against multi-target drugs compared to single-target drugs and since it is very unlikely that bacteria are able to mutate multiple target proteins simultaneously, multi-target approaches have the potential to fight the antimicrobial resistance development and reduce resistance formation.^[85–90] Therefore, recent reviews postulated that an ideal concept for antibiotic development would be to use highly reactive electrophiles that covalently engage multiple, unrelated intracellular targets.^[91,92] In order to avoid potential off-targets and deleterious side-effects in humans that are probably associated with the use of those highly reactive compounds, these electrophiles must be delivered in a caged form that is initially unreactive but gets activated by specific bacterial enzymes to release the reactive electrophile only in bacteria but not in human cells. Such a concept may be realized through the use of caged electrophiles that are intrinsically unreactive, but after specific enzymatic activation the caging group gets cleaved off and the liberated electrophile can engage multiple intracellular targets, thus preventing resistance formation (Scheme 6).^[47,90–96]



Scheme 6: Schematic representation of a generalized caged electrophile strategy. The caged electrophile is intrinsically unreactive and only after specific activation through bacterial enzymes a highly reactive electrophile gets liberated that can engage various intracellular targets simultaneously only in bacteria but not in human cells. Thereby, the chance of resistance formation and potential side-effects in human cells are reduced.^[47,90–96]

To this end, bacterial nitroreductases were utilized in many different concepts to selectively liberate reactive agents specifically only after activation.^[93–96]

1.1 Bacterial nitroreductases

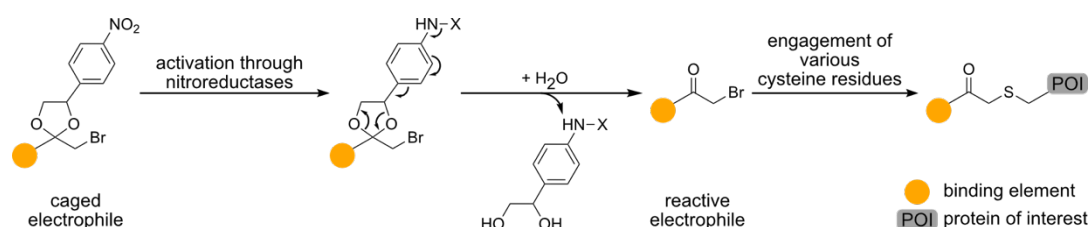
During their investigations into the mechanism of action of nitrofurantoin antibiotics, *Asnis et al.* identified that these antibiotics are activated in *Escherichia coli* through the reduction of the nitro-group catalyzed by flavoproteins.^[97] In following studies by *McCalla et al.* the corresponding enzymes were further characterized and the genes controlling the reductase activity were assigned as nitrofurantoin-sensitive genes *nfsA* and *nfsB*, respectively.^[98] In general, nitroreductases are able to catalyze the reduction of a wide variety of different nitro group-containing molecules and can be classified into oxygen-insensitive (type I) and oxygen-sensitive (type II) nitroreductases.^[99–101] The latter catalyze one electron reductions strictly under anaerobic conditions to transform the nitro-group to a nitro-anion radical. The radical gets readily re-oxidized by oxygen under aerobic conditions to its parent nitro-group in a futile cycle, which also generates superoxides that lead to oxidative stress.^[99,102,103] In contrast, the oxygen-insensitive (type I) nitroreductases catalyze consecutive two-electron reductions under aerobic conditions to form the nitroso-, hydroxylamine- and finally amine-derivative.^[99,102–107] There are reports that suggest that nitrofurantoin antibiotics are further converted to the respective open-chain nitrile derivatives after a six-electron reduction.^[104,105] The hydroxylamine, which is formed after two consecutive two-electron reductions, is believed to be a toxic and cancerogenic intermediate that can react with bacterial proteins and DNA leading to strand breaks in the latter.^[99,107–111] The aforementioned major nitroreductase NfsA and minor nitroreductase NfsB from *E. coli* belong to the oxygen-insensitive (type I) group. NfsA has a monomeric molecular weight of 26.8 kDa and is tightly associated with flavin mononucleotide (FMN) as a prosthetic group. It is active as a homodimer with one FMN per subunit and it uses nicotinamide adenine dinucleotide phosphate (NADPH) as reducing equivalent.^[99–101,112] Similarly, NfsB is also active as homodimer with one FMN associated to each monomer and has a monomeric molecular weight of 24 kDa. In contrast to NfsA, NfsB can accept both, NADPH and nicotinamide adenine dinucleotide (NADH), as electron donor for reductions.^[101,111–114] Although NfsA and NfsB are structurally different and have only very little sequence similarity, both enzymes display similar catalytic properties and can reduce a wide variety of different nitro-group containing molecules according to a ping-pong bi-bi mechanism.^[99–102,106,111–114] The fact that both enzymes only catalyze obligatory two-electron reductions can probably be attributed to the extreme instability of their FMN semiquinone redox state.^[99–102,106,111–114]

In general, nitroreductases are widely distributed among bacteria and most bacteria contain even several different nitroreductase. In *E. coli*, in addition to the aforementioned NfsA and

NfsB, at least one other nitroreductase, YdjA is present.^[95,103,112] Additionally, a recent study identified another *E. coli* nitroreductase, AhpF, that was also able to reduce nitrofurantoin derivatives.^[115] Strikingly, *Staphylococcus aureus* even contains at least four different nitroreductases.^[116] It was also shown that *E. coli* has to mutate both, the major nitroreductase NfsA and the minor nitroreductase NfsB in order to develop resistance towards nitrofurantoin antibiotics in two consecutive steps.^[98,110–112] Even those mutants that were resistant against nitrofurantoin, an antibiotic belonging to the nitrofurantoin class, showed overall decreased growth in the absence of the antibiotic and in presence of the antibiotic their growth was further decreased suggesting that they are unable to cause an infection in humans.^[117] Additionally, no cross-resistance towards other antibiotics was identified for resistant strains against the nitrofurantoin antibiotic furazolidone.^[118] Apart from bacteria, nitroreductases can also be found under hypoxic conditions in tumor cells and tumorous tissues. This nitroreductase activity was utilized in different studies for the selective activation of fluorescent dyes to visualize tumorous tissues and their hypoxic status.^[119–123] The nitroreductase DT-diaphorase, that is present in tumors, was utilized to selectively activate the prodrug CB1954 in Walker rat carcinoma cells. After reduction of the nitro-group, a highly potent DNA crosslinking agent is generated to exhibit its cytotoxic effect. Nevertheless, human tumors were insensitive towards CB1954, since the mammalian enzyme showed slower reaction kinetics.^[124–129] However, it was found that the *E. coli* NfsB was able to reduce and activate CB1954 up to 60 times faster compared to the mammalian enzyme.^[124] Consequently, NfsB was utilized in many suicide gene therapy approaches, where an exogenous enzyme is delivered specifically to the target cells to activate a prodrug site-specifically. Therefore, NfsB is either coupled directly to an antibody in an antibody-directed enzyme prodrug therapy (ADEPT) or its respective gene gets delivered to and expressed in the target cells through appropriate vector systems in the so-called viral- or gene-directed enzyme prodrug therapy (VDEPT and GDEPT).^[124–130] In addition to NfsB, also NfsA was utilized in such strategies showing the potential of bacterial nitroreductases to selectively activate prodrugs at the targeted cells.^[131,132] Other studies even report the complete absence of nitroreductase activity in healthy human cells or at least a low catalytic activity and different substrate specificity of the corresponding mammalian equivalents.^[93–96,133] Due to these reasons, bacterial nitroreductases are prime candidates for the development of specifically activatable prodrugs that are only released or activated at the specific site without targeting healthy human cells which can drastically reduce unwanted side-effects.^[93–96,133] However, recent studies could also detect some nitroreductase activity in mitochondria in healthy human cells, which necessitates careful fine-tuning of the prodrug activation.^[134,135]

1.2 Concept of caged electrophiles

The aforementioned concept of caged electrophiles (Scheme 6) that are initially unreactive, but are activated specifically by enzymes only present at the targeted cells^[91,92] has so far *e.g.* been applied for the reductive activation of nitrogen mustards,^[136] the generation of alkynylketones from alkynylcarbinols^[137] and for the release of isothiocyanates from glucosinolates.^[138,139] However, these systems only lead to the release of a specific subset of electrophiles and are also limited towards the activation by specific enzymes. In this work, we wanted to develop and establish a modular concept of caged electrophiles that can deliver a wide variety of different electrophilic functional groups and that is additionally also modular in regard to its activating enzyme. Therefore, we adapted a previously described strategy, where the carbonyl functionality of bromomethyl ketones was caged as an acetal, which renders them unreactive towards cellular cysteines and, thereby, prevents cytotoxic effects. This studies, however, do not utilize enzymatic activation of the caged electrophiles, but rely on UV-irradiation of a photolabile acetal protecting group to liberate a highly reactive bromomethyl ketone in living cells.^[140,141] Additionally, we were encouraged by the fact that carbonyl functionalities are responsible for the reactivity of many different electrophiles that were shown to react with *e.g.* cysteines (halomethyl ketones,^[142] peptide aldehydes,^[142,143] α,β -unsaturated ketones,^[144] alkynylketones^[137]), lysines (ethynylbenzaldehydes,^[45,145] boronic acid-substituted benzaldehydes,^[146,147] alkynylketones,^[137] salicylaldehydes^[148,149]), serines (trifluoromethyl ketones,^[142,150] peptide aldehydes^[142,143]), arginines (phenyl glyoxals)^[45,151] and protein *N*-termini (ethynylbenzaldehydes,^[45,145] pyridine carboxaldehydes,^[152] triazol carboxaldehydes^[153]). Finally, we designed and developed a modular concept of caged electrophiles based on cysteine-reactive bromomethyl ketones that are initially caged as an acetal and can further be specifically activated by bacterial nitroreductases (Scheme 7).^[45,93,94,96,120,123,140–142]



Scheme 7: Overview of the modular concept of caged electrophiles and proposed mechanism for the activation of the caged electrophiles through nitroreductases. The nitro-group gets reduced by bacterial nitroreductases to the corresponding hydroxylamine- ($X = \text{OH}$) or amine- ($X = \text{H}$) group, which increases the electron density and leads to a 1,6-elimination process that liberates the highly reactive electrophile that can then engage various intracellular cysteine residues.^[45,93,94,96,120,123,140–142]

In our concept of caged electrophiles, we chose bromomethyl ketones as electrophiles since it was already shown that caging them as acetals renders them unreactive and their promiscuous cysteine-directed reactivity was already established.^[45,140–142] Furthermore, we chose bacterial nitroreductases as activating enzymes due to the absence of nitroreductase activity in healthy human cells, respectively the low catalytic activity of their mammalian equivalents, thus preventing off-target engagement and corresponding side-effects in human cells.^[93–96,133] In this way, the initially caged electrophiles are intrinsically unreactive and after reduction of the nitro-group to the corresponding hydroxylamine- or amine-group by bacterial nitroreductases, the electron density in the ring system increases, leading to a consecutive 1,6-elimination process to liberate the highly reactive electrophile that can engage multiple intracellular cysteine residues simultaneously.^[45,93,94,96,120,123,140–142] In general, this concept should not only be modular in regards to the different carbonyl-containing electrophiles that could be used, but also different activating enzymes should be utilizable to activate the caged electrophiles, since there are many reported enzyme families that can liberate the for the fragmentation needed amine-functionality, *e.g.* proteases,^[154] β -lactamases,^[155] azoreductases^[156] or cytochrome P450 enzymes (CYP450).^[157] Additionally, altering the structure of the acetal and the corresponding caging group should allow optimization of the activation properties of the caged electrophiles as shown in related prodrug strategies.^[133] Overall, the modular nature of this concept should enable the fine-tuning of the biological activity, physicochemical properties, and permeability of the caged electrophiles through structural changes in one or more of the respective elements of the caged electrophiles.

2 Scope of the project

In this part of the thesis, we establish our proposed concept of caged electrophiles based on bromomethyl ketones that are caged as acetals to render them initially unreactive. After specific activation by bacterial nitroreductases, the highly reactive electrophile gets liberated to engage multiple intracellular proteins at their cysteine residues simultaneously (Scheme 7).^[45,93,94,96,120,123,140–142]

First of all, we aimed to synthesize the free electrophile probe and the corresponding first-generation caged electrophile to perform proof-of-concept studies through gel-based labelling experiments in bacterial lysate after preincubation with nitroreductase.

After these initial successes, we set out to further improve the labelling conditions by adjusting the experimental setup and the used cofactors. While the overall labelling could be significantly improved to better represent the native conditions in living bacteria, our first-generation caged electrophile still labelled the proteome significantly less efficient compared to the free electrophile indicating insufficient activation.

Therefore, we synthesized a library of second-generation caged electrophiles based on different caging groups with altered electronic properties and activation mechanisms and evaluated their activation potential with the optimized labelling conditions. Thereby, we identified a promising thiophene-based caged electrophile, which was selected for more detailed investigations in another gel-based experiment. We could demonstrate that even endogenous nitroreductase activity, still present in the bacterial lysate, was sufficient for notable activation of the improved caged electrophile.

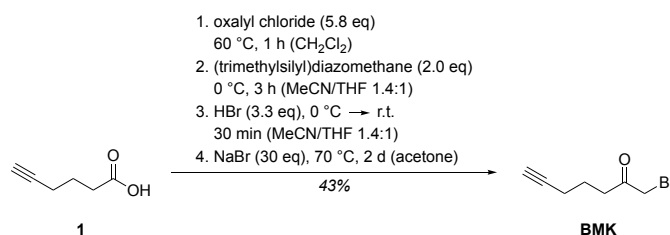
We further expanded our studies to living bacteria, where we could verify reactivity of the optimized caged electrophile comparable to the free electrophile. Using the same experimental setup in a human cell line did not lead to the activation of the caged electrophiles, demonstrating their selectivity towards bacteria.

Finally, we wanted to further analyze the exact mass of modifications and amino acid selectivity of the caged electrophiles as well as to quantify the labelled peptides using an unbiased chemoproteomic approach developed in our group based on the isoDTB-ABPP workflow^[45] in combination with the MSFragger-based FragPipe computational platform^[76–84] for data analysis.

3 Results and discussion

3.1 Synthesis of the first-generation caged electrophile

To establish the concept of caged electrophiles, we first set out to synthesize a bromomethyl ketone probe with an alkyne-handle to enable further downstream analysis of the labelling properties of the probe and its caged derivatives using ABPP experiments.^[54,56–59] Therefore, analogously to the concept of light-activatable caged electrophiles, we synthesized the corresponding bromomethyl ketone probe **BMK** starting from 5-hexynoic acid (**1**) using a modified procedure (Scheme 8).^[140,141,158]

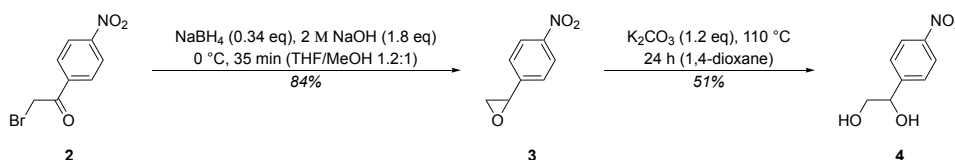


Scheme 8: Synthesis of the bromomethyl ketone probe **BMK** starting from 5-hexynoic acid (**1**) according to a modified procedure of *Abo* and coworkers,^[140,141] followed by a *Finkelstein*-reaction analogously to a patent procedure with an overall yield of 43%.^[158]

In the first step of this procedure, 5-hexynoic acid (**1**) was reacted with oxalyl chloride to form the corresponding acid chloride that immediately after evaporation of excess oxalyl chloride was converted to the diazomethyl ketone intermediate through nucleophilic attack of (trimethylsilyl)diazomethane. The nearly complete removal of excess oxalyl chloride was crucial for the success of the whole synthesis since (trimethylsilyl)diazomethane most likely was quenched by the excess reagent in initially failed syntheses. The intermediate was further reacted with hydrobromic acid to form the desired bromomethyl ketone **BMK**.^[140,141] After flash column purification and the isolation of one single spot, the ¹H-NMR indicated the presence of an additional compound that could not be separated from **BMK** by different solvent combinations for flash column chromatography or high performance liquid chromatography (HPLC). After extensive investigations, we were able to identify the second compound as the corresponding chloromethyl ketone. We hypothesized that this side product could be formed through a direct nucleophilic attack of chloride-anions, that were generated after the reaction of (trimethylsilyl)diazomethane with the acid chloride intermediate, at the diazomethyl ketone. Alternatively, a halogen exchange reaction of bromide to chloride in the final product occurred through the excess chloride-anions present in the solution. Consequently, the mixture of chloro-substituted analog and **BMK** was reacted in a *Finkelstein*-reaction with

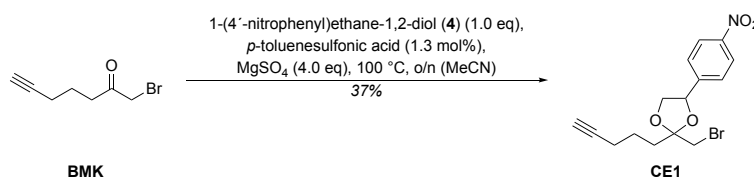
sodium bromide until complete conversion was indicated by $^1\text{H-NMR}$.^[158] In this way, we were able to synthesize **BMK** with high purity in an overall yield of 43%.

Next, we wanted to synthesize a caging group to generate the first caged derivative of **BMK**. For this first-generation of caged electrophile, we chose a *para*-nitrophenyl caging group since it is the most widely used motif in literature and since it uses a homologous structure to the light-activatable approach.^[93,94,96,123,133,140,141] Therefore, we started from 2-bromo-acetophenone (**2**) and converted it to the respective epoxide **3** with a yield of 84% through a reduction of the ketone functionality with sodium borohydride and an internal cyclization reaction *via* a nucleophilic attack of the deprotonated hydroxy-group with bromide as a leaving group (Scheme 9).^[159]



Scheme 9: Reduction of 2-bromo-acetophenone (**2**) with sodium borohydride, followed by intramolecular nucleophilic substitution yields epoxide **3** in a yield of 84%,^[159] which was further opened with aqueous potassium carbonate to obtain the caging group **4** with 51% yield.^[160]

The epoxide **3** was further opened through the reaction with aqueous potassium carbonate under reflux according to a published procedure and converted to the caging group **4** in a yield of 51% (Scheme 9).^[160] Finally, the first-generation caged electrophile **CE1** could be synthesized as a mixture of diastereoisomers according to a published procedure through the acid-catalyzed acetalization of **BMK** with the caging group **4** in a yield of 37% (Scheme 10).^[141]



Scheme 10: Acetalization reaction of **BMK** with caging group **4** under acid-catalysis to generate the first-generation caged electrophile **CE1** as a mixture of diastereomers in a yield of 37%.^[141]

The obtained yield was lower compared to the literature value of similar compounds.^[141] It was believed that this was due to an insufficient removal of water generated during the acetalization reaction. In this procedure, magnesium sulfate was added to remove the water, but evidently this could not be achieved in sufficient quantity.^[141] Nevertheless, the first-generation caged electrophile **CE1** could be successfully synthesized to enable proof-of-concept studies.

3.2 Proof-of-concept studies

Next, we wanted to verify the general feasibility of the concept of caged electrophiles by comparing the labelling intensities of the free electrophile **BMK** with the labelling properties of the caged electrophile **CE1** in a gel-based ABPP experiment. In this experiment, the labelling properties of **BMK** represented the positive control and the reference for the caged electrophile **CE1**, as the complete activation of **CE1** by bacterial nitroreductases should lead to the quantitative liberation of **BMK** and therefore to the same labelling pattern and intensity. We chose the *E. coli* nitroreductase NfsB for our first studies, because it is one of the most widely used and well-studied bacterial nitroreductase for similar concepts with a specific activation of prodrugs.^[124–130] NfsB was cloned from *E. coli* BW25113^[161] with a *N*-terminal 6×histidine (His)-tag and recombinantly expressed and purified utilizing standard techniques from a previous literature report from our group^[75] and identical with the same plasmid and expression strain constructs that were already generated during my Master's thesis.^[162]

For the proof-of-concept studies, according to a protocol established in my Master's thesis^[162] we preincubated either **BMK** or **CE1** in a concentration of 20 μM together with different combinations of the *E. coli* nitroreductase NfsB (25.3 μM) and NADH (1 mM) as a cofactor^[101,111–114] in 50 mM phosphate buffer in a total volume of 100 μL . The addition of dimethyl sulfoxide (DMSO) instead of probe was used as a solvent control experiment to assess the background labelling. After the preincubation for one hour at room temperature, 100 μL *S. aureus* SH1000^[163] lysate (1 mg/mL) were added and incubated with the reaction mixture for another hour at room temperature to lead to a proteome-wide labelling with **BMK** and uncaged **CE1**. The resulting final concentrations in this experiment after addition of bacterial lysate were, therefore, 10 μM **BMK** or **CE1** together with 12.6 μM NfsB and 500 μM NADH. Subsequently, the probe-labelled proteins were clicked to the fluorescent dye 5-carboxytetramethylrhodamine-azide (TAMRA-azide) using CuAAC,^[60–63] separated by SDS-PAGE and finally visualized by in-gel fluorescence scanning (Figure 3). Additionally, a Coomassie staining of the gel was performed to determine the protein concentration in the individual lanes to verify the equal sample loading in all gel lanes, which is shown for a representative cut-out below the fluorescence gel (Figure 3).

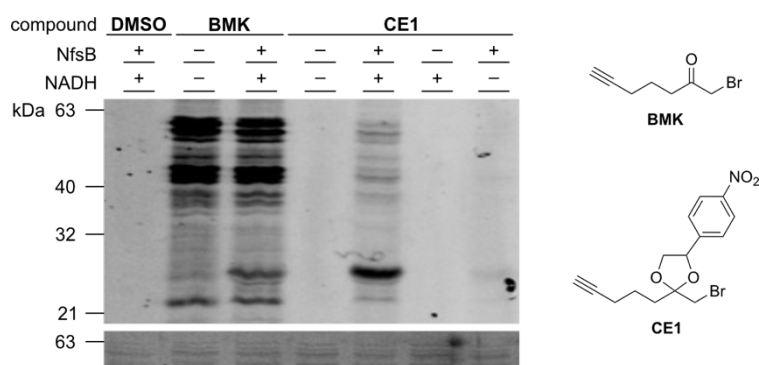


Figure 3: Gel-based labelling experiment for proof-of-concept studies for the caged electrophiles. Free electrophile **BMK** and caged electrophile **CE1** (final concentration of 10 μM) were preincubated with different combinations of *E. coli* nitroreductase NfsB (final concentration of 12.6 μM) and NADH (final concentration of 500 μM) in 50 mM phosphate buffer. DMSO was added instead of probe in a control experiment. After preincubation for one hour at room temperature, *S. aureus* SH1000^[163] lysate (1 mg/mL) was added and incubated for another hour to lead to a proteome-wide labelling. The labelled proteins were further clicked by CuAAC^[60–63] to TAMRA-azide, separated by SDS-PAGE and visualized by in-gel fluorescence scanning. The following Coomassie staining verified equal protein concentrations in all gel lanes and is shown below the fluorescence gel.

Free electrophile **BMK** promiscuously labeled the whole proteome independently of nitroreductase NfsB and NADH addition. The additional very strong protein band at around 24 kDa, that is only observed in the presence of NfsB, most likely corresponded to the added NfsB itself. In accordance with our hypothesis, the caged electrophile **CE1** did show a very similar labelling pattern after preincubation with both, NfsB and NADH, but with overall lower intensity. In contrast, caged electrophile **CE1** did not show any visible labelling at all in the absence of both, NfsB and NADH, and in the absence of only NfsB. In the case of only NfsB addition, a slight labelling pattern could be detected probably due to residual NADH that was present in the bacterial lysate in a sufficient amount to lead to the activation of **CE1** with the added NfsB. Overall, this gel-based experiment verified that the caged electrophile **CE1** could get activated by NfsB to generate a reactive electrophile that showed labelling properties similar to free **BMK**. Additionally, it could be proven that the caged electrophile **CE1** did not have any visible proteome-reactivity without activation by bacterial nitroreductases. While we were able to verify that the activation of **CE1** by NfsB led to a proteomic labelling pattern similar to the free **BMK**, this experiment did not give direct evidence for the presence of **BMK**. Nevertheless, we were encouraged as this experiment generally demonstrated the feasibility of this modular approach of caged electrophiles that are specifically activatable by bacterial nitroreductases.

3.3 Optimization of labelling conditions

After the general verification of our concept of caged electrophiles, we set out to further improve and optimize the labelling conditions to further improve the labelling intensity of the caged electrophile **CE1**, since they were significantly weaker compared to **BMK** in the initial gel-based experiment (Figure 3). Therefore, we compared the activation properties of NfsB with the major *E. coli* nitroreductase NfsA, where we substituted NADH with NADPH, since NfsA is reported to only accept NADPH as electron donor.^[99–101,112] Additionally, we tested the influence of the addition of FMN on the overall labelling intensity because both nitroreductases NfsA and NfsB were described to use FMN as prosthetic group (Figure 4).^[99–101,111–114]

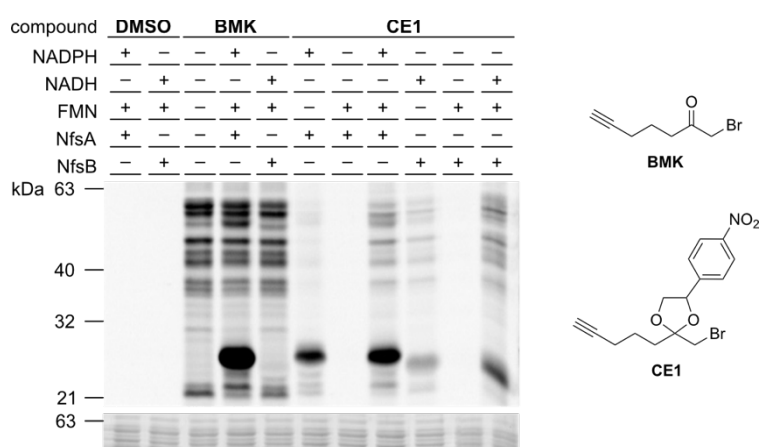


Figure 4: Gel-based labelling experiment for the optimization of labelling conditions of caged electrophiles. Free electrophile **BMK** and caged electrophile **CE1** (final concentration of 10 μM) were preincubated with different combinations of either *E. coli* nitroreductase NfsA (final concentration of 12.7 μM) or NfsB (final concentration of 12.6 μM) with FMN (final concentration of 12.5 μM) and NAD(P)H (final concentration of 500 μM) in 50 mM phosphate buffer. DMSO was added instead of probe in a control experiment. After preincubation for one hour at room temperature, *S. aureus* SH1000^[163] lysate (1 mg/mL) was added and incubated for another hour to lead to a proteome-wide labelling. The labelled proteins were further clicked by CuAAC^[60–63] to TAMRA-azide, separated by SDS-PAGE and visualized by in-gel fluorescence scanning. The following Coomassie staining verified equal protein concentrations in all gel lanes and is shown below the fluorescence gel.

Firstly, we could show that both *E. coli* nitroreductases NfsA and NfsB were able to activate caged electrophile **CE1** to lead to a proteome-wide labelling with a comparable pattern to free **BMK**. This finding was in accordance with literature reports demonstrating that both nitroreductases were responsible for the activation of nitrofurans and that bacteria needed to mutate both in consecutive steps in order to develop resistance.^[98,110–112] Since our caged electrophile **CE1** was also activated by both nitroreductases nearly equally, we assumed

and hypothesized that possible resistance development against this class of compounds also happens in multiple consecutive steps which is assumed to make resistance development overall slow.^[98,110–112] As expected, the addition of FMN further drastically increased the overall labelling intensity and the activation properties of **CE1**.

Nevertheless, we could still detect significant protein labelling at around 24 kDa that probably represented the labelling of the used nitroreductases NfsA or NfsB, respectively. This direct reaction of the electrophile with the activation enzyme pointed to the fact that during the preincubation period large amounts of electrophile were captured by the nitroreductase itself leading to a reduction in labelling of other proteins as well as to a probable inactivation of the enzyme. Consequently, we investigated the activation and labelling of **CE1** in a coincubation experiment, where **BMK** or **CE1** were added directly together with NfsA/NfsB, FMN and NAD(P)H in *S. aureus* SH1000^[163] lysate (Figure 5).

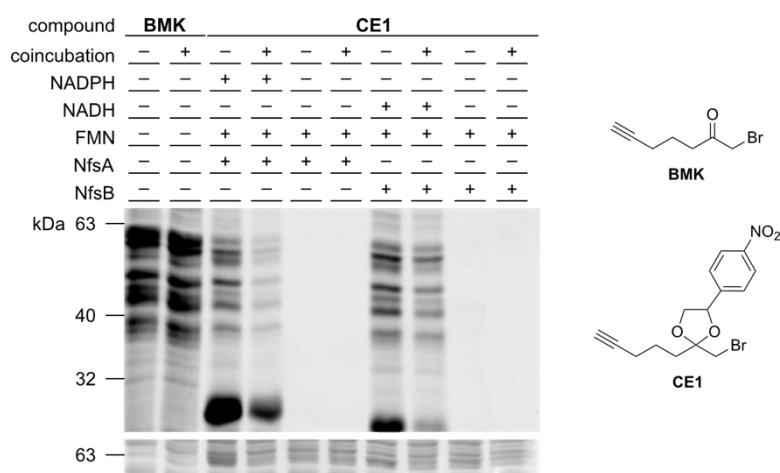


Figure 5: Gel-based labelling experiment for the optimization of labelling conditions of caged electrophiles. For preincubation experiments, free electrophile **BMK** and caged electrophile **CE1** (final concentration of 10 μM) were preincubated with different combinations of either *E. coli* nitroreductase NfsA (final concentration of 12.7 μM) or NfsB (final concentration of 12.6 μM) with FMN (final concentration of 12.5 μM) and NAD(P)H (final concentration of 500 μM) in 50 mM phosphate buffer. DMSO was added instead of probe in a control experiment. After preincubation for one hour at room temperature, *S. aureus* SH1000^[163] lysate (1 mg/mL) was added and incubated for another hour. Alternatively, for coincubation experiments **BMK** and **CE1** (final concentration of 10 μM) were incubated with different combinations of either NfsA (final concentration of 12.7 μM) or NfsB (final concentration of 12.6 μM) with FMN (final concentration of 12.5 μM) and NAD(P)H (final concentration of 500 μM) in *S. aureus* SH1000^[163] lysate (1 mg/mL) in a total volume of 200 μL phosphate-buffered saline (PBS) for one hour at room temperature. For both experiments, the labelled proteins were further clicked by CuAAC^[60–63] to TAMRA-azide, separated by SDS-PAGE and visualized by in-gel fluorescence scanning. The following Coomassie staining verified equal protein concentrations in all gel lanes and is shown below the fluorescence gel.

In the case of the coincubation experiment, we exchanged the 50 mM phosphate buffer with phosphate-buffered saline (PBS), since the activation directly occurred within the bacterial lysate that was prepared in PBS. In order to directly compare the labelling intensities of the coincubation with the preincubation experiment, the coincubation was performed in a total volume of 200 μL by dilution with PBS to obtain the same volume and concentrations of all reagents as in the preincubation setup. As we hypothesized, the labelling of the used nitroreductases significantly decreased in coincubation experiments, especially in the case of NfsB activation. Unfortunately, the overall labelling intensity also slightly decreased compared to the preincubation experiment, but not to the same extent as the labelling of the individual nitroreductases. Nevertheless, we could show that **CE1** was also activated in the presence of the whole proteome as background and since these coincubation conditions represented more closely the realistic conditions in living bacteria, we decided to further continue with the coincubation setup.

Finally, we wanted to assess the influence of the temperature on the activation properties of the caged electrophile **CE1**. Therefore, we performed the identical experiment under coincubation conditions at either room temperature (25 $^{\circ}\text{C}$) or at 37 $^{\circ}\text{C}$, since we assumed that nitroreductases have increased activity at this elevated temperature (Figure 6).

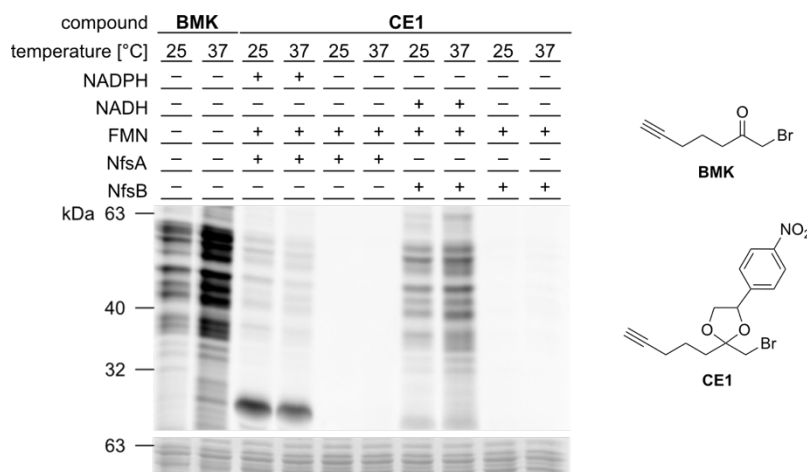
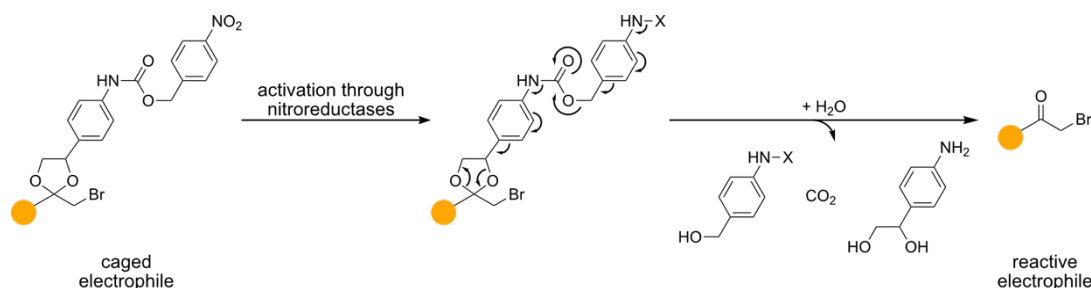


Figure 6: Gel-based labelling experiment for the optimization of labelling conditions of caged electrophiles. Free **BMK** and caged electrophile **CE1** (final concentration of 20 μM) were incubated with different combinations of either NfsA (final concentration of 25.5 μM) or NfsB (final concentration of 25.3 μM) with FMN (final concentration of 25 μM) and NAD(P)H (final concentration of 1 mM) in *S. aureus* SH1000^[163] lysate (1 mg/mL) in a total volume of 100 μL phosphate-buffered saline (PBS) for one hour at either room temperature (25 $^{\circ}\text{C}$) or at 37 $^{\circ}\text{C}$. DMSO was added instead of probe in a control experiment. The labelled proteins were further clicked by CuAAC^[60-63] to TAMRA-azide, separated by SDS-PAGE and visualized by in-gel fluorescence scanning. The following Coomassie staining verified equal protein concentrations in all gel lanes and is shown below the fluorescence gel.

It has to be mentioned that starting from this experiment, the final concentrations of all reagents were doubled compared to the previous experiments, but the ratio of reagents to bacterial lysate remained unchanged due to the fact that the additional dilution to make preincubation and coincubation directly comparable was not necessary anymore. It could be seen that at 37 °C the labelling intensity of **CE1** increased in the case of NfsB, whereas for NfsA the labelling was nearly unchanged or potentially even decreased to some degree. However, NfsB led to stronger labelling in this experiment in accordance with all previous experiments. Therefore, we focused on the activation with NfsB in all further experiments and chose 37 °C as reaction temperature. Summarizing, through different optimization studies we identified the activation of **CE1** to be most efficient in a coincubation setup with the use of NfsB as activation enzyme in the presence of NADH and FMN at 37 °C.

3.4 Design and synthesis of second-generation caged electrophiles

Even after the optimization of the labelling conditions, we still could detect significantly weaker labelling of **CE1** compared to free **BMK** that indicated only partial activation and uncaging of **CE1** by the bacterial nitroreductases. A previous literature report that investigated different caging groups for nitroreductase-based activation of prodrugs identified thiophene-, furane- and imidazole-based analogs of the *para*-nitrophenyl caging group that showed drastically increased activation properties.^[133] Additionally, we adapted the concept of so-called self-immolative linkers to our concept of caged electrophiles utilizing caging groups with a carbamate functionality.^[164,165] Upon activation through bacterial nitroreductases, a cascade of elimination processes can occur to liberate the reactive electrophile and three additional reaction products (Scheme 11).^[93,94,96,120,123,140,141,164,165]

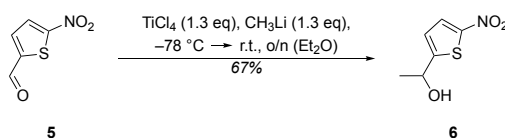


Scheme 11: Overview of the modular concept of caged electrophiles with self-immolative linkers and proposed mechanism for the activation through nitroreductases. The nitro-group gets reduced by bacterial nitroreductases to the corresponding hydroxylamine- ($X = OH$) or amine- ($X = H$) group, which increases the electron density and leads to a cascade of elimination processes that liberate the highly reactive electrophile.^[93,94,96,120,123,140,141,164,165]

The use of this longer self-immolative linker system is described to shorten the distance between the catalytically active center and the nitro-group and, thereby, to improve the activation kinetics.^[164] Additionally, the activation and the resulting fragmentation are entropically favored since three compounds are released in addition to the reactive electrophile, especially carbon dioxide that can evolve from the reaction.^[165] Therefore, we started to synthesize the respective caging groups and the corresponding caged electrophiles.

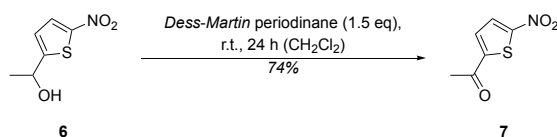
3.4.1 Synthesis of improved caging groups

Generally, we wanted to use a similar synthetic strategy as for the *para*-nitrophenyl group **4** and, therefore, aimed to synthesize the corresponding bromomethyl ketone intermediates. For the thiophene-based group, aldehyde **5** was methylated to the corresponding secondary alcohol **6** using methyllithium and titanium(IV) chloride according to a published procedure (Scheme 12).^[166]



Scheme 12: Methylation of aldehyde **5** with methyllithium and titanium(IV) chloride according to a published procedure to generate the secondary alcohol **6** with a yield of 67%.^[166]

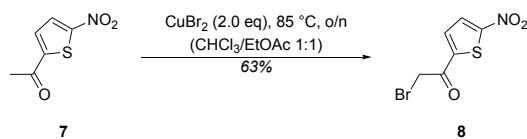
This synthesis could be successfully completed, and the reaction product **6** was obtained after flash column chromatography in high purity with a yield of 67%. The yield was lower compared to the literature report^[166] maybe due to insufficiently anhydrous reaction conditions, but in an acceptable range to continue with the further reactions. The generated alcohol **6** was directly re-oxidized with *Dess-Martin* periodinane to the respective ketone **7** described in the same literature report (Scheme 13).^[166]



Scheme 13: Oxidation of alcohol **6** with *Dess-Martin* periodinane to the ketone **7** according to a literature report with a yield of 74%.^[166]

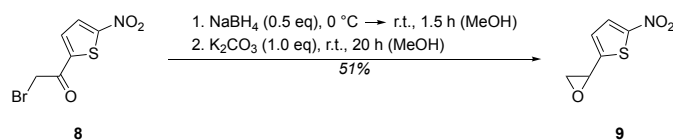
After flash chromatography, again a highly pure product could be obtained in a yield of 74%, which was also lower compared to literature.^[166] This decreased yield could probably be attributed to the partial decomposition of *Dess-Martin* periodinane, but again was in an acceptable range. The respective bromomethyl ketone **8** could then be synthesized analogously

to a literature procedure through the reaction of methyl ketone **7** with copper(II) bromide under reflux (Scheme 14).^[167]



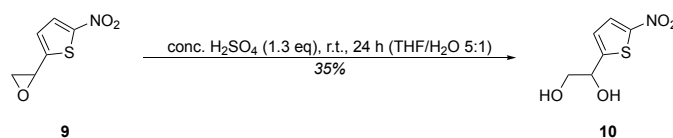
Scheme 14: Bromination of methyl ketone **7** to the bromomethyl ketone **8** using copper(II) bromide with a yield of 63% analogously to a published procedure.^[167]

In this reaction, a double brominated derivative was also generated that could be separated by flash chromatography but reduced the obtained yield to moderate 63%. Similar to the synthesis of the *para*-nitrophenyl caging group **4**, the bromomethyl ketone **8** was converted to the epoxide **9** using a similar literature procedure (Scheme 15).^[168]



Scheme 15: Reduction of bromomethyl ketone **8** with sodium borohydride, followed by the intramolecular nucleophilic substitution and cyclization after addition of potassium carbonate yielded the epoxide **9** in a yield of 51%.^[168]

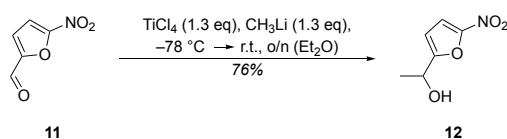
After the reduction of the ketone functionality with sodium borohydride to the corresponding secondary alcohol, the addition of potassium carbonate led to the intramolecular cyclization reaction to generate epoxide **9** with a total yield of 51%.^[168] In the final step of the synthesis, epoxide **9** was opened to give the thiophene-based caging group **10** (Scheme 16).^[168]



Scheme 16: Epoxide **9** was opened by the addition of sulfuric acid to the corresponding 1,2-diol and thiophene-based caging group **10** in a yield of 35%.^[168]

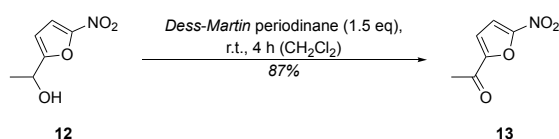
Using the identical experimental procedure^[160] as for the *para*-nitrophenyl group **4** was not successful, therefore another synthetic strategy described in literature was used, where the epoxide **9** was hydrolyzed and opened to the corresponding 1,2-diol **10** through the addition of sulfuric acid with a yield of 35%.^[168] Unfortunately, this yield was relatively low, but indeed a significant improvement compared to other procedures where we could only identify traces of the desired product. Overall, the thiophene-based caging group **10** could be successfully synthesized over five steps with a total yield of 6%.

The furane-based caging group was then synthesized using the identical synthetic strategy, starting with the methylation of the furane-based aldehyde **11** to the secondary alcohol **12** according to the already described literature procedure (Scheme 17).^[166]



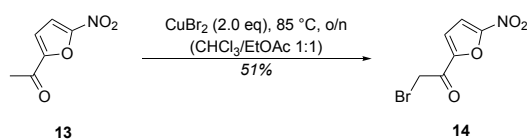
Scheme 17: Methylation of aldehyde **11** with methyllithium and titanium(IV) chloride according to a published procedure to generate the secondary alcohol **12** with a yield of 76%.^[166]

After flash chromatography, the methylated secondary alcohol **12** could be obtained with high purity in a yield of 76%. The yield for this furane-based intermediate **12** was higher than for the corresponding thiophene-derivative **6** and nearly identical to the literature value of 81%.^[166] The small difference in yield was probably again due to the sensitivity of the reaction towards water, which resulted in decreasing yield if no completely dry reaction conditions were achieved. Nevertheless, the obtained yield was overall sufficient, and it was continued with the oxidation to the ketone **13** using *Dess-Martin* periodinane according to the literature procedure (Scheme 18).^[166]



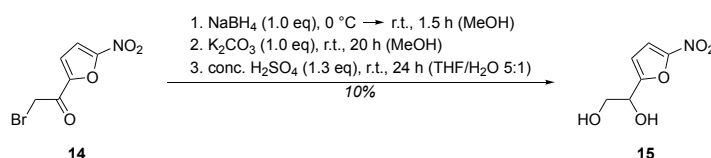
Scheme 18: Oxidation of alcohol **12** with *Dess-Martin* periodinane to the ketone **13** according to a literature report with a yield of 87%.^[166]

We could also observe the same trend in the yield for this reaction, where the obtained 87% after flash chromatography exceeded the 74% yield of the thiophene-analog **7**. In this case, we also outperformed the literature report^[166] and, generally, the synthetic route for the furane-analogs seemed to work more efficiently compared with the thiophene-derivatives. However, this was not true for the α -bromination of the methyl ketone **13** to the bromomethyl ketone **14** with copper(II) bromide that was performed using an adapted literature procedure (Scheme 19).^[167]



Scheme 19: Bromination of methyl ketone **13** to the bromomethyl ketone **14** using copper(II) bromide with a yield of 51% analogously to a published procedure.^[167]

The obtained yield of 51% was significantly lower compared to the thiophene-based bromomethyl ketone **8**. This could be attributed to a complex separation problem with flash chromatography since the product **14** and the respective double brominated side-product nearly matched in retention time on the column. Despite performing the flash chromatography carefully, a mixed fraction of product **14** and side-product was obtained, which was discarded. Nevertheless, the obtained yield of 51% was still acceptable, and the overall purity of the product **14** was very high. Surprisingly, the following epoxide formation was unsuccessful in many tries, even though we used the same experimental procedure that we adapted from literature.^[168] After thorough troubleshooting, we concluded that the epoxide intermediate initially identified by mass spectrometry (MS) was formed during the reaction but could not be isolated. This hinted towards a probable decomposition on the silica column rather than to problems with the synthesis itself. Therefore, we again generated the epoxide derivative with the same literature procedure,^[168] where bromomethyl ketone **14** was reduced to the corresponding alcohol with sodium borohydride, followed by the intramolecular substitution reaction after potassium carbonate addition (Scheme 20). After aqueous work-up and removal of the solvent, we consequently did not perform any purification procedure. However, we directly subjected the formed intermediate to hydrolysis with sulfuric acid according to the same literature report^[168] to successfully obtain the furane-based caging group **15** with a yield of 10% over these two steps (Scheme 20).



Scheme 20: Reduction of bromomethyl ketone **14** with sodium borohydride, followed by the intramolecular nucleophilic substitution and cyclization after addition of potassium carbonate yielded an epoxide intermediate. The crude reaction product was opened by the addition of sulfuric acid to the corresponding 1,2-diol and furane-based caging group **15** in a yield of 10% over two steps.^[168]

The corresponding synthesis of the thiophene-based caging group **10** achieved a total yield of 18% over these two steps, which was significantly higher than for the furane-analog **15**. This was indeed not surprising, since we were not able to isolate and purify the epoxide intermediate in this reaction, but we were successful for the thiophene-based epoxide **9**. Consequently, the decreased yield could probably be attributed to the use of a crude reaction product, where other formed side-products maybe interfered with the final hydrolysis of the epoxide. Since it was the last step in this synthesis of the caging group **15** and we obtained a sufficient amount, this low yield was acceptable. Overall, we could successfully synthesize also the furane-based

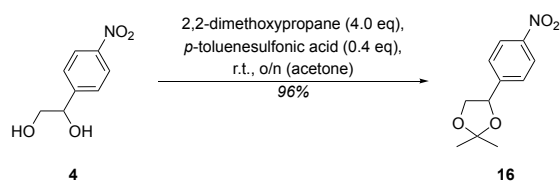
caging group **15** with a total yield of 3% over four steps which was significantly lower compared to the thiophene-analog **10**, mostly due to the poor yield of the last transformation.

In contrast to the aforementioned synthetic routes to the thiophene-based **10** and furane-based **15** caging group, the synthesis of the corresponding imidazole-analog was more complex and included multiple steps. Unfortunately, the α -bromination of the respective methyl ketone intermediate could not be successfully completed, even though many different experimental procedures were used for this transformation. Additionally, further different routes towards this caging group were tried, but none of them led to success. Consequently, we could not synthesize the imidazole-based caging group, but we continued with the already synthesized groups **10** and **15** together with the self-immolative caging groups (*vide infra*). The synthetic steps until the α -bromination for the imidazole-based caging group will not be discussed here, as they were also part of the synthesis towards the imidazole-based caging group with a self-immolative linker, which is discussed in the following part of this thesis.

3.4.2 Synthesis of caging groups with self-immolative linkers

For the synthesis of the caging groups with self-immolative linker systems (Scheme 11),^[164,165] we first synthesized a common linker motif with a 1,2-diol functionality to enable the acetal formation. On the other side, this linker motif could be modified *via* a carbamate formation with the different activation elements of the caging groups to generate a *para*-nitrophenyl-, thiophene-, furane- and imidazole-based group with self-immolative linker.

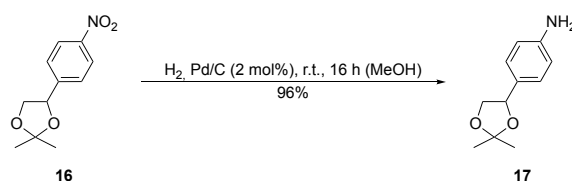
We chose to generate a common linker based on the *para*-nitrophenyl caging group **4**, where we first needed to protect the 1,2-diol functionality to enable the further transformations. For this purpose, we protected 1,2-diol **4** as an acetonide **16** through the acetal formation with 2,2-dimethoxypropane under acid-catalysis according to a published patent procedure (Scheme 21).^[169]



Scheme 21: Protection of the 1,2-diol **4** as an acetonide **16** in a yield of 96% through acetalization with 2,2-dimethoxypropane under acid-catalysis.^[169]

After flash chromatography, we could successfully obtain the protected acetonide **16** with high purity in an excellent yield of 96%, which largely exceeded the literature value.^[169] To finally

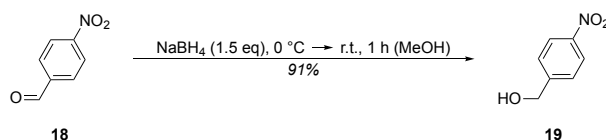
enable the carbamate formation, the nitro-group was reduced according to the same patent procedure through hydrogenation in presence of palladium on carbon to generate the amine **17** (Scheme 22).^[169]



Scheme 22: Hydrogenation in presence of palladium on carbon to convert the nitro-group **16** into the amine **17** in a yield of 96% following a patent procedure.^[169]

The common linker motif **17** could be obtained with very high purity directly after filtration, and no further purification was necessary. Despite achieving a slightly lower yield than the patent procedure,^[169] the obtained 96% were very high with only minimal loss probably during the filtration process.

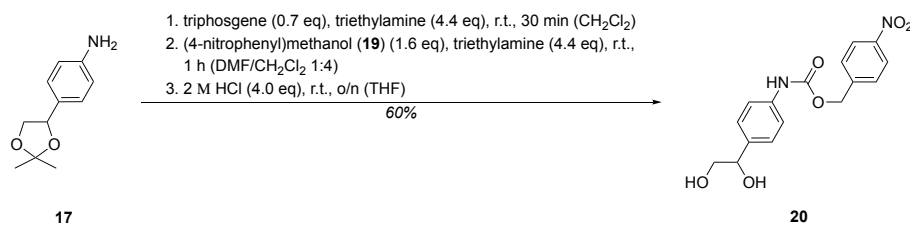
After the successful synthesis of the common linker motif **17**, we set out to generate the respective activation elements as corresponding primary alcohols to enable a carbamate formation. We started with the reduction of commercially available *para*-nitrophenyl aldehyde **18** with sodium borohydride to the primary alcohol **19** (Scheme 23).^[170]



Scheme 23: Reduction of the *para*-nitrophenyl aldehyde **18** with sodium borohydride to the primary alcohol **19** in a yield of 91%.^[170]

The product **19** could be obtained in very high purity with an excellent yield of 91%, that was just slightly lower than the literature value.^[170]

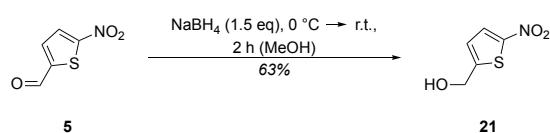
The following carbamate formation together with the common linker motif **17** was conducted according to an adapted and modified literature procedure.^[171] Therefore, the amine **17** was reacted with triphosgene in the presence of triethylamine, followed by the addition of alcohol **19** which was already pretreated with triethylamine (Scheme 24).^[171]



Scheme 24: The common linker motif **17** was reacted with triphosgene in the presence of triethylamine, followed by the addition of *para*-nitrophenyl alcohol **19** that was pretreated with also triethylamine to form a carbamate functionality. After the reaction was quenched by the addition of diluted hydrochloric acid, stirring was continued to deprotect the acetonide, which finally resulted in the formation of the *para*-nitrophenyl-based caging group with a self-immolative linker **20** in a yield of 60%.^[171]

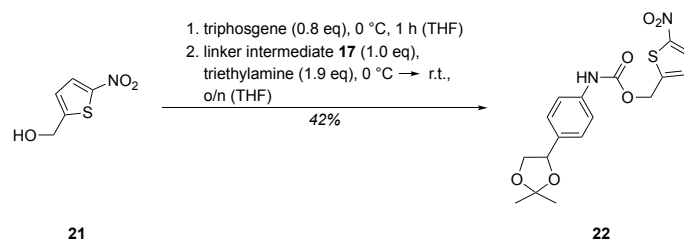
The reaction progress of amine **17** together with triphosgene alone and the final carbamate formation with alcohol **19** could be monitored by MS. After the starting materials were completely consumed, the reaction was quenched by the addition of diluted hydrochloric acid. We chose to end the reaction with acidic conditions since we were then able to continue stirring in the same reaction vessel under these acidic conditions in order to cleave the acetonide to generate the final 1,2-diol containing *para*-nitrophenyl-based caging group with self-immolative linker system **20** in an overall satisfying yield of 60%.

Next, we used thiophene aldehyde **5** as precursor for the synthesis of the thiophene-based caging group with a self-immolative linker. We reduced it with sodium borohydride according to a literature procedure to the corresponding alcohol **21** (Scheme 25).^[166]



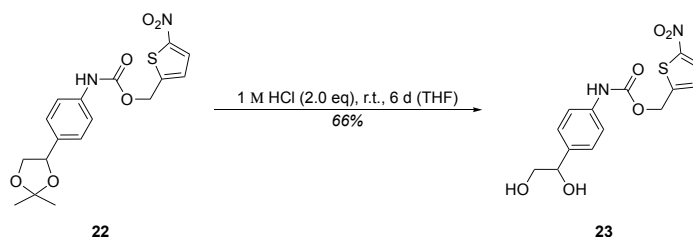
Scheme 25: Reduction of the thiophene aldehyde **5** with sodium borohydride to the primary alcohol **21** in a yield of 63%.^[166]

Unfortunately, the obtained yield was significantly lower compared to the literature^[166] but still sufficient to proceed the synthesis without the need of reaction optimization. For the subsequent carbamate formation, we chose and adapted a different literature procedure in order to evaluate, if a change in the reaction sequence and the isolation of the carbamate that is still protected as acetonide prior to the deprotection leads to an improved yield.^[172] Therefore, alcohol **21** was reacted with triphosgene first, followed by the addition of linker intermediate **17**, which was pretreated with triethylamine, and subsequent isolation and purification of the acetonide-protected carbamate intermediate **22** (Scheme 26).^[172]



Scheme 26: The alcohol **21** was first reacted with triphosgene, followed by the addition of linker intermediate **17** that was pretreated with triethylamine to form the acetonide-protected carbamate derivative **22** with a yield of 42%.^[172]

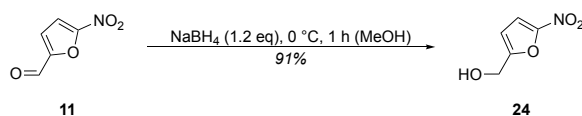
The acetonide-protected derivative **22** could be successfully synthesized and isolated after flash chromatography in a moderate yield of 42%. Subsequently, this intermediate **22** was subjected to diluted hydrochloric acid to hydrolyze the acetonide and form the respective thiophene-based caging group with self-immolative linker **23** (Scheme 27).



Scheme 27: Hydrolysis of acetonide-protected intermediate **22** through the addition of diluted hydrochloric acid generated the thiophene-based caging group with a self-immolative linker **23** in a yield of 66%.

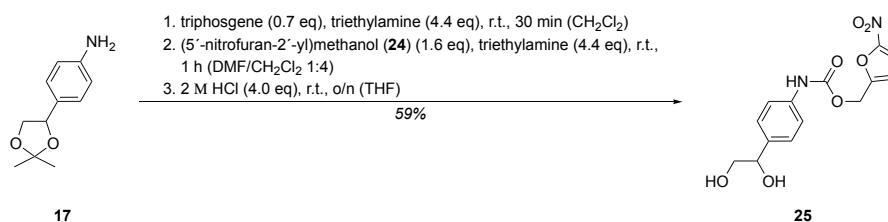
We could isolate the desired caging group **23** in very high purity in a yield of 66% after flash chromatography. Therefore, we could verify the feasibility of this different synthetic approach to generate the carbamate-containing caging groups. However, the overall yield of the carbamate formation followed by the acetonide deprotection, in this case, was lower compared to the aforementioned procedure. Since these procedures were tested on different chemical scaffolds, no direct comparisons can be made, but due to the more rapid and easier synthetic procedure, we decided to use the experimental procedure of the *para*-nitrophenyl derivative **20** also for the following carbamate-containing caging groups.

Next, we continued with the synthesis of the furane-based alcohol **24** through the reduction of the corresponding aldehyde **11** with sodium borohydride (Scheme 28).^[166]



Scheme 28: Reduction of the furane aldehyde **11** with sodium borohydride to the primary alcohol **24** in a yield of 91%.^[166]

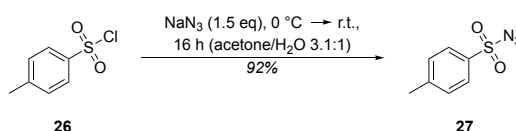
In contrast to the reduction to the thiophene alcohol **21**, we decreased the amount of added sodium borohydride since we hypothesized that the excess reagent was responsible for the relatively moderate yield. Indeed we were able to increase the yield in this synthesis drastically to 91%, which also exceeded the reported value in literature.^[166] Utilizing the general synthetic strategy, we first reacted the common linker motif **17** with triphosgene and triethylamine, followed by the addition of alcohol **24** that was pretreated with triethylamine (Scheme 29).^[171]



Scheme 29: The common linker motif **17** was reacted with triphosgene in the presence of triethylamine, followed by the addition of furane alcohol **24** that was pretreated with also triethylamine to form a carbamate functionality. After the reaction was quenched by the addition of diluted hydrochloric acid, stirring was continued to deprotect the acetone, which finally resulted in the formation of the furane-based caging group with a self-immolative linker **25** in a yield of 59%.^[171]

After the carbamate formation was completed as indicated by MS, we again quenched the reaction with diluted hydrochloric acid and continued stirring to obtain the furane-based caging group with a self-immolative linker **25** in a yield of 59% after flash chromatography. This obtained yield nearly completely matched the reaction towards the *para*-nitrophenyl derivative **20** and exceeded the yield of the thiophene-based caging group **23**, which verified our previous hypothesis that this synthetic procedure is more efficient for this transformation.

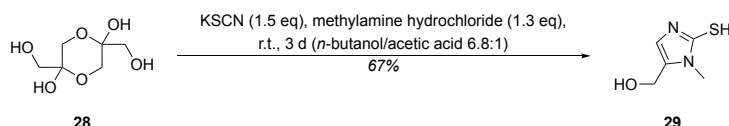
Next, we set out to conduct the synthesis of an imidazole-based caging group with a self-immolative linker, where unfortunately the synthesis of the aforementioned caging group without the linker failed. Through a pseudo-halogen exchange of sodium azide with tosyl chloride **26**, we first synthesized tosyl azide (TsN₃) **27** according to a literature procedure,^[173] since it was needed as a reagent within the following multi-step reaction sequence (Scheme 30).



Scheme 30: Nucleophilic substitution of sodium azide with tosyl chloride **26** to generate tosyl azide **27** in a yield of 92%.^[173]

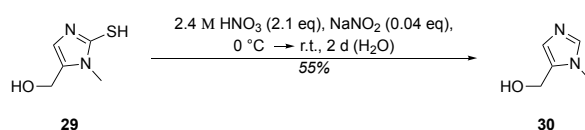
Tosyl azide **27** could be obtained in very high purity without the need of any purification and in an excellent yield of 92%. It has to be mentioned that there was some residual solvent present

in the final product, but due to the potential explosive properties of tosyl azide **27**, we did not further decrease the pressure or increase the temperature to completely remove the solvent. Additionally, the low amount of residual solvent was not believed to negatively influence the reaction, in which it was used as a reagent. Starting with the synthesis of the imidazole-based caging group itself, we build up the imidazole scaffold through a *Marckwald* cyclization of dihydroxyacetone dimer **28** with potassium thiocyanate and methylamine hydrochloride to obtain imidazole derivative **29** (Scheme 31).^[174–176]



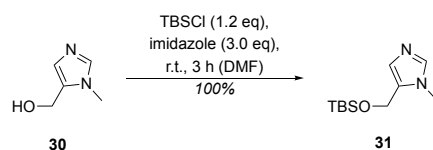
Scheme 31: *Marckwald* cyclization of dihydroxyacetone dimer **28** with potassium thiocyanate and methylamine hydrochloride to form the imidazole scaffold **29** in a yield of 67%.^[174–176]

The product **29** precipitated during this reaction and could be isolated by filtration without the need of any further purification in a yield of 67%, which nearly matched the literature report.^[176] In the next step of the synthesis, the thiol-group of **29** was removed through a desulfurization reaction with sodium nitrite and nitric acid to generate **30** (Scheme 32).^[176]



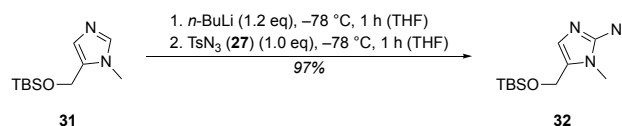
Scheme 32: Desulfurization reaction of the thiol **29** with sodium nitrite and nitric acid to generate imidazole intermediate **30** in a yield of 55%.^[176]

This transformation also did not require any further purification steps and intermediate **30** could be obtained in high purity with a yield of 55%, which was significantly lower compared to the literature value.^[176] Nevertheless, this reaction represented the highest yielding example of our attempts, and the loss of yield could probably be attributed to the complicated extraction of the product from the crude reaction mixture with hot chloroform. Since the obtained amount was sufficient for the following reactions, we continued with the protection of the hydroxy-group with *tert*-butyldimethylsilyl chloride (TBSCl) to form TBS-protected **31** (Scheme 33).^[177]



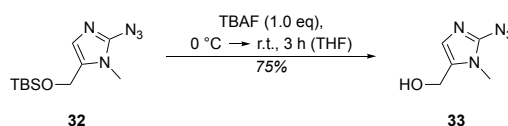
Scheme 33: Protection of alcohol **30** with *tert*-butyldimethylsilyl chloride to generate the TBS-protected imidazole analogue **31** with a yield of 100%.^[177]

Without any purification, the TBS-protected imidazole derivative **31** could be obtained in high purity with quantitative yield, that exceeded the literature value.^[177] The successful protection of the hydroxy-group enabled the generation of a carbon nucleophile after deprotonation with *n*-butyllithium (*n*-BuLi) that underwent a nucleophilic substitution reaction with the previously synthesized tosyl azide **27** to generate an azide-functionalized imidazole scaffold **32** (Scheme 34).^[178]



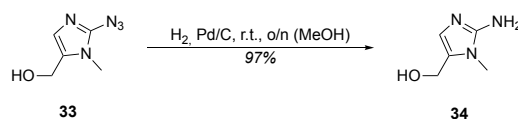
Scheme 34: Deprotonation of **31** with *n*-butyllithium generated a carbon nucleophile that subsequently was used in a nucleophilic substitution reaction with tosyl azide **27** to obtain azide **32** in a yield of 97%.^[178]

In this synthetic step, our obtained yield of 97% largely exceeded the literature value,^[178] and we could obtain the azide **32** in high purity. After completing the nucleophilic substitution reaction, we were able to deprotect the hydroxy-group again. For this purpose, we first tried the literature procedure by using hydrochloric acid, but unfortunately, this led to decomposition of the desired product.^[178] However, analogously to an unrelated literature procedure, we conducted the deprotection reaction with tetrabutylammonium fluoride (TBAF) to successfully obtain alcohol **33** with a yield of 75% (Scheme 35).^[179]



Scheme 35: Deprotection reaction of the TBS-protected hydroxy-group in **32** with tetrabutylammonium fluoride to obtain alcohol **33** in a yield of 75%.^[179]

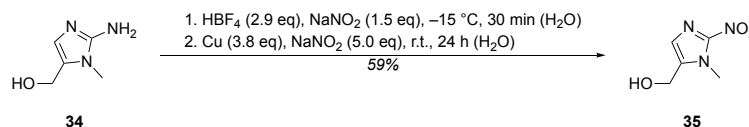
Through the hydrogenation with palladium on carbon as catalyst, we subsequently reduced the azide-functionality to an amine **34**, which was obtained in high purity after filtration without any further purification steps (Scheme 36).^[178]



Scheme 36: Hydrogenation with palladium on carbon catalysis to reduce the azide **33** to the amine **34** in a yield of 97%.^[178]

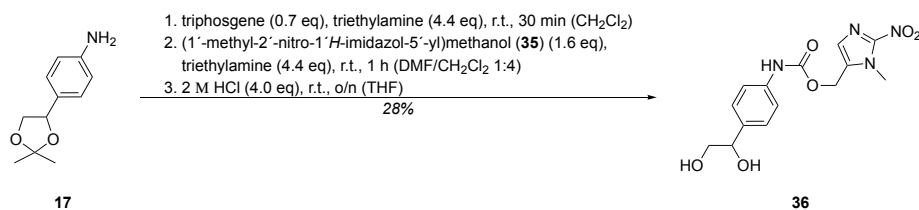
The achieved yield of 97% was excellent and was nearly identical to the literature.^[178] In the final reaction step of this synthetic route towards the imidazole-based alcohol **35**, we wanted to introduce the nitro-group into the structure. Therefore, analogously to a literature report, we

converted the amine-group into a diazonium tetrafluoroborate salt with sodium nitrite and tetrafluoroboric acid, followed by the reaction with additional sodium nitrite with copper powder as catalyst to successfully generate the final nitro-group containing imidazole derivative **35** (Scheme 37).^[178]



Scheme 37: Generation of a diazonium tetrafluoroborate salt through the reaction of amine **34** with sodium nitrite and tetrafluoroboric acid, followed by the reaction with sodium nitrite under catalysis with copper powder successfully formed the nitro-group containing imidazole derivative **35** with a yield of 59%.^[178]

Despite initial problems with this reaction due to the large amounts of evolving nitrogen and the insolubility of copper powder, which together led to excessive foam formation within the reaction flask, the final obtained yield of 59% was in accordance with the literature procedure.^[178] Having the alcohol **35** in hand, we were able to synthesize the imidazole-based caging group with a self-immolative linker **36** according to the previously described procedure (Scheme 38).^[171]



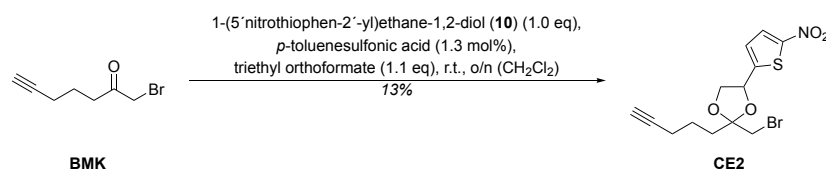
Scheme 38: The common linker motif **17** was reacted with triphosgene in the presence of triethylamine, followed by the addition of imidazole alcohol **35** that was pretreated with also triethylamine to form a carbamate functionality. After the reaction was quenched by the addition of diluted hydrochloric acid, stirring was continued to deprotect the acetonide, which finally resulted in the formation of the imidazole-based caging group with a self-immolative linker **36** in a yield of 28%.^[171]

After flash chromatography, the imidazole-based caging group with a self-immolative linker **36** could be obtained in high purity with a yield of 28%. This yield was lower compared to the previous carbamate formations potentially due to some interference of the imidazole scaffold with this reaction, but we could obtain the final product **36** in sufficient amounts and therefore no further reaction optimization was necessary at this point. Additionally, due to the high-yielding intermediate steps in the synthetic route, we could obtain the caging group **36** in a sufficient yield of 4% over eight steps.

Overall, we could successfully synthesize all planned caging groups with the self-immolative linker system, the *para*-nitrophenyl- **20**, thiophene- **23**, furane- **25** and imidazole-based **36** groups, and could continue with the synthesis of the corresponding caged electrophiles in the following part.

3.4.3 Synthesis of second-generation caged electrophiles

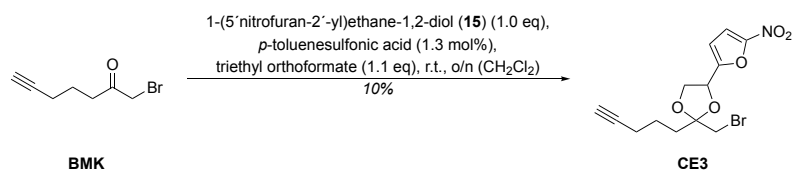
For the synthesis of the second-generation caged electrophiles, we again used our previously developed probe **BMK** to cage it as an acetal with the different newly synthesized caging groups. Unfortunately, the acetalization reaction with the thiophene-based caging group **10** using the same literature procedure^[141] as in the synthesis of **CE1** did not work, and we could not even detect traces of the desired caged electrophile. Again, we attributed this to insufficient removal of water that was generated during the reaction. During my Master's thesis^[162] we had similar issues and adapted another literature procedure^[180] to optimize the acetalization reaction. According to this protocol, we performed the acetalization reaction of **BMK** with the thiophene-based caging group **10** under acid-catalysis, where we additionally added triethyl orthoformate to remove the generated water (Scheme 39).^[180]



Scheme 39: Acetalization reaction of **BMK** with the caging group **10** under acid-catalysis and with the use of triethyl orthoformate for removal of the generated water to obtain the thiophene-based caged electrophile **CE2** as a mixture of diastereoisomers in a yield of 13%.^[180]

With this optimized synthetic procedure, we accomplished the synthesis of the thiophene-based caged electrophile **CE2** as a mixture of diastereoisomers in a yield of 13% and with high purity after HPLC purification. Unfortunately, the obtained yield was very low, which we again attributed to insufficient water removal. We hypothesized that this problem was further increased, since we performed this last step reaction from a multi-step procedure on a very small scale, where on the one hand the efficient removal of small amounts of water got more complicated and on the other hand small changes in the used amounts of reagents may have significantly influenced the outcome of the reaction. Nevertheless, we could not identify a higher yielding synthetic procedure, and more importantly, we could not successfully obtain caged electrophile **CE2** with high purity in sufficient amounts for the following biological evaluation.

Using the same synthetic strategy,^[180] we also performed the acetalization of **BMK** with the furane-based caging group **15** (Scheme 40).

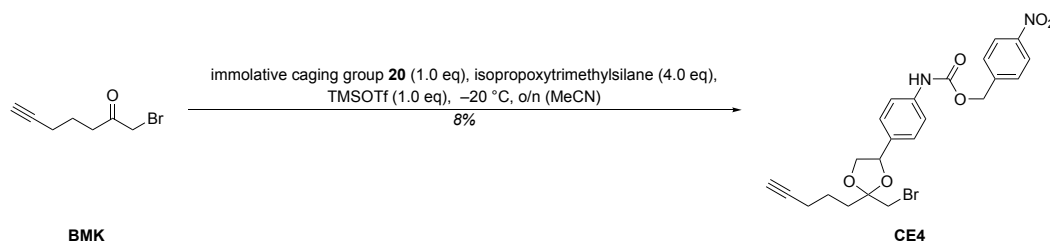


Scheme 40: Acetalization reaction of **BMK** with the caging group **15** under acid-catalysis and with the use of triethyl orthoformate for removal of the generated water to obtain the furane-based caged electrophile **CE3** as a mixture of diastereoisomers in a yield of 10%.^[180]

After HPLC purification, we could also successfully obtain furane-based caged electrophile **CE3** as a mixture of diastereoisomers in a yield of 10%. Similar to **CE2**, the obtained yield was again very low, but high enough to continue with the further experiments.

Unfortunately, the acetalization reaction towards the caged electrophiles with self-immolative linker systems did neither work with the procedure with magnesium sulfate for water removal^[141] nor with the newly adapted triethyl orthoformate procedure.^[180] We hypothesized that the carbamate functionality within the self-immolative caging groups might interfere with the acetal formation. Therefore, we searched the literature for alternative acetalization procedures that were also suitable for very small-scale reactions due to low amounts of available starting materials. We identified a procedure from *Tsunoda* and coworkers,^[181] where the acetalization was performed with ketones and silylated alcohols in the presence of catalytic amounts of trimethylsilyl trifluoromethanesulfonate (TMSOTf) as Lewis acid. The main driving force of this reaction was the formation of the very stable hexamethylsiloxane instead of water and therefore holds the potential to avoid our previously described problems with insufficient water removal.^[181] After synthesizing the TMS-protected derivative of *para*-nitrophenyl-based caging group with self-immolative linker **20**, we conducted the acetalization reaction with this new procedure.^[181] Unfortunately, this method also failed and we were not able to isolate the caged electrophile. However, in contrast to our previously used procedures, we could identify traces of the formed product in reaction controls by MS for the first time showing the general feasibility of this approach. Encouraged by this observation, we again searched the literature and found an optimized version of this synthetic approach by *Kurihara* and *Hakamata*.^[182] In this procedure, the TMS-protected alcohol was not necessary, but instead, the acetalization could be performed directly with the ketone, the unmodified alcohol, catalytic amounts of TMSOTf and the use of alkoxy silanes like isopropoxytrimethylsilane that function as a TMS-source. The authors could show that various

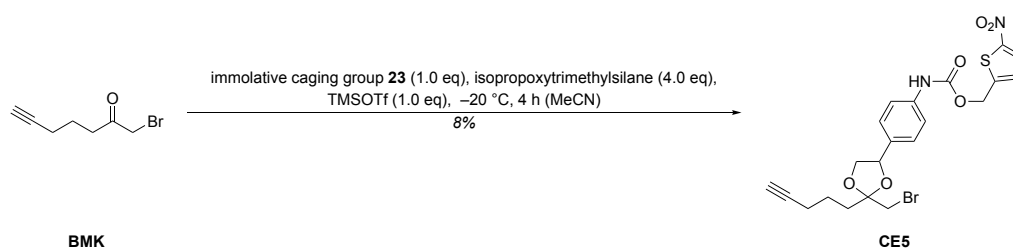
diols formed disilylated diols during the reaction in the presence of a TMS-source and catalytic amounts of TMSOTf.^[182] After thorough optimization of this procedure, we identified reaction conditions suitable for our approach, where we exchanged the used solvent from dichloromethane to acetonitrile due to solubility issues and we increased TMSOTf from catalytic to stoichiometric amounts. Applying these final conditions, we synthesized the *para*-nitrophenyl-based caged electrophile with a self-immolative linker **CE4** through the acetalization of **BMK** with caging group **20** (Scheme 41).^[182]



Scheme 41: Acetalization of **BMK** with caging group **20** with the use of TMS-source isopropoxytrimethylsilane and stoichiometric amounts of Lewis acid TMSOTf to obtain *para*-nitrophenyl-based caged electrophile with a self-immolative linker **CE4** as a mixture of diastereoisomers in a yield of 8%.^[182]

Strikingly, utilizing this optimized procedure,^[182] the caged electrophile **CE4** was successfully generated as a mixture of diastereoisomers with high purity. Indeed, the obtained yield was again very low, but comparable to the previous acetalization reactions and sufficient for further biological experiments.

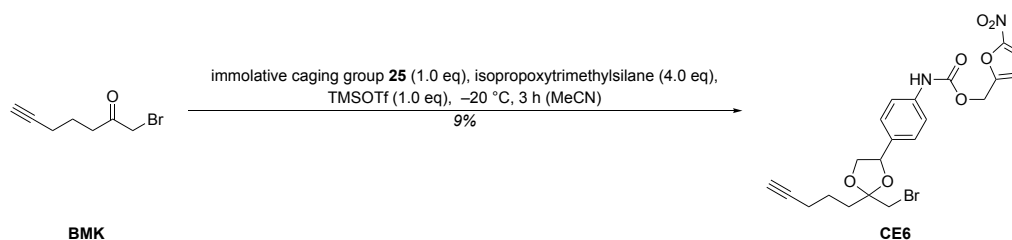
Utilizing the identical procedure, we also synthesized the respective thiophene-based caged electrophile with a self-immolative linker **CE5** (Scheme 42).^[182]



Scheme 42: Acetalization of **BMK** with caging group **23** with the use of TMS-source isopropoxytrimethylsilane and stoichiometric amounts of Lewis acid TMSOTf to obtain thiophene-based caged electrophile with a self-immolative linker **CE5** as a mixture of diastereoisomers in a yield of 8%.^[182]

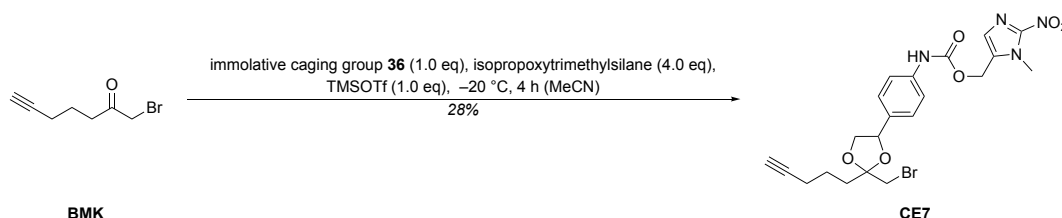
This synthesis could also be performed successfully to obtain caged electrophile **CE5** as a mixture of diastereoisomers in a yield of 8%, matching the outcome of the synthesis of **CE4** and also verifying the feasibility of this synthetic procedure for the acetalization reaction with the carbamate-containing caging groups.^[182]

Consequently, the furane-based caged electrophile with a self-immolative linker **CE6** was also synthesized as a mixture of diastereoisomers in a comparable yield of 9% (Scheme 43).^[182]



Scheme 43: Acetalization of **BMK** with caging group **25** with the use of TMS-source isopropoxytrimethylsilane and stoichiometric amounts of Lewis acid TMSOTf to obtain furane-based caged electrophile with a self-immolative linker **CE6** as a mixture of diastereoisomers in a yield of 9%.^[182]

Finally, we obtained the imidazole-based caged electrophile with a self-immolative linker **CE7** as mixture of diastereoisomers, but in this case in a significantly higher yield (Scheme 44).^[182]

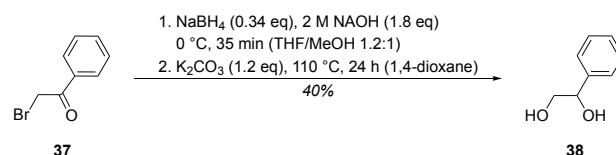


Scheme 44: Acetalization of **BMK** with caging group **36** with the use of TMS-source isopropoxytrimethylsilane and stoichiometric amounts of Lewis acid TMSOTf to obtain imidazole-based caged electrophile with a self-immolative linker **CE7** as a mixture of diastereoisomers in a yield of 28%.^[182]

Summarizing, we successfully synthesized six different second-generation caged electrophiles **CE2-CE7** as mixtures of diastereomers in very high purity.

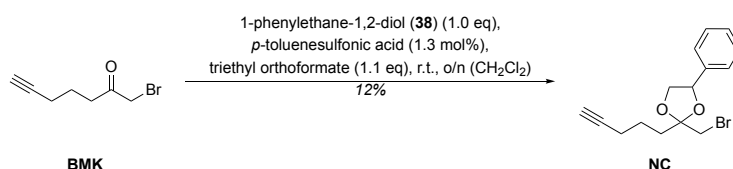
3.4.4 Synthesis of a negative control compound

Before we started with the biological evaluation of the newly obtained caged electrophiles **CE2-CE7**, we additionally wanted to synthesize an appropriate negative control compound for our subsequent studies. For this purpose, we decided already within my Master's thesis to use an unsubstituted phenyl caging group, where no nitro-group for reduction was present.^[162] According to the same synthetic strategy as for *para*-nitrophenyl-based caging group **4**, we reduced bromomethyl ketone **37** with sodium borohydride to the respective alcohol, followed by intramolecular nucleophilic substitution to generate an epoxide intermediate.^[159,162] Without further purification, we directly hydrolyzed to epoxide intermediate with potassium carbonate to open the epoxide and finally generated the phenyl-based caging group **38** in a yield of 40% over these two steps (Scheme 45).^[160,162]



Scheme 45: Reduction of bromomethyl ketone **37** with sodium borohydride, followed by intramolecular nucleophilic substitution reaction formed an intermediate epoxide,^[159,162] which was further hydrolyzed and opened with aqueous potassium carbonate to obtain phenyl-based caging group **38** in a yield of 40%.^[160,162]

As expected, we could obtain caging group **38** in comparable yields to the very similar *para*-nitrophenyl-based caging group **4**. Since there was no carbamate functionality present in the caging group **38**, we again used the previously developed acetalization procedure, where triethyl orthoformate was used for the removal of water, to synthesize the negative control **NC** as a mixture of diastereoisomers (Scheme 46).^[180]



Scheme 46: Acetalization reaction of **BMK** with the caging group **38** under acid-catalysis and with the use of triethyl orthoformate for removal of the generated water to obtain the negative control **NC** as a mixture of diastereoisomers in a yield of 12%.^[180]

Summarizing all synthetic efforts within this thesis chapter, we were able to synthesize a bromomethyl ketone probe **BMK**, seven different caged electrophiles **CE1-CE7** and a negative control **NC** that were all used for the development and optimization of our concept of caged electrophiles in the following part of this thesis (Figure 7).

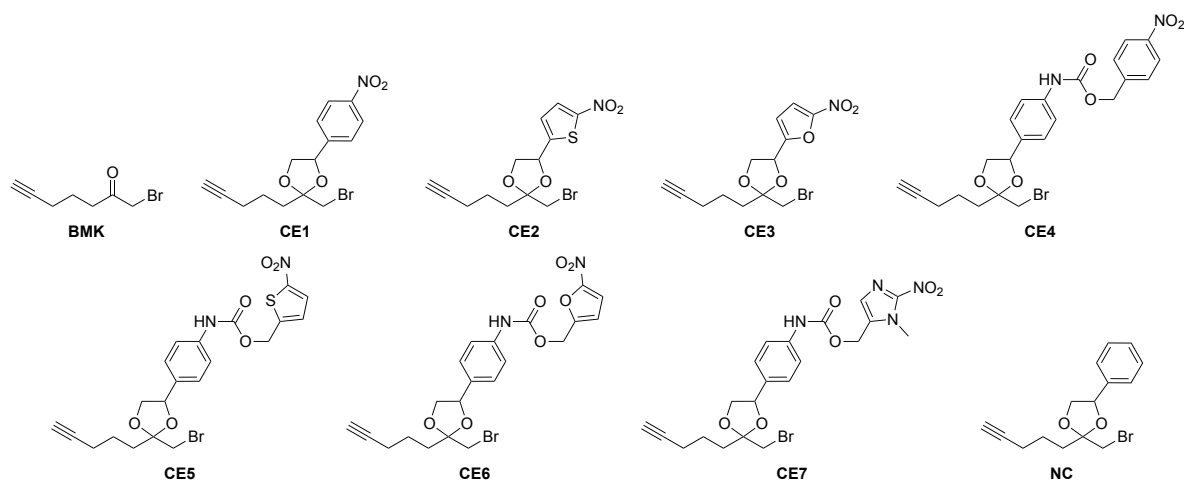


Figure 7: Overview of the synthesized compounds within this thesis for the development of the concept of caged electrophiles.

3.5 Evaluation of the labelling of the second-generation caged electrophiles

After we successfully synthesized the library of caged electrophiles **CE1-CE7** (Figure 7), we investigated and evaluated their activation potential and their labelling properties together with the free electrophile **BMK** and negative control **NC** according to our previously optimized labelling conditions (see chapter II.3.3). For this purpose, we coincubated the compounds with NAD(P)H and FMN in *S. aureus* SH1000^[163] lysate in the presence of either NfsA (Figure 8A) or NfsB (Figure 8B) as activating enzyme, followed by CuAAC^[60-63] to TAMRA-azide, SDS-PAGE separation and in-gel fluorescence scanning.

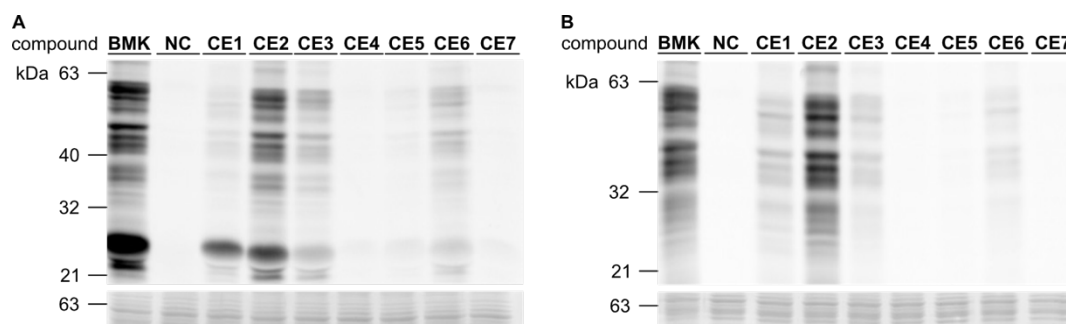


Figure 8: Gel-based labelling experiment to evaluate the activation potential and labelling properties of the library of caged electrophiles **CE1-CE7**. Free **BMK**, negative control **NC** and the caged electrophiles **CE1-CE7** (final concentration of 20 μM) were incubated with either NfsA (**A**, final concentration of 25.5 μM) or NfsB (**B**, final concentration of 25.3 μM) with FMN (final concentration of 25 μM) and either NADPH (**A**, final concentration of 1 mM) or NADH (**B**, final concentration of 1 mM) in *S. aureus* SH1000^[163] lysate (1 mg/mL) in a total volume of 100 μL PBS for one hour at 37 $^{\circ}\text{C}$. The labelled proteins were further clicked by CuAAC^[60-63] to TAMRA-azide, separated by SDS-PAGE and visualized by in-gel fluorescence scanning. The following Coomassie staining verified equal protein concentrations in all gel lanes and is shown below the fluorescence gel.

Since the trend in activation potential and labelling properties of the caged electrophiles **CE1-CE7** was very similar for both activating enzymes, NfsA and NfsB, we will discuss the results here together. Thus, we could again demonstrate and verify that both *E. coli* nitroreductases were able to activate our caged electrophiles. Additionally, we could reproduce that free electrophile **BMK** labelled the proteome strongly and that caged electrophile **CE1** reacted with a similar labelling pattern, but to a weaker extent. We further demonstrated that our hypothesized negative control **NC** indeed did not show any visible labelling, verifying that the activation by bacterial nitroreductases was responsible for the reactivity of caged electrophile **CE1**. The furane-based derivative **CE3** showed very similar or even slightly improved labelling compared to first-generation **CE1**, while the thiophene-based caged electrophile **CE2** reacted very strongly with the proteome. Strikingly, especially in the case of

NfsB as activating enzyme (Figure 8B) the labelling intensity was nearly identical to the free electrophile **BMK**, which indicated a very efficient and almost complete activation of **CE2**. Unfortunately, the caged electrophiles **CE4** (*para*-nitrophenyl-based caged electrophile with a self-immolative linker) and **CE7** (imidazole-based caged electrophile with a self-immolative linker) did not show any visible labelling at all, whereas the thiophene-based **CE5** and furane-based **CE6** caged electrophiles with a self-immolative linker only led to rather weak labelling. Therefore, the strategy with the self-immolative linkers did not work efficiently in our concept. However, we were able to successfully identify the very promising thiophene-based caged electrophile **CE2** during our optimization studies and could demonstrate that **CE2** showed nearly identical labelling as the free electrophile **BMK**. In the following part of this thesis, we will focus on caged electrophile **CE2** and further investigate its activation potential and labelling properties.

3.6 Gel-based labelling of the best caged electrophile in bacterial lysate

During our more detailed investigation on the activation of thiophene-based caged electrophile **CE2**, we first of all analyzed if we could also reduce the concentration of added nitroreductase since **CE2** was nearly completely activated in our previous experiment with a NfsB concentration of 25.3 μM . Indeed, we could show that even a NfsB concentration of 10 μM was sufficient for the nearly complete activation of **CE2** and we, therefore, changed our labelling protocol and adjusted to this concentration in the following experiments.

Next, analogously to our previous proof-of-concept investigations, we assessed the labelling potential of **CE2** compared to free electrophile **BMK** with different combinations of NADH and NfsB addition (Figure 9A).

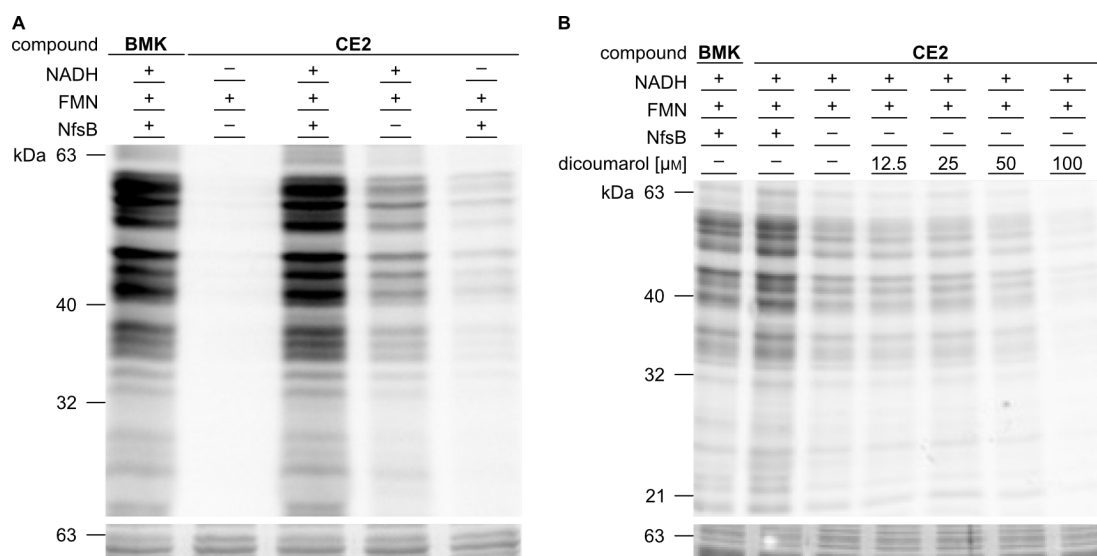


Figure 9: **A** Gel-based labelling experiment with different combinations of NADH and NfsB addition. Free electrophile **BMK** and optimized caged electrophile **CE2** (final concentration of 20 μM) were incubated with different combinations of NfsB (final concentration of 10 μM), FMN (final concentration of 25 μM) and NADH (final concentration of 1 mM) in *S. aureus* SH1000^[163] lysate (1 mg/mL) in a total volume of 100 μL PBS for one hour at 37 °C. **B** Gel-based labelling experiment with addition of increasing concentrations of the known nitroreductase inhibitor dicoumarol.^[183] Free electrophile **BMK** and optimized caged electrophile **CE2** (final concentration of 20 μM) were incubated with different combinations of NfsB (final concentration of 10 μM), FMN (final concentration of 25 μM), NADH (final concentration of 1 mM) and increasing concentrations of dicoumarol (final concentration indicated in the gel) in *S. aureus* SH1000^[163] lysate (1 mg/mL) in a total volume of 100 μL PBS for one hour at 37 °C. **A** and **B** The labelled proteins were further clicked by CuAAC^[60-63] to TAMRA-azide, separated by SDS-PAGE and visualized by in-gel fluorescence scanning. The following Coomassie staining verified equal protein concentrations in all gel lanes and is shown below the fluorescence gel.

We could successfully reproduce the very strong labelling intensity of optimized caged electrophile **CE2** that was nearly identical to the labelling with the free electrophile **BMK**. Without the addition of NfsB and NADH no labelling was observed, once more verifying that nitroreductase activation was responsible for the reactivity of the caged electrophile **CE2** and also showing the general stability of the acetal-protected caged electrophile within our reaction setup. The rather weak labelling in case of no NADH addition was attributed to residual NADH that was present in the bacterial lysate, which was also observed in our previous experiments. Surprisingly, we noticed relatively strong labelling in case of no NfsB addition, which we did not identify with our previously used caged electrophile **CE1**. We believed that this was either due to an unspecific activation or due to endogenous nitroreductase activity that was still present in the lysate. To further investigate this observation, we repeated this experiment and added a literature known nitroreductase inhibitor (dicoumarol)^[183] to analyze its influence on the labelling intensity of caged electrophile **CE2** (Figure 9B). The overall labelling intensity was strongly decreased with increasing concentrations of dicoumarol and nearly completely gone at a dicoumarol concentration of 100 μM . This observation evidently pointed to our hypothesis that the labelling of **CE2** in case of no NfsB addition was caused through the activation by residual endogenous nitroreductases rather than through a general instability or unspecific activation.

Overall, we could reproduce the strong activation potential and labelling properties of optimized caged electrophile **CE2** in bacterial lysate and we could further demonstrate that even without the addition of exogenous nitroreductase caged electrophile **CE2** was activated by endogenous nitroreductase activity.

3.7 Gel-based labelling of the best caged electrophile in living bacteria

Encouraged by the observation that endogenous nitroreductase activity was able to activate caged electrophile **CE2** to yield strong proteome-wide labelling even in bacterial lysate, we set out to take the next step in the development of our concept of caged electrophiles and moved from bacterial lysates to experiments in living bacteria.

We increased the electrophile concentration from 20 μM to 200 μM in order to see stronger labelling patterns, since we could assume that the overall labelling intensity in living bacteria will be weaker compared to bacterial lysates. Furthermore, we wanted to directly compare the reactivity of free electrophile **BMK**, first-generation caged electrophile **CE1** and optimized caged electrophile **CE2** together with the negative control **NC**. Therefore, we treated living

S. aureus SH1000^[163] with the **BMK**, **CE1**, **CE2** and **NC** in a final concentration of 200 μM without the addition of FMN, NADH and NfsB for one hour at 37 °C, followed by lysis of the bacteria, CuAAC^[60–63] to TAMRA-azide, separation by SDS-PAGE and visualization by in-gel fluorescence scanning (Figure 10).



Figure 10: Gel-based labelling experiment of caged electrophiles in living bacteria. Free **BMK**, first-generation caged electrophile **CE1**, optimized caged electrophile **CE2** and negative control **NC** (final concentration of 200 μM) were incubated in living *S. aureus* SH1000^[163] ($\text{OD}_{600} = 40$) for one hour at 37 °C. DMSO was used instead of probe in a control experiment. After lysis of the bacteria, labelled proteins were further clicked by CuAAC^[60–63] to TAMRA-azide, separated by SDS-PAGE and visualized by in-gel fluorescence scanning. The following Coomassie staining verified equal protein concentrations in all gel lanes and is shown below the fluorescence gel.

As the positive control, free electrophile **BMK** also showed very promiscuous labelling proteome-wide in living bacteria, whereas our first-generation caged electrophile **CE1** only exhibited very weak and barely detectable labelling. The negative control **NC** also only reacted very weakly with the proteome. Strikingly, our optimized caged electrophile **CE2** proved also in living bacteria to be activated very efficiently to label the proteome very strongly with a comparable labelling pattern and intensity as the free electrophile **BMK**. This observation demonstrated that optimized caged electrophile **CE2** was activated very efficiently even by the endogenous nitroreductase activity in living bacteria without the need to add any exogenous enzymes. Furthermore, this emphasized the potential of our concept of caged electrophiles to selectively deliver highly reactive electrophiles to bacteria using our initially unreactive caged electrophiles that could get specifically activated by even endogenous nitroreductases in living bacteria.

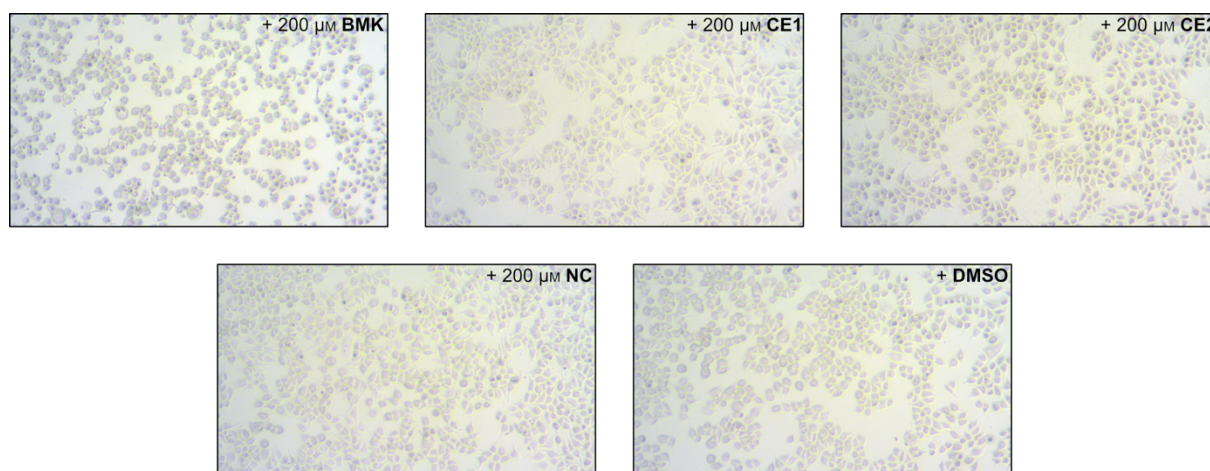


Figure 12: Microscope images of the HEK293 cells after treatment with the free electrophile **BMK**, first-generation caged electrophile **CE1**, optimized caged electrophile **CE2** and negative control **NC** (final concentration of 200 μM) for one hour at 37 $^{\circ}\text{C}$. Additionally, DMSO was used instead of probe in a control experiment.

The cells that were treated with free electrophile **BMK** showed a significant rounding, changes in their morphology and were detached from the culture dish, indicating toxic effects and corresponding cell death. In contrast to this, all caged electrophiles **CE1** and **CE2**, as well as the negative control **NC** did not lead to changes in cell morphology or cell detachment and the treated cells remained comparable to the DMSO treated cells. These observations were in agreement with the labelling patterns visible in the gel, where free electrophile **BMK** strongly labelled the proteome leading to cell death, whereas **CE1**, **CE2** and **NC** did not react with the proteins and therefore did not exhibit toxic effects on the cells.

This verified our initial hypothesis that the caged electrophiles were stable in human cells and that the nitroreductase activity in healthy human cells was comparably low and not sufficient for the activation of our caged electrophiles. Generally, this finally demonstrated the potential of our caged electrophiles towards novel antibiotics that did not show any reactivity on healthy human cells, but promiscuously engaged and labelled the bacterial proteome.

3.9 Chemoproteomic analysis of caged electrophiles in bacterial lysate

In order to fully characterize and further analyze our concept of caged electrophiles, we performed the isoDTB-ABPP workflow^[45] developed in our group that utilizes the MSFragger-based FragPipe computational platform^[76–84] for data analysis (Scheme 5).^[45,76–84] This chemoproteomic technology enabled the investigation of the mass of modification on the proteins after treatment with our caged electrophiles, their amino acid selectivity and allowed quantification of the labelled sites proteome-wide in an unbiased fashion (Figure 13).^[45]

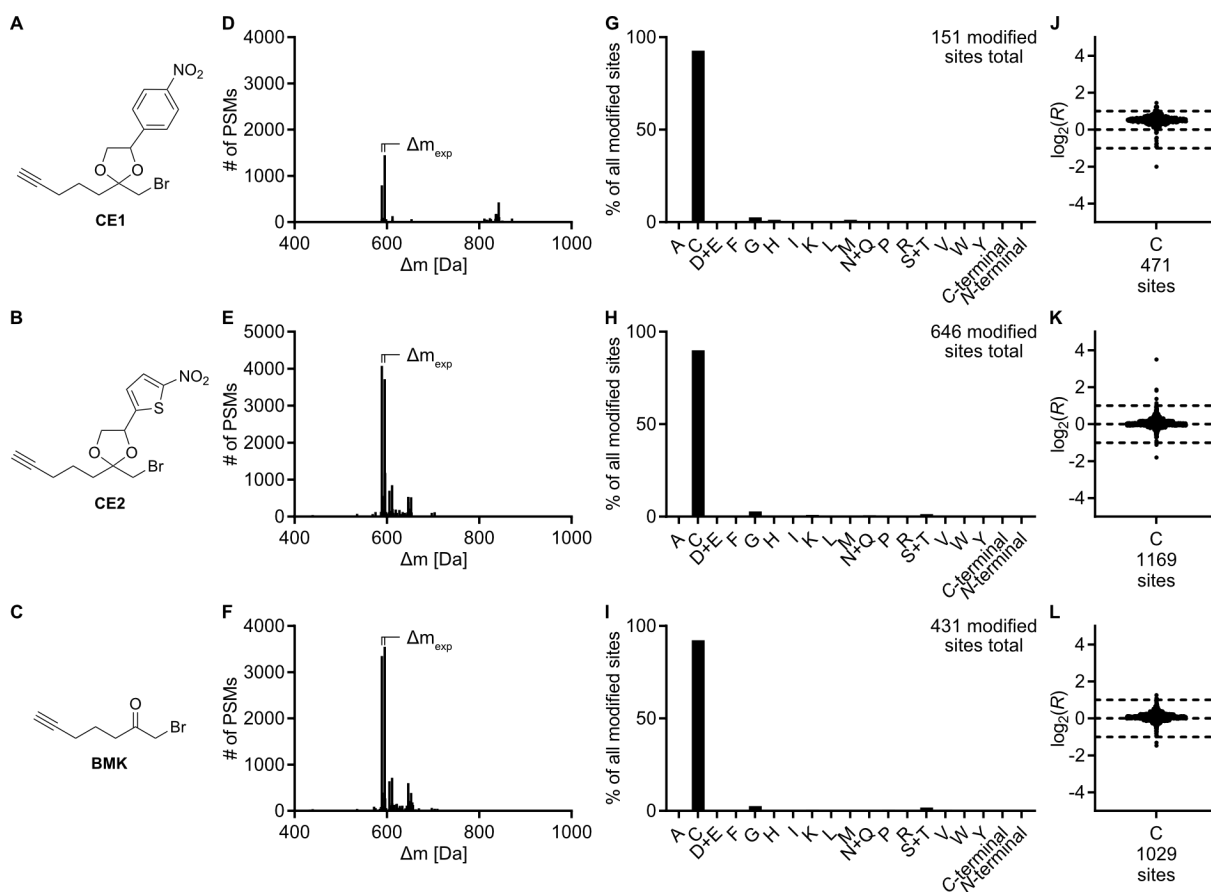


Figure 13: Structures, masses of modification, amino acid selectivity and quantification of labelled sites for **BMK**, **CE1** and **CE2** using our optimized labelling conditions in *S. aureus* SH1000^[163] lysate with addition of FMN, NADH and NfsB. **A-C** Structures of the analyzed probes (final concentration of 20 μM). **D-F** Analysis with the MSFragger Open Search^[76–83] function identified the masses of modification resulting from probe treatment, where the expected masses were marked as Δm_{exp} .^[45] PSM: peptide spectrum matches. **G-I** The pair of peaks, reflecting the isotopic pattern of the isoDTB tags with the expected mass of modification resulting from the probe,^[45] was further analyzed with the MSFragger Offset Search^[76,77,79–84] to identify to amino acid residues and termini, where the modification occurred.^[45] **J-L** Quantification of the probe-labelled cysteines using the MSFragger Closed Search^[76,77,80–83] and IonQuant^[84] quantification module, where the dashed lines show the preferred quantification window ($-1 < \log_2(R) < 1$) due to the combination of the heavy- and light-labelled peptides in a 1:1 ratio.^[45] All experiments were performed in duplicates.

We first conducted this experiment in *S. aureus* SH1000^[163] lysate using our optimized labelling conditions with coincubation of free electrophile **BMK** and caged electrophiles **CE1** and **CE2** at 37 °C and addition of FMN, NADH and NfsB. Analogously to the gel-based labelling experiment, we analyzed free electrophile **BMK**, first-generation caged electrophile **CE1** and optimized caged electrophile **CE2** with this technology in order to compare the labelling properties of the caged derivatives **CE1** and **CE2** with the positive control **BMK** and to demonstrate the improved activity of **CE2** over **CE1**. We did not include negative control **NC** in this study, since the gel-based experiment already showed its neglectable labelling. The MSFragger Open Search^[76–83] function identified for all three used probes the same peak pair of the expected masses of modification (Figure 13D-F), which was in agreement with a previous study from our group with free electrophile **BMK**.^[45] Strikingly, we now showed and proved for the first time that caged electrophiles **CE1** and **CE2** indeed led to the same modification on the labelled proteins as free electrophile **BMK**. Furthermore, this demonstrated that the activation of the caged electrophiles followed our initially proposed mechanisms with the final release of the free electrophile **BMK**. Additionally, through the MSFragger Offset Search^[76,77,79–84] we verified the expected high cysteine selectivity of our probes with >89% (Figure 13G-I), which again reproduced the results from our previous study for **BMK**.^[45] Finally, we quantified the probe-labelled cysteines using the MSFragger Closed Search^[76,77,80–83] and IonQuant^[84] quantification module (Figure 13J-L).^[45] Thereby, we could show that optimized caged electrophile **CE2** labelled 1169 cysteines and therefore was equally reactive as free electrophile **BMK**, where we could detect 1029 modified cysteines. Generally, the increased labelling of **CE2** over **BMK** could not be explained, since they were applied in the same concentration, but this small difference was in an acceptable range of the error of the experiment. Importantly, we could further verify our previous observation of the gel-based labelling experiments that the optimized caged electrophile **CE2** represented a great improvement over the first-generation caged electrophile **CE1** that only engaged 471 cysteine residues.

Summarizing, using this chemoproteomic workflow we could successfully demonstrate that after nitroreductase activation of our caged electrophiles **CE1** and **CE2** indeed a liberation of the free electrophile **BMK** occurred that was then responsible for the proteome-wide labelling. Further, we could quantitatively verify our initial observation that optimized caged electrophile **CE2** outperformed first-generation caged electrophile **CE1** and was equally active as free bromomethyl ketone **BMK**.

3.10 Chemoproteomic analysis of caged electrophiles in living bacteria

Analogously to our gel-based investigation, we next set out to also perform the isoDTB-ABPP workflow^[45] with the MSFragger-based FragPipe computational platform^[76–84] with the same probes **CE1**, **CE2** and **BMK** in living *S. aureus* SH1000^[163] without the addition of exogenous nitroreductase, FMN or NADH (Figure 14).

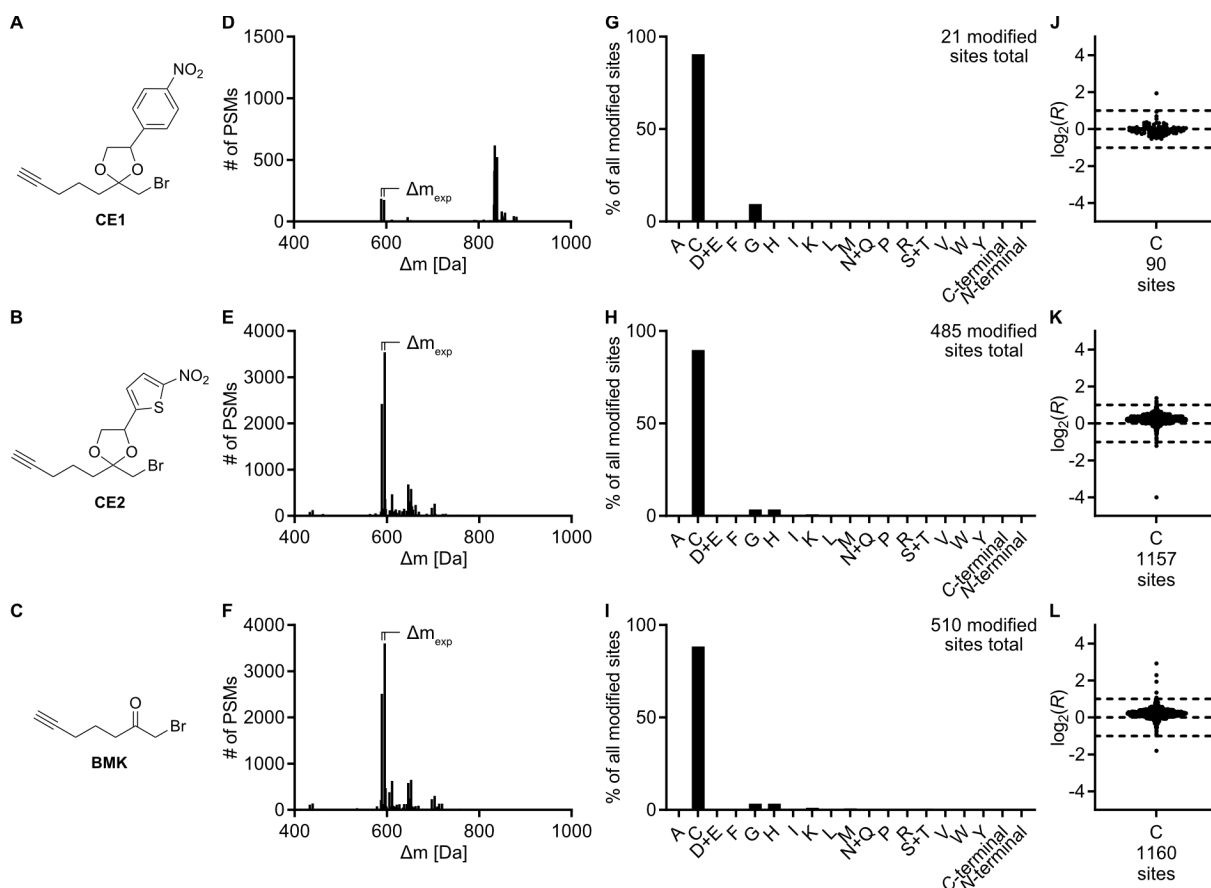


Figure 14: Structures, masses of modification, amino acid selectivity and quantification of labelled sites for **BMK**, **CE1** and **CE2** in living *S. aureus* SH1000^[163] without the addition of exogenous FMN, NADH and NfsB. **A-C** Structures of the analyzed probes (final concentration of 200 μ M). **D-F** Analysis with the MSFragger Open Search^[76–83] function identified the masses of modification resulting from probe treatment, where the expected masses were marked as Δm_{exp} .^[45] PSM: peptide spectrum matches. **G-I** The pair of peaks, reflecting the isotopic pattern of the isoDTB tags with the expected mass of modification resulting from the probe,^[45] was further analyzed with the MSFragger Offset Search^[76,77,79–84] to identify to amino acid residues and termini, where the modification occurred.^[45] **J-L** Quantification of the probe-labelled cysteines using the MSFragger Closed Search^[76,77,80–83] and IonQuant^[84] quantification module, where the dashed lines show the preferred quantification window ($-1 < \log_2(R) < 1$) due to the combination of the heavy- and light-labelled peptides in a 1:1 ratio.^[45] All experiments were performed in duplicates. **K** One cysteine residue (Q9ZAH5_C304) was quantified outside the shown region with $\log_2(R) = -7.14$.

After the MSFragger Open Search^[76-83] analysis, we could again detect the same mass of modification for all three used probes, which demonstrated that even in living bacteria without the addition of exogenous nitroreductase the liberation of the free electrophile **BMK** occurred and led to the observed proteome-wide labelling (Figure 14D-F). Not surprisingly, the MSFragger Offset Search^[76,77,79-84] also reproduced high cysteine selectivity with >88% (Figure 14G-I). Similar to our gel-based observation, the MSFragger Closed Search^[76,77,80-83] and IonQuant^[84] quantification module verified that first-generation caged electrophile **CE1**, which did show very weak labelling in the gel-based experiment, only modified 90 cysteines, which was very low compared to the 1160 sites of the free electrophile **BMK** (Figure 14J-L). More importantly, even for the treatment of living bacteria, optimized caged electrophile **CE2**, which could engage 1157 cysteines, largely exceeded the reactivity of first-generation caged electrophile **CE1** and in this case matched the reactivity of free electrophile **BMK** nearly exactly.

Overall, the obtained conclusions of the chemoproteomic experiment in bacterial lysate, that the release of free electrophile **BMK** was responsible for the reactivity of the caged electrophiles **CE1** and **CE2** and that optimized caged electrophile **CE2** was equally active as **BMK**, could be reproduced and further strengthened in this experiment and additionally it could be demonstrated that the addition of exogenous nitroreductase, FMN and NADH was not necessary for the highly efficient activation of optimized caged electrophile **CE2**.

4 Conclusion and outlook

In this part of the thesis, we proposed a modular concept of caged electrophiles based on cysteine-directed bromomethyl ketones that were rendered unreactive and caged through acetal formation and could be selectively activated by bacterial nitroreductases to engage multiple intracellular cysteine residues simultaneously, thus preventing human off-target engagement and toxic side-effects (Scheme 7).^[45,93–96,120,123,133,140–142]

For this purpose, we initially synthesized the respective free bromomethyl ketone probe **BMK** and a *para*-nitrophenyl-based caging group **4** that were used together to obtain the first-generation caged electrophile **CE1** as a mixture of diastereoisomers. First proof-of-concept studies through a gel-based labelling approach of **BMK** and **CE1** in *S. aureus* SH1000^[163] lysate with the addition of *E. coli* nitroreductase NfsB and NADH as cofactor^[101,111–114] demonstrated the general feasibility of our approach, since we could successfully observe proteome-wide labelling of **CE1** after nitroreductase activation.

Encouraged by this result, we continued with extensive labelling optimization studies, where we verified that caged electrophile **CE1** could not only get activated by NfsB, but also by the major *E. coli* nitroreductase NfsA. According to previous literature reports, resistance formation to nitrofurans antibiotics, which could also get activated by NfsA and NfsB, occurred in two consecutive mutation steps. We, therefore, hypothesized that possible resistance to the caged electrophiles also happens in two individual steps and consequently we assumed this resistance formation to be overall very slow.^[98,110–112] Additionally, we increased the overall labelling intensity through the addition of FMN as prosthetic group^[99–101,111–114] and reduced the labelling of the activating nitroreductase itself through the coincubation of caged electrophile **CE1** together with nitroreductase, NAD(P)H and FMN directly in bacterial lysate, which also represented more closely the native conditions in living bacteria. Lastly, we showed that labelling at 37 °C instead of room temperature further increased the overall intensity at least in the case of NfsB as activating nitroreductase. Together, this led to our final optimized labelling conditions of coincubation of caged electrophile together with NfsB, NADH and FMN at 37 °C directly in bacterial lysate.

Even after optimization of the conditions, the overall labelling intensity of **CE1** was relatively poor compared to free electrophile **BMK** indicating insufficient activation. The exchange of the previously used *para*-nitrophenyl caging group **4** with thiophene-, furane- and imidazole-based analogs was reported to drastically increase activation^[133] and we additionally adapted the concept of so-called self-immolative linkers, where we also expected improved

labelling properties (Scheme 11).^[93,94,96,120,123,140,141,164,165] We successfully synthesized the thiophene- **10** and furane-based caging group **15** as well as the *para*-nitrophenyl- **20**, thiophene- **23**, furane- **25** and imidazole-based caging group with self-immolative linker **36** in overall very high purity and moderate yields over multiple individual synthetic steps. Next, we performed the acetalization reactions with the aforementioned caging groups and free electrophile **BMK** to obtain the second-generation caged electrophile **CE2-CE7**. Additionally, we synthesized a respective negative control **NC** without any nitro-group based on the corresponding phenyl-based caging group **38**.

Gel-based labelling of the complete library of caged electrophiles in *S. aureus* SH1000^[163] lysate with the optimized conditions reproduced the rather weak labelling of first-generation caged electrophile **CE1**, but showed the overall stability of our caged electrophiles in the experimental setup and that nitroreductase activation was responsible for the reactivity, since negative control **NC** did not lead to significant labelling. While the caged electrophiles **CE4-CE7** with self-immolative linkers seemed to not work well within our concept, furane-based **CE3** already improved labelling, whereas thiophene-based caged electrophile **CE2** showed similar labelling intensities as free electrophile **BMK**. Another experiment with different combinations of added NfsB and NADH to **CE2** further proved that nitroreductase activation was responsible for the reactivity. However, even in the case of no nitroreductase addition, the improved activation properties of **CE2** led to sufficient activation through residual endogenous nitroreductase activity present in the bacterial lysate that could be inhibited by the addition of a known nitroreductase inhibitor dicoumarol.^[183]

Consequently, we took the next step and moved to a labelling experiment in living *S. aureus* SH1000^[163] without the addition of exogenous NfsB, NADH or FMN. The negative control **NC** only very weakly reacted with the proteome compared to free electrophile **BMK**. First-generation **CE1** also showed very weak labelling, but in accordance with our previous experiments the optimized caged electrophile **CE2** represented a huge improvement and led to nearly identical labelling as positive control **BMK**. Strikingly, we could further verify our initial hypothesis and demonstrate that our caged electrophiles **CE1** and **CE2** as well as negative control **NC** did not label the proteome in living cells of the human cell line HEK293 and did not lead to visible changes in cell morphology. In contrast, **BMK** labelled the proteome promiscuously and led to cell rounding and possibly cell death.

Finally, we investigated our concept in more detail using the chemoproteomic isoDTB-ABPP workflow^[45] with the MSFragger-based FragPipe computational platform^[76-84] to analyze the

exact modification and amino acid selectivity of the caged electrophiles and to quantify the labelled sites.^[45] We demonstrated both in bacterial lysate with addition of NfsB, NADH and FMN and in living *S. aureus* SH1000^[163] that the liberation of free electrophile **BMK** after nitroreductase activation of caged electrophiles **CE1** and **CE2** was responsible for their reactivity, since the identical masses of modification were measured as expected for the free electrophile **BMK** according to a previous study. Consequently, our caged electrophiles **CE1** and **CE2** reacted preferentially with cysteine residues in a selectivity >88%. Especially in the experiment in living bacteria, we could quantify the significant improvement of labelled sites of optimized caged electrophile **CE2** (1157 cysteines) over **CE1** (90 cysteines) and thereby also reproduce our observation from the gel-based experiments in a quantitative manner that **CE2** was equally active as free electrophile **BMK** (1160 cysteines).

In the next part of this project an antibioticly active bromomethyl ketone should be identified and equipped with our optimized thiophene-based caging group **10** to evaluate the antibiotic potential of our class of compounds. In addition to bromomethyl ketones even other carbonyl containing electrophiles, as previously mentioned, should be selected and converted to the respective caged electrophile utilizing the modular nature of our approach. This will limit future applications in drug developments based on our concept not only to bromomethyl ketone derived compounds but will expand its range to a diverse set of different electrophiles. The modularity of this concept in theory will not only allow changes in the electrophile but also in terms of the activating enzyme. As mentioned above, the caging groups may be adjusted to different activating enzyme families that are able to liberate an amine-functionality from a precursor like proteases,^[154] β -lactamases,^[155] azoreductases^[156] or CYP450 enzymes.^[157] Lastly, one could envision to further expand the application of caged electrophiles beyond antibiotics to target different diseases, *e.g.* cancer, through the selective delivery of nitroreductases or other activating enzymes to the cells of interest *via* ADEPT, VDEPT or GDEPT strategies.^[124–132]

Overall, we could successfully develop, verify and optimize our proposed concept of caged electrophiles that were selectively activated only in bacteria, but not in human cells, to engage multiple intracellular cysteine residues simultaneously, and, thereby, provide a basis for future drug development strategies.

5 Experimental part

These experimental procedures will be published identically in my corresponding publication. Some experiments were conducted identical as in my Master's thesis^[162] and some general experimental procedures are reported identically or with slight modification to previously published protocols from our group.^[45,75]

5.1 Organic synthesis

5.1.1 Materials and methods

Chemicals

All air and water sensitive reactions were carried out in dried reaction flasks under argon atmosphere using standard Schlenk techniques. Sensitive liquids and anhydrous solvents were transferred *via* argon flushed syringes. Commercially available reagents and solvents were used without further purification. Solvent mixtures are given in v/v. For reactants with given concentrations or mass fractions, the given mass corresponds to the mass of the pure reactant.

Analytical thin layer chromatography and flash chromatography

Analytical thin layer chromatography (TLC) was performed on silica-coated aluminum sheets (Merck, TLC Silicagel 60 F254). The spots were visualized using UV-light ($\lambda = 254$ nm and $\lambda = 366$ nm) and/or staining with KMnO₄ solution (1.50 g KMnO₄, 10.0 g K₂CO₃ and 1.25 mL 10 wt% aqueous NaOH in 200 mL H₂O) followed by heat treatment. Flash column chromatography was performed on silica gel (VWR, 40-63 μ m) with the indicated solvent mixture.

Nuclear magnetic resonance spectroscopy

Nuclear magnetic resonance (NMR) spectra were recorded at room temperature on an AVHD-300, AVHD-400, AVHD-500 and AVHD-500cr (Bruker). The chemical shifts (δ) are given in parts per million (ppm) and the spectra are referenced to the residual proton and carbon signal of the deuterated solvents CDCl₃, DMSO-*d*₆ and CD₃CN.

CDCl₃: δ (¹H) = 7.26 ppm, δ (¹³C) = 77.16 ppm

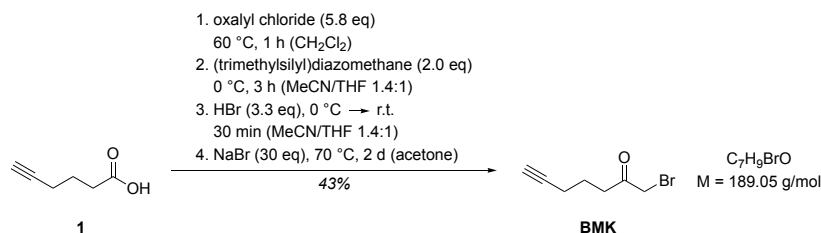
DMSO-*d*₆: δ (¹H) = 2.50 ppm, δ (¹³C) = 39.52 ppm

CD₃CN: δ (¹H) = 1.94 ppm, δ (¹³C) = 118.26 ppm

The following abbreviations were used to describe the coupling patterns: s – singlet, d – doublet, t – triplet, q – quartet, p – quintet, br – broad signal, m – multiplet, dd – doublet of doublets, dt – doublet of triplets, ddd – doublet of doublet of doublets, td – triplet of doublets, qd – quartet of doublets. The coupling constants (*J*) are reported in Hertz (Hz). If the signals of

5.1.2 Synthesis of the first-generation caged electrophile

1-bromohept-6-yn-2-one (**BMK**)

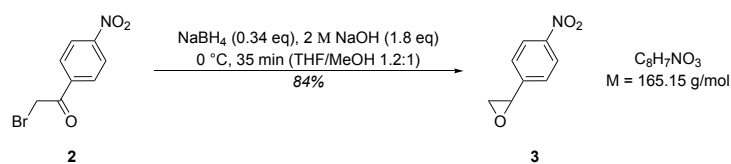


The synthesis was carried out analogously to a published procedure.^[140,141,158] Hex-5-ynoic acid (**1**) (441 μ L, 449 mg, 4.00 mmol, 1.0 eq) was dissolved in dry dichloromethane (8 mL) under argon atmosphere, oxalyl chloride (1.99 mL, 2.94 g, 23.2 mmol, 5.8 eq) was added and the reaction mixture was stirred at 60 °C for one hour. Excess oxalyl chloride and dichloromethane were evaporated under reduced pressure and the residual oil was dissolved in a mixture of dry acetonitrile (4 mL) and tetrahydrofuran (2.8 mL). The solution was cooled to 0 °C and (trimethylsilyl)diazomethane (4.00 mL, 2 M in hexane, 914 mg, 8.00 mmol, 2.0 eq) was slowly added. After stirring at 0 ° for three hours, hydrobromic acid (2.39 mL, 33 wt% in acetic acid, 1.07 g, 13.2 mmol, 3.3 eq) was added and the resulting mixture was stirred for additional 30 minutes at room temperature. It was diluted with diethyl ether (40 mL), washed with saturated sodium bicarbonate (6 \times 15 mL) and water (15 mL), dried over sodium sulfate and concentrated under reduced pressure. The crude reaction product was purified by flash chromatography (pentane/diethyl ether 95:5 \rightarrow 90:10) to yield a mixture of bromomethyl ketone **BMK** and the respective chloromethyl ketone. The mixture was dissolved in dry acetone (14 mL) under argon atmosphere and sodium bromide (6.17 g, 60.0 mmol, 15 eq) was added. The reaction mixture was stirred at 70 °C for two days in the dark and additional sodium bromide (6.17 g, 60.0 mmol, 15 eq) was added in small portions until the completion of the reaction was indicated by ¹H-NMR. Subsequently, pentane (15 mL) was added, the mixture was filtered to remove the formed solid and washed with water (7 mL). The organic phases were dried over sodium sulfate and concentrated under reduced pressure. The crude product was purified by flash chromatography (pentane/diethyl ether 95:5) to yield the bromomethyl ketone **BMK** (327 mg, 1.73 mmol, 43%) as a light-yellow oil.

TLC: $R_f = 0.23$ (pentane/diethyl ether 9:1) [KMnO₄/UV].

¹H-NMR (400 MHz, CDCl₃): δ [ppm] = 1.84 (p, ³ $J = 7.0$ Hz, 2 H), 1.98 (t, ⁴ $J = 2.7$ Hz, 1 H), 2.26 (td, ⁴ $J = 2.7$ Hz, ³ $J = 7.0$ Hz, 2 H), 2.81 (t, ³ $J = 7.0$ Hz, 2 H), 3.90 (s, 2 H).

¹³C-NMR (101 MHz, CDCl₃): δ [ppm] = 17.7 (s), 22.5 (s), 34.4 (s), 38.4 (s), 69.6 (s), 83.3 (s), 201.6 (s).

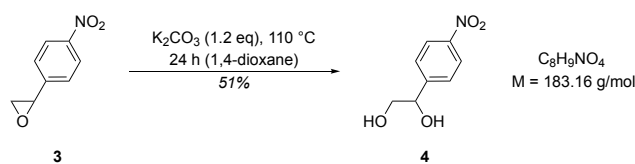
2-(4'-nitrophenyl)oxirane (**3**)

The synthesis was carried out analogously to a published procedure.^[159] To a solution of bromomethyl ketone **2** (800 mg, 3.28 mmol, 1.0 eq) in methanol (2.1 mL) and tetrahydrofuran (2.6 mL) was added sodium borohydride (42.2 mg, 1.11 mmol, 0.34 eq) and 2 M sodium hydroxide (3.00 mL, 240 mg, 6.00 mmol, 1.8 eq) at 0 °C. After stirring at 0 °C for 35 minutes, the reaction was quenched by the addition of glacial acetic acid to reach pH = 6. The resulting mixture was diluted with ethyl acetate (33 mL) and washed with saturated sodium bicarbonate (25 mL) and saturated sodium chloride (25 mL). The organic phases were dried over sodium sulfate and concentrated under reduced pressure. Without further purification epoxide **3** (456 mg, 2.76 mmol, 84%) was obtained as orange solid.

TLC: $R_f = 0.39$ (pentane/ethyl acetate 7:3) [KMnO₄/UV].

¹H-NMR (400 MHz, CDCl₃): δ [ppm] = 2.78 (dd, ³ $J = 2.5$ Hz, ² $J = 5.5$ Hz, 1 H), 3.23 (dd, ³ $J = 4.1$ Hz, ² $J = 5.5$ Hz, 1 H), 3.96 (dd, ³ $J = 4.1$ Hz, ³ $J = 2.5$ Hz, 1 H), 7.45 (d, ³ $J = 8.8$ Hz, 2 H), 8.21 (d, ³ $J = 8.8$ Hz, 2 H).

¹³C-NMR (101 MHz, CDCl₃): δ [ppm] = 51.6 (s), 51.8 (s), 124.0 (s), 126.4 (s), 145.4 (s), 148.0 (s).

1-(4'-nitrophenyl)ethane-1,2-diol (**4**)

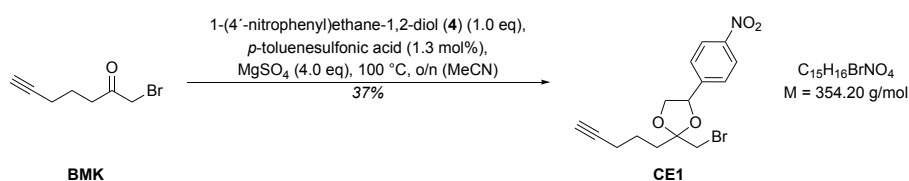
The synthesis was carried out analogously to a published procedure.^[160] Epoxide **3** (698 mg, 4.23 mmol, 1.0 eq) was dissolved in 1,4-dioxane (5.3 mL), 10% aqueous potassium carbonate (6.78 mL, 678 mg, 4.91 mmol, 1.2 eq) was added and the mixture was stirred under reflux for 24 hours. After cooling to room temperature, the reaction was quenched by the addition of 2 M hydrochloric acid until pH = 5 was reached. The reaction mixture was extracted with diethyl ether (3 × 40 mL), washed with saturated sodium chloride (25 mL), dried over sodium sulfate and concentrated under reduced pressure. The crude product was purified by flash chromatography (pentane/ethyl acetate 1:4) to yield caging group **4** (391 mg, 2.13 mmol, 51%) as a light-orange solid.

TLC: $R_f = 0.26$ (ethyl acetate) [KMnO₄/UV].

¹H-NMR (400 MHz, CDCl₃): δ [ppm] = 1.62 (br, 1 H), 2.70 (br, 1 H), 3.64 (dd, ³ $J = 7.9$ Hz, ² $J = 11.2$ Hz, 1 H), 3.85 (dd, ³ $J = 3.5$ Hz, ² $J = 11.2$ Hz, 1 H), 4.95 (dd, ³ $J = 7.9$ Hz, ³ $J = 3.4$ Hz, 1 H), 7.57 (d, ³ $J = 8.7$ Hz, 2 H), 8.23 (d, ³ $J = 8.7$ Hz, 2 H).

¹³C-NMR (126 MHz, CDCl₃): δ [ppm] = 67.8 (s), 73.9 (s), 123.9 (s), 127.0 (s), 147.8 (s, C), 147.8 (s).

HRMS (ESI): m/z calculated for C₈H₉NO₄ [M+formic acid-H]⁻: 228.0514, found: 228.0512.

First-generation caged electrophile **CE1**

The synthesis was carried out analogously to a published procedure.^[141] To a solution of bromomethyl ketone **BMK** (26.5 mg, 0.14 mmol, 1.1 eq), caging group **4** (23.3 mg, 0.13 mmol, 1.0 eq) and magnesium sulfate (67.4 mg, 0.56 mmol, 4.0 eq) in dry acetonitrile (300 μL) was added a catalytic amount of *p*-toluenesulfonic acid (1.3 mol%) under argon atmosphere. The reaction mixture was stirred at 100 °C overnight. After dilution with ethyl acetate (6 mL), the reaction mixture was washed with water (3 mL), dried over sodium sulfate and concentrated under reduced pressure. The crude product was purified by flash chromatography (pentane/diethyl ether 95:5) to yield first-generation caged electrophile **CE1** (16.7 mg, 0.05 mmol, 37%) as a light-yellow oil with a diastereomer ratio of 51:49.

TLC: $R_f = 0.39$ (pentane/diethyl ether 65:35) [KMnO_4/UV].

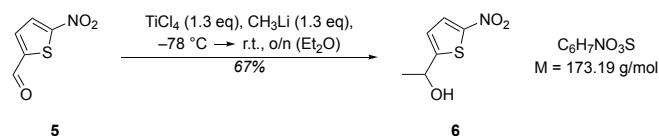
$^1\text{H-NMR}$ (400 MHz, CD_3CN): δ [ppm] = 1.60-1.75 (m, 2 H), 1.98-2.12 (m, 2 H), 2.19-2.22 (m, 1 H), 2.23-2.29 (m, 2 H), 3.59-3.78 (m, 3 H), 4.40-4.50 (m, 1 H), 5.27 (dd, $^3J = 9.1$ Hz, $^3J = 6.2$ Hz, 1 H, major), 5.29 (dd, $^3J = 8.1$ Hz, $^3J = 6.6$ Hz, 1 H, minor), 7.59-7.69 (m, 2 H), 8.17-8.26 (m, 2 H).

$^{13}\text{C-NMR}$ (101 MHz, CDCl_3): δ [ppm] = 18.7 (s), 23.3 (s, major), 23.5 (s, minor), 35.9 (s, minor), 36.0 (s, major), 36.3 (s, minor), 37.2 (s, major), 70.1 (s, major), 70.2 (s, minor), 72.7 (s, minor), 72.8 (s, major), 78.3 (s, minor), 79.0 (s, major), 84.9 (s, major), 84.9 (s, minor), 111.0 (s, major), 111.1 (s, minor), 124.6 (s, major), 124.7 (s, minor), 128.1 (s, major), 128.2 (s, minor), 146.7 (s, major), 146.9 (s, minor), 148.9 (s).

HRMS (ESI): m/z calculated for $\text{C}_{15}\text{H}_{16}\text{BrNO}_4$ [$\text{M}+\text{H}$] $^+$: 354.0335, found: 354.0336.

5.1.3 Synthesis of improved caging groups

1-(5'-nitrothiophen-2'-yl)ethan-1-ol (**6**)



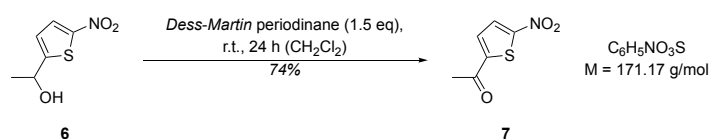
The synthesis was carried out analogously to a published procedure.^[166] Titanium(IV) chloride (12.4 mL, 1.0 M in dichloromethane, 2.35 g, 12.4 mmol, 1.3 eq) was slowly dissolved in dry diethyl ether (24 mL) under argon atmosphere. The solution was cooled to $-78\text{ }^\circ\text{C}$ and methyllithium (7.76 mL, 1.6 M in diethyl ether, 273 mg, 12.4 mmol, 1.3 eq) was added dropwise. After the reaction mixture was stirred for 1.5 hours at $-78\text{ }^\circ\text{C}$, a solution of aldehyde **5** (1.5 g, 9.55 mmol, 1.0 eq) in dry diethyl ether (30 mL) was slowly added at $-78\text{ }^\circ\text{C}$. The reaction mixture was allowed to slowly warm to room temperature overnight. Subsequently, the reaction was quenched by the addition of water (15 mL) at $0\text{ }^\circ\text{C}$ and the aqueous phase was extracted with ethyl acetate ($6 \times 12\text{ mL}$). Subsequently, the combined organic phases were washed with saturated sodium chloride (15 mL), dried over sodium sulfate and concentrated under reduced pressure. The crude product was purified by flash chromatography (pentane/ethyl acetate 4:1) to yield alcohol **6** (1.11 g, 6.42 mmol, 67%) as brown oil.

TLC: $R_f = 0.40$ (pentane/ethyl acetate 1:1) [KMnO_4/UV].

$^1\text{H-NMR}$ (500 MHz, CDCl_3): δ [ppm] = 1.62 (d, $^3J = 6.5\text{ Hz}$, 3 H), 2.17 (br, 1 H), 5.12 (qd, $^4J = 1.0\text{ Hz}$, $^3J = 6.5\text{ Hz}$, 1 H), 6.89 (dd, $^4J = 1.0\text{ Hz}$, $^3J = 4.2\text{ Hz}$, 1 H), 7.80 (d, $^3J = 4.2\text{ Hz}$, 1 H).

$^{13}\text{C-NMR}$ (101 MHz, CDCl_3): δ [ppm] = 25.5 (s), 66.7 (s), 122.2 (s), 128.8 (s), 150.7 (s), 159.0 (s).

HRMS (ESI): m/z calculated for $\text{C}_6\text{H}_7\text{NO}_3\text{S}$ [$\text{M} + \text{formic acid} - \text{H}$] $^-$: 218.0129, found: 218.0129.

1-(5'-nitrothiophen-2'-yl)ethan-1-one (**7**)

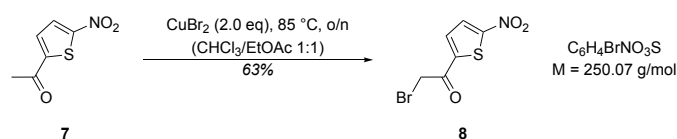
The synthesis was carried out analogously to a published procedure.^[166] To a solution of alcohol **6** (1.11 g, 6.42 mmol, 1.0 eq) dissolved in dichloromethane (75 mL) was added *Dess-Martin* periodinane (4.08 g, 9.63 mmol, 1.5 eq) in small portions. After stirring at room temperature for 24 hours, the reaction was quenched by the addition of saturated sodium thiosulfate (54 mL) and saturated sodium bicarbonate (54 mL). The mixture was filtered through Celite[®] and the aqueous phase was extracted with ethyl acetate (3 × 32 mL). The combined organic phases were washed with saturated sodium chloride (50 mL), dried over sodium sulfate and concentrated under reduced pressure. The crude product was purified by flash chromatography (pentane/ethyl acetate 4:1) to yield methyl ketone **7** (813 mg, 4.75 mmol, 74%) as light-yellow crystals.

TLC: $R_f = 0.58$ (pentane/ethyl acetate 1:1) [KMnO₄/UV].

¹H-NMR (500 MHz, CDCl₃): δ [ppm] = 2.61 (s, 3 H), 7.58 (dd, $^3J = 4.3$ Hz, 1 H), 7.89 (d, $^3J = 4.3$ Hz, 1 H).

¹³C-NMR (101 MHz, CDCl₃): δ [ppm] = 26.7 (s), 128.4 (s), 130.2 (s), 148.3 (s), 156.6 (s), 190.5 (s).

HRMS (ESI): m/z calculated for C₆H₅NO₃S [M+H]⁺: 172.0062, found: 172.0061.

2-bromo-1-(5'-nitrothiophen-2'-yl)ethan-1-one (**8**)

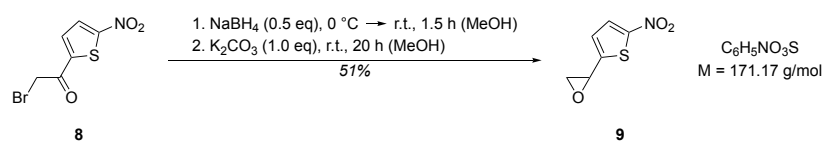
The synthesis was carried out analogously to a published procedure.^[167] The methyl ketone **7** (813 mg, 4.75 mmol, 1.0 eq) was dissolved in a 1:1 mixture of ethyl acetate (10.9 mL) and chloroform (10.9 mL). Copper(II) bromide (2.12 g, 9.49 mmol, 2.0 eq) was added and the mixture was stirred at 85°C overnight. After cooling to room temperature, the mixture was filtered through Celite[®], dried over sodium sulfate and concentrated under reduced pressure. The crude product was purified by flash chromatography (pentane/ethyl acetate 85:15) to yield bromomethyl ketone **8** (745 mg, 2.98 mmol, 63%) as light-yellow crystals.

TLC: $R_f = 0.44$ (pentane/ethyl acetate 7:3) [KMnO_4/UV].

$^1\text{H-NMR}$ (400 MHz, CDCl_3): δ [ppm] = 4.34 (s, 2 H), 7.71 (d, $^3J = 4.3$ Hz, 1 H), 7.91 (d, $^3J = 4.3$ Hz, 1 H).

$^{13}\text{C-NMR}$ (101 MHz, CDCl_3): δ [ppm] = 29.3 (s), 128.3 (s), 131.6 (s), 144.5 (s), 157.3 (s), 184.7 (s).

HRMS (ESI): m/z calculated for $\text{C}_6\text{H}_4\text{BrNO}_3\text{S}$ [M-H]⁻: 247.9022, found: 247.9023.

2-(5'-nitrothiophen-2'-yl)oxirane (**9**)

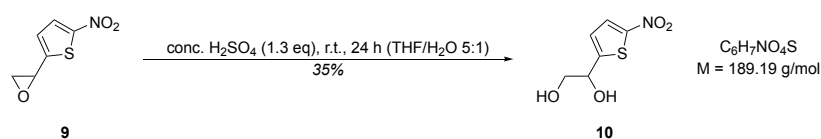
The synthesis was carried out analogously to a published procedure.^[168] To a solution of bromomethyl ketone **8** (495 mg, 1.98 mmol, 1.0 eq) in methanol (5 mL) was added sodium borohydride (37.4 mg, 0.99 mmol, 0.5 eq) at 0 °C. After the reaction mixture was stirred for 90 minutes at room temperature, potassium carbonate (274 mg, 1.98 mmol, 1.0 eq) was added in small portions. The mixture was stirred for another 20 hours at room temperature and subsequently quenched by the addition of water (4 mL). The aqueous phase was extracted with diethyl ether (3 × 5 mL) and the combined organic phases were washed with saturated sodium chloride (2 × 5 mL), dried over sodium sulfate and concentrated under reduced pressure. The crude product was purified by flash chromatography (pentane/ethyl acetate 85:15) to yield epoxide **9** (174 mg, 1.02 mmol, 51%) as brown oil.

TLC: R_f = 0.33 (pentane/ethyl acetate 6:4) [KMnO₄/UV].

¹H-NMR (400 MHz, CDCl₃): δ [ppm] = 2.93 (dd, ³ J = 2.4 Hz, ² J = 5.3 Hz, 1 H), 3.24 (dd, ³ J = 3.9 Hz, ² J = 5.3 Hz, 1 H), 4.08 (dd, ³ J = 3.9 Hz, ³ J = 2.4 Hz, 1 H), 7.06 (d, ³ J = 4.2 Hz, 1 H), 7.80 (d, ³ J = 4.2 Hz, 1 H).

¹³C-NMR (101 MHz, CDCl₃): δ [ppm] = 49.1 (s), 52.7 (s), 124.8 (s), 128.7 (s), 150.7 (s), 150.9 (s).

HRMS (ESI): m/z calculated for C₆H₅NO₃S [M+H]⁺: 172.0062, found: 172.0062.

1-(5'-nitrothiophen-2'-yl)ethane-1,2-diol (**10**)

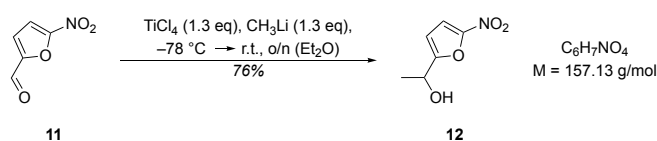
The synthesis was carried out analogously to a published procedure.^[168] Epoxide **9** (163 mg, 0.95 mmol, 1.0 eq) was dissolved in a mixture of tetrahydrofuran (7.4 mL) and water (1.5 mL) and concentrated sulfuric acid (68 μL , 121 mg, 1.23 mmol, 1.3 eq) was added at room temperature. The reaction mixture was stirred for 24 hours and neutralized by the addition of saturated sodium bicarbonate. The aqueous phase was extracted with diethyl ether ($3 \times 10 \text{ mL}$) and the combined organic phases were washed with saturated sodium chloride (10 mL), dried over sodium sulfate and concentrated under reduced pressure. The crude product was purified by flash chromatography (pentane/ethyl acetate 6:4 \rightarrow 4:6) to yield caging group **10** (62.6 mg, 0.33 mmol, 35%) as a brown solid.

TLC: $R_f = 0.07$ (pentane/ethyl acetate 6:4) [KMnO_4/UV].

$^1\text{H-NMR}$ (400 MHz, CDCl_3): δ [ppm] = 1.66-2.73 (m, 2 H), 3.75 (dd, $^3J = 6.9 \text{ Hz}$, $^2J = 11.2 \text{ Hz}$, 1 H), 3.92 (dd, $^3J = 3.6 \text{ Hz}$, $^2J = 11.2 \text{ Hz}$, 1 H), 5.05 (ddd, $^4J = 0.9 \text{ Hz}$, $^3J = 6.9 \text{ Hz}$, $^3J = 3.6 \text{ Hz}$, 1 H), 6.94 (dd, $^4J = 0.9 \text{ Hz}$, $^3J = 4.2 \text{ Hz}$, 1 H), 7.82 (d, $^3J = 4.2 \text{ Hz}$, 1 H).

$^{13}\text{C-NMR}$ (101 MHz, CDCl_3): δ [ppm] = 67.3 (s), 70.8 (s), 123.2 (s), 128.7 (s), 151.2 (s), 153.4 (s).

HRMS (ESI): m/z calculated for $\text{C}_6\text{H}_7\text{NO}_4\text{S}$ [$\text{M} + \text{formic acid} - \text{H}$] $^-$: 234.0078, found: 234.0077.

1-(5'-nitrofur-2'-yl)ethan-1-ol (**12**)

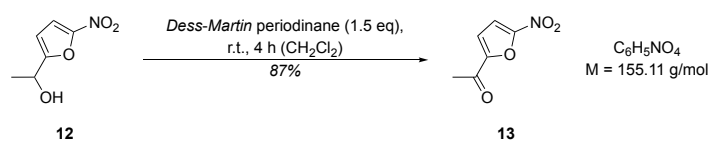
The synthesis was carried out analogously to a published procedure.^[166] Titanium(IV) chloride (27.6 mL, 1.0 M in dichloromethane, 5.24 g, 27.6 mmol, 1.3 eq) was slowly dissolved in dry diethyl ether (40 mL) under argon atmosphere. The solution was cooled to $-78\text{ }^\circ\text{C}$ and methyllithium (17.5 mL, 1.6 M in diethyl ether, 608 mg, 27.6 mmol, 1.3 eq) was added dropwise. After the reaction mixture was stirred for 1.5 hours at $-78\text{ }^\circ\text{C}$, a solution of aldehyde **11** (3.0 g, 21.3 mmol, 1.0 eq) in dry diethyl ether (48 mL) was slowly added at $-78\text{ }^\circ\text{C}$. The reaction mixture was allowed to slowly warm to room temperature overnight. Subsequently, the reaction was quenched by the addition of water (33 mL) at $0\text{ }^\circ\text{C}$ and the aqueous phase was extracted with ethyl acetate ($6 \times 26\text{ mL}$). Subsequently, the combined organic phases were washed with saturated sodium chloride (30 mL), dried over sodium sulfate and concentrated under reduced pressure. The crude product was purified by flash chromatography (pentane/ethyl acetate 4:1) to yield alcohol **12** (2.55 g, 16.2 mmol, 76%) as brown oil.

TLC: $R_f = 0.34$ (pentane/ethyl acetate 1:1) [KMnO_4/UV].

$^1\text{H-NMR}$ (500 MHz, CDCl_3): δ [ppm] = 1.61 (d, $^3J = 6.6\text{ Hz}$, 3 H), 2.16 (br, 1 H), 4.96 (q, $^3J = 6.6\text{ Hz}$, 1 H), 6.50 (dd, $^4J = 0.8\text{ Hz}$, $^3J = 3.7\text{ Hz}$, 1 H), 7.27 (d, $^3J = 3.7\text{ Hz}$, 1 H).

$^{13}\text{C-NMR}$ (126 MHz, CDCl_3): δ [ppm] = 21.6 (s), 63.9 (s), 108.7 (s), 112.6 (s), 151.8 (s), 161.3 (s).

HRMS (ESI): m/z calculated for $\text{C}_6\text{H}_7\text{NO}_4$ [$\text{M} + \text{formic acid} - \text{H}$]⁻: 202.0357, found: 202.0357.

1-(5'-nitrofur-2'-yl)ethan-1-one (**13**)

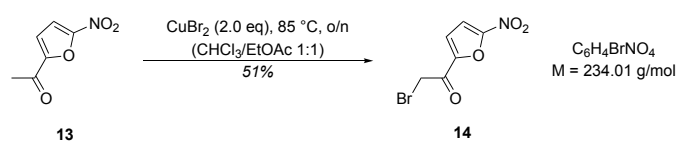
The synthesis was carried out analogously to a published procedure.^[166] To a solution of alcohol **12** (2.55 g, 16.2 mmol, 1.0 eq) dissolved in dichloromethane (189 mL) was added *Dess-Martin* periodinane (10.3 g, 24.3 mmol, 1.5 eq) in small portions. After stirring at room temperature for four hours, the reaction was quenched by the addition of saturated sodium thiosulfate (136 mL) and saturated sodium bicarbonate (136 mL). The mixture was filtered through Celite[®] and the aqueous phase was extracted with ethyl acetate (3 × 80 mL). The combined organic phases were washed with saturated sodium chloride (136 mL), dried over sodium sulfate and concentrated under reduced pressure. The crude product was purified by flash chromatography (pentane/ethyl acetate 4:1) to yield methyl ketone **13** (2.18 g, 14.1 mmol, 87%) as yellow crystals.

TLC: $R_f = 0.52$ (pentane/ethyl acetate 1:1) [KMnO₄/UV].

¹H-NMR (500 MHz, DMSO-*d*₆): δ [ppm] = 2.53 (s, 3 H), 7.70 (d, ³*J* = 3.9 Hz, 1 H), 7.80 (d, ³*J* = 3.9 Hz, 1 H).

¹³C-NMR (126 MHz, DMSO-*d*₆): δ [ppm] = 26.4 (s), 113.2 (s), 119.5 (s), 150.7 (s), 152.2 (s), 186.7 (s).

HRMS (ESI): m/z calculated for C₆H₅NO₄ [M+H]⁺: 156.0291, found: 156.0291.

2-bromo-1-(5'-nitrofuran-2'-yl)ethan-1-one (**14**)

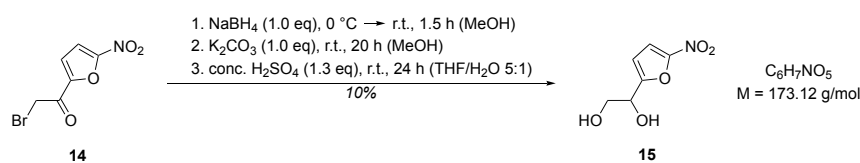
The synthesis was carried out analogously to a published procedure.^[167] The methyl ketone **13** (387 mg, 2.50 mmol, 1.0 eq) was dissolved in a 1:1 mixture of ethyl acetate (5.8 mL) and chloroform (5.8 mL). Copper(II) bromide (1.11 g, 5.00 mmol, 2.0 eq) was added and the mixture was stirred at 85°C overnight. After cooling to room temperature, the mixture was filtered through Celite[®], dried over sodium sulfate and concentrated under reduced pressure. The crude product was purified by flash chromatography (pentane/ethyl acetate 85:15 \rightarrow 7:3) to yield bromomethyl ketone **14** (300 mg, 1.28 mmol, 51%) as brown oil.

TLC: $R_f = 0.42$ (pentane/ethyl acetate 7:3) [KMnO_4/UV].

$^1\text{H-NMR}$ (500 MHz, CDCl_3): δ [ppm] = 4.40 (s, 2 H), 7.40 (d, $^3J = 3.9$ Hz, 1 H), 7.41 (d, $^3J = 3.9$ Hz, 1 H).

$^{13}\text{C-NMR}$ (101 MHz, CDCl_3): δ [ppm] = 29.4 (s), 112.1 (s), 119.1 (s), 149.2 (s), 152.2 (s), 180.5 (s).

HRMS (ESI): m/z calculated for $\text{C}_6\text{H}_4\text{BrNO}_4$ [M-H]⁻: 231.9251, found: 231.9251.

1-(5'-nitrofuranyl)ethan-1,2-diol (**15**)

The synthesis was carried out analogously to a published procedure.^[168] To a solution of bromomethyl ketone **14** (468 mg, 2.00 mmol, 1.0 eq) in dry methanol (5.1 mL) was added sodium borohydride (75.7 mg, 2.00 mmol, 1.0 eq) at 0 °C. After stirring at room temperature for 90 minutes, potassium carbonate (276 mg, 2.00 mmol, 1.0 eq) was added and stirring was continued for an additional 20 hours. The reaction was quenched by the addition of water (4.1 mL) and the aqueous phase was extracted with ethyl acetate (3 × 5 mL). The combined organic phases were washed with saturated sodium chloride (2 × 5 mL), dried over sodium sulfate and concentrated under reduced pressure. The crude reaction product was dissolved in a mixture of tetrahydrofuran (14.8 mL) and water (3 mL) and concentrated sulfuric acid (144 μL, 255 mg, 2.6 mmol, 1.3 eq) was slowly added. After stirring for 24 hours at room temperature, the reaction was neutralized by the addition of saturated sodium bicarbonate and extracted with ethyl acetate (3 × 20 mL). The combined organic phases were washed with saturated sodium chloride (20 mL), dried over sodium sulfate and concentrated under reduced pressure. The crude product was purified by flash chromatography (pentane/ethyl acetate 2:3 → 1:4) to yield caging group **15** (34.4 mg, 0.20 mmol, 10%) as brown oil.

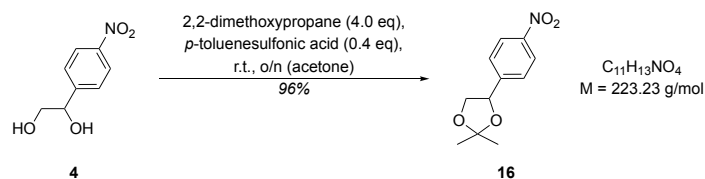
TLC: R_f = 0.17 (pentane/ethyl acetate 2:3) [KMnO₄/UV].

¹H-NMR (400 MHz, CD₃CN): δ [ppm] = 3.09 (br, 1 H), 3.74 (t, ³*J* = 5.5 Hz, 2 H), 3.86 (br, 1 H), 4.72 (t, ³*J* = 5.5 Hz, 1 H), 6.62 (d, ³*J* = 3.7 Hz, 1 H), 7.38 (d, ³*J* = 3.7 Hz, 1 H).

¹³C-NMR (126 MHz, CD₃CN): δ [ppm] = 65.0 (s), 68.9 (s), 111.4 (s), 113.9 (s), 152.7 (s), 160.6 (s).

5.1.4 Synthesis of caging groups with self-immolative linkers

2,2-dimethyl-4-(4'-nitrophenyl)-1,3-dioxolane (**16**)

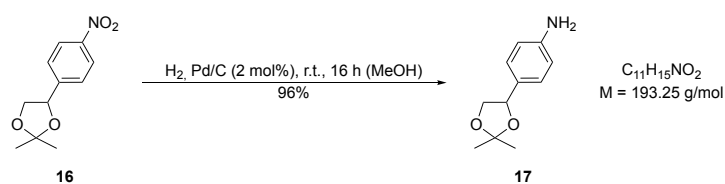


The synthesis was carried out analogously to a published procedure.^[169] To a solution of caging group **4** (183 mg, 1.00 mmol, 1.0 eq) in dry acetone (3 mL) was added 2,2-dimethoxypropane (0.49 mL, 417 mg, 4.00 mol, 4.0 eq) and *p*-toluenesulfonic acid monohydrate (76.8 mg, 0.40 mmol, 0.4 eq) and it was stirred in the dark at room temperature overnight. After the addition of water (15 mL), the aqueous phase was extracted with ethyl acetate (2 × 15 mL). The combined organic phases were washed with saturated sodium chloride (10 mL), dried over sodium sulfate and concentrated under reduced pressure. The crude product was purified by flash chromatography (pentane/ethyl acetate 9:1) to yield the acetonide **16** (214 mg, 0.96 mmol, 96%) as a yellow oil.

TLC: $R_f = 0.29$ (pentane/ethyl acetate 9:1) [KMnO₄/UV].

¹H-NMR (400 MHz, CDCl₃): δ [ppm] = 1.50 (s, 3 H), 1.56 (s, 3 H), 3.69 (t, $^2J = 8.1$ Hz, 1 H), 4.39 (dd, $^3J = 6.7$ Hz, $^2J = 8.1$ Hz, 1 H), 5.17 (t, $^3J = 6.7$ Hz, 1 H), 7.53 (d, $^3J = 8.8$ Hz, 2 H), 8.22 (d, $^3J = 8.8$ Hz, 2 H).

¹³C-NMR (101 MHz, CDCl₃): δ [ppm] = 25.9 (s), 26.6 (s), 71.5 (s), 77.0 (s), 110.7 (s), 124.0 (s), 126.9 (s), 147.2 (s), 147.8 (s).

4-(2',2'-dimethyl-1',3'-dioxolan-4'-yl)aniline (**17**)

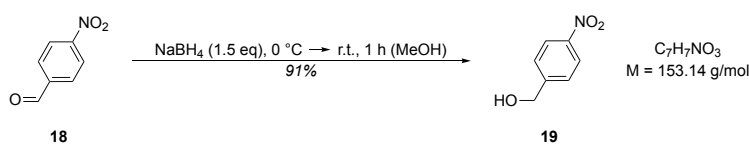
The synthesis was carried out analogously to a published procedure.^[169] Acetonide **16** (1.04 g, 4.66 mmol, 1.0 eq) was dissolved in dry methanol (9.5 mL) and palladium on carbon (99.2 mg, 10 wt% Pd, 0.09 mmol, 2 mol%) was added. The mixture was hydrogenated under a hydrogen balloon for 16 hours. The mixture was filtered through Celite[®] to remove the catalyst and the solvent was removed under reduced pressure. Without any further purification, pure amine **17** (864 mg, 4.47 mmol, 96%) was obtained as an orange oil.

TLC: $R_f = 0.13$ (pentane/ethyl acetate 4:1) [KMnO_4/UV].

¹H-NMR (400 MHz, CD_3CN): δ [ppm] = 1.38 (s, 3 H), 1.45 (s, 3 H), 3.57 (t, $^2,^3J = 8.2$ Hz, 1 H), 4.15 (dd, $^3J = 6.0$ Hz, $^2J = 8.2$ Hz, 1 H), 4.90 (dd, $^3J = 8.2$ Hz, $^3J = 6.0$ Hz, 1 H), 6.62 (d, $^3J = 8.5$ Hz, 2 H), 7.10 (d, $^3J = 8.5$ Hz, 2 H).

¹³C-NMR (101 MHz, CD_3CN): δ [ppm] = 26.2 (s), 27.0 (s), 72.1 (s), 78.8 (s), 109.7 (s), 115.2 (s), 128.4 (s), 128.6 (s), 148.9 (s).

HRMS (ESI): m/z calculated for $\text{C}_{11}\text{H}_{15}\text{NO}_2$ [$\text{M}+\text{H}$]⁺: 194.1175, found: 194.1184.

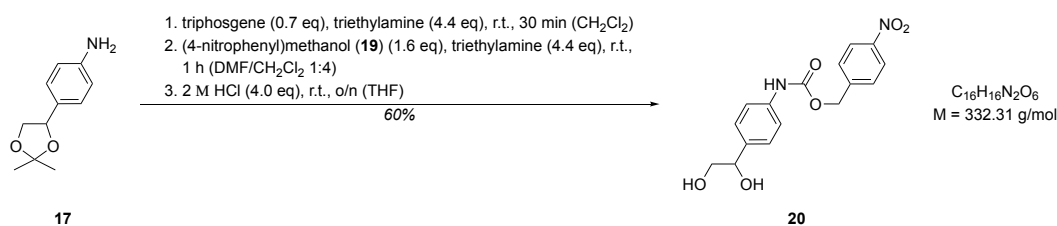
(4'-nitrophenyl)methanol (**19**)

The synthesis was carried out analogously to a published procedure.^[170] To a solution of aldehyde **18** (453 mg, 3.00 mmol, 1.0 eq) in dry methanol (6 mL) was added sodium borohydride (170 mg, 4.50 mmol, 1.5 eq) at 0 °C. After stirring for one hour at room temperature, the reaction was quenched by the addition of 1 M hydrochloric acid (4.5 mL) and it was extracted with ethyl acetate (3 × 20 mL). The combined organic phases were washed with saturated sodium chloride (10 mL), dried over sodium sulfate and concentrated under reduced pressure. The crude product was purified by flash chromatography (pentane/ethyl acetate 3:2 → 1:1) to yield the alcohol **19** (416 mg, 2.72 mmol, 91%) as a light-yellow solid.

TLC: R_f = 0.34 (pentane/ethyl acetate 1:1) [KMnO₄/UV].

¹H-NMR (400 MHz, CDCl₃): δ [ppm] = 1.86 (br, 1 H), 4.84 (s, 2 H), 7.54 (d, ³ J = 8.9 Hz, 2 H), 8.22 (d, ³ J = 8.9 Hz, 2 H).

¹³C-NMR (101 MHz, CDCl₃): δ [ppm] = 64.1 (s), 123.9 (s), 127.2 (s), 147.5 (s), 148.2 (s).

para-nitrophenyl-based caging group with a self-immolative linker **20**

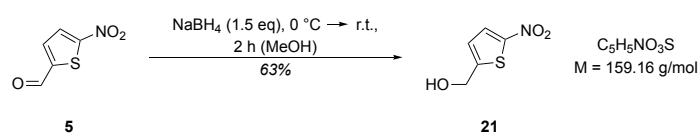
The synthesis was carried out analogously to a published procedure.^[171] To a solution of triphosgene (83.1 mg, 0.28 mmol, 0.7 eq) in dry dichloromethane (10 mL) was added a solution of amine **17** (77.3 mg, 0.40 mmol, 1.0 eq) and triethylamine (244 μ L, 178 mg, 1.76 mmol, 4.4 eq) in dry dichloromethane (10 mL) under argon atmosphere at room temperature. After stirring for 30 minutes at the same temperature, a solution of alcohol **19** (98.0 mg, 0.64 mmol, 1.6 eq) and triethylamine (244 μ L, 178 mg, 1.76 mmol, 4.4 eq) in dry *N,N*-dimethylformamide (4.5 mL) was added and stirred for another hour. The reaction was quenched by the addition of water (12 mL) and the phases were partitioned between water (80 mL) and ethyl acetate (2 \times 80 mL). The combined organic phases were washed with 5% aqueous lithium chloride solution (20 mL), dried over sodium sulfate and concentrated under reduced pressure. The crude reaction product was dissolved in dry tetrahydrofuran (4.5 mL) and diluted hydrochloric acid (800 μ L, 2 M in water, 58.3 mg, 1.60 mmol, 4.0 eq) was added and stirred at room temperature overnight. It was neutralized to pH = 6 with saturated sodium bicarbonate and extracted with ethyl acetate (3 \times 10 mL). The combined organic extracts were dried over sodium sulfate and concentrated under reduced pressure. The crude product was purified by flash chromatography (pentane/ethyl acetate 1:4) to yield the *para*-nitrophenyl-based caging group with a self-immolative linker **20** (80.3 mg, 0.24 mmol, 60%) as a light-yellow solid.

TLC: R_f = 0.16 (pentane/ethyl acetate 1:4) [KMnO₄/UV].

¹H-NMR (400 MHz, CD₃CN): δ [ppm] = 2.90 (t, ³ J = 5.6 Hz, 1 H), 3.37-3.49 (m, 2 H), 3.50-3.60 (m, 1 H), 4.60 (dt, ³ J = 7.9 Hz, ³ J = 4.0 Hz, 1 H), 5.28 (s, 2 H), 7.29 (d, ³ J = 8.7 Hz, 2 H), 7.41 (d, ³ J = 8.7 Hz, 2 H), 7.62 (d, ³ J = 8.2 Hz, 2 H), 7.94 (br, 1 H), 8.23 (d, ³ J = 8.2 Hz, 2 H).

¹³C-NMR (126 MHz, CD₃CN): δ [ppm] = 65.7 (s), 68.4 (s), 74.6 (s), 119.3 (s), 124.5 (s), 127.7 (s), 128.9 (s), 138.0 (s), 138.6 (s), 145.5 (s), 148.5 (s), 154.2 (s).

HRMS (ESI): m/z calculated for C₁₆H₁₆N₂O₆ [M-H]⁻: 331.0935, found: 331.0948.

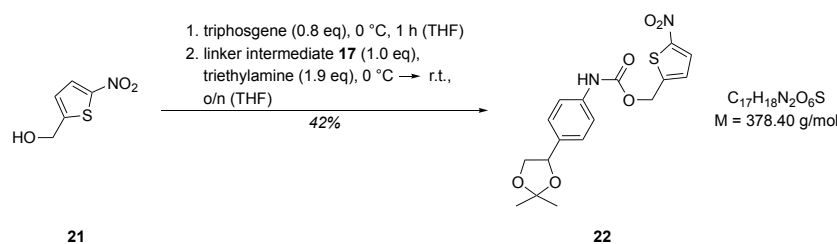
(5'-nitrothiophen-2'-yl)methanol (**21**)

The synthesis was carried out analogously to a published procedure.^[166] To a solution of aldehyde **5** (471 mg, 3.00 mmol, 1.0 eq) in dry methanol (9 mL) was added sodium borohydride (170 mg, 4.50 mmol, 1.5 eq) at 0 °C. After stirring for two hours at room temperature, the reaction was quenched by the addition of 1 M hydrochloric acid (4.5 mL) and it was extracted with ethyl acetate (3 × 20 mL). The combined organic phases were washed with saturated sodium chloride (15 mL), dried over sodium sulfate and concentrated under reduced pressure. The crude product was purified by flash chromatography (pentane/ethyl acetate 3:2) to yield the alcohol **21** (303 mg, 1.90 mmol, 63%) as a dark yellow oil.

TLC: $R_f = 0.39$ (pentane/ethyl acetate 1:1) [KMnO₄/UV].

¹H-NMR (400 MHz, CDCl₃): δ [ppm] = 2.32 (s, 1 H), 4.88 (s, 2 H), 6.93 (d, $^3J = 4.2$ Hz, 1 H), 7.81 (d, $^3J = 4.2$ Hz, 1 H).

¹³C-NMR (101 MHz, CDCl₃): δ [ppm] = 60.4 (s), 123.6 (s), 128.9 (s), 151.1 (s), 153.4 (s).

Protected thiophene-based caging group with a self-immolative linker **22**

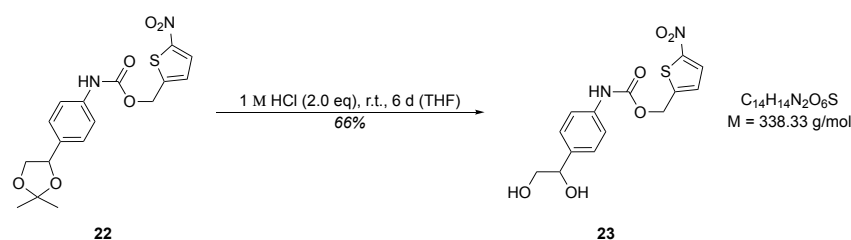
The synthesis was carried out analogously to a published procedure.^[172] To a solution of triphosgene (95.0 mg, 0.32 mmol, 0.8 eq) in dry tetrahydrofuran (2 mL) was added a solution of alcohol **21** (66.8 mg, 0.42 mmol, 1.1 eq) in dry tetrahydrofuran (2 mL) under argon atmosphere at 0 °C. After stirring for one hour at the same temperature, a solution of linker intermediate **17** (77.3 mg, 0.40 mmol, 1.0 eq) in dry tetrahydrofuran (2 mL) and triethylamine (105 μ L, 76.9 mg, 0.76 mmol, 1.9 eq) was added and the reaction was allowed to slowly warm to room temperature overnight. The reaction was quenched by the addition of water (10 mL), it was neutralized to pH = 6 with saturated sodium bicarbonate and extracted with ethyl acetate (3 \times 20 mL). The combined organic extracts were dried over sodium sulfate and concentrated under reduced pressure. The crude product was purified by HPLC (method A) to yield the product **22** (63.8 mg, 0.17 mmol, 42%) as light-yellow solid.

HPLC: t_R = 20.7 min (method A).

1H -NMR (400 MHz, CD_3CN): δ [ppm] = 1.40 (s, 3 H), 1.47 (s, 3 H), 3.59 (t, 3J = 8.0 Hz, 1 H), 4.24 (dd, 3J = 6.2 Hz, 2J = 8.2 Hz, 1 H), 5.01 (dd, 3J = 8.0 Hz, 3J = 6.2 Hz, 1 H), 5.31 (s, 2 H), 7.13 (d, 3J = 4.2 Hz, 1 H), 7.32 (d, 3J = 8.7 Hz, 2 H), 7.43 (d, 3J = 8.7 Hz, 2 H), 7.85 (d, 3J = 4.2 Hz, 1 H), 8.00 (br, 1 H).

^{13}C -NMR (101 MHz, CD_3CN): δ [ppm] = 26.1 (s), 26.8 (s), 61.8 (s), 72.2 (s), 78.2 (s), 110.2 (s), 119.7 (s), 127.8 (s), 127.9 (s), 129.8 (s), 135.6 (s), 139.0 (s), 148.6 (s), 152.7 (s), 154.0 (s).

HRMS (ESI): m/z calculated for $C_{17}H_{18}N_2O_6S$ [M-H]⁻: 377.0813, found: 377.09815.

Thiophene-based caging group with a self-immolative linker **23**

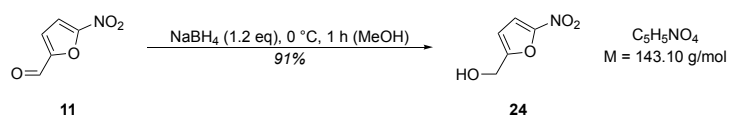
To a solution of acetone **22** (61.6 mg, 0.16 mmol, 1.0 eq) in dry tetrahydrofuran (2 mL) was added diluted hydrochloric acid (326 μ L, 1 M in water, 11.9 mg, 0.33 mmol, 2.0 eq) and it was stirred for six days at room temperature. It was neutralized to pH = 6 with saturated sodium bicarbonate and extracted with ethyl acetate (3 \times 5 mL). The combined organic extracts were dried over sodium sulfate and concentrated under reduced pressure. The crude product was purified by flash chromatography (pentane/ethyl acetate 1:4) to yield the thiophene-based caging group with a self-immolative linker **23** (36.2 mg, 0.11 mmol, 66%) as a light-yellow solid.

TLC: $R_f = 0.20$ (pentane/ethyl acetate 1:4) [KMnO₄/UV].

¹H-NMR (500 MHz, CD₃CN): δ [ppm] = 2.98 (t, $^3J = 6.0$ Hz, 1 H), 3.42-3.51 (m, 2 H), 3.51-3.60 (m, 1 H), 4.61 (dt, $^3J = 7.7$ Hz, $^3J = 3.8$ Hz, 1 H), 5.31 (s, 2 H), 7.14 (d, $^3J = 4.2$ Hz, 1 H), 7.29 (d, $^3J = 8.4$ Hz, 2 H), 7.40 (d, $^3J = 8.4$ Hz, 2 H), 7.86 (d, $^3J = 4.2$ Hz, 1 H), 7.98 (br, 1 H).

¹³C-NMR (126 MHz, CD₃CN): δ [ppm] = 61.8 (s), 68.4 (s), 74.6 (s), 119.4 (s), 127.7 (s), 127.7 (s), 129.8 (s), 138.2 (s), 138.3 (s), 148.6 (s), 152.7 (s), 153.9 (s).

HRMS (ESI): m/z calculated for C₁₄H₁₄N₂O₆S [M-H]⁻: 337.0500, found: 337.0495.

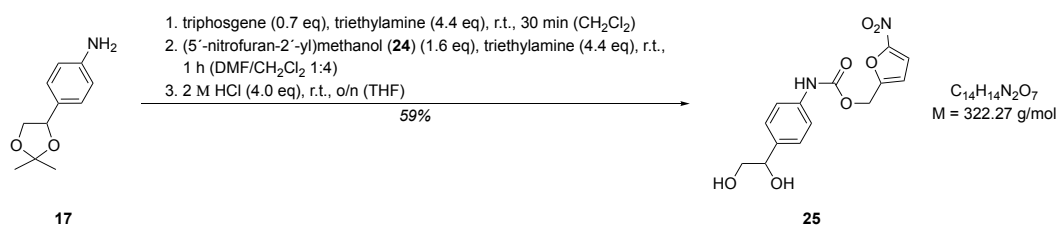
(5'-nitrofuran-2'-yl)methanol (**24**)

The synthesis was carried out analogously to a published procedure.^[166] To a solution of aldehyde **11** (705 mg, 5.00 mmol, 1.0 eq) in dry methanol (15 mL) was added sodium borohydride (227 mg, 6.00 mmol, 1.2 eq) at 0 °C. After stirring for one hour at the same temperature, the reaction was quenched by the addition of 1 M hydrochloric acid (7 mL) and it was extracted with ethyl acetate (3 × 20 mL). The combined organic phases were dried over sodium sulfate and concentrated under reduced pressure. The crude product was purified by flash chromatography (pentane/ethyl acetate 3:2 → 1:1) to yield the alcohol **24** (653 mg, 4.56 mmol, 91%) as a light-yellow solid.

TLC: $R_f = 0.35$ (pentane/ethyl acetate 2:3) [KMnO₄/UV].

¹H-NMR (400 MHz, CDCl₃): δ [ppm] = 2.21 (br, 1 H), 4.72 (s, 2 H), 6.56 (d, ³ $J = 3.6$ Hz, 1 H), 7.29 (d, ³ $J = 3.6$ Hz, 1 H).

¹³C-NMR (101 MHz, CDCl₃): δ [ppm] = 57.6 (s), 110.8 (s), 112.6 (s), 152.1 (s), 157.5 (s).

Furane-based caging group with a self-immolative linker **25**

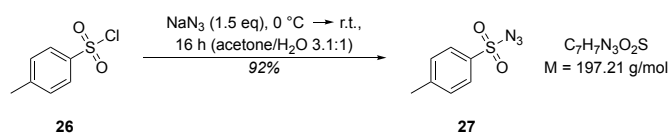
The synthesis was carried out analogously to a published procedure.^[171] To a solution of triphosgene (83.1 mg, 0.28 mmol, 0.7 eq) in dry dichloromethane (10 mL) was added a solution of amine **17** (77.3 mg, 0.40 mmol, 1.0 eq) and triethylamine (244 μ L, 178 mg, 1.76 mmol, 4.4 eq) in dry dichloromethane (10 mL) under argon atmosphere at room temperature. After stirring for 30 minutes at the same temperature, a solution of alcohol **24** (91.6 mg, 0.64 mmol, 1.6 eq) and triethylamine (244 μ L, 178 mg, 1.76 mmol, 4.4 eq) in dry *N,N*-dimethylformamide (4.5 mL) was added and stirred for another hour. The reaction was quenched by the addition of water (12 mL) and the phases were partitioned between water (80 mL) and ethyl acetate (2 \times 80 mL). The combined organic phases were washed with 5% aqueous lithium chloride solution (20 mL), dried over sodium sulfate and concentrated under reduced pressure. The crude reaction product was dissolved in dry tetrahydrofuran (4.5 mL) and diluted hydrochloric acid (800 μ L, 2 M in water, 58.3 mg, 1.60 mmol, 4.0 eq) was added and stirred at room temperature overnight. It was neutralized to pH = 6 with saturated sodium bicarbonate and extracted with ethyl acetate (3 \times 10 mL). The combined organic extracts were dried over sodium sulfate and concentrated under reduced pressure. The crude product was purified by flash chromatography (pentane/ethyl acetate 1:4) to yield the furane-based caging group with a self-immolative linker **25** (76.3 mg, 0.24 mmol, 59%) as a light-yellow solid.

TLC: R_f = 0.13 (pentane/ethyl acetate 1:4) [KMnO₄/UV].

¹H-NMR (500 MHz, CD₃CN): δ [ppm] = 3.00 (br, 1 H), 3.45 (dd, ³ J = 7.8 Hz, ² J = 11.2 Hz, 1 H), 3.50 (br, 1 H), 3.55 (dd, ³ J = 4.1 Hz, ² J = 11.2 Hz, 1 H), 4.60 (dd, ³ J = 7.8 Hz, ³ J = 4.1 Hz, 1 H), 5.18 (s, 2 H), 6.76 (d, ³ J = 3.7 Hz, 1 H), 7.29 (d, ³ J = 8.5 Hz, 2 H), 7.36-7.41 (m, 3 H), 7.93 (br, 1 H).

¹³C-NMR (126 MHz, CD₃CN): δ [ppm] = 58.7 (s), 68.4 (s), 74.6 (s), 113.6 (s), 114.3 (s), 119.4 (s), 127.7 (s), 138.1 (s), 138.3 (s), 153.1 (s), 153.7 (s), 154.5 (s).

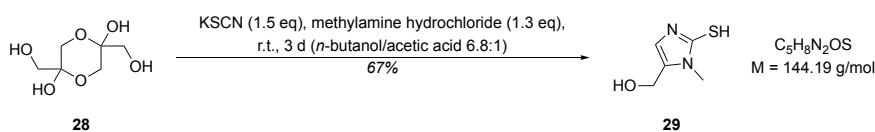
HRMS (ESI): m/z calculated for C₁₄H₁₄N₂O₇ [M-H]⁻: 321.0728, found: 321.0720.

4-methylbenzenesulfonyl azide (**27**)

The synthesis was carried out analogously to a published procedure.^[173] To a solution of tosyl chloride (**26**) (7.82 g, 41.0 mmol, 1.0 eq) in acetone (74.5 mL) was added a solution of sodium azide (4.00 g, 61.5 mmol, 1.5 eq) in water (23 mL) dropwise over one hour at 0 °C. The reaction mixture was allowed to slowly warm to room temperature and stirred for 16 hours. The acetone was removed under reduced pressure at 25 °C and the aqueous phase was extracted with diethyl ether (2 × 37 mL). The combined organic phases were washed with water (2 × 37 mL), 5% sodium bicarbonate (2 × 37 mL), water (2 × 37 mL) and were dried over sodium sulfate. After the removal of the solvent, 4-methylbenzenesulfonyl azide (**27**) (7.41 g, 37.6 mmol, 92%) was obtained as a colorless oil.

¹H-NMR (300 MHz, CDCl₃): δ [ppm] = 2.48 (s, 3 H), 7.33-7.49 (m, 2 H), 7.84 (d, ³J = 8.4 Hz, 2 H).

¹³C-NMR (76 MHz, CDCl₃): δ [ppm] = 21.9 (s), 127.7 (s), 130.4 (s), 135.7 (s), 146.3 (s).

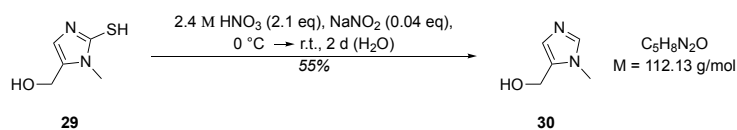
1-methyl-2-mercapto-5-hydroxymethyl-1*H*-imidazole (**29**)

The synthesis was carried out analogously to a published procedure.^[174–176] Dihydroxyacetone dimer (**28**) (20.0 g, 111 mmol, 0.5 eq), potassium thiocyanate (32.4 g, 333 mmol, 1.5 eq) and methylamine hydrochloride (18.7 mg, 278 mmol, 1.3 eq) were suspended in *n*-butanol (170 mL) and glacial acetic acid (25 mL). After the reaction mixture was stirred at room temperature for three days, the reaction was quenched by the addition of water (40 mL). Subsequently, the solid was isolated by filtration, washed with water (100 mL) and diethyl ether (100 mL) to yield 1-methyl-2-mercapto-5-hydroxymethyl-1*H*-imidazole (**29**) (21.3 g, 148 mmol, 67%) as a white powder.

TLC: $R_f = 0.10$ (ethyl acetate) [KMnO_4/UV].

$^1\text{H-NMR}$ (400 MHz, $\text{DMSO-}d_6$): δ [ppm] = 3.45 (s, 3 H), 4.32 (d, $^3J = 5.3$ Hz, 2 H), 5.19 (t, $^3J = 5.3$ Hz, 1 H), 6.80 (s, 1 H), 11.97 (s, 1 H).

$^{13}\text{C-NMR}$ (101 MHz, $\text{DMSO-}d_6$): δ [ppm] = 30.6 (s), 53.0 (s), 112.2 (s), 130.5 (s), 161.7 (s).

(1-methyl-1*H*-imidazol-5-yl)methanol (**30**)

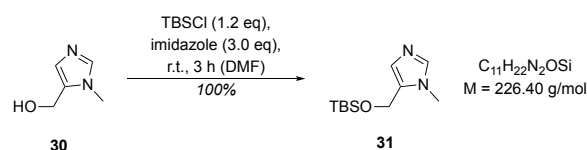
The synthesis was carried out analogously to a published procedure.^[176] Sodium nitrite (197 mg, 2.86 mmol, 0.04 eq) was dissolved in 2.4 M nitric acid (62.5 mL, 9.45 g, 150 mmol, 2.1 eq) at 0 °C and 1-methyl-2-mercapto-5-hydroxymethyl-1*H*-imidazole (**29**) (10.3 g, 71.4 mmol, 1.0 eq) was added in small portions over two hours. After the stirring for another 30 minutes at 0 °C, the reaction mixture was allowed to warm to room temperature and stirred for two days. It was cooled to 0 °C and quenched by the addition of solid sodium hydroxide until pH = 9 was reached. The solvent was removed under reduced pressure and the solid residue was extracted with hot chloroform (3 × 125 mL). After removal of the solvent under reduced pressure, (1-methyl-1*H*-imidazol-5-yl)methanol (**30**) (4.37 g, 39.0 mmol, 55%) was obtained as a light-yellow solid, which was pure enough for further transformations without purification.

TLC: R_f = 0.05 (ethyl acetate/methanol 95:5) [KMnO₄].

¹H-NMR (400 MHz, DMSO-*d*₆): δ [ppm] = 3.60 (s, 3 H), 4.24 (d, ³*J* = 5.0 Hz, 2 H), 5.01 (t, ³*J* = 5.0 Hz, 1 H), 6.76 (s, 1 H), 7.52 (s, 1 H).

¹³C-NMR (101 MHz, DMSO-*d*₆): δ [ppm] = 30.9 (s), 52.5 (s), 127.1 (s), 131.8 (s), 138.5 (s).

HRMS (ESI): *m/z* calculated for C₅H₈N₂O [M+H]⁺: 113.0709, found: 113.0708.

5-(((*tert*-butyldimethylsilyl)oxy)methyl)-1-methyl-1*H*-imidazole (**31**)

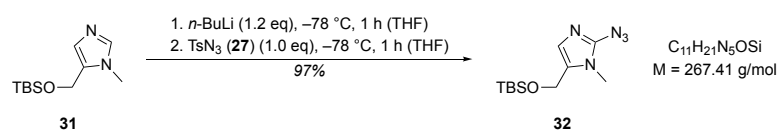
The synthesis was carried out analogously to a published procedure.^[177] To a solution of alcohol **30** (4.37 g, 39.0 mmol, 1.0 eq) in dry *N,N*-dimethylformamide (44 mL) was added imidazole (7.97 g, 117 mmol, 3.0 eq) and *tert*-butyldimethylsilyl chloride (7.05 g, 46.8 mmol, 1.2 eq) under argon atmosphere. After the mixture was stirred for three hours at room temperature, it was quenched by the addition of water (77 mL). Subsequently, it was extracted with diethyl ether ($3 \times 102 \text{ mL}$) and dried over sodium sulfate. The solvent was removed under reduced pressure to yield the protected alcohol **31** (8.83 g, 39.0 mmol, 100%) as an orange solid.

TLC: $R_f = 0.36$ (ethyl acetate/methanol 9:1) [KMnO_4/UV].

$^1\text{H-NMR}$ (500 MHz, CDCl_3): δ [ppm] = 0.05 (s, 6 H), 0.87 (s, 9 H), 3.70 (s, 3 H), 4.65 (s, 2 H), 6.93 (s, 1 H), 7.62 (s, 1 H).

$^{13}\text{C-NMR}$ (101 MHz, CDCl_3): δ [ppm] = -5.3 (s), 18.3 (s), 25.9 (s), 32.0 (s), 55.2 (s), 126.9 (s), 131.3 (s), 138.7 (s).

HRMS (ESI): m/z calculated for $\text{C}_{11}\text{H}_{22}\text{N}_2\text{OSi}$ [$\text{M}+\text{H}$] $^+$: 227.1573, found: 227.1573.

2-azido-5-(((*tert*-butyldimethylsilyl)oxy)methyl)-1-methyl-1*H*-imidazole (**32**)

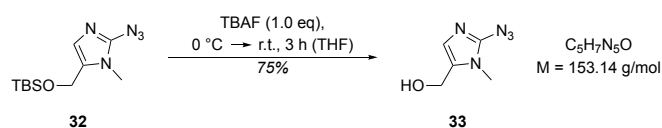
The synthesis was carried out analogously to a published procedure.^[178] *n*-Butyllithium (9.30 mL, 2.5 M in hexane, 1.49 g, 23.2 mmol, 1.2 eq) was added dropwise to a solution of the protected alcohol **31** (4.33 g, 19.1 mmol, 1.0 eq) in dry tetrahydrofuran (37.5 mL) at $-78\text{ }^{\circ}\text{C}$ under argon atmosphere. The reaction mixture was stirred for one hour at this temperature and 4-methylbenzenesulfonyl azide (**27**) (3.72 g, 18.8 mmol, 1.0 eq) was slowly added. Stirring was continued for another hour at $-78\text{ }^{\circ}\text{C}$ and it was quenched by the addition of saturated ammonium chloride (15 mL). The aqueous phase was extracted with ethyl acetate ($3 \times 40\text{ mL}$) and the combined organic phases were washed with saturated sodium chloride (20 mL), water (20 mL) and dried over sodium sulfate. The solvent was removed under reduced pressure to yield the azide **32** (4.89 g, 18.3 mmol, 97%) as a brown oil.

TLC: $R_f = 0.59$ (ethyl acetate) [KMnO₄/UV].

¹H-NMR (400 MHz, CDCl₃): δ [ppm] = 0.05 (s, 6 H), 0.87 (s, 9 H), 3.41 (s, 3 H), 4.56 (s, 2 H), 6.73 (s, 1 H).

¹³C-NMR (101 MHz, CDCl₃): δ [ppm] = -5.2 (s), 18.3 (s), 25.9 (s), 29.7 (s), 55.6 (s), 125.2 (s), 130.4 (s), 141.5 (s).

HRMS (ESI): m/z calculated for C₁₁H₂₁N₅OSi [M+H]⁺: 268.1587, found: 267.1587.

(2-azido-1-methyl-1*H*-imidazol-5-yl)methanol (**33**)

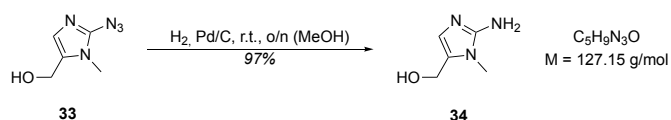
The synthesis was carried out analogously to a published procedure.^[179] To a solution of the protected alcohol **32** (9.10 g, 34.0 mmol, 1.0 eq) in dry tetrahydrofuran (102 mL) was added tetrabutylammonium fluoride (34.0 mL, 1 M in tetrahydrofuran, 8.90 g, 34.0 mmol, 1.0 eq) at 0 °C under argon atmosphere. After stirring for one hour at 0 °C, the reaction was allowed to warm to room temperature over two hours and quenched by the addition of saturated ammonium chloride (63 mL). Tetrahydrofuran was removed under reduced pressure and the aqueous phase was extracted with ethyl acetate (6 × 100 mL). The organic phases were concentrated under reduced pressure and the crude product was purified by flash chromatography (pentane/ethyl acetate 1:9 → 0:1) to yield the alcohol **33** (3.88 g, 25.3 mmol, 75%) as an orange solid.

TLC: $R_f = 0.23$ (ethyl acetate) [KMnO_4/UV].

$^1\text{H-NMR}$ (500 MHz, CDCl_3): δ [ppm] = 3.46 (s, 3 H), 4.55 (s, 2 H), 6.80 (s, 1 H).

$^{13}\text{C-NMR}$ (101 MHz, CDCl_3): δ [ppm] = 30.1 (s), 54.5 (s), 123.2 (s), 130.8 (s), 141.3 (s).

HRMS (ESI): m/z calculated for $\text{C}_5\text{H}_7\text{N}_5\text{O}$ $[\text{M}+\text{H}]^+$: 154.0723, found: 154.0722.

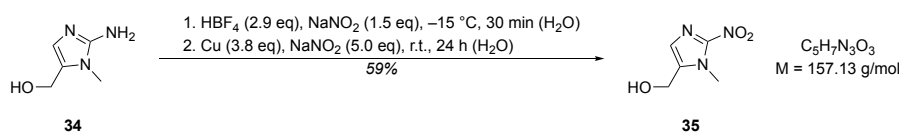
(2-amino-1-methyl-1*H*-imidazol-5-yl)methanol (**34**)

The synthesis was carried out analogously to a published procedure.^[178] Azide **33** (3.88 g, 25.3 mmol, 1.0 eq) was dissolved in dry methanol (40 mL) and palladium on carbon (404 mg, 10 wt% Pd, 0.38 mmol, 1.5 mol%) was added. The mixture was hydrogenated under a hydrogen balloon overnight. The mixture was filtered through Celite[®] to remove the catalyst and the solvent was removed under reduced pressure. Without any further purification, pure amine **34** (3.12 g, 24.5 mmol, 97%) was obtained as an orange solid.

¹H-NMR (400 MHz, DMSO-*d*₆): δ [ppm] = 3.27 (s, 3 H), 4.25 (s, 2 H), 4.73 (s, 1 H), 5.22 (s, 2 H), 6.25 (s, 1 H).

¹³C-NMR (101 MHz, DMSO-*d*₆): δ [ppm] = 28.6 (s), 53.2 (s), 122.2 (s), 126.5 (s), 150.0 (s).

HRMS (ESI): *m/z* calculated for C₅H₉N₃O [M+H]⁺: 128.0818, found: 128.0817.

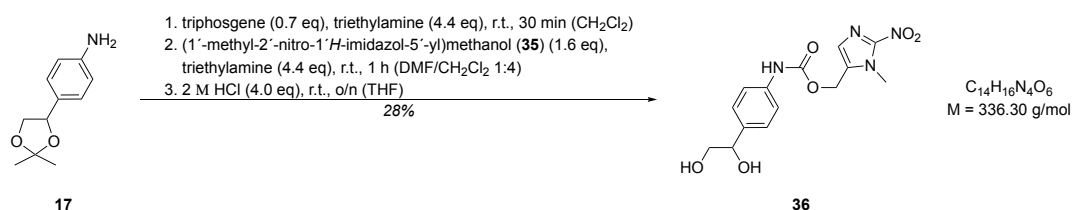
(1-methyl-2-nitro-1*H*-imidazol-5-yl)methanol (**35**)

The synthesis was carried out analogously to a published procedure.^[178] Amine **34** (636 mg, 5.00 mmol, 1.0 eq) was dissolved in tetrafluoroboric acid (2.70 mL, 48 wt% in water, 1.27 g, 14.5 mmol, 2.9 eq) and cooled to -15 °C. A solution of sodium nitrite (517 mg, 7.49 mmol, 1.5 eq) in water (1.6 mL) was added and the reaction mixture was stirred for 30 minutes at -15 °C. The mixture was then added to a suspension of copper powder (1.21 g, 19.0 mmol, 3.8 eq) and sodium nitrite (1.72 g, 24.9 mmol, 5.0 eq) in water (8 mL) at 0 °C. The suspension was allowed to warm to room temperature over 24 hours until no gas evolution was visible. It was extracted with ethyl acetate (3 × 15 mL), dried over sodium sulfate and the solvent was removed. The solid residue was extracted with dichloromethane (2 × 150 mL) under sonication, the combined organic extracts were filtered and concentrated under reduced pressure. Without any further purification, pure product **35** (466 mg, 2.97 mmol, 59%) was obtained as yellow solid.

¹H-NMR (400 MHz, DMSO-*d*₆): δ [ppm] = 3.91 (s, 3 H), 4.54 (s, 2 H), 7.11 (s, 1 H).

¹³C-NMR (101 MHz, DMSO-*d*₆): δ [ppm] = 34.1 (s), 53.0 (s), 126.6 (s), 138.6 (s), 145.7 (s).

HRMS (ESI): *m/z* calculated for C₅H₇N₃O₃ [M+H]⁺: 158.0559, found: 158.0559.

Imidazole-based caging group with a self-immolative linker **36**

The synthesis was carried out analogously to a published procedure.^[171] To a solution of triphosgene (68.3 mg, 0.23 mmol, 0.7 eq) in dry dichloromethane (8.5 mL) was added a solution of amine **17** (63.5 mg, 0.33 mmol, 1.0 eq) and triethylamine (200 μ L, 146 mg, 1.45 mmol, 4.4 eq) in dry dichloromethane (8 mL) under argon atmosphere at room temperature. After stirring for 30 minutes at the same temperature, a solution of alcohol **35** (82.6 mg, 0.53 mmol, 1.6 eq) and triethylamine (200 μ L, 146 mg, 1.45 mmol, 4.4 eq) in dry *N,N*-dimethylformamide (4 mL) was added and stirred for another hour. The reaction was quenched by the addition of water (10 mL) and the phases were partitioned between water (80 mL) and ethyl acetate (2 \times 80 mL). The combined organic phases were washed with 5% aqueous lithium chloride solution (20 mL), dried over sodium sulfate and concentrated under reduced pressure. The crude reaction product was dissolved in dry tetrahydrofuran (4 mL) and diluted hydrochloric acid (640 μ L, 2 M in water, 46.7 mg, 1.28 mmol, 4.0 eq) was added and stirred at room temperature overnight. It was neutralized to pH = 6 with saturated sodium bicarbonate and extracted with ethyl acetate (3 \times 10 mL). The combined organic extracts were dried over sodium sulfate and concentrated under reduced pressure. The crude product was purified by flash chromatography (methanol/ethyl acetate 4:96) to yield the imidazole-based caging group with a self-immolative linker **36** (31.4 mg, 0.09 mmol, 28%) as a light-yellow solid.

TLC: R_f = 0.28 (methanol/ethyl acetate 5:95) [KMnO₄/UV].

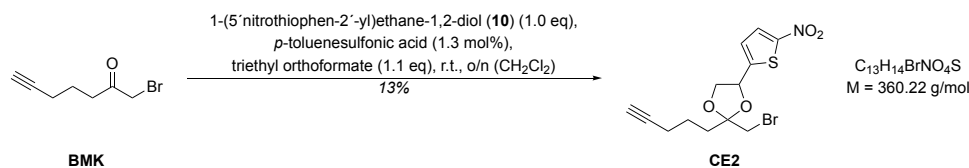
¹H-NMR (500 MHz, CD₃OD): δ [ppm] = 3.55-3.64 (m, 2 H), 4.07 (s, 3 H), 4.63 (t, ³ J = 6.0 Hz, 1 H), 5.29 (s, 2 H), 7.25 (s, 1 H), 7.30 (d, ³ J = 8.3 Hz, 2 H), 7.41 (d, ³ J = 8.3 Hz, 2 H).

¹³C-NMR (126 MHz, CD₃OD): δ [ppm] = 35.0 (s), 56.4 (s), 68.6 (s), 75.5 (s), 119.6 (s), 128.0 (s), 129.5 (s), 134.9 (s), 138.2 (s), 139.2 (s), 147.5 (s), 154.7 (s).

HRMS (ESI): m/z calculated for C₁₄H₁₆N₄O₆ [M-H]⁻: 335.0997, found: 335.0988.

5.1.5 Synthesis of second-generation caged electrophiles

Thiophene-based caged electrophile **CE2**



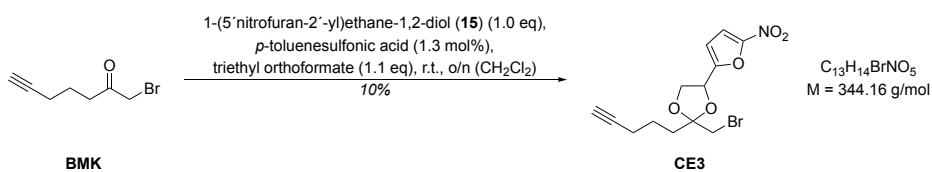
The synthesis was carried out analogously to a published procedure.^[180] To a solution of bromomethyl ketone **BMK** (30.8 mg, 0.16 mmol, 1.1 eq), caging group **10** (28.0 mg, 0.15 mmol, 1.0 eq) and triethyl orthoformate (27.0 μL , 24.1 mg, 0.16 mmol, 1.1 eq) in dry dichloromethane (300 μL) was added a catalytic amount of *p*-toluenesulfonic acid (1.3 mol%) under argon atmosphere. The reaction mixture was stirred at room temperature overnight. After dilution with dichloromethane (3 mL), the reaction mixture was washed with water (3 mL), dried over sodium sulfate and concentrated under reduced pressure. The crude product was purified by HPLC (method B) to yield thiophene-based caged electrophile **CE2** (6.90 mg, 0.02 mmol, 13%) as light-yellow oil with a diastereomer ratio of 57:43.

HPLC: $t_{\text{R}} = 8.0 \text{ min}$ (major, method B).

$t_{\text{R}} = 8.2 \text{ min}$ (minor, method B).

$^1\text{H-NMR}$ (400 MHz, CD_3CN): δ [ppm] = 1.57-1.72 (m, 2 H), 1.96-2.09 (m, 2 H), 2.20 (t, $^4J = 2.7 \text{ Hz}$, 1 H), 2.22-2.29 (m, 2 H), 3.54-3.66 (m, 2 H), 3.84 (dd, $^3J = 6.9 \text{ Hz}$, $^2J = 8.6 \text{ Hz}$, 1 H, major), 3.89 (t, $^3J = 8.4 \text{ Hz}$, 1 H, minor), 4.42-4.51 (m, 1 H), 5.41 (dd, $^4J = 6.5 \text{ Hz}$, $^3J = 8.4 \text{ Hz}$, 1 H, minor), 5.54 (t, $^3J = 6.9 \text{ Hz}$, 1 H, major), 7.09 (dd, $^4J = 6.5 \text{ Hz}$, $^3J = 4.2 \text{ Hz}$, 1 H), 7.87 (d, $^3J = 4.2 \text{ Hz}$, 1 H).

$^{13}\text{C-NMR}$ (101 MHz, CD_3CN): δ [ppm] = 18.7 (s, minor), 18.7 (s, major), 23.2 (s, minor), 23.5 (s, major), 35.7 (s, minor), 35.8 (s, major), 35.9 (s, major), 36.8 (s, minor), 70.1 (s, minor), 70.2 (s, major), 72.8 (s, major), 72.9 (s, minor), 75.4 (s, major), 75.8 (s, minor), 84.8 (s, major), 84.4 (s, minor), 111.4 (s, minor), 111.5 (s, major), 125.8 (s, major), 126.0 (s, minor), 130.1 (s, minor), 130.1 (s, major), 151.6 (s, minor), 152.0 (s), 152.3 (s, major).

Furane-based caged electrophile **CE3**

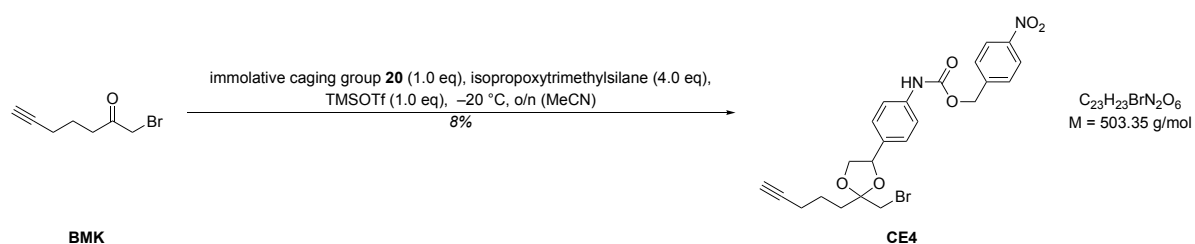
The synthesis was carried out analogously to a published procedure.^[180] To a solution of bromomethyl ketone **BMK** (45.6 mg, 0.24 mmol, 1.1 eq), caging group **15** (38.0 mg, 0.22 mmol, 1.0 eq) and triethyl orthoformate (40.2 μL , 35.8 mg, 0.24 mmol, 1.1 eq) in dry dichloromethane (440 μL) was added a catalytic amount of *p*-toluenesulfonic acid (1.3 mol%) under argon atmosphere. The reaction mixture was stirred at room temperature overnight. After dilution with dichloromethane (4 mL), the reaction mixture was washed with water (4.4 mL), dried over sodium sulfate and concentrated under reduced pressure. The crude product was purified by HPLC (method B) to yield furane-based caged electrophile **CE3** (7.20 mg, 0.02 mmol, 10%) as light-yellow oil with a diastereomer ratio of 64:36.

HPLC: $t_{\text{R}} = 7.2 \text{ min}$ (major, method B).

$t_{\text{R}} = 7.3 \text{ min}$ (minor, method B).

$^1\text{H-NMR}$ (400 MHz, CD_3CN): δ [ppm] = 1.55-1.66 (m, 2 H), 1.97-2.03 (m, 2 H), 2.16 (t, $^4J = 2.8 \text{ Hz}$, 1 H), 2.19-2.27 (m, 2 H), 3.50-3.62 (m, 2 H), 4.11-4.20 (m, 1 H), 4.37-4.44 (m, 1 H), 5.23 (t, $^3J = 7.1 \text{ Hz}$, 1 H, minor), 5.34 (t, $^3J = 6.6 \text{ Hz}$, 1 H, major), 6.73 (d, $^3J = 3.7 \text{ Hz}$, 1 H, major), 6.77 (d, $^3J = 3.7 \text{ Hz}$, 1 H, minor), 7.38 (d, $^3J = 3.7 \text{ Hz}$, 1 H).

$^{13}\text{C-NMR}$ (101 MHz, CD_3CN): δ [ppm] = 18.6 (s), 23.1 (s, minor), 23.2 (s, major), 35.4 (s, minor), 35.5 (s, major), 36.0 (s, major), 36.1 (s, minor), 69.5 (s, major), 69.5 (s, minor), 70.0 (s, major), 70.1 (s, minor), 72.4 (s, major), 72.7 (s, minor), 84.8 (s, major), 84.9 (s, minor), 111.7 (s), 112.7 (s, major), 112.8 (s, minor), 113.5 (s, major), 113.6 (s, minor), 153.3 (s), 155.9 (s, minor), 156.08 (s, major).

para-nitrophenyl-based caged electrophile with a self-immolative linker **CE4**

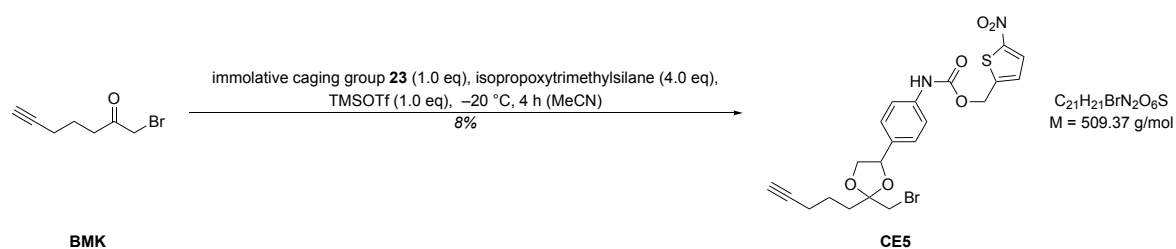
The synthesis was carried out analogously to a published procedure.^[182] Bromomethyl ketone **BMK** (26.5 mg, 0.14 mmol, 1.0 eq), immolative caging group **20** (46.6 mg, 0.14 mmol, 1.0 eq) and isopropoxytrimethylsilane (100 μL , 74.0 mg, 0.61 mmol, 4.0 eq) were dissolved in dry acetonitrile (1.5 mL) and cooled to $-20\text{ }^\circ\text{C}$. Trimethylsilyl trifluoromethanesulfonate (25.0 μL , 31.2 mg, 0.14 mmol, 1.0 eq) was added and the reaction mixture was stirred at $-20\text{ }^\circ\text{C}$ overnight. The reaction was quenched at this temperature by the addition of pyridine (100 μL) and slowly warmed to room temperature. It was diluted with ethyl acetate (10 mL), washed with saturated sodium bicarbonate (5 mL), dried over sodium sulfate and concentrated under reduced pressure. The crude product was purified by flash chromatography (diethyl ether/pentane 3:7 \rightarrow 35:65 \rightarrow 45:55 \rightarrow 55:45) and subsequently by HPLC (method C) to yield *para*-nitrophenyl-based caged electrophile with a self-immolative linker **CE4** (5.30 mg, 0.01 mmol, 8%) as colorless oil with a diastereomer ratio of 6:4.

TLC: $R_f = 0.42$ (diethyl ether/pentane 4:1) [KMnO_4/UV].

HPLC: $t_R = 24.9$ min (method C).

$^1\text{H-NMR}$ (500 MHz, CD_3CN): δ [ppm] = 1.60-1.72 (m, 2 H), 1.96-2.12 (m, 2 H), 2.20 (q, $^4J = 2.4$ Hz, 1 H), 2.21-2.28 (m, 2 H), 3.52-3.68 (m, 3 H, both and minor), 3.72 (dd, $^3J = 9.4$ Hz, $^2J = 8.3$ Hz, 1 H, major), 4.32 (dt, $^3J = 6.2$ Hz, $^2J = 8.3$ Hz, 1 H), 5.07 (dd, $^3J = 9.4$ Hz, $^3J = 6.2$ Hz, 1 H, major), 5.19 (dd, $^3J = 8.6$ Hz, $^3J = 6.3$ Hz, 1 H, minor), 5.28 (s, 2 H), 7.34 (d, $^3J = 8.6$ Hz, 2 H, minor), 7.39 (d, $^3J = 8.6$ Hz, 2 H, major), 7.46 (d, $^3J = 8.6$ Hz, 2 H), 7.62 (d, $^3J = 8.7$ Hz, 2 H), 8.03 (br, 1 H), 8.23 (d, $^3J = 8.7$ Hz, 2 H).

$^{13}\text{C-NMR}$ (126 MHz, CD_3CN): δ [ppm] = 18.7 (s), 23.3 (s, major), 23.3 (s, minor), 35.8 (s, minor), 36.0 (s, major), 36.6 (s, minor), 37.4 (s, major), 65.8 (s), 70.0 (s, major), 70.0 (s, minor), 72.9 (s, major), 73.0 (s, minor), 79.0 (s, minor), 79.7 (s, major), 84.9 (s), 110.1 (s, major), 110.2 (s, minor), 119.4 (s), 124.6 (s), 128.1 (s, minor), 128.2 (s, major), 128.9 (s), 133.3 (s, major), 133.6 (s, minor), 139.6 (s, major), 139.6 (s, minor), 145.5 (s), 148.5 (s), 154.1 (s).

Thiophene-based caged electrophile with a self-immolative linker **CE5**

The synthesis was carried out analogously to a published procedure.^[182] Bromomethyl ketone **BMK** (20.2 mg, 0.11 mmol, 1.0 eq), immolative caging group **23** (36.2 mg, 0.11 mmol, 1.0 eq) and isopropoxytrimethylsilane (76.0 μL , 56.6 mg, 0.43 mmol, 4.0 eq) were dissolved in dry acetonitrile (1.2 mL) and cooled to $-20\text{ }^\circ\text{C}$. Trimethylsilyl trifluoromethanesulfonate (19.0 μL , 23.8 mg, 0.11 mmol, 1.0 eq) was added and the reaction mixture was stirred at $-20\text{ }^\circ\text{C}$ for four hours. The reaction was quenched at this temperature by the addition of pyridine (75 μL) and slowly warmed to room temperature. It was diluted with ethyl acetate (10 mL), washed with saturated sodium bicarbonate (5 mL), dried over sodium sulfate and concentrated under reduced pressure. The crude product was purified twice by HPLC (method C and method D) to yield thiophene-based caged electrophile with a self-immolative linker **CE5** (4.60 mg, 9.03 μmol , 8%) as light-yellow oil with a diastereomer ratio of 54:46.

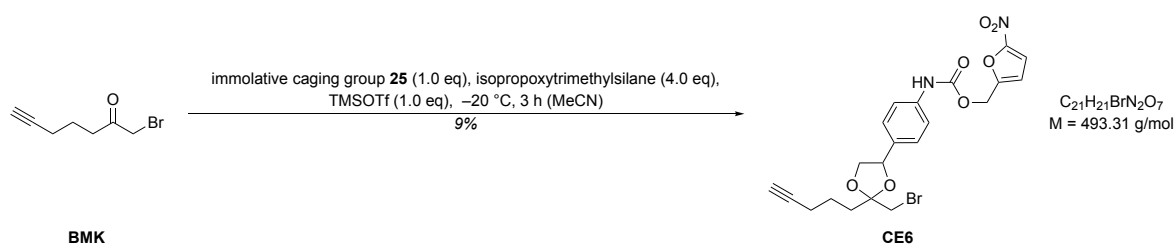
HPLC: $t_{\text{R}} = 18.1 \text{ min}$ (method D).

$^1\text{H-NMR}$ (400 MHz, CD_3CN): δ [ppm] = 1.60-1.72 (m, 2 H), 1.96-2.10 (m, 2 H), 2.19 (t, $^4J = 2.6 \text{ Hz}$, 1 H), 2.25 (td, $^4J = 2.6 \text{ Hz}$, $^3J = 7.0 \text{ Hz}$, 2 H), 3.52-3.67 (m, 3 H, both and minor), 3.72 (dd, $^3J = 9.4 \text{ Hz}$, $^2J = 8.2 \text{ Hz}$, 1 H, major), 4.32 (dd, $^3J = 6.0 \text{ Hz}$, $^2J = 8.2 \text{ Hz}$, 1 H), 5.08 (dd, $^3J = 9.4 \text{ Hz}$, $^3J = 6.0 \text{ Hz}$, 1 H, major), 5.20 (dd, $^3J = 8.6 \text{ Hz}$, $^3J = 6.3 \text{ Hz}$, 1 H, minor), 5.33 (s, 2 H), 7.15 (d, $^3J = 4.3 \text{ Hz}$, 1 H), 7.32-7.48 (m, 4 H), 7.87 (d, $^3J = 4.3 \text{ Hz}$, 1 H), 7.99 (br, 1 H).

$^{13}\text{C-NMR}$ (101 MHz, CD_3CN): δ [ppm] = 18.8 (s), 23.4 (s), 35.9 (s, minor), 36.1 (s, major), 36.6 (s, minor), 38.4 (s, major), 61.9 (s), 70.0 (s, major), 70.1 (s, minor), 73.0 (s), 79.0 (s, minor), 79.8 (s, major), 85.0 (s), 110.2 (s, major), 110.4 (s, minor), 119.7 (s), 127.8 (s), 128.2 (s, minor), 128.2 (s, major), 129.8 (s), 133.7 (s), 139.4 (s), 148.6 (s), 154.0 (s).

Due to low compound amounts the carbon next to the nitro-group could not be detected.

HRMS (ESI): m/z calculated for $\text{C}_{21}\text{H}_{21}\text{BrN}_2\text{O}_6\text{S}$ $[\text{M}-\text{H}]^-$: 507.0231, found: 507.0222.

Furane-based caged electrophile with a self-immolative linker **CE6**

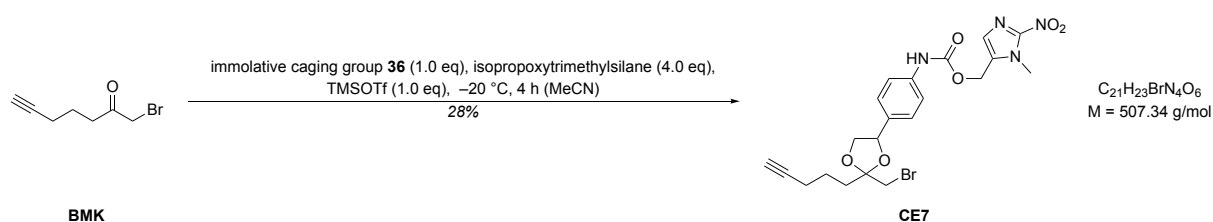
The synthesis was carried out analogously to a published procedure.^[182] Bromomethyl ketone **BMK** (18.1 mg, 0.10 mmol, 1.0 eq), immolative caging group **25** (30.8 mg, 0.10 mmol, 1.0 eq) and isopropoxytrimethylsilane (68.0 μL , 50.6 mg, 0.38 mmol, 4.0 eq) were dissolved in dry acetonitrile (1.1 mL) and cooled to $-20\text{ }^\circ\text{C}$. Trimethylsilyl trifluoromethanesulfonate (17.0 μL , 21.2 mg, 0.10 mmol, 1.0 eq) was added and the reaction mixture was stirred at $-20\text{ }^\circ\text{C}$ for three hours. The reaction was quenched at this temperature by the addition of pyridine (68 μL) and slowly warmed to room temperature. It was diluted with ethyl acetate (10 mL), washed with saturated sodium bicarbonate (5 mL), dried over sodium sulfate and concentrated under reduced pressure. The crude product was purified by HPLC (method C) to yield furane-based caged electrophile with a self-immolative linker **CE6** (4.40 mg, 8.91 μmol , 9%) as light-yellow solid with a diastereomer ratio of 57:43.

HPLC: $t_R = 22.1$ min (method C).

$^1\text{H-NMR}$ (500 MHz, CD_3CN): δ [ppm] = 1.60-1.72 (m, 2 H), 1.95-2.08 (m, 2 H), 2.17-2.20 (m, 1 H), 2.22-2.28 (m, 2 H), 3.52-3.68 (m, 3 H, both and minor), 3.72 (dd, $^3J = 9.4$ Hz, $^2J = 8.2$ Hz, 1 H, major), 4.32 (dt, $^3J = 6.2$ Hz, $^2J = 8.2$ Hz, 1 H), 5.07 (dd, $^3J = 9.4$ Hz, $^3J = 6.2$ Hz, 1 H, major), 5.17-5.23 (m, 3 H, both and minor), 6.77 (d, $^3J = 3.7$ Hz, 1 H), 7.32-7.47 (m, 5 H), 7.94 (br, 1 H).

$^{13}\text{C-NMR}$ (126 MHz, CD_3CN): δ [ppm] = 18.7 (s), 23.3 (s, major), 23.3 (s, minor), 35.8 (s, minor), 36.0 (s, major), 36.5 (s, minor), 37.3 (s, major), 58.8 (s), 70.0 (s, major), 70.0 (s, minor), 72.9 (s, major), 73.0 (s, minor), 79.0 (s, minor), 79.7 (s, major), 84.9 (s), 110.1 (s, major), 110.3 (s, minor), 113.6 (s), 114.4 (s), 119.5 (s), 128.1 (s, minor), 128.2 (s, major), 133.5 (s, major), 133.8 (s, minor), 137.9 (s, minor), 139.4 (s, major), 153.1 (s), 153.7 (s), 154.5 (s).

HRMS (ESI): m/z calculated for $\text{C}_{21}\text{H}_{21}\text{BrN}_2\text{O}_7$ $[\text{M-H}]^-$: 491.0459, found: 491.0458.

Imidazole-based caged electrophile with a self-immolative linker **CE7**

The synthesis was carried out analogously to a published procedure.^[182] Bromomethyl ketone **BMK** (17.7 mg, 0.09 mmol, 1.0 eq), immolative caging group **36** (31.4 mg, 0.09 mmol, 1.0 eq) and isopropoxytrimethylsilane (66.0 μL , 49.4 mg, 0.37 mmol, 4.0 eq) were dissolved in dry acetonitrile (1 mL) and cooled to $-20\text{ }^\circ\text{C}$. Trimethylsilyl trifluoromethanesulfonate (17.0 μL , 20.8 mg, 0.09 mmol, 1.0 eq) was added and the reaction mixture was stirred at $-20\text{ }^\circ\text{C}$ for four hours. The reaction was quenched at this temperature by the addition of pyridine (60 μL) and slowly warmed to room temperature. It was diluted with ethyl acetate (10 mL), washed with saturated sodium bicarbonate (5 mL), dried over sodium sulfate and concentrated under reduced pressure. The crude product was purified by HPLC (method C) to yield imidazole-based caged electrophile with a self-immolative linker **CE7** (13.2 mg, 26.0 μmol , 28%) as light-yellow solid with a diastereomer ratio of 57:43.

HPLC: $t_R = 18.3$ min (method C).

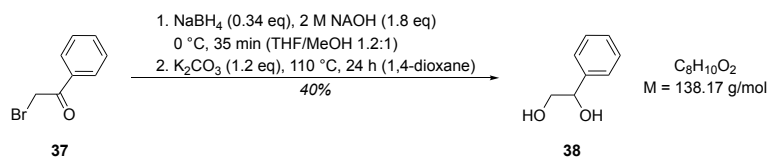
$^1\text{H-NMR}$ (500 MHz, CD_3CN): δ [ppm] = 1.59-1.71 (m, 2 H), 1.96-2.10 (m, 2 H), 2.19 (q, $^4J = 2.6$ Hz, 1 H), 2.22-2.27 (m, 2 H), 3.51-3.66 (m, 3 H, both and minor), 3.71 (dd, $^3J = 9.4$ Hz, $^2J = 8.2$ Hz, 1 H, major), 3.97 (s, 3 H), 4.31 (dt, $^3J = 6.2$ Hz, $^2J = 8.2$ Hz, 1 H), 5.06 (dd, $^3J = 9.4$ Hz, $^3J = 6.2$ Hz, 1 H, major), 5.19 (dd, $^3J = 8.6$ Hz, $^3J = 6.3$ Hz, 1 H, minor), 5.22 (s, 2 H), 7.19 (s, 1 H), 7.31-7.47 (m, 4 H), 7.99 (br, 1 H).

$^{13}\text{C-NMR}$ (126 MHz, CD_3CN): δ [ppm] = 18.7 (s), 23.3 (s, major), 23.3 (s, minor), 35.1 (s), 35.8 (s, minor), 36.0 (s, major), 36.5 (s, minor), 37.4 (s, major), 56.5 (s), 70.0 (s, major), 70.0 (s, minor), 72.9 (s, major), 72.9 (s, minor), 78.9 (s, minor), 79.7 (s, major), 84.9 (s), 110.1 (s, major), 110.2 (s, minor), 119.4 (s), 128.1 (s, minor), 128.2 (s, major), 129.6 (s), 133.4 (s, major), 133.7 (s, minor), 134.1 (s), 139.4 (s), 147.5 (s), 153.7 (s).

HRMS (ESI): m/z calculated for $\text{C}_{21}\text{H}_{23}\text{BrN}_4\text{O}_6$ $[\text{M-H}]^-$: 505.0728, found: 505.0711.

5.1.6 Synthesis of a negative control compound

1-phenylethane-1,2-diol (**38**)



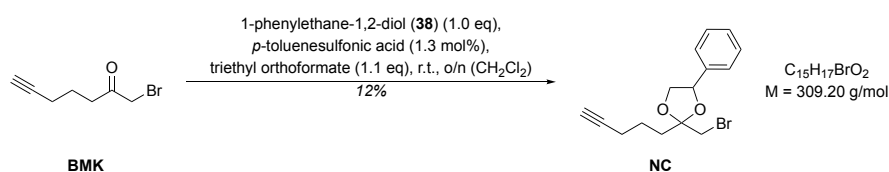
The synthesis was carried out analogously to a published procedure and identical to my Master's thesis.^[159,160,162] To a solution of bromomethyl ketone **37** (2.88 g, 15.0 mmol, 1.0 eq) in methanol (9.75 mL) and tetrahydrofuran (12 mL) was added sodium borohydride (135 mg, 5.10 mmol, 0.34 eq) and 2 M sodium hydroxide (13.7 mL, 1.10 g, 27.5 mmol, 1.8 eq). After stirring at 0°C for 35 minutes, the reaction was quenched by addition of glacial acetic acid to reach $\text{pH} = 6$. The resulting mixture was diluted with ethyl acetate (150 mL) and washed with saturated sodium bicarbonate (110 mL) and saturated sodium chloride (150 mL). It was dried over sodium sulfate and concentrated under reduced pressure. The obtained oil was dissolved in 1,4-dioxane (18 mL), 10% aqueous potassium carbonate (24.0 mL, 2.40 g, 17.4 mmol, 1.2 eq) was added and stirred under reflux for 24 hours. After cooling to room temperature, the reaction was quenched by the addition of 2 M hydrochloric acid until $\text{pH} = 5$ was reached. The reaction mixture was extracted with diethyl ether ($3 \times 54 \text{ mL}$), dried over sodium sulfate and concentrated under reduced pressure. The crude product was purified by flash chromatography (dichloromethane/ethyl acetate 1:1) to yield caging group **38** (820 mg, 5.93 mmol, 40%) as a white solid.

TLC: $R_f = 0.34$ (dichloromethane/ethyl acetate 1:1) [KMnO_4/UV].

$^1\text{H-NMR}$ (400 MHz, $\text{DMSO-}d_6$): δ [ppm] = 3.42 (dd, $^3J = 5.9 \text{ Hz}$, 2 H), 4.52 (q, $^3J = 5.9 \text{ Hz}$, $^3J = 4.2 \text{ Hz}$, 1 H), 4.70 (t, $^3J = 5.9 \text{ Hz}$, 1 H), 5.20 (d, $^3J = 4.2 \text{ Hz}$, 1 H), 7.17-7.36 (m, 5 H).

$^{13}\text{C-NMR}$ (101 MHz, $\text{DMSO-}d_6$): δ [ppm] = 67.5 (s), 73.8 (s), 126.2 (s), 126.7 (s), 127.8 (s), 143.4 (s).

Negative control (NC)



The synthesis was carried out analogously to a published procedure.^[180] To a solution of bromomethyl ketone **BMK** (31.2 mg, 0.17 mmol, 1.1 eq), caging group **38** (20.7 mg, 0.15 mmol, 1.0 eq) and triethyl orthoformate (27.4 μL , 24.4 mg, 0.17 mmol, 1.1 eq) in dry dichloromethane (300 μL) was added a catalytic amount of *p*-toluenesulfonic acid (1.3 mol%) under argon atmosphere. The reaction mixture was stirred at room temperature overnight. After dilution with dichloromethane (2.7 mL), the reaction mixture was washed with water (3 mL), dried over sodium sulfate and concentrated under reduced pressure. The crude product was purified by flash chromatography (pentane/diethyl ether 95:5) to yield negative control **NC** (5.70 mg, 0.02 mmol, 12%) as a colorless oil with a diastereomer ratio of 61:39.

TLC: $R_f = 0.55$ (pentane/diethyl ether 65:35) [KMnO_4/UV].

$^1\text{H-NMR}$ (500 MHz, CDCl_3): δ [ppm] = 1.71-1.81 (m, 2 H), 1.99 (q, $^4J = 2.8$ Hz, 1 H), 2.04-2.20 (m, 2 H), 2.28 (qd, $^4J = 2.8$ Hz, $^3J = 7.1$ Hz, 2 H), 3.45-3.61 (m, 2 H), 3.73 (dd, $^3J = 8.9$ Hz, $^2J = 8.1$ Hz, 1 H, major), 3.82 (dd, $^3J = 9.4$ Hz, $^2J = 8.3$ Hz, 1 H, minor), 4.34-4.44 (m, 1 H), 5.12 (dd, $^3J = 9.4$ Hz, $^3J = 6.0$ Hz, 1 H, minor), 5.24 (dd, $^3J = 8.9$ Hz, $^3J = 6.3$ Hz, 1 H, major), 7.31-7.45 (m, 5 H).

$^{13}\text{C-NMR}$ (101 MHz, CDCl_3): δ [ppm] = 18.6 (s, minor), 18.6 (s, major), 22.7 (s, minor), 22.7 (s, major), 35.6 (s, major), 35.7 (s, minor), 35.7 (s, major), 36.2 (s, minor), 69.0 (s, minor), 69.0 (s, major), 72.7 (s, minor), 72.8 (s, major), 79.0 (s, major), 79.5 (s, minor), 84.0 (s), 109.7 (s, minor), 109.8 (s, major), 126.4 (s, minor), 126.5 (s, major), 128.6 (s, minor), 128.8 (s, major), 128.8 (s), 137.6 (s, minor), 137.6 (s, major).

5.2 Biochemistry

5.2.1 Cloning of NfsA and NfsB

All cloning experiments were conducted according to a published procedure^[75] and identical as in my Master's thesis.^[162] *N*-terminal 6×His-tagged constructs of *E. coli* BW25113^[161] NfsA (UniProt code: P17117) and NfsB (UniProt code: P38489) were cloned into pET28a+ expression vectors using standard techniques based on polymerase chain reaction (PCR), restriction, digestion and ligation. PCRs were carried out in a CFX96 Real-time System in combination with a C1000 Thermal Cycler (BioRad). The PCR mixture contained 10 µL GC or HF buffer (NEB), 1 µL dNTP mix (10 mM), 2.5 µL forward primer (10 µM, NfsA: 5'-CTGCAGCATATGACGCCAACCATTGAACTTATTTGT-3'; NfsB: 5'-CTGCAGCATATGGATATCATTCTGTGCGCCTTAA-3'), 2.5 µL reverse primer (10 µM, NfsA: 5'-GTTAGCGGATCCTTAGCGCGTCGCCCAACCCT-3'; NfsB: 5'-GTTAGCGGATCCCGCTAAATCTTCAACCTGGGAT-3'), 1 µL overnight culture of *E. coli* BW25113^[161] as template, 0.5 µL Phusion High Fidelity DNA polymerase (NEB) and 32.5 µL ddH₂O. After initial denaturation (98 °C, 30 s), the mixtures underwent 35 cycles of denaturation (98 °C, 10 s), annealing (NfsA: 72 °C, NfsB: 71 °C, 20 s) and extension (72 °C, 54 s), before a final extension (72 °C, 10 min). PCR products were purified by agarose gel electrophoresis on a 1% agarose gel run at 90 V for 50 min. After extraction with an E.Z.N.A. Gel Extraction kit (Omega bio-tek), 500 ng of the PCR products were digested in Cut Smart buffer (NEB) in a total volume of 50 µL at 37 °C for 90 min using 5 units of the restriction enzymes NdeI (NEB) and BamHI (Promega), each, which were then inactivated by incubation at 65 °C for 20 min. Isolation of the digest was carried out using an E.Z.N.A. Gel Extraction kit (Omega bio-tek). pET28a+ vector was extracted from NEB5α *E. coli* using a NucleoSpin Plasmid EasyPure kit (Macherey-Nagel). 1 µg vector was digested in Cut Smart buffer (NEB) in a total volume of 50 µL at 37 °C for 1 h using 10 units of NdeI (NEB) and BamHI (Promega), each. In order to dephosphorylate the ends of the restriction sites, 10 units Antarctic phosphatase (NEB) in Antarctic phosphatase buffer (NEB) were added and digestion was continued for another 30 min before heat inactivation at 65 °C for 20 min. Purification of the digested vector was carried out by agarose gel electrophoresis and gel extraction. 14 fmol digested pET28a+ vector and 42 fmol digested insert were ligated using 1 µL Quick Ligase (NEB) in Quick Ligase buffer (NEB) in a total volume of 20 µL. The ligation mixture was incubated at room temperature for 5 min and 5 µL of the ligation product were subsequently transformed into XL1-blue chemically competent cells (Agilent). For this, 50 µL competent

cells were thawed on ice, cautiously mixed with the respective DNA and kept on ice for 30 min. Afterwards, the cells were heat-shocked at 42 °C for 45 s and chilled on ice for 2 min. 500 µL SOC (super optimal broth with catabolite repression, 20 g/L peptone, 5 g/L yeast extract, 600 mg/L NaCl, 200 mg/L KCl, 2 g/L MgSO₄, 20 mM D-glucose) medium were added and the cells incubated (200 rpm, 37 °C) for 1 h. The cells were harvested by centrifugation (6,000 ×g, 2 min), resuspended in SOC medium and plated on LB agar plates containing 250 µg/mL kanamycin. For preparation of the plasmids, 5 mL of LB medium (10 g/L peptone, 5 g/L NaCl, 5 g/L yeast extract, pH = 7.5) containing 250 µg/mL kanamycin were inoculated with single colonies of the transformation and incubated (200 rpm, 37 °C) overnight. Plasmid DNA was prepared using a NucleoSpin Plasmid EasyPure kit (Macherey-Nagel) according to the manufacturer's instructions and sequenced by GeneWiz.

5.2.2 Expression and purification of recombinant NfsA and NfsB

The expression and purification of the recombinant NfsA and NfsB were conducted according to a published procedure^[75] and identical as in my Master's thesis.^[162] Chemically competent *E. coli* BL21(DE3) cells were transformed with the respective plasmids for NfsA and NfsB. For protein overexpression, 20 mL LB medium containing 250 µg/mL kanamycin were inoculated with cryostocks of transformed *E. coli* BL21(DE3) cells and incubated (200 rpm, 37 °C) overnight. 1 L LB medium containing 250 µg/mL kanamycin was inoculated with 10 mL of the overnight culture and incubated (200 rpm, 37 °C). The proteins were expressed at 18 °C overnight after induction at OD₆₀₀ = 0.6 with 1 mM *isopropyl*-β-D-thiogalactoside. Cells were harvested (6,000 rpm, 10 min, 4 °C), washed with 30 mL PBS (8.18 g/L NaCl, 1.78 g/L Na₂HPO₄, 200 mg/L KCl, 240 mg/L K₂HPO₄, pH = 7.4), resuspended in 20 mL wash buffer 1 (20 mM Tris-HCl, pH = 8.0, 150 mM NaCl, 10 mM imidazole) and lysed by sonication (Bandelin Sonoplus) under constant cooling with ice. Lysate was cleared by centrifugation (18,000 rpm, 30 min, 4 °C) and the supernatant was purified. Crude soluble lysate was loaded onto 2 mL of Ni-NTA-agarose beads (Qiagen) equilibrated with wash buffer 1 and flow-through was collected. The column was sequentially washed with 10 column volumes of wash buffer 1, 10 column volumes of wash buffer 2 (20 mM Tris-HCl, pH = 8.0, 1 M NaCl, 10 mM imidazole) and 10 column volumes of wash buffer 3 (20 mM Tris-HCl, pH = 8.0, 150 mM NaCl, 20 mM imidazole). The protein was eluted in 5 mL fractions using elution buffer (20 mM Tris-HCl, pH = 8.0, 150 mM NaCl, 300 mM imidazole). 50 µL of each collected fraction were mixed with 50 µL 2× Laemmli buffer and analyzed by SDS-PAGE with

Coomassie staining. Fractions that contained the purified protein were concentrated using centrifugal filters (Merck) with a 10 kDa cut-off. During the concentration procedure, elution buffer was exchanged for a storage buffer (20 mM Tris-HCl, pH = 8.0, 150 mM NaCl). Purity of the isolated proteins was furthermore analyzed by intact protein MS (IPMS).

5.2.3 Cultivation and lysis of *S. aureus* SH1000 and HEK293 cells

The cultivation and lysis of *Staphylococcus aureus* SH1000^[163] was performed according to a published procedure.^[45,75] *S. aureus* SH1000 was a kind gift from Simon J. Foster, The Krebs Institute, Department of Molecular Biology and Biotechnology, University of Sheffield.^[163]

For experiments in lysate, day cultures were inoculated with 5 μ L of a glycerol stock into 5 mL of B medium (10 g/L peptone, 5 g/L NaCl, 5 g/L yeast extract, 1 g/L K₂HPO₄) and grown for ~8 h (200 rpm, 37 °C). B medium was inoculated 1:100 with a day culture and incubated (200 rpm, 37 °C) until 1 h after it reached the stationary phase (OD₆₀₀ \approx 6). The cells were harvested by centrifugation (6,000 \times g, 10 min, 4 °C), pellets of 100 mL initial culture were pooled and the pellets were washed two times with PBS prior to the immediate use or storage at -80 °C. 5 mL PBS were added to the bacterial pellets and the pellets were resuspended and transferred into 7 mL tubes containing 0.1 mm ceramic beads (PeqLab, 91-PCS-CK01L). Cells were lysed in a Precellys 24 bead mill (3 \times 30 s, 6,500 rpm) while cooling with an airflow that was pre-cooled with liquid nitrogen. The suspension was transferred into a microcentrifuge tube and centrifuged (20,000 \times g, 30 min, 4 °C). The supernatant of several samples was pooled and filtered through a 0.45 μ m filter. Protein concentration of the lysate was determined using a bicinchoninic acid (BCA) assay (typical concentrations were between ~2 mg/mL and ~3 mg/ml) and the concentration was adjusted to 1 mg/mL with PBS. The lysates were used immediately for all MS experiments.

For experiments in living bacteria, overnight cultures were inoculated with 5 μ L of a glycerol stock into 5 mL of B Medium and grown overnight (200 rpm, 37 °C). B medium was inoculated 1:100 with an overnight culture and incubated (200 rpm, 37 °C) until mid-exponential phase (OD₆₀₀ \approx 0.5-1.5) was reached. The cells were harvested by centrifugation (6,000 \times g, 10 min, 4 °C), pellets of 50 mL initial culture were pooled and the pellets were washed two times with PBS. The pellets were resuspended in PBS to OD₆₀₀ = 40 prior to the immediate use.

HEK293 cells were cultured in Dulbecco's Modified Eagle's Medium (DMEM, Sigma Aldrich) supplemented with 10% fetal bovine serum (FBS, Sigma Aldrich) and

2 mM L-glutamine at 37 °C with 5% CO₂. The cells were routinely tested for mycoplasma contamination. For experiments in living cells, cells were grown to ~90% confluency, washed with PBS, detached with 1 mL Accutase solution (Sigma Aldrich) and taken up in 9 mL DMEM. 20 µL of the cells were diluted 1:1 with 0.5% trypan blue solution and counted using a Neubauer improved cell counting chamber. The cells were diluted with PBS to a final concentration of 375,000 cells/mL and 2 mL of this suspension (750,000 cells) were seeded into each well of a 6-well plate that was precoated with a 0.01% poly-L-lysine hydrobromide (molecular weight 70,000-150,000 g/mol) solution. The cells were grown overnight to ~90% confluency and washed with PBS prior to the immediate use.

5.2.4 Gel-based labelling experiments in bacterial lysate

The gel-based labelling experiments in bacterial lysate were performed with different conditions to optimize the labelling properties of the respective probes according to a protocol established in my Master's thesis.^[162] As reaction buffer and for making cofactor stock solutions a 50 mM phosphate buffer (28.9 mM Na₂HPO₄, 21.1 mM NaH₂PO₄·H₂O, pH = 7.0) was used in preincubation experiments and PBS was used in coincubation experiments.

For preincubation experiments, 1 µL of the respective probe (2 mM stock in DMSO for a final concentration of 10 µM), 1 µL flavin mononucleotide (FMN, 2.5 mM stock in 50 mM phosphate buffer for a final concentration of 12.5 µM), 2 µL nicotinamide adenine dinucleotide (phosphate) (NAD(P)H, 50 mM stock in 50 mM phosphate buffer for a final concentration of 500 µM) and 5 µL NfsA/NfsB (NfsA: 509 µM stock in storage buffer for a final concentration of 12.7 µM; NfsB: 505 µM stock in storage buffer for a final concentration of 12.6 µM) were incubated in a total volume of 100 µL 50 mM phosphate buffer for 1 h at room temperature. The reaction was started with the addition of NfsA/NfsB. Different combinations of FMN, NAD(P)H and NfsA/NfsB addition were tested as indicated in the individual experiments, where 50 mM phosphate buffer was added to adjust the total volume. Dimethyl sulfoxide was used instead of probe in control experiments. Subsequently, 100 µL of *S. aureus* SH1000^[163] (1 mg/mL) lysate were added and incubated together with the reaction mixture for 1 h at room temperature.

For coincubation experiments, 1 µL of the respective probe (2 mM stock in DMSO for a final concentration of 20 µM), 1 µL FMN (2.5 mM stock in PBS for a final concentration of 25 µM), 2 µL NAD(P)H (50 mM stock in PBS for a final concentration of 1 mM) and different amounts of NfsA/NfsB (NfsA: 509 µM stock in storage buffer; NfsB: 505 µM stock in storage buffer)

were incubated with equal amounts of *S. aureus* SH1000^[163] (1 mg/mL) lysate in a total volume of 100 μ L PBS for 1 h at either room temperature without shaking or at 37 °C with shaking (300 rpm). The reaction was started with the addition of NfsA/NfsB. Different combinations of FMN, NAD(P)H and NfsA/NfsB addition were tested as indicated in the individual experiments, where PBS was added to adjust the total volume. Dimethyl sulfoxide was used instead of probe in control experiments. To directly compare pre- and coincubation, the coincubation was performed in a total volume of 200 μ L by dilution with PBS to obtain the same volume and concentrations as in the preincubation setup. In the case of dicoumarol addition, 1 μ L dicoumarol (100 \times stock in DMSO, e.g., 1 μ L 10 mM stock for a final concentration of 100 μ M) was coincubated with the reaction mixture.

The samples were clicked to 5-carboxytetramethylrhodamine-azide (TAMRA-azide) by adding 24 μ L (preincubation experiment) or 12 μ L (coincubation experiment) of a click-mix solution consisting of 240 μ L tris(benzyltriazolylmethyl)amine (TBTA, 0.9 mg/mL in 4:1 tBuOH/DMSO), 80 μ L CuSO₄·5H₂O (12.5 mg/mL in H₂O), 80 μ L tris(2-carboxyethyl)phosphine (TCEP, 13 mg/mL in H₂O) and 4 μ L TAMRA-azide (5 mM stock in DMSO). After incubation of the samples at room temperature for 1 h, the reactions were quenched by the addition of 200 μ L (preincubation experiment) or 100 μ L (coincubation experiment) 2 \times Laemmli buffer and analyzed by SDS-PAGE. Modification with TAMRA-azide was detected by in-gel fluorescence scanning and protein loading was visualized by Coomassie staining.

5.2.5 Gel-based labelling experiments in living bacteria

To 100 μ L freshly resuspended living *S. aureus* SH1000^[163] (OD₆₀₀ = 40) was added 1 μ L dimethyl sulfoxide and incubated for 1 h at 37 °C while shaking (200 rpm). Subsequently, it was added 1 μ L of the respective probe (20 mM stock in DMSO for a final concentration of 200 μ M) or 1 μ L dimethyl sulfoxide as a solvent control and incubated for 1 h at 37 °C while shaking (200 rpm). The cells were harvested by centrifugation (6,000 \times g, 10 min, 4 °C) and washed two times with PBS prior to storage at –80 °C overnight. The pellets were resuspended in 200 μ L PBS, 1 μ L lysostaphin (10 mg/mL stock in 20 mM NaOAc buffer, pH = 4.5, Sigma Aldrich) was added and incubated for 1 h at 37 °C while shaking (1,300 rpm). It was added 4 μ L sodium dodecyl sulfate (SDS, 20 wt% in PBS for a final concentration of 0.4 wt%) and sonicated (Bandelin Sonoplus, 10 s, 20% intensity). The lysate was cleared by centrifugation (21,100 \times g, 1 h, r.t.) and 100 μ L of the supernatant were transferred to a new

microcentrifuge tube. The samples were clicked to TAMRA-azide by adding 12 μL of a click-mix solution consisting of 240 μL TBTA (0.9 mg/mL in 4:1 tBuOH/DMSO), 80 μL $\text{CuSO}_4 \cdot 5\text{H}_2\text{O}$ (12.5 mg/mL in H_2O), 80 μL TCEP (13 mg/mL in H_2O) and 4 μL TAMRA-azide (5 mM stock in DMSO). After incubation of the samples at room temperature for 1 h, the reactions were quenched by the addition of 100 μL 2 \times Laemmli buffer and analyzed by SDS-PAGE. Modification with TAMRA-azide was detected by in-gel fluorescence scanning and protein loading was visualized by Coomassie staining.

5.2.6 Gel-based labelling experiments in living HEK293 cells

Solutions of the respective probes or dimethyl sulfoxide as solvent control in PBS were prepared by adding 11 μL of the respective probes (20 mM stock for a final concentration of 200 μM) or 11 μL dimethyl sulfoxide to 1.1 mL PBS. To the freshly prepared and washed HEK293 cells (~90% confluency) in a 6-well plate were added 1 mL of the respective probe or dimethyl sulfoxide solutions and incubated at 37 $^\circ\text{C}$ with 5% CO_2 for 1 h. The cells were investigated under a microscope and photos were taken to analyze the effect of the probes on living cells. The cells were scraped into microcentrifuge tubes, harvested by centrifugation (600 $\times\text{g}$, 4 min, 4 $^\circ\text{C}$) and washed with PBS prior to storage at -80 $^\circ\text{C}$ overnight. The cells were resuspended in 150 μL lysis buffer (1% NP40 substitute, 1% sodium deoxycholate and 0.1% SDS in PBS) and incubated for 10 min on ice. After sonication (Bandeling Sonoplus, 10 s, 20% intensity), the lysate was cleared by centrifugation (21,100 $\times\text{g}$, 20 min, 4 $^\circ\text{C}$) and 100 μL of the supernatant were transferred to a new microcentrifuge tube. The samples were clicked to TAMRA-azide by adding 12 μL of a click-mix solution consisting of 240 μL TBTA (0.9 mg/mL in 4:1 tBuOH/DMSO), 80 μL $\text{CuSO}_4 \cdot 5\text{H}_2\text{O}$ (12.5 mg/mL in H_2O), 80 μL TCEP (13 mg/mL in H_2O) and 4 μL TAMRA-azide (5 mM stock in DMSO). After incubation of the samples at room temperature for 1 h, the reactions were quenched by the addition of 100 μL 2 \times Laemmli buffer and analyzed by SDS-PAGE. Modification with TAMRA-azide was detected by in-gel fluorescence scanning and protein loading was visualized by Coomassie staining.

5.2.7 isoDTB-ABPP experiments in bacterial lysate

The chemoproteomic experiments were performed according to a published procedure.^[45] Two samples of 1.00 mL freshly prepared lysate of *S. aureus* SH1000^[163] (1 mg/mL) were incubated with 10 μ L flavin mononucleotide (FMN, 2.5 mM stock in PBS for a final concentration of 25 μ M), 20 μ L nicotinamide adenine dinucleotide (NADH, 50 mM stock in PBS for a final concentration of 1 mM), 20 μ L NfsB (505 μ M stock in storage buffer for a final concentration of 10 μ M) and 10 μ L of the respective probe (2 mM stock in DMSO for a final concentration of 20 μ M) at 37 °C for 1 h while shaking (300 rpm). One sample was clicked to the heavy and one to the light isoDTB tag by adding 120 μ L of a solution consisting of 60 μ L TBTA ligand (0.9 mg/mL in 4:1 ^tBuOH/DMSO), 20 μ L CuSO₄·5H₂O (12.5 mg/mL in H₂O), 20 μ L TCEP (13 mg/mL in H₂O) and 20 μ L of the respective isoDTB tag (5 mM stock in DMSO). After incubation of the samples at room temperature for 1 h, the light- and the heavy-labeled samples were combined into 8 mL cold acetone in order to precipitate all proteins. Precipitates were stored at –20 °C overnight.

5.2.8 isoDTB-ABPP experiments in living bacteria

The chemoproteomic experiments were performed according to a published procedure.^[45] Two samples of 1.00 mL freshly resuspended living *S. aureus* SH1000^[163] (OD₆₀₀ = 40) were incubated with 10 μ L of the respective probe (20 mM stock in DMSO for a final concentration of 200 μ M) at 37 °C for 1 h while shaking (200 rpm). The cells were harvested by centrifugation (6,000 \times g, 10 min, 4 °C) and washed two times with PBS prior to storage at –80 °C overnight. The pellets were resuspended in 1 mL PBS, 10 μ L lysostaphin (10 mg/mL stock in 20 mM NaOAc buffer, pH = 4.5, Sigma Aldrich) were added and incubated at 37 °C for 1 h while shaking (1,300 rpm). It was added 20 μ L sodium dodecyl sulfate (SDS, 20 wt% in PBS for a final concentration of 0.4 wt%) and sonicated (Bandelin Sonoplus, 10 s, 20% intensity). The lysate was cleared by centrifugation (21,100 \times g, 1 h, r.t.) and 900 μ L of the supernatant were transferred to a new microcentrifuge tube. One sample was clicked to the heavy and one to the light isoDTB tag by adding 108 μ L of a solution consisting of 54 μ L TBTA ligand (0.9 mg/mL in 4:1 ^tBuOH/DMSO), 18 μ L CuSO₄·5H₂O (12.5 mg/mL in H₂O), 18 μ L TCEP (13 mg/mL in H₂O) and 18 μ L of the respective isoDTB tag (5 mM stock in DMSO). After incubation of the samples at room temperature for 1 h, the light- and the heavy-labeled samples were combined into 7.2 mL cold acetone in order to precipitate all proteins. Precipitates were stored at –20 °C overnight.

5.2.9 MS sample preparation

The MS samples were prepared according to a published procedure.^[45,75] The protein precipitates were centrifuged (3,500 rpm, 10 min, r.t.) and the supernatant was removed. The precipitates were resuspended in 1 mL cold methanol by sonification and centrifuged (21,100 ×g, 10 min, 4 °C). The supernatant was removed and this wash step with methanol was repeated one more time. The pellets were dissolved in 300 μL urea (8 M in 0.1 M aqueous triethylammonium bicarbonate (TEAB)) by sonification. 900 μL TEAB (0.1 M in H₂O) were added to obtain a concentration of 2 M urea. This solution was added to 1.2 mL of washed high capacity streptavidin agarose beads (50 μL initial slurry, Fisher Scientific, 10733315) in NP40 substitute (0.2% in PBS). The samples were rotated at room temperature for 1 h in order to assure binding to the beads. The beads were centrifuged (1,000 ×g, 1 min, r.t.) and the supernatant was removed. The beads were resuspended in 600 μL NP40 substitute (0.1% in PBS) and transferred to a centrifuge column (Fisher Scientific, 11894131). Beads were washed with 2 × 600 μL NP40 substitute (0.1% in PBS), 3 × 600 μL PBS and 3 × 600 μL H₂O. The beads were resuspended in 600 μL urea (8 M in 0.1 M aqueous TEAB), transferred to a Protein LoBind tube (Eppendorf) and centrifuged (1,000 ×g, 1 min, r.t.). The supernatant was removed, the beads were resuspended in 300 μL urea (8 M in 0.1 M aqueous TEAB) and incubated with 15 μL dithiothreitol (DTT, 31 mg/mL in H₂O) at 37 °C for 45 min while shaking (200 rpm). They were further treated with 15 μL iodoacetamide (74 mg/mL in H₂O) at room temperature for 30 min while rotating and with 15 μL DTT (31 mg/mL in H₂O) at room temperature for 30 min while rotating. The samples were diluted with 900 μL TEAB (0.1 M in H₂O) and centrifuged (1,000 ×g, 1 min, r.t.). After removal of the supernatant, the beads were resuspended in 200 μL urea (2 M in 0.1 M aqueous TEAB) and incubated with 4 μL trypsin (0.5 mg/mL, Promega, V5113) at 37 °C overnight while shaking (200 rpm). The samples were diluted by adding 400 μL NP40 substitute (0.1% in PBS) and transferred to a centrifuge column (Fisher Scientific, 11894131). Beads were washed with 3 × 600 μL NP40 substitute (0.1% in PBS), 3 × 800 μL PBS and 3 × 800 μL H₂O. Peptides were eluted into Protein LoBind tubes (Eppendorf) with 1 × 200 μL and 2 × 100 μL trifluoroacetic acid (TFA, 0.1% in 50% aqueous MeCN) followed by a final centrifugation (3,000 ×g, 3 min, r.t.). The solvent was removed in a rotating vacuum concentrator (~5 h, 30 °C) and the resulting residue was dissolved in 30 μL TFA (0.1% in H₂O) by sonification for 5 min. Samples were filtered through filters (Merck, UVC30GVNB) washed with the same solvent by centrifugation (17,000 ×g, 3 min, r.t.) and transferred into MS sample vials. Samples were stored at -20 °C until measurement.

5.2.10 Sample analysis by LC-MS/MS

The samples were analyzed according to a published procedure.^[45] 5 μ L of the samples were analyzed using a Qexactive Plus mass spectrometer (ThermoFisher) coupled to an Ultimate 3000 nano HPLC system (Dionex). Samples were loaded on an Acclaim C18 PepMap100 trap column (75 μ m ID \times 2 cm, Acclaim, PN 164535) and washed with 0.1% TFA. The subsequent separation was carried out on an AURORA series AUR2-25075C18A column (75 μ m ID \times 25 cm, Serial No. IO257504282) with a flow rate of 400 nL/min using buffer A (0.1% formic acid in water) and buffer B (0.1% formic acid in acetonitrile). The column was heated to 40 °C. Analysis started with washing in 5% B for 7 min followed by a gradient from 5% to 40% buffer B over 105 min, an increase to 60% B in 10 min and another increase to 90% B in 10 min. 90% B was held for 10 min, then decreased to 5% in 0.1 min and held at 5% for another 9.9 min. The Qexactive Plus mass spectrometer was run in a TOP10 data-dependent mode. In the orbitrap, full MS scans were collected in a scan range of 300-1500 m/z at a resolution of 70,000 and an AGC target of 3e6 with 80 ms maximum injection time. The most intense peaks were selected for MS2 measurement with a minimum AGC target of 1e3 and isotope exclusion and dynamic exclusion (exclusion duration: 60 s) enabled. Peaks with unassigned charge or a charge of +1 were excluded. Peptide match was “preferred”. MS2 spectra were collected at a resolution of 17,500 aiming at an AGC target of 1e5 with a maximum injection time of 100 ms. Isolation was conducted in the quadrupole using a window of 1.6 m/z. Fragments were generated using higher-energy collisional dissociation (HCD, normalized collision energy: 27%) and finally detected in the orbitrap.

5.2.11 isoDTB-ABPP data analysis

The data analysis described in the following sections was performed according to a published procedure.^[45]

General setup of analysis software^[45]

Raw data of the LC-MS/MS analyses was converted into mzML format using the MSconvert tool (version: 3.0.19172-57d620127) of the ProteoWizard software (version: 3.0.19172 64bit)^[184] using standard settings with vendor’s peak picking enabled. For all data analysis it was used the FragPipe interface (version: 14.0) with MSFragger (version: 3.1.1),^[76–81,83]

Philosopher (version: 3.3.10),^[82] IonQuant (version 1.4.6)^[84] and Python (version 3.7.3) enabled.

A FASTA database for *S. aureus* SH1000^[163] was downloaded from www.uniprot.org using a search for “93061” as “Taxonomy [OC]” at UniProtKB on 27.02.2018.^[185] This corresponds to the FASTA database for the strain NCTC8325. Comparative sequencing of these two strains has been reported^[186] and the respective changes have been manually made to the FASTA file. These include several point mutations, the deletion of the partial proteins Q2FWJ0 and Q2FWJ1 as well as the addition of the *rsbU* gene from *S. aureus* Newman (A0A0H3KE27). The reverse sequences were manually added to the FASTA databases.

Analysis of the mass of modifications with FragPipe^[45]

To survey the landscape of all mass shifts observed on peptides in the data sets, an OpenSearch^[76-83] was performed with MSFragger. For this purpose, the following settings were used: Precursor mass tolerance –150 to 1000 Da, (initial) fragment mass tolerance 20 ppm, Calibration and Optimization “Mass calibration, parameter optimization” enabled, Isotope Error “0”, enzyme name “trypsin”, cut after “KR”, but not before “P”, cleavage “enzymatic”, missed cleavages “2”, Clip N-term N enabled, peptide length 7 to 50, peptide mass range 500 to 5,000 Da, no variable modifications, no fixed modifications, all other options were left at the standard settings. Crystal-C^[78] was enabled. PeptideProphet^[80] was run with the following setting: “--nonparam --expectscore --decoyprobs --masswidth 1000.0 --clevel -2”. PTMProphet was disabled. ProteinProphet^[81] was run with the following settings: “--maxppmdiff 2000000”. Generate report was enabled with the following settings: “--sequential --razor --mapmods --prot 0.01”. Run MS1 quant was disabled. Run TMT-Integrator was disabled. PTM-Shepherd^[79] was enabled with the following settings: Smoothing factor “2”, Precursor tolerance “0.01 Da”, Prominence ratio “0.3”, Peak picking width “0.002 Da”, Localization background “4”. Annotation tolerance “0.01 Da”, Custom mass shifts: a custom mass shift list was used including only UniMod modifications with less than 400 Da molecular weight as previously published,^[45] Ion Types for modification with “b” and “y” enabled and mass fragment charge “2”. Generate Spectral Library was disabled. For duplicates, both runs were analyzed as the same experiment. For downstream data analysis, the “global.modsummary.tsv” file was loaded and the values for the number of PSMs (“default-ptmshepherd-dataset (PTMs)”) were plotted against the “Theoretical Mass Shift” in

the mass range between 400 and 1000 Da. The expected and detected mass shifts obtained in the different experiments were listed in Table 2.

Table 2: Expected and detected mass shifts obtained from the MSFragger OpenSearch^[76–83] in the different performed experiments.

experiment	expected mass shift [Da]	detected mass shift [Da]
CE1 in bacterial lysate	589.3336 (light isoDTB tag)	589.3338 (light isoDTB tag)
	595.3411 (heavy isoDTB tag)	595.3412 (heavy isoDTB tag)
CE2 in bacterial lysate	589.3336 (light isoDTB tag)	589.3332 (light isoDTB tag)
	595.3411 (heavy isoDTB tag)	595.3390 (heavy isoDTB tag)
BMK in bacterial lysate	589.3336 (light isoDTB tag)	589.3320 (light isoDTB tag)
	595.3411 (heavy isoDTB tag)	595.3392 (heavy isoDTB tag)
CE1 in living bacteria	589.3336 (light isoDTB tag)	589.3330 (light isoDTB tag)
	595.3411 (heavy isoDTB tag)	595.3396 (heavy isoDTB tag)
CE2 in living bacteria	589.3336 (light isoDTB tag)	589.3320 (light isoDTB tag)
	595.3411 (heavy isoDTB tag)	595.3404 (heavy isoDTB tag)
BMK in living bacteria	589.3336 (light isoDTB tag)	589.3320 (light isoDTB tag)
	595.3411 (heavy isoDTB tag)	595.3390 (heavy isoDTB tag)

Analysis of amino acid selectivity with FragPipe^[45]

To analyze the amino acid selectivity an Offset Search was performed in MSFragger.^[76,77,79–84] For this purpose, the following settings were used in MSFragger: Precursor mass tolerance –20 to 20 ppm, fragment mass tolerance 20 ppm, Calibration and Optimization “None”, Isotope Error “0/1/2”, enzyme name “trypsin”, cut after “KR”, but not before “P”, cleavage “enzymatic”, missed cleavages “2”, Clip N-term N enabled, peptide length 7 to 50, peptide mass range 500 to 5,000 Da, variable modification of 57.02146 Da on C with max. 3 occurrences, no fixed modifications, mass offsets set according to the detected mass shifts (Table 2), all other options were left at the standard settings. Crystal-C^[78] was disabled. PeptideProphet^[80] was run with the following settings: “--nonparam --expectscore --decoyprobs --masswidth 1000.0 --clevel -2”. PTMProphet was disabled. ProteinProphet^[81] was run with the following settings: “--maxppmdiff 2000000”. Generate report was enabled with the following settings: “--sequential --razor --mapmods --prot 0.01”. Run MS1 quant was enabled

with the following settings: IonQuant^[84] enabled, M/Z Window “10 ppm”, RT Window “0.4 min”, Labelling based quant with the detected masses indicated in Table 2 on any amino acid as indicated by “*”, Re-quantify enabled, Top N Ions “3” Min freq. “0.5”, Min exps “1”, Min isotopes “2”, Normalize disabled. Run TMT-Integrator was disabled. PTM-Shepherd^[79] was enabled with the following settings: Smoothing factor “2”, Precursor tolerance 20 ppm, Prominence ratio “0.3”, Peak picking width “20 ppm, Localization background “4”, Annotation tolerance “0.01 Da”, Custom mass shifts: “Failed_Carbamidomethylation:-57.021464”, a custom mass shift list was used including only UniMod modifications with less than 400 Da molecular weight as previously published,^[45] Ion Types for modification with b and y enabled and mass fragment charge “2”. Generate Spectral Library was disabled. For duplicates, both runs were analyzed as the same experiment.

For downstream data analysis, the two “*.tsv” files for the two experiments were individually processed. They were filtered to retain only entries that are present in the “psm.tsv” file, which contains the PSMs filtered by 1% PSM- and protein-level FDR. The column “best locs” indicates the possible residues modified by the mass offset. MSFragger puts the mass offset on each residue one-by-one and calculates hyperscores. The residues with the highest hyperscore are indicated by lower-case letters. Only entries were retained that were localized to a unique residue as seen by containing one lower-case letter (If there is no lower-case letter, the score for the unmodified peptide was higher than that for the best modified peptide and therefore no localization was performed). Next, the entries were filtered for a delta score > 1 , where delta score is the difference of the highest hyperscore and the second highest hyperscore during the localization. For each entry, the UniProt Code was isolated from the column “Protein” and the full protein sequence was linked into the table. Based on this information, all peptide sequences that do not occur exactly once in the identified protein were excluded and the residue number of the modified residue was determined. If the *N*-terminus (modification at amino acid 1 or amino acid 2 if amino acid 1 is not present in the peptide (clipping of *N*-terminal methionine)) or the *C*-terminus (last amino acid of the protein) were modified, this was only counted and labelled as modification of the terminus and not of the respective amino acid at that position. For each entry, an identifier was generated in the format “UniProtCode”_X_”residue number”, where X is the one letter code of the modified amino acid or “N-terminal” or “C-terminal” for terminal modifications. Duplicates of entries with the same identifier were retained only once. The data of both experiments was then combined and only residues were counted in the final analysis that were present in both replicates. The fraction off all sites that was modified at each

amino acid and the termini was reported. In some cases, amino acids with the same reactive group (D+E, N+Q and S+T) were clustered together.

Quantification with FragPipe^[45]

To quantify specific amino acids a Closed Search was performed in MSFragger.^[76,77,80–84] For this purpose, the following settings were used in MSFragger. Precursor mass tolerance –50 to 50 ppm, fragment mass tolerance 20 ppm, Calibration and Optimization “none”, Isotope Error “0/1/2”, enzyme name “trypsin”, cutter after “KR”, but not before “P”, cleavage “enzymatic”, missed cleavages “2”, Clip N-term N enabled, peptide length 7 to 50, peptide mass range 500 to 5,000 Da, no fixed modifications, no mass offsets, all other options were left at the standard settings. Variable modifications were set to the detected masses indicated in Table 2 on cysteines with max. 1 occurrence and additionally a variable modification of 57.02146 Da on cysteines with max. 3 occurrences was added. Crystal-C^[78] was disabled. PeptideProphet^[80] was run with the following settings: “--decoyprobs --ppm --accmass --nonparam --expectscore”. PTMProphet was disabled. ProteinProphet^[81] was run with the following settings: “--maxppmdiff 2000000”. Generate report was enabled with the following settings: “--sequential --razor --mapmods --prot 0.01”. Run MS1 quant was enabled with the following settings: IonQuant^[84] enabled, M/Z Window “10 ppm”, RT Window “0.4 min”, Labelling based quant with the detected masses indicated in Table 2 on cysteines, Re-quantify enabled, Top N ions “3” Min freq. “0.5”, Min expts “1”, Min isotopes “2”, Normalize disabled. Run TMT-Integrator was disabled. PTM-Shepherd^[79] was disabled. Generate Spectral Library was disabled. For duplicates, both runs were analyzed as different experiments.

For downstream data analysis, the “ion_label_quant.tsv” files of the two experiments were analyzed separately. For each entry, the “Modified peptide” was generated as either the “Light Modified Peptide” or the “Heavy Modified Peptide” based on the entry with the higher “PeptideProphet Propability”. The masses of probe modification in the “Modified Peptide” were replaced by an “*” and the mass of carbamidomethylation ([57.0215]) in this entry was deleted, if present. The full protein sequence was linked into the table. Based on this information, all peptide sequences that do not occur exactly once in the same protein were excluded and the residue number of the modified residue was determined. The “identifier” was generated in the format “UniProtCode”_C_”residue number”, where C is the one letter code of the modified amino acid cysteine. For each “identifier”, the averaged “Log2 ratio HL”, which is the log₂ transformed ratio of heavy and light ions, was determined as average of the “Log2

ratio HL” of all corresponding ions weighted with the “Total intensity” of the ion, which was calculated as the sum of “Light Intensity” and “Heavy Intensity” for each ion. The value was disregarded if the standard deviation of the “Log2 ratio HL” values for all ions of the same “Identifier” was > 1.41 . Furthermore, for each “Identifier” the “Total Intensity”, “Total Light Intensity” and “Total Heavy Intensity” were calculated as the sum of all “Total Intensity”, “Light Intensity” and “Heavy Intensity” values of the individual ions, respectively. If several different “Modified peptides” were detected for the same “Identifier”, the “Modified Peptide” and the “Peptide Sequence” with the shortest sequence were kept. For all identifiers, the data for both replicates was now combined into one table. If different “Modified peptides” were detected for the same “Identifier” in the different replicates, the “Modified Peptide” and “Peptide Sequence” with the shortest sequence were kept. The “Total Intensity”, “Total Light Intensity” and “Total Heavy Intensity” was calculated as the sum of all “Total Intensity”, “Total Light Intensity” and “Total Heavy Intensity” values for all replicates, respectively. The “Log2 ratio HL” values for the replicates were named “Log2 ratio HL replicate 1” and “Log2 ratio HL replicate 2”. The average of these two values was calculated and named “Log2 ratio HL”. The value was disregarded, if the standard deviation between the replicates was > 1.41 or if the identifier was only quantified in one of the replicates. The “Log2 ratio HL” data for all “Identifiers” was plotted as a violin plot with all individual values shown. The expected value for the ratio ($\log_2(R) = 0$) as well as the preferred quantification window ($-1 < \log_2(R) < 1$) were indicated by dashed lines.

III Chemoproteomic analysis of the covalent ligandability of *Moraxella catarrhalis*

This chapter is based on the following publication:

M. Zollo, M. Pfanzelt, A. P. A. Janssen, S. M. Hacker, *In situ* chemoproteomic profiling identifies new target proteins for narrow-spectrum antibiotics against the Gram-negative human pathogen *Moraxella catarrhalis*. *Manuscript in preparation*.

Some results of this chapter are further included in the following conference presentation:

M. Zollo, C. Schmidt, P. R. A. Zanon, R. Bonsignore, A. Casini, S. A. Sieber, S. M. Hacker, New Chemoproteomic Technologies and Chemical Modalities for Antibiotic Discovery. *poster presentation and flash talk, EFMC-ISMIC, 4th-8th September 2022*, Nice, France.

Contributions:

MZ and SMH planned the project and all experiments. MZ conducted all experiments and data evaluation. MP developed the assay to determine the enzymatic activity of SirA-like protein. APAJ provided figures for the AlphaFold predictions and established procedures for mining of protein data. MZ and SMH prepared the manuscript for publication with input from all others.

1 The Gram-negative pathogen *Moraxella catarrhalis*

Moraxella catarrhalis is a Gram-negative aerobic diplococcus that in the past was well-known as a harmless commensal bacterium in the human upper respiratory tract.^[187] Over the last decades it became clear that *M. catarrhalis* is also responsible for many diseases of the upper respiratory tract, especially in children, as well as for lower respiratory tract infections in people suffering from chronic obstructive pulmonary disease (COPD). Consequently, *M. catarrhalis* was reclassified and is nowadays accepted as pathogenic bacterium.^[187–189] The most common diseases in children caused by *M. catarrhalis* are sinusitis and otitis media, but also bronchitis and even pneumonia.^[187] Particularly noteworthy is acute otitis media as the major cause for antibiotic usage in childhood, since it was estimated that nearly 80% of all children at least once suffered from this infection by the age of three years. *M. catarrhalis* accounts for approximately 15 to 20% of otitis media infections and thereby belongs to the three major causes for this disease together with *Streptococcus pneumoniae* and *Haemophilus influenzae*.^[187–190] Similarly, together with these two organisms, *M. catarrhalis* was also found in the sputum of adults with COPD representing the second most frequent cause of exacerbations during COPD infection after *H. influenzae*. In total, *M. catarrhalis* thereby is responsible for around 10% of exacerbations, which are two to four million cases annually alone in the US.^[187–189,191] Additionally, some *M. catarrhalis* strains mostly isolated directly from patients suffering from acute otitis media or COPD were reported to be resistant to human serum, which probably increases their overall virulence.^[189,190,192,193] Even more important, the majority of all *M. catarrhalis* strains, that were clinically isolated, show resistance to β -lactam antibiotics due to the production of different β -lactamases. After the first observation of resistance in 1976, the number of resistant strains strongly increased to over 90% of the clinical isolates nowadays, where also reduced susceptibility towards amoxicillin-clavulanic acid was reported, hinting towards additional resistance mechanisms besides β -lactamases.^[187–190,194–197] In addition to the β -lactam resistance of *M. catarrhalis* itself, the production of β -lactamases by *M. catarrhalis* strains also rendered other respiratory tract pathogens e.g. *S. pneumoniae* and *H. influenzae* resistant or less susceptible to a treatment with this class of antibiotics leading to a protective effect of *M. catarrhalis* in coinfections with these other pathogens.^[187–190,194–197]

Overall, *M. catarrhalis* represents an emerging pathogen of the human respiratory tract system and the increasing use of pneumococcal vaccines could further increase the number of respiratory tract infections caused by *M. catarrhalis*.^[187,189,193,198]

2 Scope of the project

In this part of the thesis we aimed to identify the antibacterial activity of a library of electrophiles against Gram-negative *M. catarrhalis* and to study the ligandable cysteinome in living *M. catarrhalis* to develop novel narrow-spectrum antibiotics^[199] that selectively target infections caused by *M. catarrhalis*.

Initially, we investigated a library of more than 200 electrophiles mainly consisting of α -chloroacetamides and α -bromoamides, which were previously analyzed for their ligandability in *S. aureus*,^[75] for their antibacterial activity in *M. catarrhalis* DSM9143 and the β -lactamase-producing *M. catarrhalis* DSM11994.^[200] Further, we selected 14 of the most potent compounds and additionally determined their antibacterial activity in a selection of other Gram-negative and Gram-positive bacteria to evaluate their potential as narrow-spectrum antibiotics.

Next, we aimed to analyze the cysteine reactivity in *M. catarrhalis* DSM11994^[200] analogously to a previous study^[75] in *S. aureus* SH1000^[163] using the residue-specific isoDTB-ABPP workflow.^[75] Thereby, we obtained broad knowledge about the cysteine reactivity in *M. catarrhalis* and could determine that the higher susceptibility of *M. catarrhalis* towards our electrophiles was probably not due to an increased overall cysteine reactivity.

Afterwards, we optimized the residue-specific, competitive isoDTB-workflow^[75] to profile the cysteine ligandability not only in bacterial lysate, but also in living bacteria to also account for uptake or metabolic inactivation of the tested electrophiles.^[75] We could successfully demonstrate the feasibility of our approach in living bacteria and determined a bacterial density of $OD_{600} = 4$ as optimal conditions for future experiments. Using these conditions, we profiled the selected electrophiles to obtain insights into the ligandable cysteinome of *M. catarrhalis* DSM11994.^[200]

Finally, we investigated three ligandable hotspot cysteines in three essential proteins,^[201] C60 in ThiD, C26 in PdxJ and C15 in SirA-like protein that were targeted by many of our tested electrophiles in gel-based and intact protein MS (IPMS) experiments to verify the site-specific binding of our compounds.^[75] Furthermore, we aimed to unravel the enzymatic activity of the poorly characterized SirA-like protein and to show its inhibition upon compound binding. This demonstrated that our chemoproteomic workflow^[75] is capable of identifying novel target proteins that can be exploited in future antibiotic developments.

3 Results and discussion

3.1 Antibacterial activity screening

In the second project of this thesis, we approached antibiotic development from a different angle by developing narrow-spectrum antibiotics that selectively target and kill only specific bacteria. While most of the available antibiotics are active against multiple different bacterial strains simultaneously, the use of these broad-spectrum antibiotics leads to bacterial resistance formation and to the consecutive selection for this resistance not only in the bacterial strain causing the infection, but also in all other pathogenic and non-pathogenic strains present in the human body that are also exposed to the antibiotic. Especially resistance formation in commensal non-pathogenic bacteria can have severe effects since these bacteria can store the resistance information and can possibly transfer their resistance genes to other pathogenic bacteria in the future leading to complicated antibacterial treatments in future infections.^[199] Additionally, broad-spectrum antibiotics not only kill the bacterial strain responsible for the infection, but also target and harm the host microbiome. Disruptions in the microbiome are reported to have long-term negative effects on the human body. Therefore, the use of narrow-spectrum antibiotics selectively targeting only the bacterial strain responsible for the respective infection can have beneficial effects.^[199]

We screened a library of more than 200 electrophilic small molecules consisting of mainly α -chloroacetamides and α -bromoamides, that was previously investigated for their ligandability in *S. aureus* in a study from our group,^[75] for their antibacterial activity in multiple different Gram-positive and Gram-negative bacterial strains. Thereby, we identified that the Gram-negative pathogen *M. catarrhalis* was highly susceptible towards these covalent fragments. In our initial screen in the strain *M. catarrhalis* DSM9143 at a single-point concentration of 12.5 μM , we could identify that 82 of 211 compounds were antibiologically active, which represents a hit rate of $\sim 39\%$. Consequently, we repeated the screening at a lower concentration of 6.3 μM and still found 39 compounds, or 18%, as active. Strikingly, in a screening in the β -lactamase-producing strain *M. catarrhalis* DSM11994^[200] 33 compounds ($\sim 16\%$ hit rate) were still identified as antibiologically active at the lower concentration. Encouraged by these findings of the high susceptibility of *M. catarrhalis* towards our electrophile library, we selected and prioritized 43 compounds based on their initial activity and on structural diversity and performed minimum inhibitory concentration (MIC) assays to determine their antibacterial activity in a concentration-dependent manner starting from 50 μM as the highest tested concentration followed by a two-fold series dilution (Figure 15A).

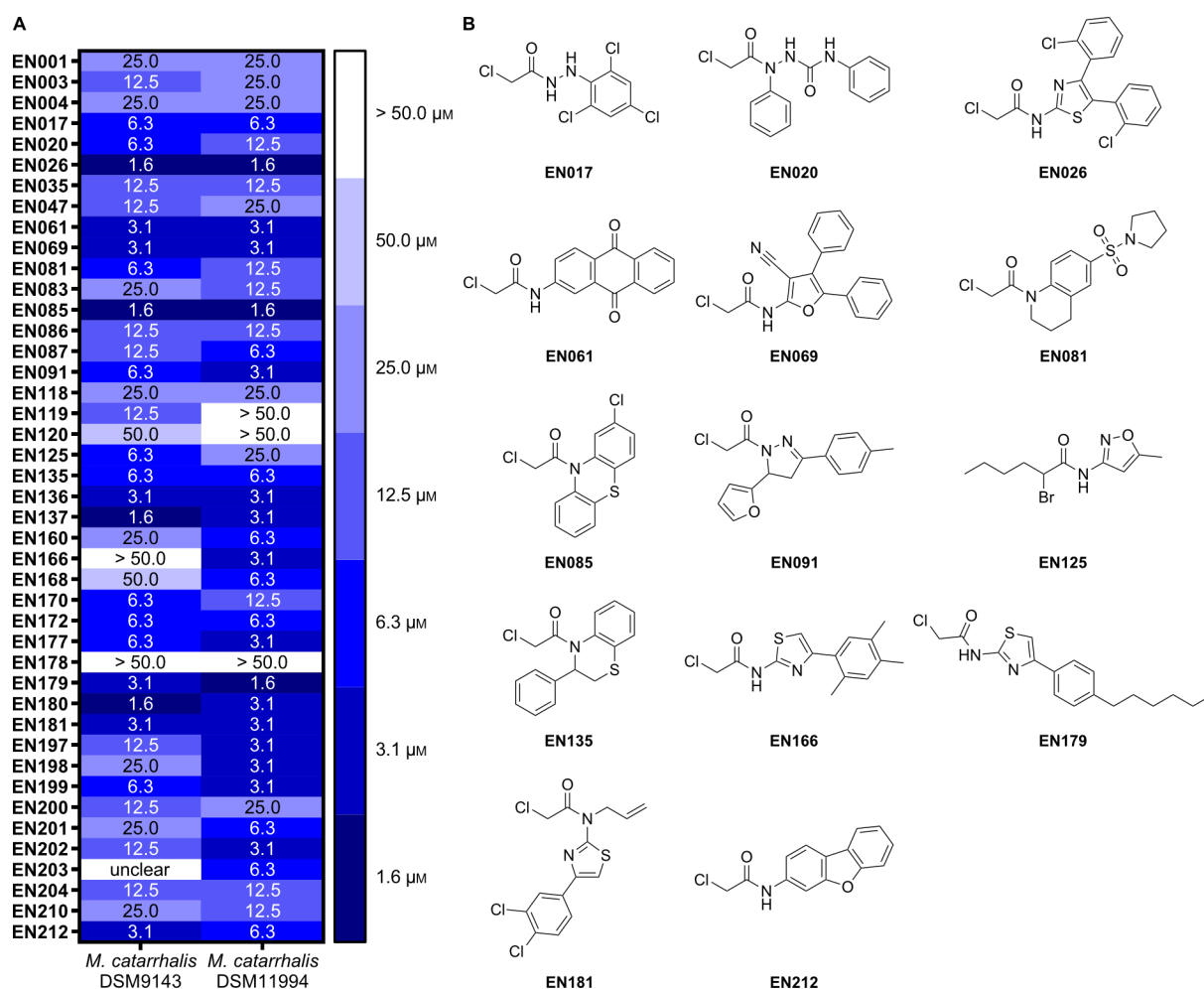


Figure 15: **A** Minimum inhibitory concentration (MIC) in μM of the selected 43 electrophiles in *M. catarrhalis* DSM9143 and in the β -lactamase-producing *M. catarrhalis* DSM11994.^[200] The MIC was determined through the measurement of the optical density of the bacterial culture after 24 h incubation and no growth was defined as $\text{OD}_{600} < 0.1$. The experiments were performed in duplicates and if different concentrations as MIC value were obtained, the higher value was reported as final MIC. If there was bacterial growth at higher concentrations of compound, followed by at least three consecutive lower concentrations without bacterial growth, the lower concentration was reported. In other cases, the MIC was reported as “unclear”. **B** Structures of the 14 compounds that were selected for further cellular target engagement studies.

In this way, we could again verify the high susceptibility of both *M. catarrhalis* strains against our electrophile library and could identify many different compounds displaying high antibacterial activity in the low micromolar concentration range. We further selected 14 of these compounds (Figure 15B) for further target engagement investigations based on their MIC values. 13 of those 14 compounds showed antibacterial activity with $\text{MIC} \leq 6.3 \mu\text{M}$ in *M. catarrhalis* DSM9143 and, more importantly, even 10 of these 13 active compounds remained active with still $\text{MIC} \leq 6.3 \mu\text{M}$ in the β -lactamase-producing strain *M. catarrhalis* DSM11994.^[200] Additionally, we identified **EN166** as not active ($\text{MIC} > 50 \mu\text{M}$)

in *M. catarrhalis* DSM9143, but as active (MIC = 3.1 μM) in the resistant strain *M. catarrhalis* DSM11994.^[200] After we obtained the selection of 14 compounds with promising antibacterial activity in both tested strains, we wanted to investigate their potential as narrow-spectrum antibiotics against *M. catarrhalis* and determined their antibiotic activity at a comparable high concentration of 25.0 μM in a selection of different Gram-positive (*Staphylococcus aureus* SH1000^[163] and *Streptococcus pneumoniae* DSM20566) and Gram-negative (*Klebsiella pneumoniae* DSM30104, *Acinetobacter baumannii* DSM30007 and *Pseudomonas aeruginosa* DSM22644) strains (Figure 16).

EN017	active	active	inactive	inactive	inactive	inactive	inactive	inactive	inactive
EN020	active	active	inactive	inactive	inactive	inactive	inactive	inactive	
EN026	active	active	active	active	inactive	inactive	inactive	inactive	
EN061	active	active	inactive	inactive	inactive	inactive	inactive	inactive	
EN069	active	active	inactive	inactive	inactive	inactive	inactive	inactive	
EN081	active	active	inactive	active	inactive	inactive	inactive	inactive	
EN085	active	active	active	active	inactive	inactive	inactive	inactive	
EN091	active	active	inactive	inactive	inactive	inactive	inactive	inactive	
EN125	active	active	inactive	inactive	inactive	inactive	inactive	inactive	
EN135	active	active	active	active	inactive	inactive	inactive	inactive	
EN166	inactive	active	inactive	inactive	inactive	inactive	inactive	inactive	
EN179	active	active	inactive	inactive	inactive	inactive	inactive	inactive	
EN181	active	active	active	inactive	inactive	inactive	inactive	inactive	
EN212	active	active	inactive	inactive	inactive	inactive	inactive	inactive	
	<i>M. catarrhalis</i> DSM9143	<i>M. catarrhalis</i> DSM11994	<i>S. aureus</i> SH1000	<i>S. pneumoniae</i> DSM20566	<i>K. pneumoniae</i> DSM30104	<i>A. baumannii</i> DSM30007	<i>P. aeruginosa</i> DSM22644	active	

Figure 16: Antibiotic activity of the selected 14 electrophilic compounds at a concentration of 25 μM in both previously tested *M. catarrhalis* strains^[200] and in the Gram-positive *Staphylococcus aureus* SH1000^[163] and *Streptococcus pneumoniae* DSM20566 and in the Gram-negative *Klebsiella pneumoniae* DSM30104, *Acinetobacter baumannii* DSM30007 and *Pseudomonas aeruginosa* DSM22644. The experiment was performed in duplicates and the measured OD₆₀₀ values were averaged. If the averaged OD₆₀₀ < 0.1, the compound was defined as “active”, otherwise as “inactive”.

Even at this relatively high concentration of 25 μM , 9 of the 14 selected compounds did not show any antibiotic activity against the tested Gram-positive strains and even all 14 compounds remained inactive against all three investigated Gram-negative strains.

Summarizing, the high antibacterial activity in the low micromolar concentration range of the selected 14 compounds in *M. catarrhalis* and the overall absence of activity at 25 μM of most of these compounds in all other tested bacterial strains indicated their potential use as narrow-spectrum antibiotics against *M. catarrhalis*.

3.2 Chemoproteomic analysis of cysteine reactivity in *M. catarrhalis*

In the next part of this project and before we investigated the respective targets of the selected 14 compounds, we wanted to assess the overall cysteine reactivity in *M. catarrhalis* to analyze, if the higher susceptibility towards our cysteine-directed electrophiles was due to an enhanced overall cysteine reactivity.

Therefore, we used the residue-specific isoDTB-ABPP workflow developed in our group (Scheme 4).^[75] We adapted the identical workflow with the same cut-off values and definitions as the previous study from our group developed for the analysis of the cysteine reactivity in *S. aureus* in order to directly compare the obtained results from *M. catarrhalis* with the previous findings from *S. aureus*.^[75] In this and all further investigations, we focused only on the resistant, β -lactamase-producing strain *M. catarrhalis* DSM11994.^[200] To analyze the cysteine reactivity, one sample of bacterial lysate was treated with a lower concentration of 10 μ M IA-alkyne and probe-labelled proteins were clicked to the light-labelled isoDTB tag by CuAAC,^[60-63] whereas another sample of lysate was treated with a higher concentration of 100 μ M IA-alkyne and clicked to the respective heavy-labelled isoDTB tag. Afterwards, the two samples were combined, enriched on (strept)avidin and digested with trypsin. The probe-labelled peptides were further eluted from the beads and analyzed by LC-MS/MS. Due to the isotopic pattern of the used isoDTB tags, a reactivity ratio $R_{10:1}$ was generated reflecting the difference in MS1 signal intensity of heavy-labelled (high concentration, 100 μ M) and light-labelled (low concentration, 10 μ M) peptides.^[71,75] While at high concentrations (heavy-labelled) nearly all cysteine will most likely be engaged by IA-alkyne, at a lower concentration (light-labelled) only the more reactive cysteines will be targeted. Consequently, a reactivity ratio $R_{10:1} \gg 1$ was expected for the majority of cysteines and only very highly reactive cysteines will also be quantitatively engaged even at a lower concentration and, therefore, display a ratio of $R_{10:1} \sim 1$. We classified the respective cysteines in three distinct reactivity groups: low reactive cysteines with $R_{10:1} > 5$, medium reactive cysteines with $5 > R_{10:1} > 3$ and high reactive cysteines with $R_{10:1} < 3$. Additionally, we performed the same experiment with both samples treated at the higher concentration of 100 μ M IA-alkyne as a control experiment, where we expected an overall ratio of $R_{1:1} \sim 1$.^[75] We further only analyzed the cysteines that were detected in both experiments. Thereby, we could quantify and detect 1218 different cysteines and the overall ratio $R_{1:1}$ was as expected close to 1 (Figure 17A). Through the reactivity experiment, we could classify 47 of the detected cysteines as highly reactive ($R_{10:1} < 3$, 3.9%), 106 cysteines as medium reactive ($5 > R_{10:1} > 3$, 8.7%) and 1065 cysteines as lowly reactive ($R_{10:1} > 5$, 87.4%).

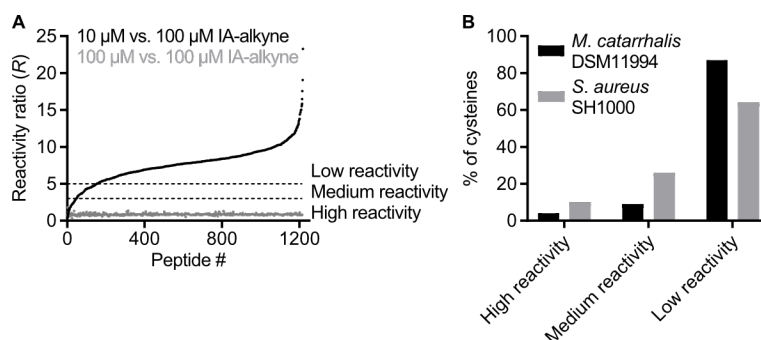


Figure 17: **A** Graph of the reactivity data obtained from *M. catarrhalis* DSM11994.^[200] The reactivity ratio $R_{10:1}$ that was generated by comparing the labelling intensities of samples treated with high concentration (100 μM) with samples treated with low concentration (10 μM) IA-alkyne is displayed in black. The control experiment where both samples were treated at high concentration (100 μM) IA-alkyne and the respective ratio $R_{1:1}$ is displayed in grey.^[75] **B** Comparison of the fraction of cysteines that was classified as highly reactive ($R_{10:1} < 3$), medium reactive ($5 > R_{10:1} > 3$) and lowly reactive ($R_{10:1} > 5$) in *M. catarrhalis* DSM11994^[200] with the respective fractions in *S. aureus* SH1000^[163] determined by a previous study from our group.^[75]

When comparing the obtained fractions of cysteines in the different reactivity groups with the data obtained in *S. aureus* SH1000^[163] by a previous study from our group^[75] (Figure 17B), it could be seen that in *S. aureus* a higher fraction of highly reactive (9.6% vs. 3.9%) and medium reactive (26.1% vs. 8.7%) cysteines were identified.^[75] Consequently, the overall cysteine reactivity in *S. aureus* SH1000^[163] was even higher compared to the investigated reactivity in *M. catarrhalis* DSM11994^[200] and, therefore, the higher sensitivity of *M. catarrhalis* towards the tested electrophile library could not be attributed to enhanced cysteine reactivity.^[75] The observed higher susceptibility despite a lower overall cysteine reactivity peaked our interest to study the reactive cysteinome of *M. catarrhalis* in more detail (Figure 18).

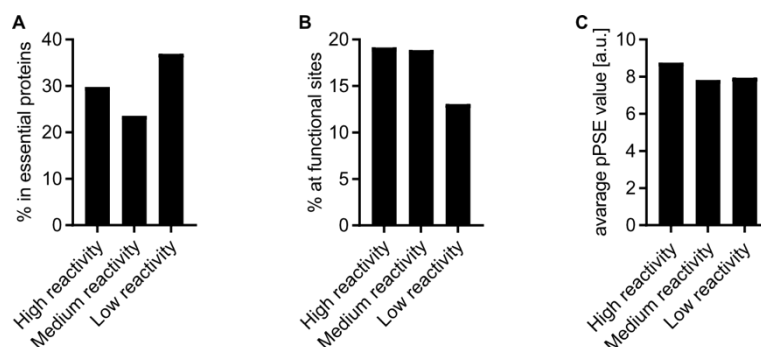


Figure 18: **A, B** Fraction of cysteines in *M. catarrhalis* DSM11994^[200] in the different reactivity groups that were in essential proteins (**A**)^[201] or at functional sites^[185] (**B**).^[75] **C** Averaged pPSE values of the cysteines in the different reactivity groups that were calculated with a recently published tool^[202,203] based on AlphaFold structures^[204,205] to assess the cysteine accessibility.^[202,203]

We found that highly reactive (29.8%) and medium reactive (23.6%) cysteines were less frequently located in essential proteins^[201] compared to lowly reactive cysteines (36.9%, Figure 18A). This observation was in agreement with the previous study from our group in *S. aureus* and probably indicated that highly reactive cysteines are intentionally avoided in essential proteins in order to avoid binding of reactive electrophiles and corresponding toxicity issues.^[75] Similarly, in agreement with the previous study in *S. aureus*^[75] and with a study in human cells,^[71] we identified an enrichment of highly (19.1%) and medium reactive (18.9%) cysteines over lowly reactive cysteines (13.1%) at functional sites^[185] of proteins (Figure 18B), which further strengthened the previous hypothesis that cysteine reactivity might hint towards possible functionality.^[71,75] Furthermore, we wanted to assess if the cysteines in the different reactivity groups also differed in terms of their accessibility for small molecules. Therefore, we utilized a recently published tool^[202,203] that calculates prediction-aware part-sphere exposure (pPSE) values based on AlphaFold structures.^[204,205] These pPSE values were generated through the construction of a cone around the amino acid side chains (12 Å radius, 70° angle), followed by the calculation of how many other C α s of proximal amino acids were within this cone. Consequently, high pPSE values indicate many proximal C α s and therefore a more buried or less accessible cysteine and low pPSE values reflect cysteines that are less buried and more accessible.^[202,203] However, we could only detect minor changes in the pPSE values of the cysteines in the different reactivity groups with only slightly less accessibility of highly reactive cysteines compared to the others (Figure 18C). Due to the only very small differences, no significant correlation of accessibility and reactivity could be obtained.

Nevertheless, in our data we could identify many different highly and medium reactive cysteines at functional sites^[185] in essential proteins.^[201] Furthermore, these proteins are involved in key pathways like tRNA modification (C83 at the active site of GatA (UniProt code: D5V8F8) and C281 at the ATP binding site of Serine-tRNA-ligase (UniProt code: D5VAV4)), RedOx biology (C54 in the RedOx-active disulfide of the Thiol:disulfide interchange protein (UniProt code: D5V944)), the synthesis of lipoylated proteins (C198 forming the acyl-thioester intermediate in LipB (UniProt code: D5VCL4) and C101 and C105 within an iron-sulfur cluster of LipA (UniProt code: D5VA92)), thymidylate synthesis (active site nucleophile C162 of Thymidylate synthase (UniProt code: D5V859)) and cofactor synthesis (C148 at the substrate binding site of RibB involved in the riboflavin synthesis (UniProt code: D5V9A7) and C349 at the CTP binding site of CoaBC involved in CoA synthesis (UniProt code: D5VD96)).^[185]

Summarizing, we could show that the high susceptibility of *M. catarrhalis* was not directly due to enhanced cysteine reactivity and could identify many reactive cysteines within key pathways.

3.3 Chemoproteomic analysis of cysteine ligandability in *M. catarrhalis*

Next, we set out to explore the intracellular target proteins of the previously selected 14 compounds (Figure 15B) utilizing the residue-specific, competitive isoDTB-ABPP workflow (Scheme 4).^[75] In contrast to the above-mentioned reactivity experiments, one sample of bacteria was treated with the respective electrophile, whereas another identical sample was treated with DMSO as a solvent control instead.^[75] Afterwards, both samples were treated with the broadly-reactive IA-alkyne at equal concentrations and the compound-treated samples were clicked by CuAAC^[60–63] to the light-labelled isoDTB tag, whereas the DMSO-treated samples were clicked by CuAAC^[60–63] to the heavy-labelled isoDTB tag.^[75] After combining both samples, the probe-labelled proteins were enriched on (strept)avidin, digested with trypsin and eluted from the beads followed by LC-MS/MS analysis. This again generated a competition ratio R between the heavy- (DMSO-treated) and light- (compound-treated) labelled peptides. Therefore, cysteines, that were engaged by the respective compound in the compound-treated sample, were quantified more strongly in the DMSO-treated sample leading to higher R values, whereas cysteines, that were not targeted by the analyzed compound, were quantified equally in both samples leading to R values of close to 1. This workflow was previously used in our group to study the cysteine ligandability in *S. aureus* lysate and, therefore, did not account for uptake of different compounds or other metabolic inactivation of the compounds.^[75] In this thesis, we set out to optimize and adjust this chemoproteomic technology to study living bacteria, where we incubate with the respective compound or the DMSO solvent control in living cells and after cell lysis apply the broadly reactive IA-alkyne, followed by the identical further workflow.^[75] In this way, it should be possible to identify the intracellular targets of electrophiles within the environment of intact living bacteria and thereby also account for possible reduced uptake or other metabolic processes.

3.3.1 Optimization and adjustment of the isoDTB-ABPP workflow

Before we started with the analysis of the intracellular targets of the selected 14 compounds (Figure 15B), we set out to optimize and adjust the residue-specific, competitive isoDTB-ABPP workflow for the profiling of living bacteria.^[75] For the first benchmark studies, we selected the α -chloroacetamide **EN085** as we expected to observe strong competition due to its high antibacterial activity (1.6 μM) in *M. catarrhalis* and its already shown proteome-wide reactivity in *S. aureus* lysate.^[75] Instead of using lysate, we grew the resistant β -lactamase-producing *M. catarrhalis* DSM11994^[200] to the early stationary phase, harvested the cells, washed them

with PBS and resuspended in PBS to give $OD_{600} = 40$. Initially, we chose this high bacterial density as we wanted to reduce the amount of needed compound, while still obtaining sufficient protein concentrations for the subsequent chemoproteomic workflow. We treated the resuspended cells with $100 \mu\text{M}$ (Figure 19A) or $20 \mu\text{M}$ **EN085** (Figure 19B). In this way, we demonstrated that the residue-specific, competitive isoDTB-ABPP workflow can in principle be applied to study living bacteria as the approximately 1700 quantified cysteines were comparable in number to the previous study of *S. aureus* lysate.^[75]

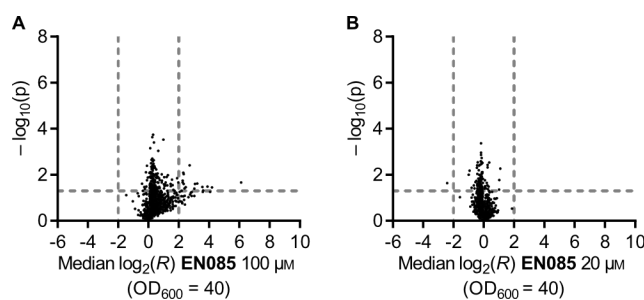


Figure 19: Volcano plots for **EN085** at $100 \mu\text{M}$ (A) and $20 \mu\text{M}$ (B) in *M. catarrhalis* DSM11994^[200] at a bacterial density of $OD_{600} = 40$. The plots show the median $\log_2(R)$ reflecting the difference in MS1 signal intensity between the heavy- (DMSO-treated) and light- (compound-treated) labelled peptides and the statistical significance $-\log_{10}(p)$ obtained through a one-sample t-test for all quantified cysteines. All data result from two biologically independent replicates. The dashed grey lines indicate the cut-off values for cysteine ligandability of $\log_2(R) > 2$ and $-\log_{10}(p) > 1.30$.^[75]

We further chose the identical cut-off values to determine ligandability as in the previous study, where we classified a cysteine as ligandable or engaged by a certain compound and as a hit of this compound, if $\log_2(R) > 2$ and additionally if the $\log_2(R)$ was statistically significantly different from 0 according to a one-sample t-test with $p < 0.05$ ($-\log_{10}(p) > 1.30$).^[75] In the experiment at a concentration of $100 \mu\text{M}$ **EN085**, we identified 16 engaged cysteines (Figure 19A), whereas in the experiment at $20 \mu\text{M}$ **EN085** we could not detect a single cysteine as engaged (Figure 19B). Even without the filter for statistical significance, there was no cysteine with $\log_2(R) > 2$ quantified. This observation was surprising as **EN085** showed broad proteome-wide reactivity in *S. aureus* in a previous study^[75] and since a concentration of $20 \mu\text{M}$ still represented approximately 10-fold MIC value, where the engagement of at least some cysteines was expected. Due to the absence of any engaged cysteines despite the relatively low MIC value, we reconsidered the protocol for our chemoproteomic labelling approach and identified bacterial density as one major difference between the chemoproteomic and MIC experiment. Whereas in MIC experiments the bacterial density is initially very low, we used an extremely high density of $OD_{600} = 40$ in the isoDTB-ABPP workflow.^[75] We hypothesized that at these high bacterial densities highly reactive electrophiles, like **EN085**, might be quenched

by different thiols present in the bacterial culture before the compound reaches its intracellular target proteins. Therefore, we repeated the identical chemoproteomic experiments at 100 μM (Figure 20A) and at 20 μM **EN085** (Figure 20B) at a bacterial density of $\text{OD}_{600} = 4$, where we additionally increased the volume of culture and added compound 10-fold to maintain identical protein concentrations after bacterial lysis.

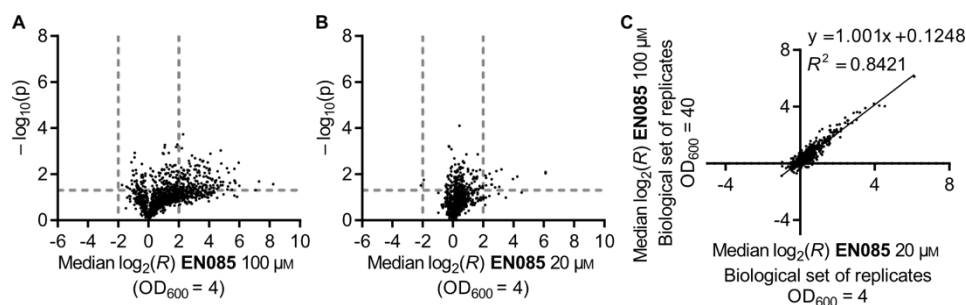


Figure 20: Volcano plots for **EN085** at 100 μM (A) and 20 μM (B) in *M. catarrhalis* DSM11994^[200] at a bacterial density of $\text{OD}_{600} = 4$. The plots show the median $\log_2(R)$ reflecting the difference in MS1 signal intensity between the heavy- (DMSO-treated) and light- (compound-treated) labelled peptides and the statistical significance $-\log_{10}(p)$ obtained through a one-sample t-test for all quantified cysteines. All data result from two biologically independent replicates. The dashed grey lines indicate the cut-off values for cysteine ligandability of $\log_2(R) > 2$ and $-\log_{10}(p) > 1.30$.^[75] C Plot to visualize the correlation between the chemoproteomic experiment with **EN085** at 100 μM at a bacterial density of $\text{OD}_{600} = 40$ and at 20 μM at a bacterial density of $\text{OD}_{600} = 4$. The plot shows the median $\log_2(R)$ reflecting the difference in MS1 signal intensity between the heavy- (DMSO-treated) and light- (compound-treated) labelled peptides.^[75] All data result from two biologically independent replicates. Simple linear regression analysis was conducted with GraphPad Prism version 9.5.0 for Windows (GraphPad Software, San Diego, California USA, www.graphpad.com) resulting in a slope = 1.001 and a goodness of fit $R^2 = 0.84$.

With the adjusted conditions of the workflow, we were still able to detect a similar number of cysteines with 1549 at 100 μM **EN085** and 1695 cysteines at 20 μM **EN085**. Additionally, we significantly increased the number of hit cysteines at 100 μM **EN085** from 16 to 157 representing an increase of hit rate from $\sim 1\%$ to $\sim 10\%$ from the $\text{OD}_{600} = 40$ to $\text{OD}_{600} = 4$ experiment. This showed that the adjusted protocol also was applicable for our approach and that it largely increased the number of engaged cysteines as we hypothesized. Nevertheless, the newly obtained hit rate of $\sim 10\%$ was at the limit that we considered useful for further analysis. Strikingly, the same trend was also observed in the experiment at 20 μM **EN085**, where we now could identify 15 engaged cysteines (hit rate $\sim 1\%$), whereas in the previous setup at high bacterial density no single cysteine was hit. Furthermore, among these hit cysteine we could identify five cysteines that were described to be in essential proteins.^[201] We further saw similarities to the previously obtained data at the higher concentration and correlated the data

at 100 μM **EN085** at $\text{OD}_{600} = 40$ with the data at 20 μM **EN085** at $\text{OD}_{600} = 4$ (Figure 20C). We could verify a strong correlation between these experiments after a simple linear regression analysis (GraphPad Prism version 9.5.0 for Windows, GraphPad Software, San Diego, California USA, www.graphpad.com) with an obtained slope of 1.001 and a goodness of fit of $R^2 = 0.84$. This further verified our initial hypothesis that our reactive electrophiles were quenched at high bacterial densities by different thiols present in the bacterial culture prior to reaching their intracellular target proteins. Since we assumed that reactive electrophiles like **EN085**, that also showed high antibacterial activity (MIC = 1.6 μM in *M. catarrhalis* DSM9143 and *M. catarrhalis* DSM11994^[200]), reasonably engage different intracellular cysteine residues covalently that explain their activity, we decided to continue all further chemoproteomic investigations with the optimized workflow at a bacterial density of $\text{OD}_{600} = 4$ to obtain more relevant and significant information on the intracellular targets of the other selected compounds.

3.3.2 Analysis of cysteine ligandability

Using the optimized residue-specific, competitive isoDTB-ABPP workflow^[75] at a bacterial density of $\text{OD}_{600} = 4$, we next investigated the intracellular target cysteines of the 13 other selected electrophiles (Figure 15B) in duplicates. Importantly, treatment with DMSO as a solvent control verified that in this setup all cysteines were unaffected and quantified with $R \sim 1$. Among the other tested electrophiles, we identified **EN026** (31% of quantified cysteines with median $\log_2(R) > 2$, Figure 21A), **EN179** (52% of quantified cysteines with median $\log_2(R) > 2$, Figure 21A) and **EN181** (41% of quantified cysteines with median $\log_2(R) > 2$, Figure 21A) as highly reactive and highly promiscuous compounds that strongly targeted a large fraction of all detected cysteines. Since we reasoned that these highly promiscuous compounds were not suitable for further drug development or target identification studies, we excluded these three compounds from all further data analysis. On the other side, we detected **EN017** without any hit cysteine and **EN125** with only one hit cysteine that was not described to be essential.^[201] Due to that, we decided to not further investigate these compounds but did not exclude them from further data analysis. Consequently, we selected the remaining eight compounds and performed an additional experiment in duplicates to obtain a total of four replicates for these interesting compounds to obtain more significant and reliable results. The obtained results of our chemoproteomic investigation of the additionally investigated 13 compounds at 100 μM were visualized as volcano plots (Figure 21B-O).

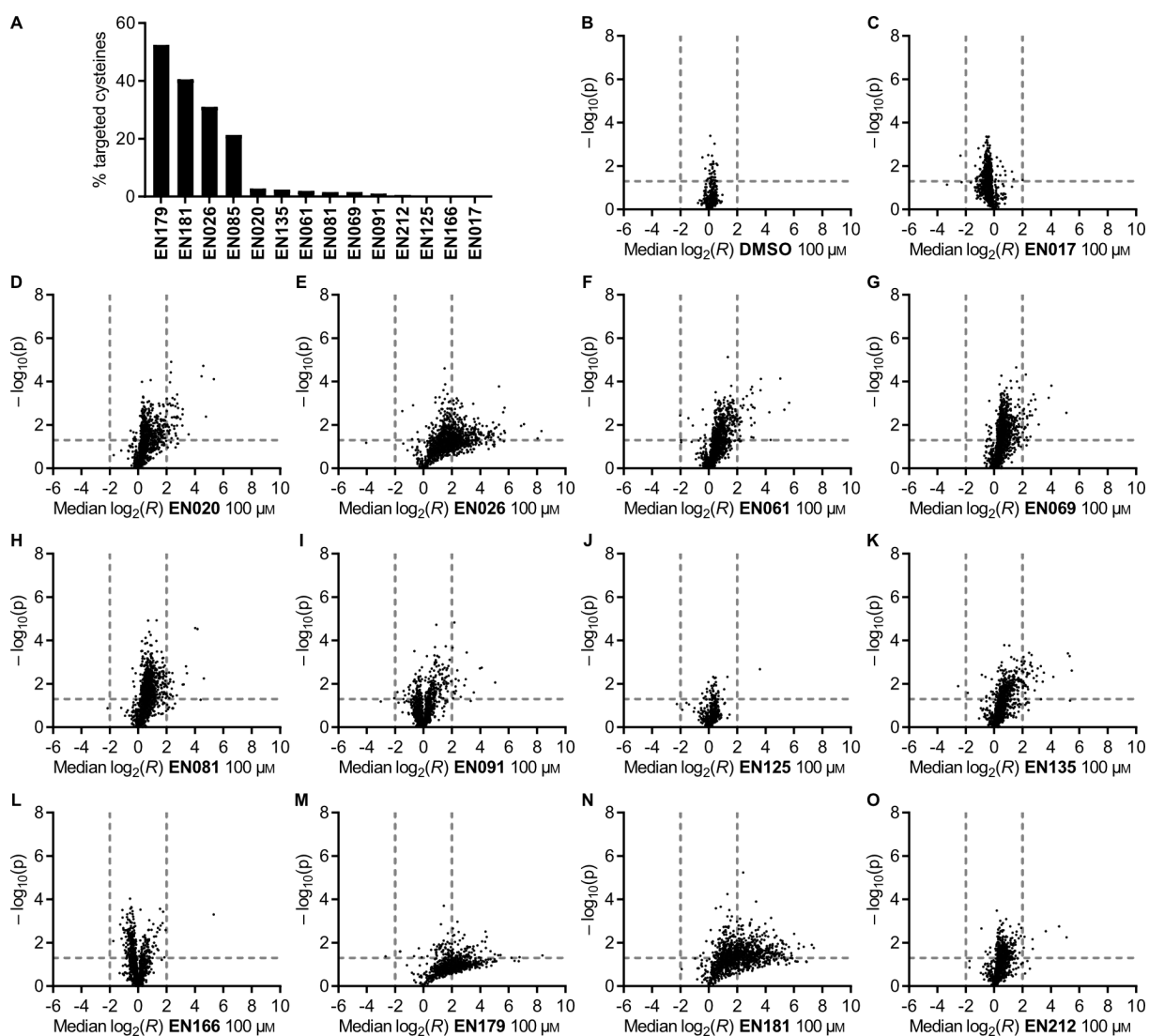


Figure 21: A Bar graph of the promiscuity of all investigated compounds in the residue-specific, competitive isoDTB-ABPP workflow^[75] at 100 μM in *M. catarrhalis* DSM11994^[200] at a bacterial density of $\text{OD}_{600} = 4$. The percentage of targeted cysteines was determined as the percentage of cysteines with median $\log_2(R) > 2$ from all quantified cysteines of the respective electrophile.^[75] **B-O** Volcano plots for all tested electrophiles at 100 μM (excluding **EN085**) and for the control experiment with DMSO in *M. catarrhalis* DSM11994^[200] at a bacterial density of $\text{OD}_{600} = 4$. The plots show the median $\log_2(R)$ reflecting the difference in MS1 signal intensity between the heavy- (DMSO-treated) and light- (compound-treated) labelled peptides and the statistical significance $-\log_{10}(p)$ obtained through a one-sample t-test for all quantified cysteines. All data result from two biologically independent replicates (**B, C, E, J, M** and **N**) or from four biologically independent replicates (**D, F, G, H, I, K, L** and **O**). The dashed grey lines indicate the cut-off values for cysteine ligandability of $\log_2(R) > 2$ and $-\log_{10}(p) > 1.30$.^[75]

Similarly to our data analysis in the benchmark studies with **EN085** (Figure 20C), we correlated the obtained median $\log_2(R)$ values of the two sets of biologically independent replicates of the compounds, where the chemoproteomic experiment was performed in a total of four replicates (Figure 22).

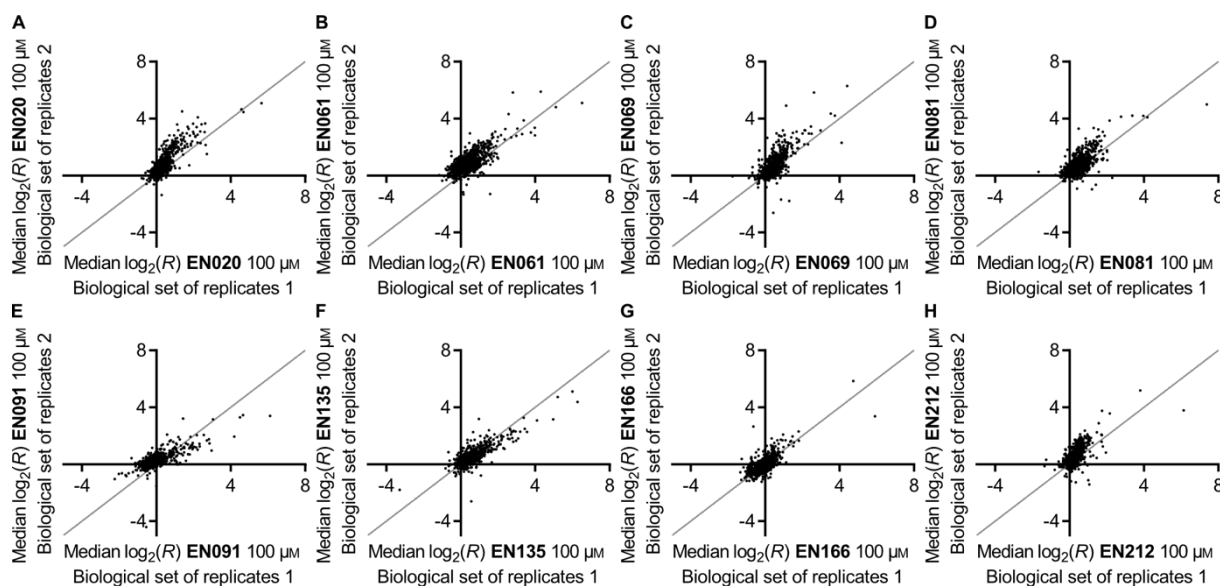


Figure 22: Plots to visualize the correlation between the two sets of biologically independent replicates of the residue-specific, competitive isoDTB-ABPP workflow^[75] with **EN020** (A), **EN061** (B), **EN069** (C), **EN081** (D), **EN091** (E), **EN135** (F), **EN166** (G), and **EN212** (H) at 100 μM in *M. catarrhalis* DSM11994^[200] at a bacterial density of $\text{OD}_{600} = 4$. The plots show the median $\log_2(R)$ reflecting the difference in MS1 signal intensity between the heavy- (DMSO-treated) and light- (compound-treated) labelled peptides. The added lines indicate a perfect correlation of 1.^[75]

Strikingly, all evaluated compounds showed a relatively good correlation between the two sets of two biologically independent replicates, which again verified the reproducibility of our approach even between different biological replicates in living bacteria.

Even though we could already obtain much information on the ligandable cysteinome of *M. catarrhalis* and proved the general feasibility of our method, we profiled all compounds so far at a relatively high concentration of 100 μM , especially considering the relatively low MIC values of the respective compounds (Figure 15A). Therefore, we selected six compounds (**EN020**, **EN061**, **EN069**, **EN091**, **EN135** and **EN166**) based on their reactivity profiles to also analyze their ligandable cysteines at a lower concentration of 20 μM in again two sets of two biologically independent replicates (Figure 23A-F)

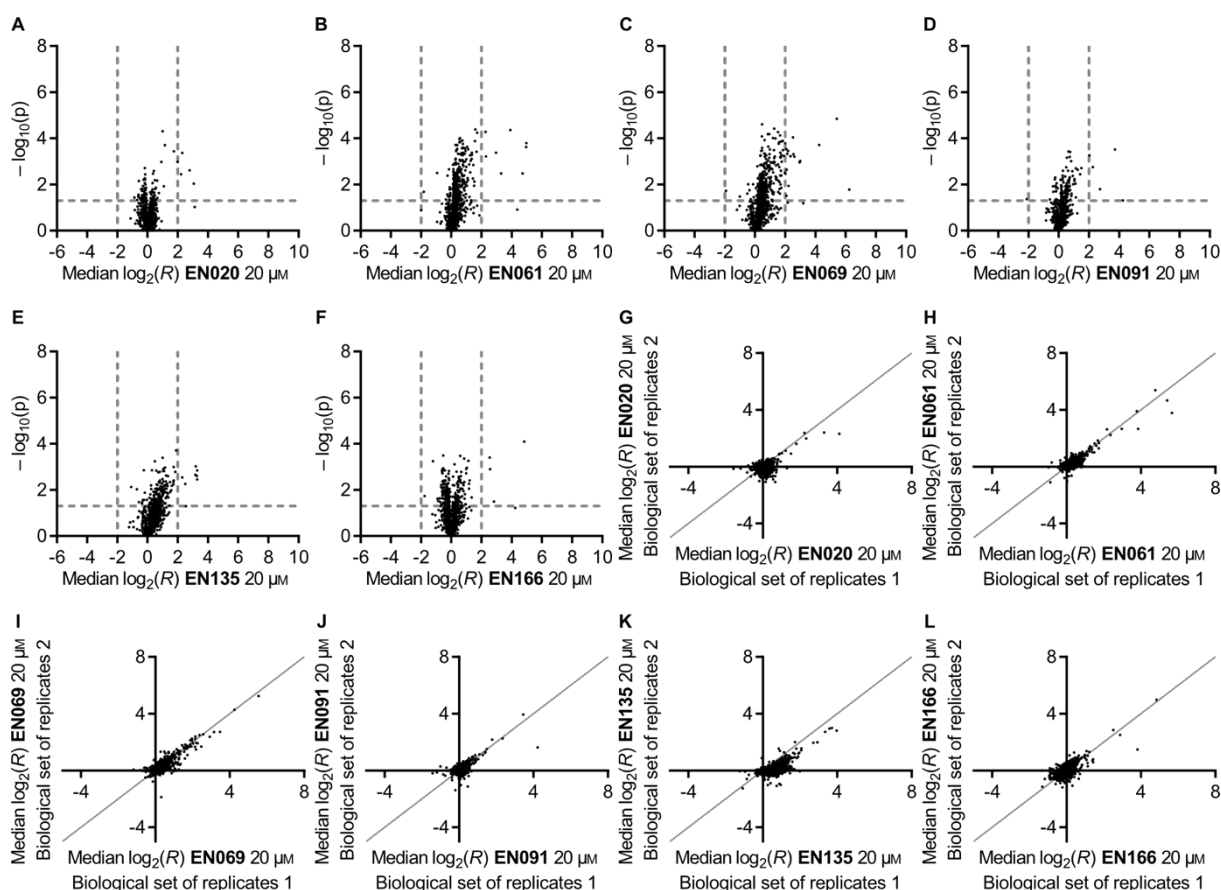


Figure 23: A-F Volcano plots for EN020 (A), EN061 (B), EN069 (C), EN091 (D), EN135 (E), and EN166 (F) at 20 μM in *M. catarrhalis* DSM11994^[200] at a bacterial density of $\text{OD}_{600} = 4$. The plots show the median $\log_2(R)$ reflecting the difference in MS1 signal intensity between the heavy- (DMSO-treated) and light- (compound-treated) labelled peptides and the statistical significance $-\log_{10}(p)$ obtained through a one-sample t-test for all quantified cysteines. All data result from two sets of two biologically independent replicates. The dashed grey lines indicate the cut-off values for cysteine ligandability of $\log_2(R) > 2$ and $-\log_{10}(p) > 1.30$.^[75] G-L Plots to visualize the correlation between the two sets of biologically independent replicates of the residue-specific, competitive isoDTB-ABPP workflow^[75] with EN020 (G), EN061 (H), EN069 (I), EN091 (J), EN135 (K), and EN166 (L) at 20 μM in *M. catarrhalis* DSM11994^[200] at a bacterial density of $\text{OD}_{600} = 4$. The plots show the median $\log_2(R)$ reflecting the difference in MS1 signal intensity between the heavy- (DMSO-treated) and light- (compound-treated) labelled peptides. The added lines indicate a perfect correlation of 1.^[75]

Even at the lower concentration of 20 μM , we still could detect several hit cysteines (4 hits for EN020, 8 hits for EN061, 18 hits for EN069, 5 hits for EN091, 7 hits for EN135, and 4 hits for EN166) with all tested electrophiles in living *M. catarrhalis* DSM11994.^[200] Again demonstrating the reproducibility of our results, we obtained an overall good correlation between the two sets of two biologically independent replicates (Figure 23G-L). Finally, we combined all data from our experiments at a bacterial density of $\text{OD}_{600} = 4$ with the three highly promiscuous compounds EN026, EN179 and EN181 excluded, which resulted in data for

eleven compounds at 100 μM , six compounds at 20 μM and the DMSO control to give a total amount of 19 different conditions. Furthermore, we excluded all cysteines that were quantified in less than three of these conditions from our further analysis. Taken these results together, we were able to quantify 2073 different cysteines within 817 different proteins, where 228 of the cysteines (Figure 24A) and 173 of the proteins (Figure 24B) were detected to be ligandable by at least one of the tested conditions. Interestingly, in 63% of the detected proteins (518 of 817 detected proteins) more than one single cysteine was quantified, whereas in 74% of the ligandable proteins (128 of 173 ligandable proteins) only one cysteine was engaged (Figure 24C) indicating that even our reactive electrophiles generated specificity in terms of cysteine engagement.

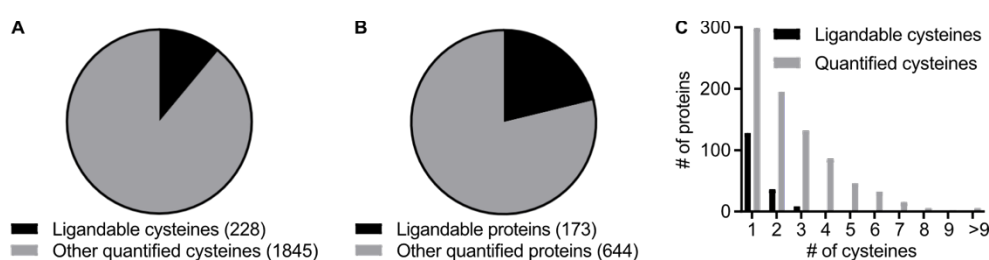


Figure 24: **A** Pie chart indicating the fraction of ligandable cysteines (228) and other quantified cysteines (1845) among all detected cysteines (2073). **B** Pie chart indicating the fraction of ligandable proteins (173) and other quantified proteins (644) among all detected proteins (817). **C** Bar graph showing the number of ligandable and quantified cysteines within different proteins. **A-C** Cysteines and proteins were grouped as follows: ligandable cysteines/proteins: cysteines that were engaged by at least one compound with median $\log_2(R) > 2$ and $-\log_{10}(p) > 1.30$, and proteins that were engaged by at least one compound on at least one cysteine residue, respectively; other quantified cysteines/proteins: cysteines that were quantified in our data but not engaged by any compound, and proteins that were quantified but no single cysteine residue was engaged by any compound, respectively; quantified cysteines: total number of quantified cysteines including the hit and non-hit cysteines.^[75]

Generally, we detected an equal fraction of ligandable cysteines (30%) and other quantified cysteines (31%) in essential proteins^[201] that were both higher compared to the amount of essential proteins^[201] (23%) within the complete genome of *M. catarrhalis* DSM11994^[200] (Figure 25A).^[185,201] This indicated that we detected more selectively cysteines within essential proteins^[201] with our approach compared to cysteines in non-essential proteins. Similarly, we identified more cysteines at functional sites^[185] within our data compared to all cysteines in *M. catarrhalis* at functional sites^[185] (9%). Additionally, we found an enrichment of functional site^[185] cysteines among the ligandable cysteines (23%) compared to the other quantified cysteines (13%, Figure 25B). This indicated that a large fraction of cysteines that were ligandable with our electrophile library additionally were located at the functional sites^[185] of

the corresponding proteins. We hypothesized that these ligandable cysteines at functional sites^[185] were maybe responsible for the high antibacterial activity of our library. We further classified the ligandable and other detected cysteines into their functional classes based on their Gene Ontology (GO) terms^[206–209] that were reported on UniProt (Figure 25C).^[185]

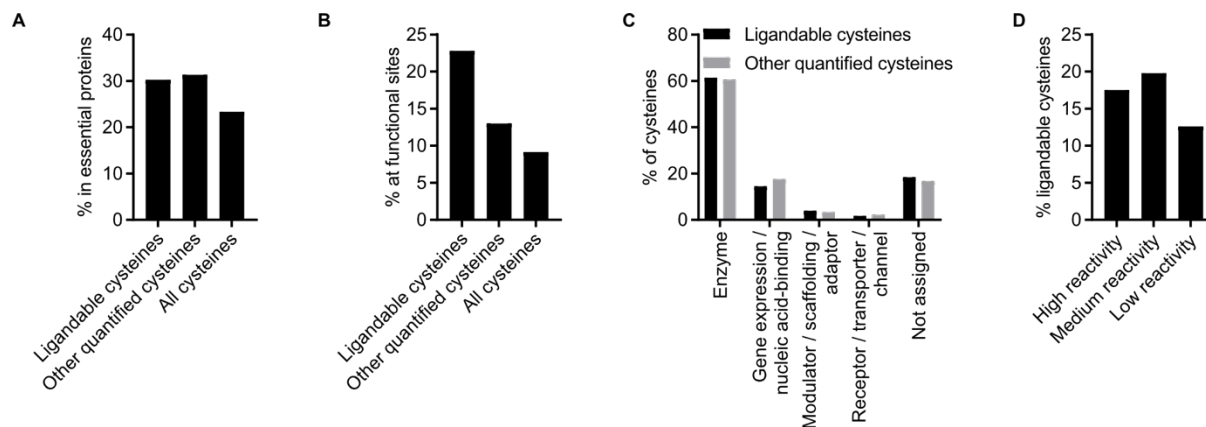


Figure 25: **A, B** Fraction of cysteines in *M. catarrhalis* DSM11994^[200] in ligandable, other quantified and all cysteines that were in essential proteins (**A**)^[201] or at functional sites (**B**).^[185] **C** Classification of the fraction of cysteines in *M. catarrhalis* DSM11994^[200] in ligandable and other quantified cysteines into their different functional classes based on their Gene Ontology (GO) terms^[206–209] on UniProt.^[185] **A-C** Cysteines were grouped as follows: ligandable cysteines: cysteines that were engaged by at least one compound with median $\log_2(R) > 2$ and $-\log_{10}(p) > 1.30$; other quantified cysteines: cysteines that were quantified in our data but not engaged by any compound; all cysteines: all cysteines that were present in the genome of *M. catarrhalis* DSM11994^[200] according to UniProt^[185] independently if they were quantified in our data.^[75] **D** Fraction of ligandable cysteines in *M. catarrhalis* DSM11994^[200] in the different reactivity groups with high reactivity ($R_{10:1} < 3$), medium reactivity ($5 > R_{10:1} > 3$) and low reactivity ($R_{10:1} > 5$).^[75]

We could detect that ligandable (61%) and non-ligandable cysteines (60%) were found nearly to the same extent in enzymes as the major functional class among all detected cysteines with also a similar distribution among the other classified functional classes.^[185,206–209] We further referenced our obtained data about cysteine ligandability with our previous results on cysteine reactivity to show that ligandable cysteines were more likely located in highly (18%) and medium reactive (20%) cysteines than in cysteines with low reactivity (13%, Figure 25D). This pointed to the fact that cysteine reactivity strongly correlated with cysteine ligandability, but strikingly we also detected 129 ligandable cysteines within the low reactivity group, which demonstrated that beyond cysteine reactivity also more specific interactions between our electrophiles and the proteins occurred. Furthermore, we again analyzed the accessibility of the ligandable, other quantified and all cysteines in the genome^[185] utilizing a recently published

tool^[202,203] to calculate the pPSE values of the respective cysteines based on AlphaFold^[204,205] structures (Figure 26).^[202,203]

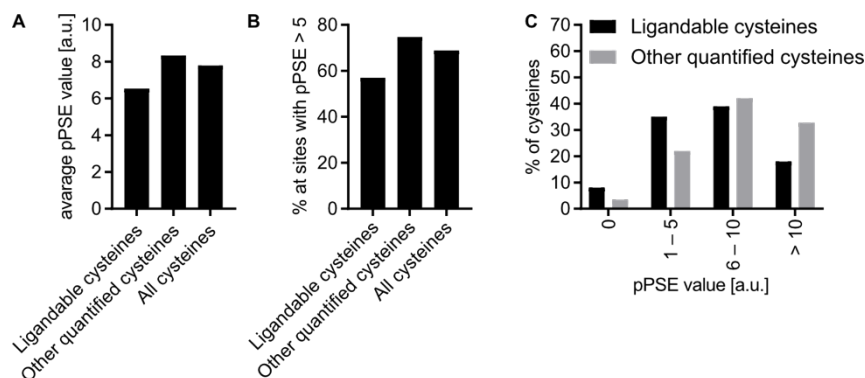


Figure 26: **A** Averaged pPSE values of the ligandable, other quantified and all cysteines in *M. catarrhalis* DSM11994.^[200] **B** Percentage of ligandable, other quantified and all cysteines with an pPSE value > 5 in *M. catarrhalis* DSM11994.^[200] **C** Classification of the fraction of cysteines in *M. catarrhalis* DSM11994^[200] in ligandable and other quantified cysteines into highly accessible (pPSE = 0), accessible ($1 \leq \text{pPSE} \leq 5$), slightly buried ($6 \leq \text{pPSE} \leq 10$) and highly buried (pPSE > 10) sites. **A-C** Cysteines were grouped as follows: ligandable cysteines: cysteines that were engaged by at least one compound with median $\log_2(R) > 2$ and $-\log_{10}(p) > 1.30$; other quantified cysteines: cysteines that were quantified in our data but not engaged by any compound; all cysteines: all cysteines that were present in the genome of *M. catarrhalis* DSM11994^[200] according to UniProt^[185] independently if they were quantified in our data.^[75] The pPSE values were calculated with a recently published tool^[202,203] based on AlphaFold^[204,205] structures to assess the cysteine accessibility.^[202,203]

The calculated average of the pPSE values (Figure 26A) of the ligandable cysteines (pPSE = 6.5) was slightly lower compared to the not engaged cysteines (pPSE = 8.3) and to all cysteines (pPSE = 7.8) present in the genome,^[185] which indicated that more accessible cysteines were more likely engaged by our electrophiles compared to the others. The same trend could be observed within the less accessible cysteines (pPSE > 5, Figure 26B) that a lower percentage of ligandable cysteines (57%) were detected compared to non-hit cysteines (75%) and all cysteines (69%). Additionally, we classified the cysteines according to their pPSE values into highly accessible (pPSE = 0), accessible ($1 \leq \text{pPSE} \leq 5$), slightly buried ($6 \leq \text{pPSE} \leq 10$) and highly buried (pPSE > 10) sites (Figure 26C) and identified a higher fraction of ligandable cysteines within the two more accessible groups, whereas not engaged cysteines represented the majority in the two more buried or less accessible groups.^[202,203] This further strengthened our previous hypothesis that ligandable cysteines were more accessible compared to non-ligandable cysteines but more research specifically into this direction has to be done in order to analyze and verify this observation in more detail.

Next, we set out to analyze some ligandable cysteines in more detail (Figure 27A).

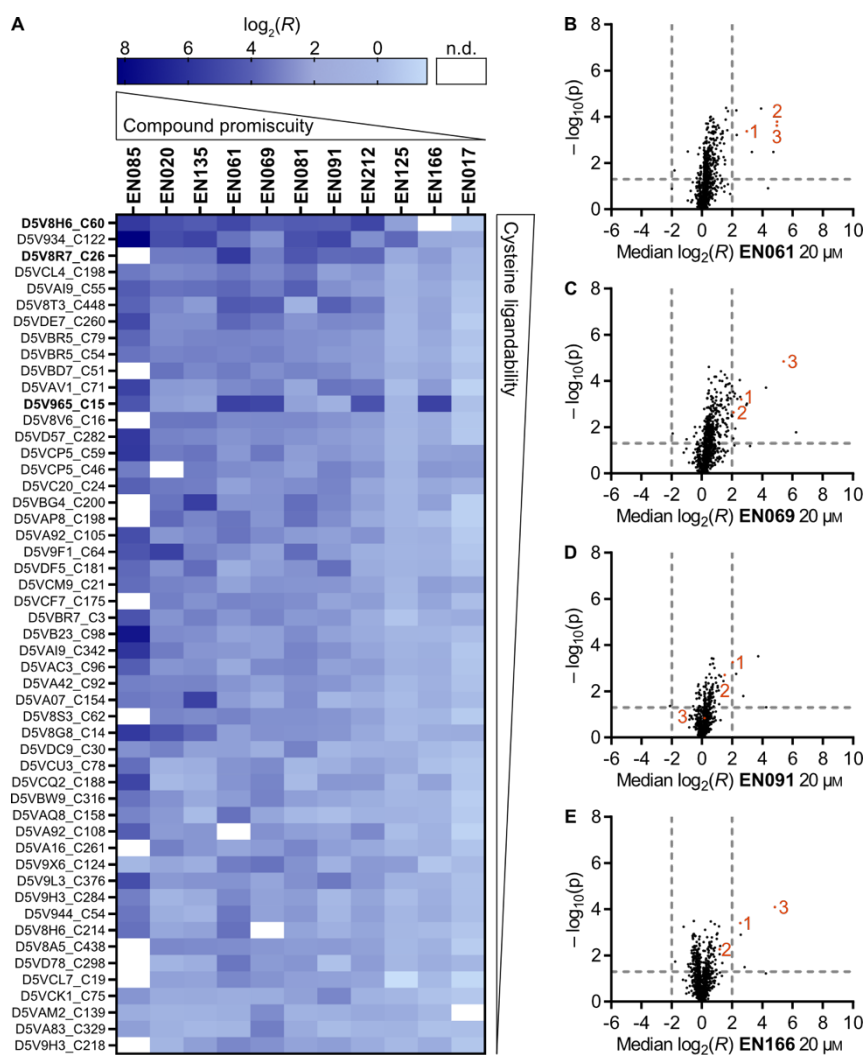


Figure 27: A Heat map showing the median $\log_2(R)$ of the selected electrophiles at 100 μM for a set of different ligandable cysteines. The electrophiles were listed by decreasing promiscuity (percentage of engaged cysteines) from left to right and the selected cysteines were listed by decreasing ligandability (number of identified electrophiles that engaged the respective cysteines) from top to bottom. The cysteines that were further investigated in the following part of this thesis were marked in bold. Data for **EN017**, **EN085**, and **EN125** results from two biologically independent replicates, whereas all data for the other electrophiles results from two sets of two biologically independent replicates.^[75] **B-E** Volcano plots for **EN061** (B), **EN069** (C), **EN091** (D), and **EN166** (E) at 20 μM in *M. catarrhalis* DSM11994^[200] at a bacterial density of $\text{OD}_{600} = 4$. The plots show the median $\log_2(R)$ reflecting the difference in MS1 signal intensity between the heavy- (DMSO-treated) and light- (compound-treated) labelled peptides and the statistical significance $-\log_{10}(p)$ obtained through a one-sample t-test for all quantified cysteines. All data result from two sets of two biologically independent replicates. The dashed grey lines indicate the cut-off values for cysteine ligandability of $\log_2(R) > 2$ and $-\log_{10}(p) > 1.30$. The cysteines that were further investigated in the following part of this thesis were marked in red. 1: C60 of ThiD (UniProt code: D5V8H6); 2: C26 of PdxJ (UniProt code: D5V8R7); 3: C15 of SirA-like protein (UniProt code: D5V965).^[75,185]

Overall, we could observe that indeed compounds with increasing promiscuity also predominantly engaged cysteines with increasing reactivity (top left corner of the heat map), which was not surprising. More interesting were the more specific interactions, where we could detect also moderately engaged cysteines by compounds with lower promiscuity (right side of the heat map), which further strengthened our previous hypothesis that besides cysteine reactivity and compound promiscuity also more specific interactions between our electrophiles and certain cysteines occurred. Especially of interest were the engaged cysteines at functional sites^[185] in essential proteins,^[201] which again include the already discussed highly and medium reactive cysteines C105 of LipA (UniProt code: D5VA92), C198 of LipB (UniProt code: D5VCL4) and C54 of the Thiol:disulfide interchange protein (UniProt code: D5V944).^[185] Further, we again detected several cysteines as engaged in key pathways including tRNA modification (C333 in a zinc binding site of Threonine-tRNA ligase (UniProt code: D5VDF5), C374 close to the ATP binding site of Serine-tRNA ligase (UniProt code: D5VAV4) and C116 and C217 in the active site of MnmA (UniProt code: D5VB14)), carbohydrate metabolism (the catalytically active nucleophile C2 of GlmS (UniProt code: D5V915)), amino acid metabolism (C75 and C222 in the active site of Diaminopimelate epimerase (UniProt code: D5V853)), cofactor synthesis (C85 in a zinc binding site of RibD (UniProt code: D5V9B6) involved in riboflavin synthesis), fatty acid synthesis (C194 in the active site of FabF (UniProt code: D5V963)) and peptidoglycan synthesis (C408 near the substrate binding site of MurE (UniProt code: D5V8Z3)).^[185] Interestingly, we identified many engaged cysteines that were involved in Fe-S clusters (C86, C105 and C108 of LipA (UniProt code: D5VA92), C160 and C163 of NfuA (UniProt code: D5V8M3) and C12 and C96 of IspH (UniProt code: D5VAC3)) indicating that this pathway represented a prime target for our electrophile library and probably generally for covalent inhibitors.^[185] Strikingly, we could further observe that among the six most engaged cysteines three were located in essential proteins^[201] pointing to the hypothesis that the engagement of these cysteines with our electrophiles led to the high antibacterial activity of our compounds and even further that these cysteines could represent ligandable hotspots for future antibiotic development (marked in bold in Figure 27A). These ligandable hotspots were at C60 of ThiD (UniProt code: D5V8H6) involved in thiamin biosynthesis, at C26 of PdxJ (UniProt code: D5V8R7) involved in pyridoxal phosphate synthesis and at C15 of the uncharacterized SirA-like protein (UniProt code: D5V965).^[185] These cysteines could all be detected and in most cases even engaged for many different compounds even at lower concentrations of 20 μ M, which could be seen in the already previously shown volcano plots of **EN061**, **EN069**, **EN091**, and **EN166** with the respective cysteines now highlighted in red (Figure 27B-E).

3.4 Target engagement and verification studies

In the next part of this project, we aimed to analyze these potential hotspot ligandable cysteines in the essential proteins^[201] ThiD, PdxJ and SirA-like protein in more detail. Furthermore, as the isoDTB-ABPP workflow^[75] identified these cysteines in a competitive manner, we also set out to verify the covalent binding of the respective electrophiles to these cysteines through follow-up experiments.^[75] Therefore, we cloned and recombinantly expressed these proteins with a *C*-terminal (for ThiD and PdxJ) or an *N*-terminal (for SirA-like protein) 6×His-tag to enable protein purification using standard techniques that were previously developed in our group.^[75] Further, we generated and expressed the respective cysteine to alanine mutants by site-directed mutagenesis also according to the previously developed protocol.^[75] In the case of ThiD, in addition to the C60A mutant we cloned and expressed also a C214A mutant and the respective C60A C214A double mutant, since cysteine C214 was also engaged by some of the tested electrophiles (Figure 27A). First, we performed a gel-based competitive labelling experiment with compounds **EN061**, **EN069**, and **EN091** on ThiD and its respective cysteine to alanine mutants analogously as previously published (Figure 28).^[75]

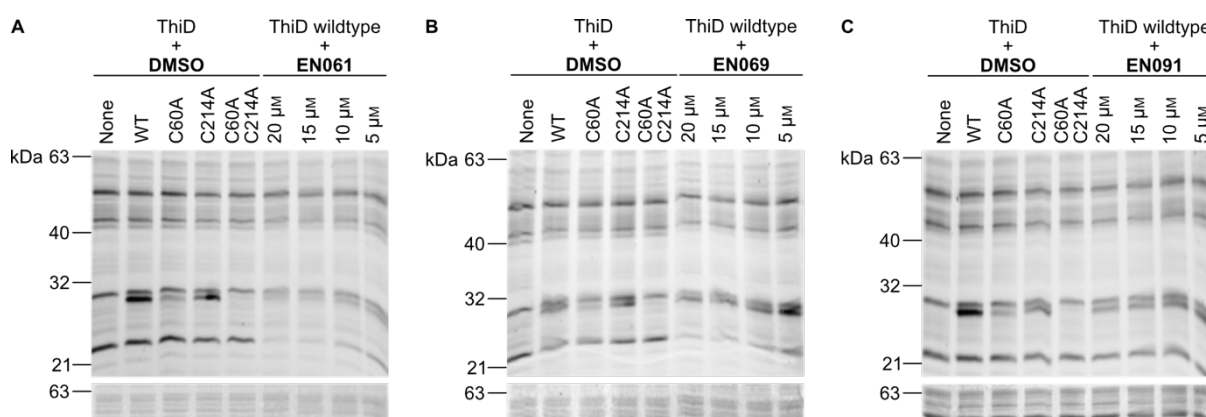


Figure 28: Gel-based competitive labelling experiment for target verification studies of ThiD. **EN061** (A), **EN069** (B) or **EN091** (C) were preincubated at the indicated concentrations with ThiD wildtype (1 μ M final concentration) in *M. catarrhalis* DSM11994^[200] lysate (1 mg/mL) for one hour at room temperature. DMSO instead of electrophile and the cysteine to alanine mutants instead of ThiD wildtype or no protein were used in control experiments. After another incubation for one hour at room temperature with IA-alkyne (10 μ M final concentration), the labelled proteins were clicked by CuAAC^[60–63] to TAMRA-azide, separated by SDS-PAGE and visualized by in-gel fluorescence scanning. The following Coomassie staining verified equal protein concentrations in all gel lanes and is shown below the fluorescence gels.^[75] WT: wildtype.

We preincubated the electrophiles at the indicated concentrations with ThiD wildtype (1 μ M final concentration) in *M. catarrhalis* DSM11994^[200] lysate (1 mg/mL) in a total volume of 50 μ L. The addition of DMSO to the cysteine to alanine mutants of ThiD or to only bacterial

lysate was used in control experiments. After the preincubation for one hour at room temperature, the broadly reactive IA-alkyne (10 μM final concentration) was added and, after another incubation for one hour at room temperature, the labelled proteins were clicked to TAMRA-azide using CuAAC,^[60–63] separated by SDS-PAGE and visualized by in-gel fluorescence scanning. Additionally, a Coomassie staining was performed to verify equal protein loading in all gel lanes, which is shown for a representative cut-out below the fluorescence gel. Since we performed again a competitive labelling experiment, similarly to the isoDTB-ABPP experiments, electrophile binding to the cysteines was indicated by decreasing band intensity.^[75] Thereby, we could detect that ThiD was engaged by **EN061** in a concentration-dependent manner (Figure 28A), which was in agreement with the obtained results from the chemoproteomic experiments ($\log_2(R) = 3.0$ at 20 μM (Figure 27B) and $\log_2(R) = 5.0$ at 100 μM (Figure 21F)). At higher compound concentrations, we could even detect a further decrease in signal intensity beyond the band of the C60A mutant indicating that probably also C214 was targeted by this compound. Unfortunately, in the case of **EN069** (Figure 28B) and **EN091** (Figure 28C) we could not observe any significant or only slight reduction in labelling intensity hinting towards a possible modification of different cysteines present in ThiD with IA-alkyne that were not engaged and competed by our electrophiles, which made the verification of compound binding through this gel-based approach impossible. Nevertheless, we continued with the identical gel-based competitive labelling experiment to verify electrophile binding to PdxJ (Figure 29).^[75]

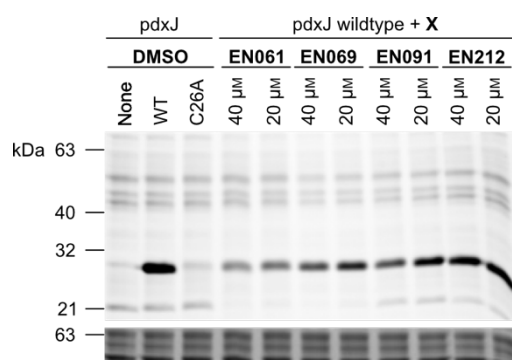


Figure 29: Gel-based competitive labelling experiment for target verification studies of PdxJ. **EN061**, **EN069**, **EN091** or **EN212** were preincubated at the indicated concentrations with PdxJ wildtype (1 μM final concentration) in *M. catarrhalis* DSM11994^[200] lysate (1 mg/mL) for one hour at room temperature. DMSO instead of electrophile and the C26A mutant instead of PdxJ wildtype or no protein were used in control experiments. After another incubation for one hour at room temperature with IA-alkyne (10 μM final concentration), the labelled proteins were clicked by CuAAC^[60–63] to TAMRA-azide, separated by SDS-PAGE and visualized by in-gel fluorescence scanning. The following Coomassie staining verified equal protein concentrations in all gel lanes and is shown below the fluorescence gels.^[75] WT: wildtype.

Similar to the target verification experiments of ThiD, we could again verify binding of **EN061** to C26 of PdxJ, which again was in agreement with our chemoproteomic experiments ($\log_2(R) = 5.0$ at 20 μM (Figure 27B) and $\log_2(R) = 5.7$ at 100 μM (Figure 21F)). Unfortunately, the other investigated electrophiles **EN069** and **EN091** only slightly decreased the labelling of PdxJ, whereas **EN212** did not show any target engagement at all in this experiment again pointing towards possible difficulties in the target verification with this gel-based approach.

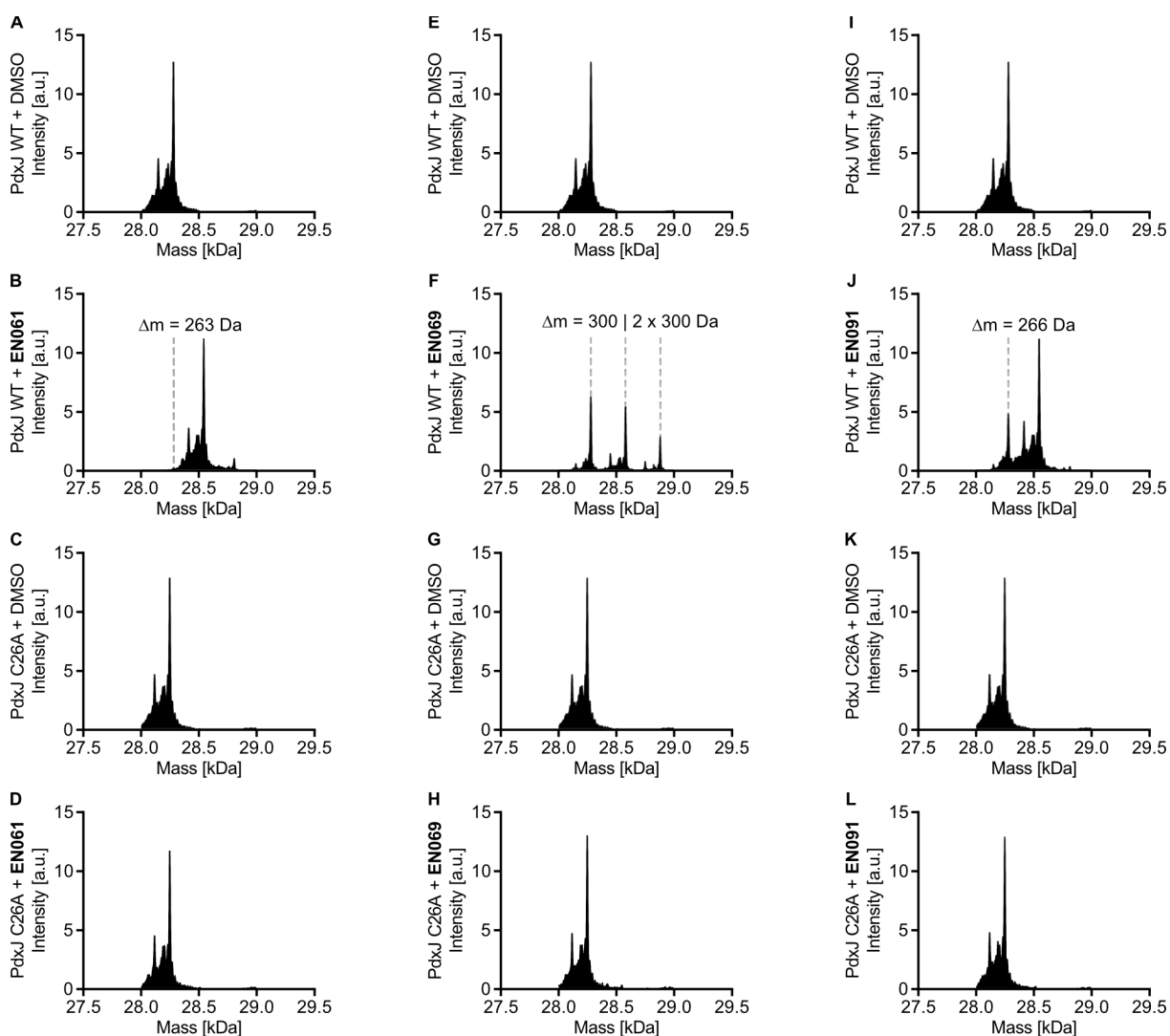


Figure 30: IPMS experiments for target verification studies of PdxJ. PdxJ wildtype (5 μM final concentration) was incubated with either DMSO as a control experiment (identical experiment shown in **A**, **E** and **I**) or with **EN061** (**B**), **EN069** (**F**) or **EN091** (**J**) (40 μM final concentration), and C26A PdxJ mutant (5 μM final concentration) was incubated also with either DMSO as a control experiment (identical experiment shown in **C**, **G** and **K**) or with **EN061** (**D**), **EN069** (**H**) or **EN091** (**L**) (40 μM final concentration) in a total volume of 100 μL PBS for one hour at 37 $^{\circ}\text{C}$. All samples were analyzed by LC-MS and the spectra are shown in the relevant mass range of 27.5-29.5 kDa after deconvolution. The dashed grey lines indicate the unmodified wildtype protein or the respective modified proteins shifted according to the expected masses of the modification with the respective compounds ($\Delta m = 263$ Da for **EN061**, $\Delta m = 300$ Da for **EN069**, and $\Delta m = 266$ Da for **EN091**).^[75] WT: wildtype.

Therefore, we set out to perform intact protein MS (IPMS) experiments with **EN061**, **EN069** and **EN091** on isolated PdxJ wildtype and the corresponding C26A mutant according to a previously published protocol (Figure 30).^[75] While impurities were detected for the recombinantly expressed PdxJ wildtype (identical experiment shown in Figure 30A, E and I) and PdxJ C26A mutant (identical experiment shown in Figure 30C, G and K), we could still detect that after incubation with **EN061** the wildtype protein was selectively modified only once with the expected mass resulting from **EN061** ($\Delta m = 263$ Da, Figure 30B), whereas the C26A mutant was not engaged by **EN061** (Figure 30D) verifying the site-specific engagement of C26 in PdxJ. Unfortunately, **EN069** led to a single and additionally to a double modification of PdxJ wildtype ($\Delta m = 300$ Da and $\Delta m = 2 \times 300$ Da, Figure 30F), even though C26A mutant was not targeted at all (Figure 30H). This indicated that C26 was indeed modified by **EN069** ($\log_2(R) = 2.1$ at $20 \mu\text{M}$ (Figure 27C) and $\log_2(R) = 2.6$ at $100 \mu\text{M}$ (Figure 21G)), but an additional cysteine was most likely also engaged by this compound. For **EN091**, we could again detect a single modification of PdxJ wildtype ($\Delta m = 266$ Da, Figure 30J) and no target engagement of PdxJ C26A mutant (Figure 30L). In this case, PdxJ wildtype was selectively targeted at C26 by **EN091**, but not modified quantitatively at the used concentration, which was in line with the smaller $\log_2(R)$ at lower concentrations in our chemoproteomic experiment ($\log_2(R) = 1.5$ at $20 \mu\text{M}$ (Figure 27D) and $\log_2(R) = 3.5$ at $100 \mu\text{M}$ (Figure 21I)).

Finally, we were especially interested in the SirA-like protein (UniProt code: D5V965) since it was targeted by many different of our tested electrophiles and described to be an essential enzyme,^[201] whose activity was not well understood.^[185]

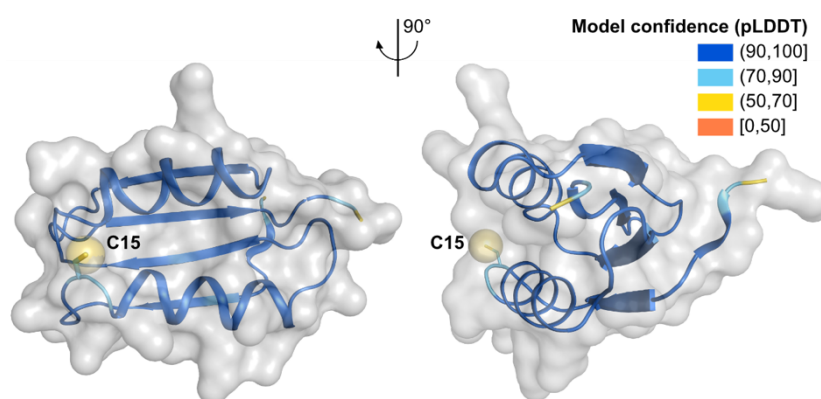


Figure 31: Visualization of the targeted cysteine C15 (highlighted with a yellow sphere) in the AlphaFold^[204,205] model of SirA-like protein (UniProt code: D5V965),^[185] which was colored according to the predicted local-distance difference test (pLDDT) indicating the model confidence. The protein was rendered as cartoon with the solvent-accessible surface shown.^[204,205] This representation was generated by A. P. A. Janssen (Leiden University).

We hypothesized that there was a small binding pocket around the targeted C15 (highlighted with a yellow sphere) visible in the AlphaFold predicted structure indicating that our electrophiles probably could engage this pocket and thereby potentially inhibit the activity of SirA-like protein (Figure 31).^[204,205] Analogously to the previously studied targets, we started with the identical gel-based competitive labelling experiment to verify binding of **EN061**, **EN069** and **EN166** to C15 of SirA-like protein (Figure 32).^[75]

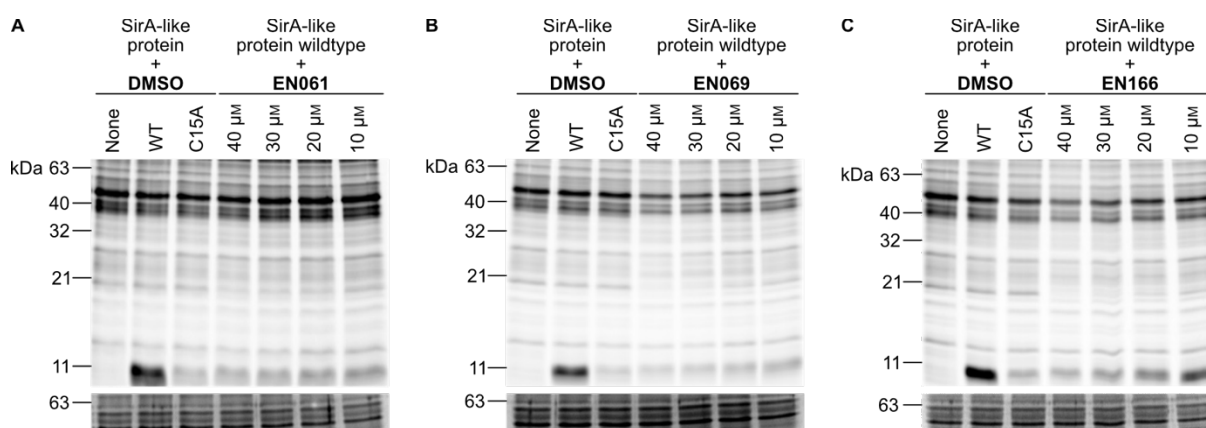


Figure 32: Gel-based competitive labelling experiment for target verification studies of SirA-like protein. **EN061** (A), **EN069** (B) or **EN166** (C) were preincubated at the indicated concentrations with SirA-like protein wildtype (4 μM final concentration) in *M. catarrhalis* DSM11994^[200] lysate (1 mg/mL) for one hour at room temperature. DMSO instead of electrophile and the C15A mutant instead of SirA-like protein wildtype or no protein were used in control experiments. After another incubation for one hour at room temperature with IA-alkyne (40 μM final concentration), the labelled proteins were clicked by CuAAC^[60–63] to TAMRA-azide, separated by SDS-PAGE and visualized by in-gel fluorescence scanning. The following Coomassie staining verified equal protein concentrations in all gel lanes and is shown below the fluorescence gels.^[75] WT: wildtype.

Strikingly, we could detect a concentration-dependent engagement of C15 of SirA-like protein for **EN061** (Figure 32A), **EN069** (Figure 32B) as well as for **EN166** (Figure 32C) in line with the chemoproteomic data for **EN061** ($\log_2(R) = 4.9$ at 20 μM (Figure 27B) and $\log_2(R) = 5.3$ at 100 μM (Figure 21F)), **EN069** ($\log_2(R) = 5.4$ at 20 μM (Figure 27C) and $\log_2(R) = 5.1$ at 100 μM (Figure 21G)) and **EN166** ($\log_2(R) = 4.8$ at 20 μM (Figure 27D) and $\log_2(R) = 5.3$ at 100 μM (Figure 21L)).

We also performed IPMS experiments on isolated SirA-like protein wildtype and the C15A mutant according to the identical protocol (Figure 33).^[75] Thereby, we detected both proteins as two individual peaks with a mass difference of 178 Da (identical experiments shown in Figure 33A, E and I, respectively in C, G and K). The detected mass shift most likely resulted from a *N*-gluconoylation of both proteins, which was described in previous literature reports for other proteins with a similar *N*-terminal 6 \times His-tag protein starting sequence.^[210,211]

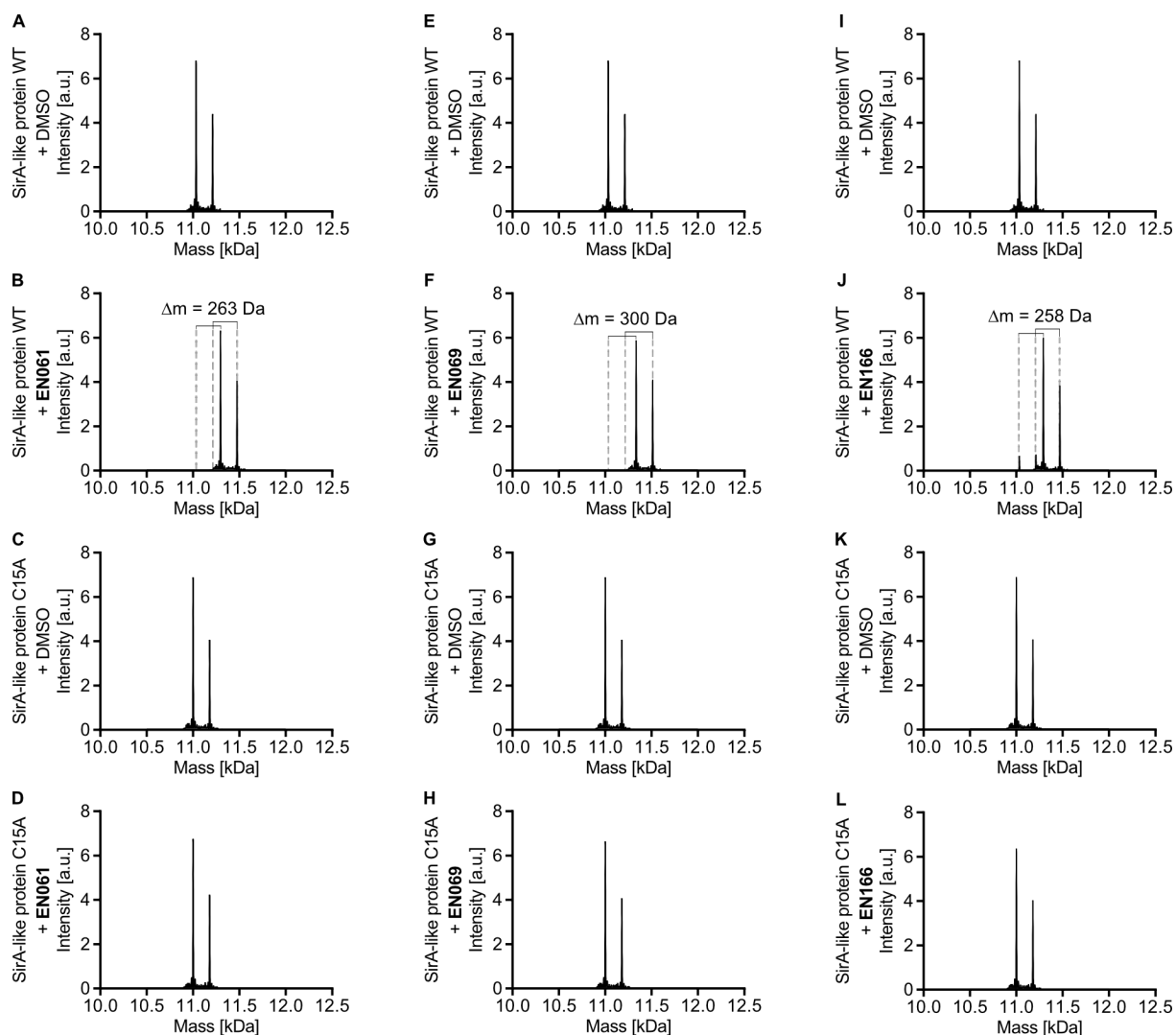


Figure 33: IPMS experiments for target verification studies of SirA-like protein. SirA-like protein wildtype ($5 \mu\text{M}$ final concentration) was incubated with either DMSO as a control experiment (identical experiment shown in A, E and I) or with **EN061** (B), **EN069** (F) or **EN166** (J) ($40 \mu\text{M}$ final concentration), and C15A SirA-like protein mutant ($5 \mu\text{M}$ final concentration) was incubated also with either DMSO as a control experiment (identical experiment shown in C, G and K) or with **EN061** (D), **EN069** (H) or **EN166** (L) ($40 \mu\text{M}$ final concentration) in a total volume of $100 \mu\text{L}$ PBS for one hour at 37°C . All samples were analyzed by LC-MS and the spectra are shown in the relevant mass range of $10.0\text{--}12.5$ kDa after deconvolution. The dashed grey lines indicate the unmodified wildtype protein or the respective modified proteins shifted according to the expected masses of the modification with the respective compounds ($\Delta m = 263$ Da for **EN061**, $\Delta m = 300$ Da for **EN069**, and $\Delta m = 258$ Da for **EN166**).^[75] Each protein was detected as two individual peaks with a mass difference of 178 Da corresponding to a *N*-gluconoylation of the proteins after expression.^[210,211] WT: wildtype.

Reproducing the results from the gel-based labelling experiment, **EN061** (Figure 33B), **EN069** (Figure 33F) and **EN166** (Figure 33J) all nearly quantitatively engaged C15 of SirA-like protein

with both protein peaks shifted according to the expected masses, while the respective C15A mutant remained unchanged (Figure 33D, L and H).

After we verified that compounds **EN061**, **EN069** and **EN166** indeed strongly target C15 of SirA-like protein, we were also interested if compound binding led to inhibition of its activity. Since the activity of SirA-like protein was not completely known or described, we performed homology searches on UniProt and, thereby, identified structural homology to TusA from different bacterial strains.^[185] Even though there was only little structural homology with TusA from *E. coli*, we utilized the detailed annotation of *E. coli* to hypothesize the activity of SirA-like protein.^[185] TusA is described as a sulfur carrier protein that can accept a sulfur from the protein IscS to form a persulfide intermediate on its catalytically active cysteine residue. This sulfur can be further transferred by TusA to TusD, which represents an essential pathway towards the synthesis of 2-thiouridine as precursor for the generation of the wobble base 5-methylaminomethyl-2-thiouridine in bacterial tRNAs. In the first step of this sulfur mediation process, IscS acts as a cysteine desulfurase converting L-cysteine to L-alanine followed by the transport of the generated persulfide to TusA. Further, it was reported that TusA enhances the cysteine desulfurase activity of IscS approximately 3-fold.^[212–214] While searching the literature for other similar enzymes, we identified an assay to determine the hypothesized enzymatic activity of SirA-like protein (Figure 34A).^[215,216]

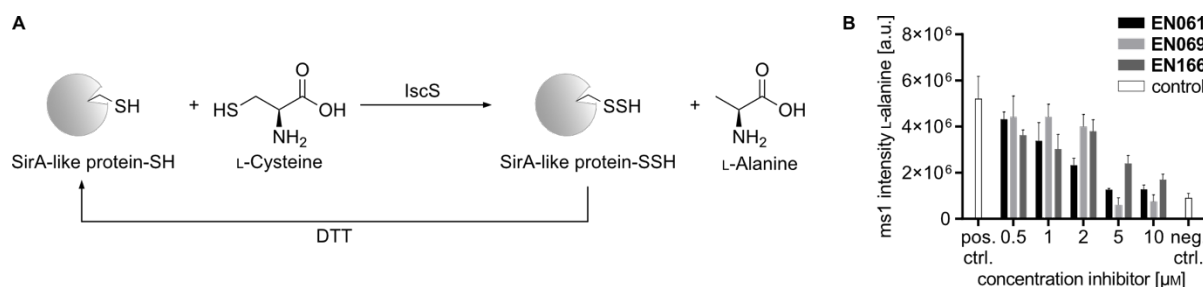


Figure 34: **A** Proposed enzymatic activity of SirA-like protein and the corresponding assay to determine the activity through the MS-based measurement and quantification of the generated L-alanine in a coupled assay with IscS. DTT was used to regenerate the cysteine of SirA-like protein.^[212–216] **B** Results of the activity assay of SirA-like protein in the coupled assay with IscS. The amount of generated L-alanine was quantified as the ms1 intensity and plotted against the used concentration of inhibitor. A positive control experiment (pos. ctrl.) was performed with IscS and SirA-like protein and the addition of DMSO as solvent control to determine the maximum amount of generated L-alanine, whereas a negative control experiment (neg. ctrl.) was performed with only IscS and addition of DMSO to determine the cysteine desulfurase activity in complete absence of SirA-like protein.^[215,216]

Therefore, we recombinantly expressed also IscS from *M. catarrhalis* DSM11994^[200] according to a previously developed protocol in our group.^[75] Next, we adapted the previously

described assay to our conditions and reasoned that we could probably determine the activity of SirA-like protein through the MS-based measurement and quantification of the generated L-alanine in a coupled assay with IscS. We used DTT to regenerate the cysteine of SirA-like protein and referenced our obtained results to a positive control consisting of IscS and SirA-like protein and to the negative control representing only the desulfurase activity of IscS alone.^[215,216] Strikingly, we could detect that SirA-like protein indeed showed the expected activity as sulfur carrier protein (pos. ctrl. Figure 34B) and enhanced the cysteine desulfurase activity of IscS significantly (neg. ctrl. Figure 34B) as described in literature for homologous proteins.^[212–214] Furthermore, we could detect a concentration-dependent inhibition of the enzymatic activity of SirA-like protein with **EN061**, **EN069** and **EN166** and could, thereby, prove that C15 was the cysteine residue to form the persulfide intermediate,^[212–214] which was then covalently blocked by our electrophiles.

Overall, these target verification experiments proved the site-specific engagement of C60 of ThiD, C26 of PdxJ and C15 of SirA-like protein by our tested electrophiles and demonstrated that our chemoproteomic data in living *M. catarrhalis* indeed gave valuable insights into ligandable cysteines that could be further verified by follow-up experiments. Furthermore, we could unravel the activity of the poorly characterized SirA-like protein and demonstrate its inhibition upon electrophile binding.

4 Conclusion and outlook

In the second project of this thesis, we aimed to develop novel narrow-spectrum antibiotics against the Gram-negative pathogen *M. catarrhalis* that is the cause of many respiratory tract infections especially in children and people suffering from COPD with an increasing emergence of β -lactamase-producing strains in clinical isolates.^[187–189] The identification of narrow-spectrum antibiotics offers several advantages over broad-spectrum antibiotics since the natural occurring human microbiome stays unharmed and the spread of the resistance between different bacteria will be minimized as the selection for resistance will only occur in the targeted bacterial species.^[199]

We screened a library of more than 200 electrophiles mainly consisting of α -chloroacetamides and α -bromoamides from a previous study from our group^[75] against two *M. catarrhalis* strains and identified a high susceptibility of both strains towards our electrophile library with a hit rate of ~18% in *M. catarrhalis* DSM9143 and of ~16% in the β -lactamase-producing *M. catarrhalis* DSM11994^[200] at a concentration of 6.3 μ M. Encouraged by these results, we further profiled a selection of 43 compounds in a concentration-dependent MIC experiment and verified their antibiotic activities even in the low micromolar range. We then selected 14 of these compounds and investigated their antibiotic activity at a comparably high concentration of 25 μ M in two Gram-positive and three other Gram-negative strains and detected that 9 of the 14 compounds were inactive against the Gram-positive and that all compounds were inactive against the other Gram-negative bacteria indicating the potential use as narrow-spectrum antibiotics against *M. catarrhalis*.

Next, we set out to investigate the overall cysteine reactivity in lysate of the β -lactamase-producing *M. catarrhalis* DSM11994^[200] with the residue-specific isoDTB-ABPP workflow that was previously developed by our group to study the cysteine reactivity in *S. aureus*.^[75] In total, we could detect 1218 cysteines and classified them into highly reactive ($R_{10:1} < 3$, 3.9%), medium reactive ($5 > R_{10:1} > 3$, 8.7%) and lowly reactive ($R_{10:1} > 5$, 87.4%) cysteines.^[75] Surprisingly, when comparing the data with the previous study in *S. aureus*,^[75] we identified a smaller fraction of cysteines in both, the high and medium reactive group, which indicated that an overall increased cysteine reactivity was not responsible for the higher susceptibility of *M. catarrhalis* towards our electrophiles. Furthermore, we could observe the same trends as in the study with *S. aureus*^[75] that highly reactive cysteines were less frequently located in essential proteins,^[201] whereas they were enriched at functional sites^[185] of proteins indicating that cysteine reactivity might hint towards possible functionalities of the

corresponding protein.^[75] Additionally, we identified several high and medium reactive cysteines that were present in functional sites^[185] of essential proteins^[201] that could possibly be exploited as future targets of covalent drugs.

After we obtained a broad overview of the cysteine reactivity in *M. catarrhalis*, we continued to profile the cysteine ligandability and the intracellular target proteins of the selection of 14 electrophiles in *M. catarrhalis* DSM11994^[200] using the residue-specific, competitive isoDTB-ABPP workflow that was previously used to study cysteine ligandability in lysate of *S. aureus*.^[75] To do so, we selected the highly reactive **EN085** for our first benchmark studies to adjust and optimize this chemoproteomic workflow for studies in living bacteria instead of bacterial lysate to also account for uptake or metabolic inactivation of our electrophiles. First, we treated living bacteria at a relatively high bacterial density of $OD_{600} = 40$ and could successfully prove that this chemoproteomic experiment was generally feasible to study living bacteria as we identified approximately 1700 cysteines with 16 cysteines engaged ($\log_2(R) > 2$ and $-\log_{10}(p) > 1.30$) at a concentration of 100 μM . Even though **EN085** showed high antibacterial activity in the MIC experiments (1.6 μM), we could surprisingly not detect any engaged cysteines at a still relatively high concentration of 20 μM . Since we strongly expected to identify cysteines as engaged or ligandable by **EN085**,^[75] we reconsidered our protocol and hypothesized that at high bacterial densities different thiols present in the bacterial culture might react and quench our reactive electrophile before they are able to engage their target proteins. Consequently, we repeated the experiment at a bacterial density of $OD_{600} = 4$ and could still detect a similar number of cysteines (1549 at 100 μM **EN085** and 1695 at 20 μM **EN085**), while increasing the hit rate from $\sim 1\%$ (16 engaged cysteines) to $\sim 10\%$ (157 engaged cysteine) at 100 μM and from none to $\sim 1\%$ (15 engaged cysteines) at 20 μM . Furthermore, we detected a very strong correlation between the experiment at 100 μM at $OD_{600} = 40$ with the experiment at 20 μM at $OD_{600} = 4$ (slope of 1.001 and goodness of fit of $R^2 = 0.84$). Since we reasoned that our electrophiles most likely engage several intracellular cysteines explaining their antibacterial activity, we decided to continue with all further chemoproteomic investigations at the bacterial density of $OD_{600} = 4$ to obtain more relevant information.

In the following part, we investigated the other 13 compounds at 100 μM with the residue-specific, competitive isoDTB-ABPP workflow^[75] with the optimized conditions as well as DMSO in a control experiment and identified **EN026**, **EN179**, and **EN181** as highly reactive and promiscuous electrophiles probably not suitable for future drug development, which we therefore excluded from our further data analysis. For eight of the remaining compounds, we performed another set of two biological replicates and found an overall good correlation

between the two sets of two independent biological replicates indicating the reproducibility of our approach. Furthermore, six compounds were selected based on their initial hit profiles and investigated at the lower concentration of 20 μM again in two sets of two independent biological replicates with also a very good correlation with each other. Combining all acquired data, we could in total detect 2073 cysteines in 817 different proteins and could identify 228 cysteines and 173 different proteins as ligandable by at least one compound. We could further show that detected cysteines were more frequently found in essential proteins^[201] and ligandable sites were especially enriched at functional sites^[185] in proteins compared to all cysteines present in the genome.^[185,201] Furthermore, we could observe a trend that ligandable cysteines were in general more accessible compared to non-ligandable cysteines according to the calculated pPSE values^[202,203] based on their AlphaFold^[204,205] structures.^[202,203]

Lastly, we investigated the potential hotspot cysteines in essential proteins^[201] that were liganded by many different of our investigated compounds pointing to the hypothesis that these cysteines might represent ideal targets for future drug developments. Thereby, we used a gel-based competitive labelling experiment that was previously developed in our group^[75] to verify that **EN061** engaged C60 of ThiD in a concentration-dependent manner. This gel-based approach^[75] also identified binding of **EN061** to C26 of PdxJ, which was further verified by IPMS experiments^[75] showing that **EN061**, **EN069** and **EN091** covalently engaged PdxJ wildtype, whereas the respective C26A mutant was not targeted. Nevertheless, **EN069** led to multiple modifications of PdxJ in this experiment pointing to the fact that also other cysteine residues were targeted by this compound. We were especially interested in the poorly characterized SirA-like protein that was targeted at C15 by **EN061**, **EN069** and **EN166**. We reasoned a possible binding pocket around C15 in the AlphaFold^[204,205] predicted structure that could be engaged by our electrophiles to inhibit its activity. We successfully verified by gel-based and IPMS experiments^[75] that all three compounds nearly quantitatively engaged C15 of SirA-like protein, which was in accordance with our chemoproteomic data. Furthermore, through homology search on UniProt^[185] and literature studies^[212–216] we identified the activity of SirA-like protein as a sulfur-carrier protein in a coupled assay with the cysteine desulfurase IscS and could further demonstrate its concentration-dependent inhibition upon compound binding indicating that the targeted C15 acted as the cysteine residue forming the persulfide intermediate.^[212–216]

Overall, we could identify several small electrophilic fragments with high antibacterial activity against the β -lactamase-producing *M. catarrhalis* DSM11994^[200] and could successfully optimize the residue-specific, competitive isoDTB-ABPP workflow^[75] to profile living

bacteria. Thereby, we could obtain much information on the ligandable cysteinome of *M. catarrhalis* and identified several ligandable hotspots for future drug development. Furthermore, we could unravel the activity of the poorly characterized SirA-like protein and verify concentration-dependent electrophile binding and the resulting inhibition of its activity. Summarizing, this work should be the foundation and pave the way for the development of novel narrow-spectrum antibiotics to treat infections with *M. catarrhalis* selectively.

5 Experimental part

These experimental procedures will be published identically in my corresponding publication. Some general experimental procedures are reported identically or with slight modification to previously published protocols from our group.^[45,75]

5.1 Cultivation and lysis of bacterial strains

The cultivation and lysis of bacteria were performed according to a published procedure.^[45,75] The following strains were used and grown in the respective media as indicated in Table 3.

Table 3: List of the used bacterial strains and the respective growth media.

Strain Name	Growth Media
<i>Moraxella catarrhalis</i> DSM9143	PPM ^[a]
<i>Moraxella catarrhalis</i> DSM11994 ^[200]	PPM ^[a]
<i>Staphylococcus aureus</i> SH1000 ^[b]	B ^[c]
<i>Klebsiella pneumoniae</i> DSM30104	BHB ^[d]
<i>Streptococcus pneumoniae</i> DSM20566	BHB ^[d]
<i>Pseudomonas aeruginosa</i> DSM22644	LB ^[e]
<i>Acinetobacter baumannii</i> DSM3007	LB ^[e]

[a] PPM medium: 15 g/L peptone, 1 g/L soluble starch, 5 g/L NaCl, 4 g/L KH₂PO₄, 1 g/L K₂HPO₄, pH = 7.5.^[217] [b] *Staphylococcus aureus* SH1000 was a kind gift from Simon J. Foster, The Krebs Institute, Department of Molecular Biology and Biotechnology, University of Sheffield.^[163] [c] B medium: 10 g/L peptone, 5 g/L NaCl, 5 g/L yeast extract, 1 g/L K₂HPO₄. [d] BHB medium: 7.5 g/L brain infusion, 10 g/L heart infusion, 10 g/L peptone, 5 g/L NaCl, 2.5 g/L Na₂HPO₄, 2 g/L D-glucose, pH = 7.4. [e] LB medium: 10 g/L peptone, 5 g/L NaCl, 5 g/L yeast extract, pH = 7.5.

Overnight cultures of bacteria were inoculated with 5 µL of a glycerol stock into 5 mL of the indicated medium and grown overnight (200 rpm, 37 °C; for *Streptococcus pneumoniae* DSM30104: 5% CO₂ atmosphere, 37 °C without shaking).

For experiments in lysate of *M. catarrhalis* DSM11994,^[200] PPM medium was inoculated 1:100 with an overnight culture and incubated (200 rpm, 37 °C) until 1 h after it reached the stationary phase ($OD_{600} \approx 3$). The cells were harvested by centrifugation (6,000 \times g, 10 min, 4 °C), pellets of 100 mL initial culture were pooled and the pellets washed two times with PBS (10 mM Na_2HPO_4 , 1.8 mM KH_2PO_4 , 140 mM NaCl, 2.7 mM KCl, pH = 7.4) prior to the immediate use or storage at -80 °C. 5 mL PBS were added to the bacterial pellets and the pellets were resuspended and transferred into 7 mL tubes containing 0.1 mm ceramic beads (PeqLab, 91-PCS-CK01L). Cells were lysed in a Precellys 24 bead mill (3 \times 30 s, 6,500 rpm) while cooling with an airflow that was pre-cooled with liquid nitrogen. The suspension was transferred into a microcentrifuge tube and centrifuged (13,000 \times g, 30 min, 4 °C). The supernatant of several samples was pooled and filtered through a 0.45 μ m filter. Protein concentration of the lysate was determined using a bicinchoninic acid (BCA) assay (typical concentrations were between ~2 mg/mL and ~3 mg/ml) and the concentration was adjusted to 1 mg/mL with PBS. The lysates were either used immediately (for all MS experiments) or stored at -20 °C.

For experiments in living *M. catarrhalis* DSM11994,^[200] day cultures were inoculated with 5 μ L of a glycerol stock into 5 mL of PPM medium and grown for ~8 h (200 rpm, 37 °C). PPM medium was inoculated 1:100 with a day culture and incubated (200 rpm, 37 °C) until 1 h after it reached the stationary phase ($OD_{600} \approx 3$). The cells were harvested by centrifugation (6,000 \times g, 10 min, 4 °C) and washed two times with PBS. The pellets were resuspended in PBS to either $OD_{600} = 40$ or $OD_{600} = 4$ prior to the immediate use.

5.2 Determination of MIC values

The minimum inhibitory concentration (MIC) was determined according to a published procedure.^[75] Bacterial overnight cultures were diluted 1:10,000 in the respective growth medium and 100 μ L of this dilution was pipetted into a sterile 96-well plate. 1 μ L of the respective compound (100 \times stock in dimethyl sulfoxide) was added. The addition of 1 μ L DMSO to the bacterial suspension served as a growth control, whereas the use of only 100 μ L of the respective medium with addition of 1 μ L DMSO served as a sterile control in several replicates on every plate. The plates were incubated (200 rpm, 37 °C; for *Streptococcus pneumoniae* DSM30104: 5% CO_2 atmosphere, 37 °C without shaking) for 20 h. The MIC was determined through the measurement of the OD_{600} using an infinite-pro plate reader M200pro (Tecan). For single-point concentration investigations, the measured OD_{600} values of the

replicates were averaged and, if the averaged $OD_{600} < 0.1$, the compound was defined as active at the tested concentration, otherwise as inactive. For concentration-dependent investigations, the MIC was determined for each replicate as the lowest concentration for which no bacterial growth was observed, which was defined as the measured $OD_{600} < 0.1$. If different MIC values were obtained for the biologically independent replicates, the higher value was reported as final MIC. If there was bacterial growth at higher concentrations of compound, followed by at least three consecutive lower concentrations without bacterial growth, the lower concentration was reported. In other cases, the MIC was reported as “unclear”.

5.3 isoDTB-ABPP experiments in lysate to investigate cysteine reactivity

The chemoproteomic experiment was performed according to a published procedure.^[75] 1.00 mL freshly prepared lysate of *M. catarrhalis* DSM11994^[200] were incubated with 20 μ L IA-alkyne (5 mM stock in DMSO for a final concentration of 100 μ M, high concentration) at room temperature for 1 h. Another 1.00 mL sample of lysate was incubated with 20 μ L IA-alkyne (500 μ M stock in DMSO for a final concentration of 10 μ M, low concentration) at room temperature for 1 h. In additional control experiments, both samples were treated with high concentration of IA-alkyne. The samples were clicked to the heavy (high concentration) and light (low concentration) isoDTB tags by adding 120 μ L of a solution consisting of 60 μ L tris(benzyltriazolylmethyl)amine (TBTA, 0.9 mg/mL in 4:1 t -BuOH/DMSO), 20 μ L $CuSO_4 \cdot 5H_2O$ (12.5 mg/mL in H_2O), 20 μ L tris(2-carboxyethyl)phosphine (TCEP, 13 mg/mL in H_2O) and 20 μ L of the respective isoDTB tag (5 mM stock in DMSO). After incubation of the samples at room temperature for 1 h, the light- and the heavy-labeled samples were combined into 8 mL cold acetone in order to precipitate all proteins. Precipitates were stored at -20 °C overnight.

5.4 Competitive isoDTB-ABPP experiments in living bacteria

The chemoproteomic experiment was performed according to a published procedure.^[75]

For experiments in high bacterial density ($OD_{600} = 40$), 1.00 mL freshly resuspended living *M. catarrhalis* DSM11994^[200] ($OD_{600} = 40$) were incubated with 10 μ L of the respective compound (100 \times stock in DMSO; *e.g.*, 10 μ L 10 mM stock for a final concentration of 100 μ M) at 37 °C for 1 h while shaking (200 rpm). Another 1.00 mL sample of resuspended living bacteria ($OD_{600} = 40$) was incubated with 10 μ L DMSO. The cells were harvested by

centrifugation (6,000 ×g, 10 min, 4 °C) and washed two times with PBS prior to storage at –80 °C overnight.

For experiments in low bacterial density ($OD_{600}=4$), 10.0 mL freshly resuspended living *M. catarrhalis* DSM11994^[200] ($OD_{600}=4$) were incubated with 100 µL of the respective compound (100× stock in DMSO; e.g., 100 µL 10 mM stock for a final concentration of 100 µM) at 37 °C for 1 h while shaking (200 rpm). Another 10.0 mL sample of resuspended living bacteria ($OD_{600}=4$) was incubated with 100 µL DMSO. The cells were harvested by centrifugation (6,000 ×g, 10 min, 4 °C) and washed two times with PBS prior to storage at –80 °C overnight.

For all experiments, the pellets were resuspended in 1 mL PBS and 20 µL sodium dodecyl sulfate (SDS, 20 wt% in PBS for a final concentration of 0.4 wt%) was added and sonicated (Bandelin Sonoplus, 10 s, 20% intensity). The lysate was cleared by centrifugation (21,100 ×g, 1 h, r.t.) and 900 µL of the supernatant were transferred to a new microcentrifuge tube. Subsequently, 9 µL IA-alkyne (10 mM stock in DMSO for a final concentration of 100 µM) were separately added to the lysate with and without competitor and incubated at room temperature for 1 h. The samples were clicked to the heavy (DMSO-treated) and light (compound-treated) isoDTB tags by adding 108 µL of a solution consisting of 54 µL TBTA ligand (0.9 mg/mL in 4:1 ^tBuOH/DMSO), 18 µL CuSO₄·5H₂O (12.5 mg/mL in H₂O), 18 µL TCEP (13 mg/mL in H₂O) and 18 µL of the respective isoDTB tag (5 mM stock in DMSO). After incubation of the samples at room temperature for 1 h, the light- and the heavy-labeled samples were combined into 7.2 mL cold acetone in order to precipitate all proteins. Precipitates were stored at –20 °C overnight.

5.5 MS sample preparation

The MS samples were prepared according to a published procedure.^[45,75] The protein precipitates were centrifuged (3,500 rpm, 10 min, r.t.) and the supernatant was removed. The precipitates were resuspended in 1 mL cold methanol by sonification and centrifuged (21,100 ×g, 10 min, 4 °C). The supernatant was removed and this wash step with methanol was repeated one more time. The pellets were dissolved in 300 µL urea (8 M, 0.1 M aqueous triethylammonium bicarbonate (TEAB)) by sonification. 900 µL TEAB (0.1 M in H₂O) were added to obtain a concentration of 2 M urea. This solution was added to 1.2 mL of washed high capacity streptavidin agarose beads (50 µL initial slurry, Fisher Scientific, 10733315) in NP40 substitute (0.2% in PBS). The samples were rotated at room temperature

for 1 h in order to assure binding to the beads. The beads were centrifuged ($1,000 \times g$, 1 min, r.t.) and the supernatant was removed. The beads were resuspended in 600 μL NP40 substitute (0.1% in PBS) and transferred to a centrifuge column (Fisher Scientific, 11894131). Beads were washed with $2 \times 600 \mu\text{L}$ NP40 substitute (0.1% in PBS), $3 \times 600 \mu\text{L}$ PBS and $3 \times 600 \mu\text{L}$ H_2O . The beads were resuspended in 600 μL urea (8 M in 0.1 M aqueous TEAB), transferred to a Protein LoBind tube (Eppendorf) and centrifuged ($1,000 \times g$, 1 min, r.t.). The supernatant was removed, the beads were resuspended in 300 μL urea (8 M in 0.1 M aqueous TEAB) and incubated with 15 μL dithiothreitol (DTT, 31 mg/mL in H_2O) at 37 °C for 45 min while shaking (200 rpm). They were further treated with 15 μL iodoacetamide (74 mg/mL in H_2O) at room temperature for 30 min while rotating and with 15 μL DTT (31 mg/mL in H_2O) at room temperature for 30 min while rotating. The samples were diluted with 900 μL TEAB (0.1 M in H_2O) and centrifuged ($1,000 \times g$, 1 min, r.t.). After removal of the supernatant, the beads were resuspended in 200 μL urea (2 M in 0.1 M aqueous TEAB) and incubated with 4 μL trypsin (0.5 mg/mL, Promega, V5113) at 37 °C overnight while shaking (200 rpm). The samples were diluted by adding 400 μL NP40 substitute (0.1% in PBS) and transferred to a centrifuge column (Fisher Scientific, 11894131). Beads were washed with $3 \times 600 \mu\text{L}$ NP40 substitute (0.1% in PBS), $3 \times 800 \mu\text{L}$ PBS and $3 \times 800 \mu\text{L}$ H_2O . Peptides were eluted into Protein LoBind tubes (Eppendorf) with $1 \times 200 \mu\text{L}$ and $2 \times 100 \mu\text{L}$ trifluoroacetic acid (TFA, 0.1% in 50% aqueous MeCN) followed by a final centrifugation ($3,000 \times g$, 3 min, r.t.). The solvent was removed in a rotating vacuum concentrator (~ 5 h, 30 °C) and the resulting residue was dissolved in 30 μL formic acid (1% in H_2O) or 30 μL TFA (0.1% in H_2O) by sonification for 5 min. Samples were filtered through filters (Merck, UVC30GVNB) washed with the same solution by centrifugation ($17,000 \times g$, 3 min, r.t.) and transferred into MS sample vials. Samples were stored at -20 °C until measurement.

5.6 Sample analysis by LC-MS/MS

The samples were analyzed according to a published procedure.^[45] 5 μL of the samples were analyzed using a Qexactive Plus mass spectrometer (ThermoFisher) coupled to an Ultimate 3000 nano HPLC system (Dionex). Samples were loaded on an Acclaim C18 PepMap100 trap column (75 μm ID \times 2 cm, Acclaim, PN 164535) and washed with 0.1% TFA. The subsequent separation was carried out on an AURORA series AUR2-25075C18A column (75 μm ID \times 25 cm, Serial No. IO257504282) with a flow rate of 400 nL/min using

buffer A (0.1% formic acid in water) and buffer B (0.1% formic acid in acetonitrile). The column was heated to 40 °C. Analysis started with washing in 5% B for 7 min followed by a gradient from 5% to 40% buffer B over 105 min, an increase to 60% B in 10 min and another increase to 90% B in 10 min. 90% B was held for 10 min, then decreased to 5% in 0.1 min and held at 5% for another 9.9 min. The Qexactive Plus mass spectrometer was run in a TOP10 data-dependent mode. In the orbitrap, full MS scans were collected in a scan range of 300-1500 m/z at a resolution of 70,000 and an AGC target of 3e6 with 80 ms maximum injection time. The most intense peaks were selected for MS2 measurement with a minimum AGC target of 1e3 and isotope exclusion and dynamic exclusion (exclusion duration: 60 s) enabled. Peaks with unassigned charge or a charge of +1 were excluded. Peptide match was “preferred”. MS2 spectra were collected at a resolution of 17,500 aiming at an AGC target of 1e5 with a maximum injection time of 100 ms. Isolation was conducted in the quadrupole using a window of 1.6 m/z. Fragments were generated using higher-energy collisional dissociation (HCD, normalized collision energy: 27%) and finally detected in the orbitrap.

5.7 isoDTB-ABPP data analysis

The data analysis described in the following sections was performed according to published procedures.^[45,75]

Data analysis using MaxQuant^[45,75]

A FASTA database for *M. catarrhalis* DSM11994^[200] was downloaded from www.uniprot.org using a search for “1236608” as “Taxonomy [OC]” at UniProtKB on 20.05.2020.^[185] This corresponds to the FASTA database for the strain *M. catarrhalis* BBH18.^[193]

Quantification with MaxQuant^[218] was performed according to a published procedure utilizing a workaround to also allow quantification of peptides that contain one or more carbamidomethylated cysteines in addition to the isoDTB tag-labelled cysteine.^[45,75] Briefly, in this workaround “U”, which normally stands for selenocysteine, is used as a placeholder amino acid for the modified cysteine. To accomplish this, each cysteine in the FASTA database was individually replaced with a “U” generating n different sequences with a single “U” for a protein with n cysteines. For each individual replacement, an entry in the FASTA database was created, which was named in the format “UniProt code”_”C””number of the cysteine”. The unmodified sequence was deleted from the FASTA database, except if the protein did not contain any cysteine, in which case the unmodified entry was renamed to “UniProt Code”_”C0” and kept

in the database. In this way, for each cysteine in the database, a unique sequence was created, in which it was marked as the modified cysteine (by being replaced by the placeholder “U”) and all other cysteines were marked as unmodified (were remaining “C” in the database). In this way, there was always only one modified cysteine in each peptide to be detected and quantified. MS raw data were analyzed using MaxQuant software (version 1.6.17.0).^[218] Standard settings were used with the following changes and additions: The modified FASTA database with individual substitutions of cysteines with the placeholder “U” were used. Labels were set on the placeholder amino acid “U” for the light isoDTB tag as light label ($C_{28}H_{46}N_{10}O_6S_1Se_{.1}$) and the heavy isoDTB tag as heavy label ($C_{24}^{13}C_4H_{46}N_8^{15}N_2O_6S_1Se_{.1}$). A multiplicity of 2 was set and a maximum number of labelled amino acids of 1. The digestion enzyme was set to Trypsin/P with a maximum number of missed cleavages of 2. No variable modifications were included. The “Re-quantify” option was enabled. Carbamidomethyl (C_2H_3NO) was used as fixed modification on cysteine. Contaminants were included. Peptides were searched with a minimum peptide length of 7 and a maximum peptide mass of 4,600 Da. “Second peptides” and “Dependent peptides” were disabled and the option “Match between run” was enabled with a Match time window of 0.7 min and an alignment window of 20 min. An FDR of 0.01 was used for Protein FDR, PSM FDR and XPSM FDR. The “peptides.txt” file of the MaxQuant analysis was used for further analysis. All peptide sequences without a modified cysteine (placeholder “U”) and all reverse sequences were deleted. Only the columns “Sequence”, “Leading Razor Protein”, “Start Position” and the columns for “Ratio H/L” for all replicates were kept. The “Leading Razor Protein” was renamed to the UniProt Code without the indicator for the number of the cysteine. All individual ratios were filtered out if they were “NaN” and all other values were transformed into log₂-scale. For each peptide, the data was filtered out, if it was not present in at least two replicates or if the standard deviation between the replicates exceeded a value of 1.41. For each peptide, an identifier was generated in the form “UniProt Code”_”C”_”residue number of the modified cysteine”. The data for the same replicate for all peptides with the same identifier, and therefore the same modified cysteine, were combined. Here, the median of the data was used. The data was filtered out if the standard deviation exceeded a value of 1.41. Each modified cysteine was kept in the dataset once with the shortest peptide sequence as the reported sequence. For each modified cysteine, the values of the replicates were combined, but the individual values were also reported. The values were combined as the median and the data was filtered out if there was data not in at least two of the replicates or if the standard deviation exceeded a value of

1.41. These are the final ratios that are reported. The information on the “Gene Name” and “Name” was linked back from the FASTA database.

Downstream analysis for the reactivity experiments^[75]

The data for the reactivity experiments was analyzed according to a published procedure.^[75] Only the cysteines that are quantified in both the experiment comparing high and low concentration of IA-alkyne, as well as in the control experiment comparing two samples with high concentration of IA-alkyne were included. The data was finally transformed back into the linear scale from the \log_2 -scale. Cysteines with ratios $R_{10:1}$ in the experiment comparing high and low concentration of IA-alkyne are grouped into three bins: high reactivity cysteines: $R_{10:1} < 3$; medium reactivity cysteines: $3 < R_{10:1} < 5$; low reactivity cysteines: $R_{10:1} > 5$.

Downstream analysis for the competitive experiments^[75]

The data for the competitive experiments was analyzed according to a published procedure^[75] using the Perseus software.^[219] All individual values for each modified cysteine for the same condition were loaded into Perseus and analyzed using a one-sample t-test against a value of $\log_2(R) = 0$. Conditions with $p < 0.05$ were considered significant and compounds were deemed to engage a certain cysteine at a specific condition and called a “hit” if the statistical significance was $p < 0.05$ and the median ratio was $\log_2(R) > 2$. For volcano plots, the median values for $\log_2(R)$ and the $-\log_{10}(p)$ values derived from Perseus are used. In order to analyze the reproducibility between the two sets of two biologically independent replicates, the data for the sets of replicates was processed independently and the values for all cysteines detected in both sets of replicates were plotted. For the final data analysis, the highly promiscuous compounds **EN026**, **EN179** and **EN181** and all cysteines that were quantified in less than three conditions were excluded. A cysteine was defined as ligandable cysteine if it was engaged by at least one of the conditions with $p < 0.05$ and $\log_2(R) > 2$. For the comparison of the reactivity data with the ligandability data obtained from the competitive experiments, only cysteines were included that were quantified in both filtered data sets. The information on the ligandability of a certain cysteine was linked to its respective reactivity group (high reactivity, medium reactivity and low reactivity) and the fraction of ligandable cysteines among all cysteines within one reactivity group was calculated.

Analysis of protein essentiality^[45,75]

The analysis of protein essentiality was performed similarly as in previous publications.^[45,75] The essentiality data for *M. catarrhalis* DSM11994^[200] was derived from a literature report^[201] of the essential proteins in *M. catarrhalis* BBH18, which was used as the FASTA for our data evaluation, and all entries with values of $\log_2(\text{FC}) \leq -4.70$ were used to obtain an essentiality data sheet containing the $\log_2(\text{FC})$ and adjusted p-values. This information was linked into the data tables.^[185,193]

Analysis of functional sites^[75]

The analysis of functional sites was performed according to a published procedure.^[75] For all entries in the generated FASTA database for *M. catarrhalis* DSM11994,^[200] which was the FASTA database of *M. catarrhalis* BBH18,^[193] functional site annotations were downloaded using the *.gff files from UniProt on 21.02.2023.^[185] The site information was extracted, and a list was generated, in which all residues within annotated sites or five amino acid residues or less away from them were kept. Only annotations for cysteines were kept and only the following site annotations were considered: Active site, Binding site, Disulfide bond, DNA binding, Lipidation, Metal binding, Modified residue, Nucleotide binding, Site, Zinc finger. If a cysteine was in or five amino acids or less away from any of these sites, it was considered a functional site residue.

Analysis of functional protein classes^[75]

The analysis of functional protein classes was performed according to a published procedure.^[75] Gene Ontology terms^[206–209] for all entries in the generated FASTA database for *M. catarrhalis* DSM11994,^[200] which was the FASTA database for *M. catarrhalis* BBH18,^[193] in the category “GO – Molecular function” were downloaded from UniProt.^[185] For each term that was present in the database at least once, a functional class was annotated manually. In this way, each term for each protein was assigned to a functional class, if possible. If a protein was only associated with terms from one functional class, it was assigned to that functional class. If a protein was associated with terms from different functional classes, the functional class of the protein was assigned according to this order of priority: enzyme, modulator / scaffolding / adaptor, receptor / transporter / channel and then gene expression / nucleic acid-binding. If no functional class was assigned to any of the terms, the protein was classified as “not assigned”.

Analysis of protein accessibility

Information on residue accessibility was extracted using StructureMap^[202,203] with the adjustment that all releases of AlphaFold^[204,205] were searched for matches to the respective UniProt^[185] code keeping the latest match. The script determines the number of C α atoms in a cone with a maximum distance of 12 Å and an angle of 70° around the respective residue. The residue identifier was generated for each residue and the accessibility information was only retained for cysteines and if the quality was 70 or higher. The column “nAA_12_70_pae” was renamed to pPSE (nAA_12_70_pae), for which a value ≤ 5 was considered high accessibility and a value > 5 was considered low accessibility.^[202,203]

5.8 Cloning

All cloning experiments were conducted according to a published procedure.^[75] *N*-terminal 6 \times His-tagged (UniProt ID: D5V965) and *C*-terminal 6 \times His-tagged (UniProt ID: D5V8R7, D5V8H6 and D5VB25) constructs of *M. catarrhalis* DSM11994^[200] were cloned into pET28a+ expression vectors using standard techniques based on polymerase chain reaction (PCR), restriction, digestion and ligation. Genomic DNA was extracted from 1 mL *M. catarrhalis* DSM11994^[200] culture (OD₆₀₀ = 1) with a Bacterial DNA Kit (peqlab). PCRs were carried out in a CFX96 Real-time System in combination with a C1000 Thermal Cycler (BioRad). The PCR mixture contained 10 μ L GC or HF buffer (NEB), 1 μ L dNTP mix (10 mM), 2.5 μ L forward primer (10 μ M, D5V965: 5'-CTGCAGCATATGACCACGATTAACCACACATTAG-3'; D5V8R7: 5'-CTGCAGCCATGGGCAATATACCATTATTAGGTGTCAATATCG-3'; D5V8H6: 5'-CTGCAGCCATGGGCCAAATCCATCAAATGCGACCGAC-3'; D5VB25: 5'-CTGCAGCCATGGGCAGCCAGACTTCACTCATCTATTTA-3'), 2.5 μ L reverse primer (10 μ M, D5V965: 5'-GTTAGCGGATCCTTATGTGTGCTTTTTTTG AACCAAGTA-3'; D5V8R7: 5'-GTTAGCCTCGAGATGATTGGTCGTTTTATCTTGAACAAA-3'; D5V8H6: 5'-GTTAGCCTCGAGAATAAAACGATTTGGGATAAGCTGG-3'; D5VB25: 5'-GTTAGCCTCGAGATGCTCTTGCCACTCAACGG-3'), 1 μ L genomic DNA as template (31 ng), 0.5 μ L Phusion High Fidelity DNA polymerase (NEB) and 32.5 μ L ddH₂O. After initial denaturation (98 °C, 30 s), the mixtures underwent 35 cycles of denaturation (98 °C, 10 s), annealing (D5V965: 71 °C, D5V8R7, D5V8H6 and D5VB25: 72 °C, 20 s) and extension (72 °C, D5V965 and D5V8R7: 57 s; D5V8H6 and D5VB25: 74 s), before a final extension (72 °C, 10 min). PCR products were purified by agarose gel electrophoreses on a 1% agarose gel run at 90 V for 50 min. After extraction with an E.Z.N.A.

Gel Extraction Kit (Omega bio-tek), 500 ng of the PCR products were digested in Cut Smart buffer (NEB) in a total volume of 50 μ L at 37 °C for 90 min using 5 units of the restriction enzymes (D5V965: NdeI and BamHI; D5V8R7, D5V8H6 and D5VB25: NcoI and XhoI), each, which were then inactivated by incubation at 80 °C for 20 min. Isolation of the digest was carried out using an E.Z.N.A. Gel Extraction Kit (Omega bio-tek). pET28a+ vector was extracted from NEB5 α *E. coli* using a NucleoSpin Plasmid EasyPure kit (Macherey-Nagel). 500 ng vector for each construct was digested in Cut Smart buffer (NEB) in a total volume of 50 μ L at 37 °C for 1 h using 5 units of the respective restriction enzymes, each. In order to dephosphorylate the ends of the restriction sites, 5 units Antarctic phosphatase (NEB) in Antarctic phosphatase buffer (NEB) were added, each, and digestion was continued for another 30 min before heat inactivation at 80 °C for 20 min. Purification of the digested vector was carried out by agarose gel electrophoresis and gel extraction. 14 fmol digested pET28a+ vector and 42 fmol digested insert were ligated using 1 μ L Quick Ligase (NEB) in Quick Ligase buffer (NEB) in a total volume of 20 μ L. The ligation mixture was incubated at room temperature for 5 min and 15 μ L (D5V965 and D5V8R7) or 10 μ L (D5V8H6 and D5VB25) of the ligation product were subsequently transformed into XL1-blue chemically competent cells (Agilent). For this, 100 μ L (D5V965 and D5V8R7) or 50 μ L (D5V8H6 and D5VB25) competent cells were thawed on ice, cautiously mixed with the respective DNA and kept on ice for 30 min. Afterwards, the cells were heat-shocked at 42 °C for 45 s and chilled on ice for 2 min. 500 μ L SOC (super optimal broth with catabolite repression, 20 g/L peptone, 5 g/L yeast extract, 600 mg/L NaCl, 200 mg/L KCl, 2 g/L MgSO₄, 20 mM D-glucose) medium were added and the cells incubated (200 rpm, 37 °C) for 1 h. The cells were harvested (6,000 \times g, 2 min, r.t.), resuspended in SOC medium and plated on LB agar plates containing 250 μ g/mL kanamycin. For preparation of the plasmids, 5 mL LB medium containing 250 μ g/mL kanamycin were inoculated with single colonies of the transformation and incubated (200 rpm, 37 °C) overnight. Plasmid DNA was prepared using a NucleoSpin Plasmid EasyPure kit (Macherey-Nagel) according to the manufacturer's instructions and sequenced by GeneWiz.

5.9 Site-directed mutagenesis

The Site-directed mutagenesis was performed according to a published procedure.^[75] The QuickChange site-directed mutagenesis system (Agilent) was used to construct the respective point mutants starting from the isolated wildtype plasmid DNA, respectively starting from the

generated D5V8H6 C60A plasmid DNA for the double point mutant D5V8H6 C60A C214A. The PCR mixture contained 10 μ L GC buffer (NEB), 1 μ L dNTP mix (10 mM), 1 μ L forward primer (10 μ M, D5V965 C15A: 5'-GATACCAAAGGGCTGATTGCGCCCGAACCTGTCATGCTAC-3'; D5V8R7 C26A: 5'-GGTGTGCGGCTATCCTGCGCCCATTAAGGAGCGCTG-3'; D5V8H6 C60A: 5'-GGCTTTGAACCTGTTGCGCATCAGCTGCTAAAGGCACAAG-3'; D5V8H6 C214A: 5'-GGTGAATTTTCATGGATCAGGAGCGTCA TTAGCCAGCCATATTGCAG-3'; D5V8H6 C60A C214A: 5'-GGTGAATTTTCATGGATCAGGAGCGTCATTAGCCAGCCATATTGCAG-3'), 1 μ L reverse primer (10 μ M, D5V965 C15A: 5'-GTAGCATGACAGGTTTCGGGCGCAATCAGCCCTTTGGTATC-3'; D5V8R7 C26A: 5'-CAGCGCTCCTTTAATGGGCGCAGGATAGCCGACACC-3'; D5V8H6 C60A: 5'-CTTGTGCCTTTAGCAGCTGATGCGCAACAGGTTCAAAGCC-3'; D5V8H6 C214A: 5'-CTGCAATATGGCTGGCTAATGACGCTCCTGATCCATGAAATTCACC-3'; D5V8H6 C60A C214A: 5'-CTGCAATATGGCTGGCTAATGACGCTCCTGATCCATGAAATTCACC-3'), 1 μ L template DNA (64-102 ng), 0.5 μ L Phusion High Fidelity DNA polymerase (NEB), 1-3 μ L DMSO and 34.5-32.5 μ L ddH₂O. After initial denaturation (95 °C, 30 s), the mixtures underwent 19 cycles of denaturation (95 °C, 15 s), annealing (55 °C, 30 s) and extension (72 °C, 5 min), before a final extension (72 °C, 10 min). 10 μ L of the PCR mixture were digested with 20 units DpnI at 37 °C for 4 h before transformation into XL1-blue cells was carried out as described above. Plasmid DNA was prepared using a NucleoSpin Plasmid EasyPure kit (Macherey-Nagel) according to the manufacturer's instructions and sequenced by GeneWiz.

5.10 Expression and purification of recombinant proteins

The expression and purification of the recombinant proteins were conducted according to a published procedure.^[75] Chemically competent *E. coli* BL21(DE3) cells were transformed with the respective plasmid. For protein overexpression, 20 mL LB medium containing 250 μ g/mL kanamycin were inoculated with the cryostocks of transformed *E. coli* BL21(DE3) cells and incubated (200 rpm, 37 °C) overnight. 1 L LB medium containing 250 μ g/mL kanamycin was inoculated with 10 mL of the overnight culture and incubated (200 rpm, 37 °C). The proteins were expressed at 18 °C overnight after induction at OD₆₀₀ = 0.6 with 1 mM *isopropyl*- β -D-thiogalactoside. Cells were harvested (6,000 rpm, 10 min, 4 °C), washed with 30 mL PBS, resuspended in 20 mL wash buffer 1 (20 mM Tris-HCl, pH = 8.0, 150 mM NaCl, 10 mM imidazole) and lysed by sonication (Bandelin Sonoplus) under constant

cooling with ice. Lysate was cleared by centrifugation (18,000 rpm, 30 min, 4 °C) and the supernatant was purified. Crude soluble lysate was loaded onto 2 mL of Ni-NTA-agarose beads (Qiagen) equilibrated with wash buffer 1 and flow-through was collected. The column was sequentially washed with 10 column volumes of wash buffer 1, 10 column volumes of wash buffer 2 (20 mM Tris-HCl, pH = 8.0, 1 M NaCl, 10 mM imidazole) and 10 column volumes of wash buffer 3 (20 mM Tris-HCl, pH = 8.0, 150 mM NaCl, 20 mM imidazole). The protein was eluted in 5 mL fractions using elution buffer (20 mM Tris-HCl, pH = 8.0, 150 mM NaCl, 300 mM imidazole). 50 μ L of each collected fraction were mixed with 50 μ L 2 \times Laemmli buffer and analyzed by SDS-PAGE with Coomassie staining. Fractions that contained the purified protein were concentrated using centrifugal filters (Merck, D5V965 and D5V965 C15A: 3 kDa cut-off, D5V8R7, D5V8R7 C26A, D5V8H6, D5V8H6 C60A, D5V8H6 C214A and D5V8H6 C60A C214A: 10 kDa cut-off, D5VB25: 30 kDa cut-off). During the concentration procedure, elution buffer was exchanged for a storage buffer (20 mM Tris-HCl, pH = 8.0, 150 mM NaCl). Purity of the isolated proteins was furthermore analyzed by intact protein MS (IPMS).

5.11 Gel-based competitive labelling experiments

The gel-based competitive labelling experiments were performed according to a published procedure.^[75] SirA-like protein (UniProt code: D5V965, 4 μ M final concentration), PdxJ (UniProt code: D5V8R7, 1 μ M final concentration) or ThiD (UniProt code: D5V8H6, 1 μ M final concentration) wildtype were added to lysate of *M. catarrhalis* DSM11994^[200] (1 mg/mL) to give a total volume of 50 μ L. The addition of no protein or the addition of the respective single or double-point mutants (D5V965 C15A: 4 μ M final concentration, all others: 1 μ M final concentration) instead of the wildtype proteins served as control experiments. 1 μ L of the respective compound (50 \times stock in DMSO; e.g., 1 μ L 2 mM stock for a final concentration of 40 μ M) at the indicated concentrations, respectively 1 μ L DMSO as a solvent control was added and it was incubated at room temperature for 1 h. Subsequently, 1 μ L IA-alkyne (D5V8R7 and D5V8R7 C15A: 2 mM stock in DMSO for a final concentration of 40 μ M, all others: 500 μ M stock in DMSO for a final concentration of 10 μ M) was added and incubated for another 1 h at room temperature. The samples were clicked to 5-carboxytetramethylrhodamine-azide (TAMRA-azide) by adding 6 μ L of a click-mix solution consisting of 240 μ L TBTA ligand (0.9 mg/mL in 4:1 ^tBuOH/DMSO), 80 μ L CuSO₄·5H₂O (12.5 mg/mL in H₂O), 80 μ L TCEP (13 mg/mL in H₂O)

and 4 μL TAMRA-azide (5 mM stock in DMSO). After incubation for 1 h at room temperature, the reaction mixtures were quenched by the addition of 50 μL 2 \times Laemmli buffer and analyzed by SDS-PAGE. Modification with TAMRA-azide was detected by in-gel fluorescence scanning and protein loading was visualized by Coomassie staining.

5.12 Intact protein MS (IPMS) experiments

The IPMS experiments were performed according to a published procedure.^[75] High-resolution IPMS was performed to validate the identity of the recombinantly expressed proteins, as well as to measure the degree of covalent modification of the respective cysteines with the indicated compounds. Therefore, 10 μL of the respective expressed proteins (50 μM stock in PBS for a final concentration of 5 μM) and 5 μL of the different compounds (20 \times stock in DMSO; *e.g.*, 5 μL 800 μM stock for a final concentration of 40 μM) or DMSO as a solvent control were added into 85 μL PBS and incubated for 1 h at 37 $^{\circ}\text{C}$. All samples were measured on a Dionex Ultimate 3000 HPLC system (Thermo Scientific) coupled to an LTQ Orbitrap XL mass spectrometer (Thermo Scientific) with an electrospray ionization source (spray voltage 4.0 kV, tube lens 110 V, capillary voltage 31 V, sheath gas 30 a.u., aux gas 15 a.u.). The mass spectrometer was operated in positive ion mode collecting full scans at high resolution ($R = 100,000$) in a range of $m/z = 300\text{--}2000$. The protein spectra were deconvoluted using UniDec 2.6.7.

5.13 Activity assay for SirA-like protein

The inhibition of the activity of SirA-like protein was determined by quantification of the product L-alanine by LC-MS and was performed according to a published procedure.^[215,216] SirA-like protein (2 μM final concentration) or no SirA-like protein as a control were preincubated with 1 μL of the respective compound (100 \times stock in DMSO; *e.g.*, 1 μL 1 mM stock for a final concentration of 10 μM) or 1 μL DMSO as a control for 1 h at 37 $^{\circ}\text{C}$ in 95 μL 3-(morpholin-4-yl)propane-1-sulfonic acid buffer (MOPS, 50 mM, pH = 7.4). To the reaction mixtures were added 1 μL DTT (500 mM stock in MOPS buffer for a final concentration of 5 mM), 1 μL IscS (465 μM stock in storage buffer for a final concentration of 4.65 μM), 1 μL pyridoxal phosphate (1 mM stock in MOPS buffer for a final concentration of 10 μM) and 2 μL L-cysteine (500 mM stock in MOPS buffer for a final concentration of 10 mM) to reach a final volume of 100 μL and the reactions were incubated for another 30 min at 37 $^{\circ}\text{C}$.

A heat control (protein preincubation at 95 °C for 10 min) and samples with the addition of only one of the two proteins were included as control experiments. All samples were performed in triplicates. After incubation, 400 µL of cold acetone was added in order to precipitate the proteins and the samples were stored at –20 °C overnight. The proteins were then pelletized by centrifugation (21,100 ×g, 20 min, 4 °C) and the supernatant was transferred into new microcentrifuge tubes. The solvent was removed in a rotating vacuum concentrator (45 °C) and the residues were dissolved in 50 µL formic acid (0.1% in 2:1 H₂O/MeCN) by sonification for 5 min. The samples were clarified by another centrifugation (21,100 ×g, 10 min, r.t.) and transferred into MS sample vials. The samples were measured on a Dionex Ultimate 3000 HPLC system (Thermo Scientific) coupled to an LTQ Orbitrap XL mass spectrometer (Thermo Scientific). The subsequent separation was carried out on an Accucore HILIC column (150×2.1 mm, 2.6 µm, Serial No. 17526-152130, Thermo Scientific) with a flow rate of 400 µL/min using buffer A (0.1% formic acid and 5 mM ammonium acetate in 50:50 H₂O/MeCN) and buffer B (0.1% formic acid and 5 mM ammonium acetate in 5:95 H₂O/MeCN). The column was heated to 25 °C. The analysis started with an equilibration with 5% buffer A for 2 min followed by sample injection and an elution with a linear gradient from 5% to 50% buffer A over 12 min, an increase to 100 % buffer A over 3 min, a decrease to 5% buffer A over 3 min and an additional 2 min at 5% buffer A. The mass spectrometer was operated in positive ion mode collecting full scans (R = 60,000) and SIM scans (R = 30,000) in a range of m/z = 50-500 (full scan), respectively in a range of m/z = 89.55-90.55 (SIM scan) with the following settings: spray voltage 3.5 kV, tube lens 25 V, capillary voltage 6 V, capillary temperature 350 °C, sheath gas 40 a.u.. The spectra were analyzed with XCalibur 2.2 (Thermo Scientific) and the amount of generated L-alanine was quantified by integrating the corresponding peak of the SIM scan and by directly comparing the peak areas.

IV Bibliography

- [1] A. Fleming, On the Antibacterial Action of Cultures of a *Penicillium*, with Special Reference to their Use in the Isolation of *B. influenzae*. *Br J Exp Pathol.* **1929**, *10*, 226–236.
- [2] J. Davies, Where Have all the Antibiotics Gone? *Canadian Journal of Infectious Diseases and Medical Microbiology* **2006**, *17*, 287–290.
- [3] E. C. Bragginton, L. J. V. Piddock, UK and European Union public and charitable funding from 2008 to 2013 for bacteriology and antibiotic research in the UK: an observational study. *The Lancet Infectious Diseases* **2014**, *14*, 857–868.
- [4] A. Fleming, “Nobel Lecture: Penicillin” available at: <https://www.nobelprize.org/uploads/2018/06/fleming-lecture.pdf>. (accessed: 25th January **2023**).
- [5] World Health Organization, “Antimicrobial resistance” available at: <https://www.who.int/news-room/fact-sheets/detail/antimicrobial-resistance>. (accessed: 7th February **2023**).
- [6] J. O’Neill, Antimicrobial Resistance: Tackling a crisis for the health and wealth of nations. *The Review on Antimicrobial Resistance* **2014**.
- [7] J. O’Neill, Tackling drug-resistant infections globally: Final report and recommendations. *The Review on Antimicrobial Resistance* **2016**.
- [8] Centers for Disease Control and Prevention (U.S.), National Center for Emerging Zoonotic and Infectious Diseases (U.S.), National Center for HIV/AIDS, Viral Hepatitis, STD, and TB Prevention (U.S.), National Center for Immunization and Respiratory Diseases (U.S.), *Antibiotic Resistance Threats in the United States, 2013*, Centers For Disease Control And Prevention (U.S.), **2013**.
- [9] Centers for Disease Control and Prevention (U.S.), National Center for Emerging Zoonotic and Infectious Diseases (U.S.). Division of Healthcare and Quality Promotion. Antibiotic Resistance Coordination and Strategy Unit, *Antibiotic Resistance Threats in the United States, 2019*, Centers For Disease Control And Prevention (U.S.), **2019**.
- [10] C. J. Murray, K. S. Ikuta, F. Sharara, L. Swetschinski, G. Robles Aguilar, A. Gray, C. Han, C. Bisignano, P. Rao, E. Wool, S. C. Johnson, A. J. Browne, M. G. Chipeta, F. Fell, S. Hackett, et al., Global burden of bacterial antimicrobial resistance in 2019: a systematic analysis. *The Lancet* **2022**, *399*, 629–655.

- [11] D. M. P. De Oliveira, B. M. Forde, T. J. Kidd, P. N. A. Harris, M. A. Schembri, S. A. Beatson, D. L. Paterson, M. J. Walker, Antimicrobial Resistance in ESKAPE Pathogens. *Clin Microbiol Rev* **2020**, *33*, e00181-19.
- [12] World Health Organization, “Global priority list of antibiotic-resistant bacteria to guide research, discovery, and development of new antibiotics” available at: https://www.who.int/medicines/publications/WHO-PPL-Short_Summary_25Feb-ET_NM_WHO.pdf?ua=1. (accessed: 12th August **2019**).
- [13] T. Kostyanev, M. J. M. Bonten, S. O’Brien, H. Steel, S. Ross, B. François, E. Tacconelli, M. Winterhalter, R. A. Stavenger, A. Karlén, S. Harbarth, J. Hackett, H. S. Jafri, C. Vuong, A. MacGowan, et al., The Innovative Medicines Initiative’s New Drugs for Bad Bugs programme: European public–private partnerships for the development of new strategies to tackle antibiotic resistance. *Journal of Antimicrobial Chemotherapy* **2016**, *71*, 290–295.
- [14] M. Lakemeyer, W. Zhao, F. A. Mandl, P. Hammann, S. A. Sieber, Thinking Outside the Box–Novel Antibacterials To Tackle the Resistance Crisis. *Angewandte Chemie International Edition* **2018**, *57*, 14440–14475.
- [15] A. D. Russell, Antibiotic and biocide resistance in bacteria: Introduction. *Journal of Applied Microbiology* **2002**, *92*, 1S-3S.
- [16] K. Poole, Mechanisms of bacterial biocide and antibiotic resistance. *Journal of Applied Microbiology* **2002**, *92*, 55S-64S.
- [17] H. Nikaido, Multiple antibiotic resistance and efflux. *Current Opinion in Microbiology* **1998**, *1*, 516–523.
- [18] H. F. Chambers, Methicillin resistance in staphylococci: molecular and biochemical basis and clinical implications. *Clin. Microbiol. Rev.* **1997**, *10*, 781–791.
- [19] G. D. Wright, Aminoglycoside-modifying enzymes. *Current Opinion in Microbiology* **1999**, *2*, 499–503.
- [20] K. S. Thomson, E. Smith Moland, Version 2000: the new β -lactamases of Gram-negative bacteria at the dawn of the new millennium. *Microbes and Infection* **2000**, *2*, 1225–1235.
- [21] S. Zhao, J. W. Adamiak, V. Bonifay, J. Mehla, H. I. Zgurskaya, D. S. Tan, Defining new chemical space for drug penetration into Gram-negative bacteria. *Nat Chem Biol* **2020**, *16*, 1293–1302.
- [22] S. B. Levy, Active efflux mechanisms for antimicrobial resistance. *Antimicrob. Agents Chemother.* **1992**, *36*, 695–703.

- [23] A. Tuley, W. Fast, The Taxonomy of Covalent Inhibitors. *Biochemistry* **2018**, *57*, 3326–3337.
- [24] L. Boike, N. J. Henning, D. K. Nomura, Advances in covalent drug discovery. *Nat Rev Drug Discov* **2022**, *21*, 881–898.
- [25] J. Singh, R. C. Petter, T. A. Baillie, A. Whitty, The resurgence of covalent drugs. *Nat Rev Drug Discov* **2011**, *10*, 307–317.
- [26] J. Singh, The Ascension of Targeted Covalent Inhibitors. *J. Med. Chem.* **2022**, *65*, 5886–5901.
- [27] B. K. Park, A. Boobis, S. Clarke, C. E. P. Goldring, D. Jones, J. G. Kenna, C. Lambert, H. G. Lavery, D. J. Naisbitt, S. Nelson, D. A. Nicoll-Griffith, R. S. Obach, P. Routledge, D. A. Smith, D. J. Tweedie, et al., Managing the challenge of chemically reactive metabolites in drug development. *Nat Rev Drug Discov* **2011**, *10*, 292–306.
- [28] J. R. Vane, Inhibition of Prostaglandin Synthesis as a Mechanism of Action for Aspirin-like Drugs. *Nature New Biology* **1971**, *231*, 232–235.
- [29] G. J. Roth, N. Stanford, P. W. Majerus, Acetylation of prostaglandin synthase by aspirin. *Proc. Natl. Acad. Sci. U.S.A.* **1975**, *72*, 3073–3076.
- [30] D. J. Tipper, J. L. Strominger, Mechanism of action of penicillins: a proposal based on their structural similarity to acyl-D-alanyl-D-alanine. *Proc. Natl. Acad. Sci. U.S.A.* **1965**, *54*, 1133–1141.
- [31] R. Fernandes, P. Amador, C. Prudêncio, β -Lactams: chemical structure, mode of action and mechanisms of resistance. *Reviews in Medical Microbiology* **2013**, *24*, 7–17.
- [32] R. Lonsdale, R. A. Ward, Structure-based design of targeted covalent inhibitors. *Chem. Soc. Rev.* **2018**, *47*, 3816–3830.
- [33] F. Sutanto, M. Konstantinidou, A. Dömling, Covalent inhibitors: a rational approach to drug discovery. *RSC Med. Chem.* **2020**, *11*, 876–884.
- [34] S. De Cesco, J. Kurian, C. Dufresne, A. K. Mittermaier, N. Moitessier, Covalent inhibitors design and discovery. *European Journal of Medicinal Chemistry* **2017**, *138*, 96–114.
- [35] T. Zhang, J. M. Hatcher, M. Teng, N. S. Gray, M. Kostic, Recent Advances in Selective and Irreversible Covalent Ligand Development and Validation. *Cell Chemical Biology* **2019**, *26*, 1486–1500.
- [36] M. Gehring, S. A. Laufer, Emerging and Re-Emerging Warheads for Targeted Covalent Inhibitors: Applications in Medicinal Chemistry and Chemical Biology. *J. Med. Chem.* **2019**, *62*, 5673–5724.

- [37] S. M. Drawz, R. A. Bonomo, Three Decades of β -Lactamase Inhibitors. *Clin Microbiol Rev* **2010**, *23*, 160–201.
- [38] D. Hendlin, E. O. Stapley, M. Jackson, H. Wallick, A. K. Miller, F. J. Wolf, T. W. Miller, L. Chaiet, F. M. Kahan, E. L. Foltz, H. B. Woodruff, J. M. Mata, S. Hernandez, S. Mochales, Phosphonomycin, a New Antibiotic Produced by Strains of *Streptomyces*. *Science* **1969**, *166*, 122–123.
- [39] S. Eschenburg, M. Priestman, E. Schönbrunn, Evidence That the Fosfomycin Target Cys115 in UDP-N-acetylglucosamine Enolpyruvyl Transferase (MurA) Is Essential for Product Release. *Journal of Biological Chemistry* **2005**, *280*, 3757–3763.
- [40] F. A. Kuehl, F. J. Wolf, N. R. Trenner, R. L. Peck, R. P. Buhs, E. Howe, I. Putter, B. D. Hunnewell, R. Ormond, G. Downing, J. E. Lyons, E. Newstead, L. Chaiet, K. Folkers, D-4-AMINO-3-ISOXAZOLIDONE, A NEW ANTIBIOTIC. *J. Am. Chem. Soc.* **1955**, *77*, 2344–2345.
- [41] P. H. Hidy, E. B. Hodge, V. V. Young, R. L. Harned, G. A. Brewer, W. F. Phillips, W. F. Runge, H. E. Stavely, A. Pohland, H. Boaz, H. R. Sullivan, STRUCTURE AND REACTIONS OF CYCLOSERINE. *J. Am. Chem. Soc.* **1955**, *77*, 2345–2346.
- [42] E. H. Robitzek, I. J. Selikoff, Hydrazine derivatives of isonicotinic acid (rimifon marsilid) in the treatment of active progressive caseous-pneumonic tuberculosis; a preliminary report. *Am Rev Tuberc* **1952**, *65*, 402–428.
- [43] R. A. M. Serafim, L. Haarer, J. G. B. Pedreira, M. Gehringer, Covalent chemical probes for protein kinases. *Current Research in Chemical Biology* **2023**, *3*, 100040.
- [44] A. K. Ghosh, I. Samanta, A. Mondal, W. R. Liu, Covalent Inhibition in Drug Discovery. *ChemMedChem* **2019**, *14*, 889–906.
- [45] P. R. A. Zanon, F. Yu, P. Musacchio, L. Lewald, M. Zollo, K. Krauskopf, D. Mrdović, P. Raunft, T. E. Maher, M. Cigler, C. Chang, K. Lang, F. D. Toste, A. I. Nesvizhskii, S. M. Hacker, Profiling the proteome-wide selectivity of diverse electrophiles. **2021**, DOI 10.26434/chemrxiv-2021-w7rss-v2.
- [46] W. Lu, M. Kostic, T. Zhang, J. Che, M. P. Patricelli, L. H. Jones, E. T. Chouchani, N. S. Gray, Fragment-based covalent ligand discovery. *RSC Chem. Biol.* **2021**, *2*, 354–367.

- [47] D. E. Mortenson, G. J. Brighty, L. Plate, G. Bare, W. Chen, S. Li, H. Wang, B. F. Cravatt, S. Forli, E. T. Powers, K. B. Sharpless, I. A. Wilson, J. W. Kelly, “Inverse Drug Discovery” Strategy To Identify Proteins That Are Targeted by Latent Electrophiles As Exemplified by Aryl Fluorosulfates. *J. Am. Chem. Soc.* **2018**, *140*, 200–210.
- [48] W. C. Chan, S. Sharifzadeh, S. J. Buhrlage, J. A. Marto, Chemoproteomic methods for covalent drug discovery. *Chem. Soc. Rev.* **2021**, *50*, 8361–8381.
- [49] S. Wang, Y. Tian, M. Wang, M. Wang, G. Sun, X. Sun, Advanced Activity-Based Protein Profiling Application Strategies for Drug Development. *Front. Pharmacol.* **2018**, *9*, 353.
- [50] R. E. Moellering, B. F. Cravatt, How Chemoproteomics Can Enable Drug Discovery and Development. *Chemistry & Biology* **2012**, *19*, 11–22.
- [51] M. J. Niphakis, B. F. Cravatt, Enzyme Inhibitor Discovery by Activity-Based Protein Profiling. *Annual Review of Biochemistry* **2014**, *83*, 341–377.
- [52] B. F. Cravatt, E. J. Sorensen, Chemical strategies for the global analysis of protein function. *Curr Opin Chem Biol* **2000**, *4*, 663–668.
- [53] G. C. Adam, E. J. Sorensen, B. F. Cravatt, Chemical strategies for functional proteomics. *Mol Cell Proteomics* **2002**, *1*, 781–790.
- [54] M. Fonović, M. Bogyo, Activity-based probes as a tool for functional proteomic analysis of proteases. *Expert Review of Proteomics* **2008**, *5*, 721–730.
- [55] B. F. Cravatt, A. T. Wright, J. W. Kozarich, Activity-Based Protein Profiling: From Enzyme Chemistry to Proteomic Chemistry. *Annual Review of Biochemistry* **2008**, *77*, 383–414.
- [56] S. H. L. Verhelst, K. M. Bongers, L. I. Willems, Bioorthogonal Reactions in Activity-Based Protein Profiling. *Molecules* **2020**, *25*, 5994.
- [57] D. G. Hoch, D. Abegg, A. Adibekian, Cysteine-reactive probes and their use in chemical proteomics. *Chemical Communications* **2018**, *54*, 4501–4512.
- [58] M. H. Wright, S. A. Sieber, Chemical proteomics approaches for identifying the cellular targets of natural products. *Natural Product Reports* **2016**, *33*, 681–708.
- [59] J. Martell, E. Weerapana, Applications of Copper-Catalyzed Click Chemistry in Activity-Based Protein Profiling. *Molecules* **2014**, *19*, 1378–1393.
- [60] V. V. Rostovtsev, L. G. Green, V. V. Fokin, K. B. Sharpless, A Stepwise Huisgen Cycloaddition Process: Copper(I)-Catalyzed Regioselective “Ligation” of Azides and Terminal Alkynes. *Angew. Chem. Int. Ed.* **2002**, *41*, 2596–2599.

- [61] C. W. Tornøe, C. Christensen, M. Meldal, Peptidotriazoles on Solid Phase: [1,2,3]-Triazoles by Regiospecific Copper(I)-Catalyzed 1,3-Dipolar Cycloadditions of Terminal Alkynes to Azides. *J. Org. Chem.* **2002**, *67*, 3057–3064.
- [62] A. E. Speers, G. C. Adam, B. F. Cravatt, Activity-Based Protein Profiling in Vivo Using a Copper(I)-Catalyzed Azide-Alkyne [3 + 2] Cycloaddition. *J. Am. Chem. Soc.* **2003**, *125*, 4686–4687.
- [63] A. E. Speers, B. F. Cravatt, Profiling Enzyme Activities In Vivo Using Click Chemistry Methods. *Chemistry & Biology* **2004**, *11*, 535–546.
- [64] N. J. Agard, J. A. Prescher, C. R. Bertozzi, A Strain-Promoted [3 + 2] Azide–Alkyne Cycloaddition for Covalent Modification of Biomolecules in Living Systems. *J. Am. Chem. Soc.* **2004**, *126*, 15046–15047.
- [65] N. J. Agard, J. M. Baskin, J. A. Prescher, A. Lo, C. R. Bertozzi, A Comparative Study of Bioorthogonal Reactions with Azides. *ACS Chem. Biol.* **2006**, *1*, 644–648.
- [66] J. M. Baskin, J. A. Prescher, S. T. Laughlin, N. J. Agard, P. V. Chang, I. A. Miller, A. Lo, J. A. Codelli, C. R. Bertozzi, Copper-free click chemistry for dynamic *in vivo* imaging. *Proc. Natl. Acad. Sci. U.S.A.* **2007**, *104*, 16793–16797.
- [67] P. V. Chang, J. A. Prescher, E. M. Sletten, J. M. Baskin, I. A. Miller, N. J. Agard, A. Lo, C. R. Bertozzi, Copper-free click chemistry in living animals. *Proc. Natl. Acad. Sci. U.S.A.* **2010**, *107*, 1821–1826.
- [68] K. M. Backus, B. E. Correia, K. M. Lum, S. Forli, B. D. Horning, G. E. González-Páez, S. Chatterjee, B. R. Lanning, J. R. Teijaro, A. J. Olson, D. W. Wolan, B. F. Cravatt, Proteome-wide covalent ligand discovery in native biological systems. *Nature* **2016**, *534*, 570–574.
- [69] A. E. Speers, B. F. Cravatt, A Tandem Orthogonal Proteolysis Strategy for High-Content Chemical Proteomics. *J. Am. Chem. Soc.* **2005**, *127*, 10018–10019.
- [70] E. Weerapana, A. E. Speers, B. F. Cravatt, Tandem orthogonal proteolysis-activity-based protein profiling (TOP-ABPP)—a general method for mapping sites of probe modification in proteomes. *Nat Protoc* **2007**, *2*, 1414–1425.
- [71] E. Weerapana, C. Wang, G. M. Simon, F. Richter, S. Khare, M. B. D. Dillon, D. A. Bachovchin, K. Mowen, D. Baker, B. F. Cravatt, Quantitative reactivity profiling predicts functional cysteines in proteomes. *Nature* **2010**, *468*, 790–795.
- [72] C. Wang, E. Weerapana, M. M. Blewett, B. F. Cravatt, A chemoproteomic platform to quantitatively map targets of lipid-derived electrophiles. *Nature Methods* **2014**, *11*, 79–85.

- [73] K. Senkane, E. V. Vinogradova, R. M. Suciu, V. M. Crowley, B. W. Zaro, J. M. Bradshaw, K. A. Brameld, B. F. Cravatt, The Proteome-Wide Potential for Reversible Covalency at Cysteine. *Angewandte Chemie International Edition* **2019**, *58*, 11385–11389.
- [74] S. M. Hacker, K. M. Backus, M. R. Lazear, S. Forli, B. E. Correia, B. F. Cravatt, Global profiling of lysine reactivity and ligandability in the human proteome. *Nature Chemistry* **2017**, *9*, 1181–1190.
- [75] P. R. A. Zanon, L. Lewald, S. M. Hacker, Isotopically Labeled Desthiobiotin Azide (isoDTB) Tags Enable Global Profiling of the Bacterial Cysteinome. *Angewandte Chemie International Edition* **2020**, *59*, 2829–2836.
- [76] A. T. Kong, F. V. Leprevost, D. M. Avtonomov, D. Mellacheruvu, A. I. Nesvizhskii, MSFragger: ultrafast and comprehensive peptide identification in mass spectrometry-based proteomics. *Nat Methods* **2017**, *14*, 513–520.
- [77] F. Yu, G. C. Teo, A. T. Kong, S. E. Haynes, D. M. Avtonomov, D. J. Geiszler, A. I. Nesvizhskii, Identification of modified peptides using localization-aware open search. *Nat Commun* **2020**, *11*, 4065.
- [78] H.-Y. Chang, A. T. Kong, F. da Veiga Leprevost, D. M. Avtonomov, S. E. Haynes, A. I. Nesvizhskii, Crystal-C: A Computational Tool for Refinement of Open Search Results. *J. Proteome Res.* **2020**, *19*, 2511–2515.
- [79] D. J. Geiszler, A. T. Kong, D. M. Avtonomov, F. Yu, F. da V. Leprevost, A. I. Nesvizhskii, PTM-Shepherd: Analysis and Summarization of Post-Translational and Chemical Modifications From Open Search Results. *Molecular & Cellular Proteomics* **2021**, *20*, 100018.
- [80] A. Keller, A. I. Nesvizhskii, E. Kolker, R. Aebersold, Empirical Statistical Model To Estimate the Accuracy of Peptide Identifications Made by MS/MS and Database Search. *Anal. Chem.* **2002**, *74*, 5383–5392.
- [81] A. I. Nesvizhskii, A. Keller, E. Kolker, R. Aebersold, A Statistical Model for Identifying Proteins by Tandem Mass Spectrometry. *Anal. Chem.* **2003**, *75*, 4646–4658.
- [82] F. da Veiga Leprevost, S. E. Haynes, D. M. Avtonomov, H.-Y. Chang, A. K. Shanmugam, D. Mellacheruvu, A. T. Kong, A. I. Nesvizhskii, Philosopher: a versatile toolkit for shotgun proteomics data analysis. *Nat Methods* **2020**, *17*, 869–870.
- [83] G. C. Teo, D. A. Polasky, F. Yu, A. I. Nesvizhskii, Fast Deisotoping Algorithm and Its Implementation in the MSFragger Search Engine. *J. Proteome Res.* **2021**, *20*, 498–505.

- [84] F. Yu, S. E. Haynes, G. C. Teo, D. M. Avtonomov, D. A. Polasky, A. I. Nesvizhskii, Fast Quantitative Analysis of timsTOF PASEF Data with MSFragger and IonQuant. *Molecular & Cellular Proteomics* **2020**, *19*, 1575–1585.
- [85] L. Otvos, C. Snyder, B. Condie, P. Bulet, J. D. Wade, Chimeric Antimicrobial Peptides Exhibit Multiple Modes of Action. *International Journal of Peptide Research and Therapeutics* **2005**, *11*, 29–42.
- [86] P. Csermely, V. Agoston, S. Pongor, The efficiency of multi-target drugs: the network approach might help drug design. *Trends in Pharmacological Sciences* **2005**, *26*, 178–182.
- [87] T. Korcsmáros, M. S. Szalay, C. Böde, I. A. Kovács, P. Csermely, How to design multi-target drugs: target search options in cellular networks. *Expert Opinion on Drug Discovery* **2007**, *2*, 799–808.
- [88] J.-J. Lu, W. Pan, Y.-J. Hu, Y.-T. Wang, Multi-Target Drugs: The Trend of Drug Research and Development. *PLoS ONE* **2012**, *7*, e40262.
- [89] K. Li, L. A. Schurig-Briccio, X. Feng, A. Upadhyay, V. Pujari, B. Lechartier, F. L. Fontes, H. Yang, G. Rao, W. Zhu, A. Gulati, J. H. No, G. Cintra, S. Bogue, Y.-L. Liu, et al., Multitarget Drug Discovery for Tuberculosis and Other Infectious Diseases. *Journal of Medicinal Chemistry* **2014**, *57*, 3126–3139.
- [90] A. Talevi, Multi-target pharmacology: possibilities and limitations of the “skeleton key approach” from a medicinal chemist perspective. *Front. Pharmacol.* **2015**, *6*, DOI 10.3389/fphar.2015.00205.
- [91] K. Lewis, Persister cells, dormancy and infectious disease. *Nat Rev Microbiol* **2007**, *5*, 48–56.
- [92] K. Lewis, Platforms for antibiotic discovery. *Nat Rev Drug Discov* **2013**, *12*, 371–387.
- [93] K. A. Pardeshi, T. A. Kumar, G. Ravikumar, M. Shukla, G. Kaul, S. Chopra, H. Chakrapani, Targeted Antibacterial Activity Guided by Bacteria-Specific Nitroreductase Catalytic Activation to Produce Ciprofloxacin. *Bioconjugate Chemistry* **2019**, *30*, 751–759.
- [94] K. Sharma, K. Sengupta, H. Chakrapani, Nitroreductase-activated nitric oxide (NO) prodrugs. *Bioorganic & Medicinal Chemistry Letters* **2013**, *23*, 5964–5967.
- [95] A. Çelik, G. Yetiş, An unusually cold active nitroreductase for prodrug activations. *Bioorganic & Medicinal Chemistry* **2012**, *20*, 3540–3550.

- [96] P. Shukla, V. S. Khodade, M. SharathChandra, P. Chauhan, S. Mishra, S. Siddaramappa, B. E. Pradeep, A. Singh, H. Chakrapani, "On demand" redox buffering by H₂S contributes to antibiotic resistance revealed by a bacteria-specific H₂S donor. *Chemical Science* **2017**, *8*, 4967–4972.
- [97] R. E. Asnis, The reduction of Furacin by cell-free extracts of Furacin-resistant and parent-susceptible strains of *Escherichia coli*. *Archives of Biochemistry and Biophysics* **1957**, *66*, 208–216.
- [98] D. R. McCalla, C. Kaiser, M. H. Green, Genetics of nitrofurazone resistance in *Escherichia coli*. *J. Bacteriol.* **1978**, *133*, 10–16.
- [99] T. Kobori, H. Sasaki, W. C. Lee, S. Zenno, K. Saigo, M. E. P. Murphy, M. Tanokura, Structure and Site-directed Mutagenesis of a Flavoprotein from *Escherichia coli* That Reduces Nitrocompounds: ALTERATION OF PYRIDINE NUCLEOTIDE BINDING BY A SINGLE AMINO ACID SUBSTITUTION. *Journal of Biological Chemistry* **2001**, *276*, 2816–2823.
- [100] S. Zenno, H. Koike, A. N. Kumar, R. Jayaraman, M. Tanokura, K. Saigo, Biochemical characterization of NfsA, the *Escherichia coli* major nitroreductase exhibiting a high amino acid sequence homology to Frp, a *Vibrio harveyi* flavin oxidoreductase. *Journal of Bacteriology* **1996**, *178*, 4508–4514.
- [101] S. Zenno, H. Koike, M. Tanokura, K. Saigo, Gene Cloning, Purification, and Characterization of NfsB, a Minor Oxygen-Insensitive Nitroreductase from *Escherichia coli*, Similar in Biochemical Properties to FRase I, the Major Flavin Reductase in *Vibrio fischeri*. *Journal of Biochemistry* **1996**, *120*, 736–744.
- [102] R. S. Boddu, O. Perumal, D. K., Microbial nitroreductases: A versatile tool for biomedical and environmental applications. *Biotechnology and Applied Biochemistry* **2020**, 1518–1530.
- [103] M. D. Roldán, E. Pérez-Reinado, F. Castillo, C. Moreno-Vivián, Reduction of polynitroaromatic compounds: the bacterial nitroreductases. *FEMS Microbiol Rev* **2008**, *32*, 474–500.
- [104] J. J. Gavin, F. F. Ebetino, R. Freedman, W. E. Waterbury, The aerobic degradation of 1-(5-nitrofurfurylideneamino)-2-imidazolidinone (NF-246) by *Escherichia coli*. *Archives of Biochemistry and Biophysics* **1966**, *113*, 399–404.
- [105] F. J. Peterson, R. P. Mason, J. Hovsepian, J. L. Holtzman, Oxygen-sensitive and -insensitive nitroreduction by *Escherichia coli* and rat hepatic microsomes. *Journal of Biological Chemistry* **1979**, *254*, 4009–4014.

- [106] B. Valiauga, L. Misevičienė, M. H. Rich, D. F. Ackerley, J. Šarlauskas, N. Čėnas, Mechanism of Two-/Four-Electron Reduction of Nitroaromatics by Oxygen-Insensitive Nitroreductases: The Role of a Non-Enzymatic Reduction Step. *Molecules* **2018**, *23*, 1672.
- [107] K. Nepali, H.-Y. Lee, J.-P. Liou, Nitro-Group-Containing Drugs. *Journal of Medicinal Chemistry* **2019**, *62*, 2851–2893.
- [108] A. S. Breeze, E. E. Obaseiki-Ebor, Mutations to Nitrofurantoin and Nitrofurazone Resistance in Escherichia coli K12. *Microbiology* **1983**, *129*, 99–103.
- [109] C. C. McOsker, P. M. Fitzpatrick, Nitrofurantoin: Mechanism of action and implications for resistance development in common uropathogens. *Journal of Antimicrobial Chemotherapy* **1994**, *33*, 23–30.
- [110] D. R. McCalla, A. Reuvers, C. Kaiser, Mode of Action of Nitrofurazone. *J Bacteriol* **1970**, *104*, 1126–1134.
- [111] P. R. Race, A. L. Lovering, R. M. Green, A. Oссор, S. A. White, P. F. Searle, C. J. Wrighton, E. I. Hyde, Structural and Mechanistic Studies of *Escherichia coli* Nitroreductase with the Antibiotic Nitrofurazone: reversed binding orientations in different redox states of the enzyme. *Journal of Biological Chemistry* **2005**, *280*, 13256–13264.
- [112] J. Whiteway, P. Koziarz, J. Veall, N. Sandhu, P. Kumar, B. Hoecher, I. B. Lambert, Oxygen-insensitive nitroreductases: analysis of the roles of nfsA and nfsB in development of resistance to 5-nitrofur derivatives in Escherichia coli. *J. Bacteriol.* **1998**, *180*, 5529–5539.
- [113] G. N. Parkinson, J. V. Skelly, S. Neidle, Crystal Structure of FMN-Dependent Nitroreductase from *Escherichia coli* B: A Prodrug-Activating Enzyme^{†‡}. *Journal of Medicinal Chemistry* **2000**, *43*, 3624–3631.
- [114] A. L. Lovering, E. I. Hyde, P. F. Searle, S. A. White, The structure of Escherichia coli nitroreductase complexed with nicotinic acid: three crystal forms at 1.7 Å, 1.8 Å and 2.4 Å resolution. *Journal of Molecular Biology* **2001**, *309*, 203–213.
- [115] V. V. H. Le, I. G. Davies, C. D. Moon, D. Wheeler, P. J. Biggs, J. Rakonjac, Novel 5-Nitrofurantoin-Activating Reductase in Escherichia coli. *Antimicrob Agents Chemother* **2019**, *63*, e00868-19.
- [116] A. F. N. Tavares, L. S. Nobre, A. M. P. Melo, L. M. Saraiva, A Novel Nitroreductase of Staphylococcus aureus with S-Nitrosoglutathione Reductase Activity. *Journal of Bacteriology* **2009**, *191*, 3403–3406.

- [117] L. Sandegren, A. Lindqvist, G. Kahlmeter, D. I. Andersson, Nitrofurantoin resistance mechanism and fitness cost in *Escherichia coli*. *Journal of Antimicrobial Chemotherapy* **2008**, *62*, 495–503.
- [118] S. Martínez-Puchol, C. Gomes, M. J. Pons, L. Ruiz-Roldán, A. Torrents de la Peña, T. J. Ochoa, J. Ruiz, Development and analysis of furazolidone-resistant *Escherichia coli* mutants. *APMIS* **2015**, *123*, 676–681.
- [119] L.-L. Wu, Q. Wang, Y. Wang, N. Zhang, Q. Zhang, H.-Y. Hu, Rapid differentiation between bacterial infections and cancer using a near-infrared fluorogenic probe. *Chem. Sci.* **2020**, *11*, 3141–3145.
- [120] Z. Li, X. Li, X. Gao, Y. Zhang, W. Shi, H. Ma, Nitroreductase Detection and Hypoxic Tumor Cell Imaging by a Designed Sensitive and Selective Fluorescent Probe, 7-[(5-Nitrofuranyl)methoxy]-3-*H*-phenoxazin-3-one. *Anal. Chem.* **2013**, *85*, 3926–3932.
- [121] L. Cui, Y. Zhong, W. Zhu, Y. Xu, Q. Du, X. Wang, X. Qian, Y. Xiao, A New Prodrug-Derived Ratiometric Fluorescent Probe for Hypoxia: High Selectivity of Nitroreductase and Imaging in Tumor Cell. *Org. Lett.* **2011**, *13*, 928–931.
- [122] Y. Liu, W. Liu, H. Li, W. Yan, X. Yang, D. Liu, S. Wang, J. Zhang, Two-photon fluorescent probe for detection of nitroreductase and hypoxia-specific microenvironment of cancer stem cell. *Analytica Chimica Acta* **2018**, *1024*, 177–186.
- [123] J. Zhang, H.-W. Liu, X.-X. Hu, J. Li, L.-H. Liang, X.-B. Zhang, W. Tan, Efficient Two-Photon Fluorescent Probe for Nitroreductase Detection and Hypoxia Imaging in Tumor Cells and Tissues. *Anal. Chem.* **2015**, *87*, 11832–11839.
- [124] G. M. Anlezark, R. G. Melton, R. F. Sherwood, B. Coles, F. Friedlos, R. J. Knox, The bioactivation of 5-(aziridin-1-yl)-2,4-dinitrobenzamide (CB1954)—I. *Biochemical Pharmacology* **1992**, *44*, 2289–2295.
- [125] F. Friedlos, W. A. Denny, B. D. Palmer, C. J. Springer, Mustard Prodrugs for Activation by *Escherichia coli* Nitroreductase in Gene-Directed Enzyme Prodrug Therapy. *Journal of Medicinal Chemistry* **1997**, *40*, 1270–1275.
- [126] I. Niculescu-Duvaz, C. J. Springer, Antibody-directed enzyme prodrug therapy (ADEPT): a review. *Advanced Drug Delivery Reviews* **1997**, *26*, 151–172.
- [127] P. F. Searle, M.-J. Chen, L. Hu, P. R. Race, A. L. Lovering, J. I. Grove, C. Guise, M. Jaberipour, N. D. James, V. Mautner, L. S. Young, D. J. Kerr, A. Mountain, S. A. White, E. I. Hyde, NITROREDUCTASE: A PRODRUG-ACTIVATING ENZYME FOR CANCER GENE THERAPY. *Clinical and Experimental Pharmacology and Physiology* **2004**, *31*, 811–816.

- [128] E. Johansson, G. N. Parkinson, W. A. Denny, S. Neidle, Studies on the Nitroreductase Prodrug-Activating System. Crystal Structures of Complexes with the Inhibitor Dicoumarol and Dinitrobenzamide Prodrugs and of the Enzyme Active Form. *Journal of Medicinal Chemistry* **2003**, *46*, 4009–4020.
- [129] G. Dachs, M. Hunt, S. Syddall, D. Singleton, A. Patterson, Bystander or No Bystander for Gene Directed Enzyme Prodrug Therapy. *Molecules* **2009**, *14*, 4517–4545.
- [130] M. P. Hay, R. F. Anderson, D. M. Ferry, W. R. Wilson, W. A. Denny, Synthesis and Evaluation of Nitroheterocyclic Carbamate Prodrugs for Use with Nitroreductase-Mediated Gene-Directed Enzyme Prodrug Therapy. *Journal of Medicinal Chemistry* **2003**, *46*, 5533–5545.
- [131] S. O. Vass, D. Jarrom, W. R. Wilson, E. I. Hyde, P. F. Searle, E. coli NfsA: an alternative nitroreductase for prodrug activation gene therapy in combination with CB1954. *British Journal of Cancer* **2009**, *100*, 1903–1911.
- [132] A. V. Sharrock, S. P. McManaway, M. H. Rich, J. S. Mumm, I. F. Hermans, M. Tercel, F. B. Pruijn, D. F. Ackerley, Engineering the Escherichia coli Nitroreductase NfsA to Create a Flexible Enzyme-Prodrug Activation System. *Front. Pharmacol.* **2021**, *12*, 701456.
- [133] T. D. Gruber, C. Krishnamurthy, J. B. Grimm, M. R. Tadross, L. M. Wysocki, Z. J. Gartner, L. D. Lavis, Cell-Specific Chemical Delivery Using a Selective Nitroreductase–Nitroaryl Pair. *ACS Chemical Biology* **2018**, *13*, 2888–2896.
- [134] A. Chevalier, Y. Zhang, O. M. Khmour, J. B. Kaye, S. M. Hecht, Mitochondrial Nitroreductase Activity Enables Selective Imaging and Therapeutic Targeting. *J. Am. Chem. Soc.* **2016**, *138*, 12009–12012.
- [135] Z. Thiel, P. Rivera-Fuentes, Single-Molecule Imaging of Active Mitochondrial Nitroreductases Using a Photo-Crosslinking Fluorescent Sensor. *Angewandte Chemie International Edition* **2019**, *58*, 11474–11478.
- [136] K. M. Johnson, Z. D. Parsons, C. L. Barnes, K. S. Gates, Toward Hypoxia-Selective DNA-Alkylating Agents Built by Grafting Nitrogen Mustards onto the Bioreductively Activated, Hypoxia-Selective DNA-Oxidizing Agent 3-Amino-1,2,4-benzotriazine 1,4-Dioxide (Tirapazamine). *J. Org. Chem.* **2014**, *79*, 7520–7531.
- [137] P. Demange, E. Joly, J. Marcoux, P. R. Zanon, D. Listunov, P. Rullière, C. Barthes, C. Noirot, J.-B. Izquierdo, A. Rozié, K. Pradines, R. Hee, M. V. de Brito, M. Marcellin, R.-F. Serre, et al., SDR enzymes oxidize specific lipidic alkynylcarbinols into cytotoxic protein-reactive species. *eLife* **2022**, *11*, e73913.

- [138] A. Aires, V. R. Mota, M. J. Saavedra, E. A. S. Rosa, R. N. Bennett, The antimicrobial effects of glucosinolates and their respective enzymatic hydrolysis products on bacteria isolated from the human intestinal tract. *Journal of Applied Microbiology* **2009**, *106*, 2086–2095.
- [139] C. P. Glindemann, A. Backenköhler, M. Strieker, U. Wittstock, P. Klahn, Synthesis and Biochemical Evaluation of an Artificial, Fluorescent Glucosinolate (GSL). *ChemBioChem* **2019**, *20*, 2341–2345.
- [140] M. Abo, E. Weerapana, A Caged Electrophilic Probe for Global Analysis of Cysteine Reactivity in Living Cells. *Journal of the American Chemical Society* **2015**, *137*, 7087–7090.
- [141] M. Abo, D. W. Bak, E. Weerapana, Optimization of Caged Electrophiles for Improved Monitoring of Cysteine Reactivity in Living Cells. *ChemBioChem* **2017**, *18*, 81–84.
- [142] J. C. Powers, J. L. Asgian, Ö. D. Ekici, K. E. James, Irreversible Inhibitors of Serine, Cysteine, and Threonine Proteases. *Chemical Reviews* **2002**, *102*, 4639–4750.
- [143] S. I. Al-Gharabli, S. T. A. Shah, S. Weik, M. F. Schmidt, J. R. Mesters, D. Kuhn, G. Klebe, R. Hilgenfeld, J. Rademann, An Efficient Method for the Synthesis of Peptide Aldehyde Libraries Employed in the Discovery of Reversible SARS Coronavirus Main Protease (SARS-CoV M^{pro}) Inhibitors. *ChemBioChem* **2006**, *7*, 1048–1055.
- [144] E. Weerapana, G. M. Simon, B. F. Cravatt, Disparate proteome reactivity profiles of carbon electrophiles. *Nat Chem Biol* **2008**, *4*, 405–407.
- [145] J.-R. Deng, N. C.-H. Lai, K. K.-Y. Kung, B. Yang, S.-F. Chung, A. S.-L. Leung, M.-C. Choi, Y.-C. Leung, M.-K. Wong, N-Terminal selective modification of peptides and proteins using 2-ethynylbenzaldehydes. *Commun Chem* **2020**, *3*, 67.
- [146] P. M. S. D. Cal, J. B. Vicente, E. Pires, A. V. Coelho, L. F. Veiros, C. Cordeiro, P. M. P. Gois, Iminoboronates: A New Strategy for Reversible Protein Modification. *J. Am. Chem. Soc.* **2012**, *134*, 10299–10305.
- [147] R. M. Reja, W. Wang, Y. Lyu, F. Haeffner, J. Gao, Lysine-Targeting Reversible Covalent Inhibitors with Long Residence Time. *J. Am. Chem. Soc.* **2022**, *144*, 1152–1157.
- [148] G. Sacco, D. Arosio, M. Paolillo, A. Gloger, J. Scheuermann, L. Pignataro, L. Belvisi, A. Dal Corso, C. Gennari, RGD cyclopeptide equipped with a lysine-engaging salicylaldehyde shows enhanced integrin affinity and cell detachment potency. *Chemistry A European J* **2023**, chem.202203768.

- [149] T. Yang, A. Cuesta, X. Wan, G. B. Craven, B. Hirakawa, P. Khamphavong, J. R. May, J. C. Kath, J. D. Lapek, S. Niessen, A. L. Burlingame, J. D. Carelli, J. Taunton, Reversible lysine-targeted probes reveal residence time-based kinase selectivity. *Nat Chem Biol* **2022**, *18*, 934–941.
- [150] B. Imperiali, R. H. Abeles, Inhibition of serine proteases by peptidyl fluoromethyl ketones. *Biochemistry* **1986**, *25*, 3760–3767.
- [151] I. Dovgan, S. Erb, S. Hessmann, S. Ursuegui, C. Michel, C. Muller, G. Chaubet, S. Cianférani, A. Wagner, Arginine-selective bioconjugation with 4-azidophenyl glyoxal: application to the single and dual functionalisation of native antibodies. *Org. Biomol. Chem.* **2018**, *16*, 1305–1311.
- [152] J. I. MacDonald, H. K. Munch, T. Moore, M. B. Francis, One-step site-specific modification of native proteins with 2-pyridinecarboxyaldehydes. *Nat Chem Biol* **2015**, *11*, 326–331.
- [153] A. Onoda, N. Inoue, E. Sumiyoshi, T. Hayashi, Triazolecarbaldehyde Reagents for One-Step N-Terminal Protein Modification. *ChemBioChem* **2020**, *21*, 1274–1278.
- [154] M. Poreba, Protease-activated prodrugs: strategies, challenges, and future directions. *FEBS J* **2020**, *287*, 1936–1969.
- [155] M. L. Rodrigues, P. Carter, C. Wirth, S. Mullins, A. Lee, B. K. Blackburn, Synthesis and β -lactamase-mediated activation of a cephalosporin-taxol prodrug. *Chemistry & Biology* **1995**, *2*, 223–227.
- [156] S. A. Misal, K. R. Gawai, Azoreductase: a key player of xenobiotic metabolism. *Bioresour. Bioprocess.* **2018**, *5*, 17.
- [157] L. J. O'Connor, I. N. Mistry, S. L. Collins, L. K. Folkes, G. Brown, S. J. Conway, E. M. Hammond, CYP450 Enzymes Effect Oxygen-Dependent Reduction of Azide-Based Fluorogenic Dyes. *ACS Cent. Sci.* **2017**, *3*, 20–30.
- [158] P. Jones, M. E. Di Francesco, A. Petrocchi, J. Marszalek, G. Liu, Heterocyclic Modulators of HIF Activity for Treatment of Disease. **2014**, US2014057914A1.
- [159] W. Wierenga, A. W. Harrison, B. R. Evans, C. G. Chidester, Antibacterial benzisoxazolones. An unusual rearrangement product from o-nitrostyrene oxide en route to the photolabile carbonyl protecting group, (o-nitrophenyl)ethylene glycol. *The Journal of Organic Chemistry* **1984**, *49*, 438–442.
- [160] Y. Ji, J. Yang, L. Wu, L. Yu, X. Tang, Photochemical Regulation of Gene Expression Using Caged siRNAs with Single Terminal Vitamin E Modification. *Angewandte Chemie International Edition* **2016**, *55*, 2152–2156.

- [161] K. A. Datsenko, B. L. Wanner, One-step inactivation of chromosomal genes in *Escherichia coli* K-12 using PCR products. *Proceedings of the National Academy of Sciences* **2000**, *97*, 6640–6645.
- [162] M. Zollo, Evaluation of the Antibiotic Potential of Bromomethyl Ketones for the Development of Latent Electrophiles, Master's Thesis, Technical University of Munich, **2019**.
- [163] M. J. Horsburgh, J. L. Aish, I. J. White, L. Shaw, J. K. Lithgow, S. J. Foster, σ^B Modulates Virulence Determinant Expression and Stress Resistance: Characterization of a Functional *rsbU* Strain Derived from *Staphylococcus aureus* 8325-4. *J Bacteriol* **2002**, *184*, 5457–5467.
- [164] J. Ning, T. Liu, P. Dong, W. Wang, G. Ge, B. Wang, Z. Yu, L. Shi, X. Tian, X. Huo, L. Feng, C. Wang, C. Sun, J. Cui, T. D. James, et al., Molecular Design Strategy to Construct the Near-Infrared Fluorescent Probe for Selectively Sensing Human Cytochrome P450 2J2. *Journal of the American Chemical Society* **2019**, *141*, 1126–1134.
- [165] A. Alouane, R. Labruère, T. Le Saux, F. Schmidt, L. Jullien, Self-Immolative Spacers: Kinetic Aspects, Structure-Property Relationships, and Applications. *Angew. Chem. Int. Ed.* **2015**, *54*, 7492–7509.
- [166] B. A. Winn, Z. Shi, G. J. Carlson, Y. Wang, B. L. Nguyen, E. M. Kelly, R. D. Ross, E. Hamel, D. J. Chaplin, M. L. Trawick, K. G. Pinney, Bioreductively activatable prodrug conjugates of phenstatin designed to target tumor hypoxia. *Bioorganic & Medicinal Chemistry Letters* **2017**, *27*, 636–641.
- [167] E. Bellale, M. Naik, V. Vb, A. Ambady, A. Narayan, S. Ravishankar, V. Ramachandran, P. Kaur, R. McLaughlin, J. Whiteaker, S. Morayya, S. Guptha, S. Sharma, A. Raichurkar, D. Awasthy, et al., Diarylthiazole: An Antimycobacterial Scaffold Potentially Targeting PrrB-PrrA Two-Component System. *Journal of Medicinal Chemistry* **2014**, *57*, 6572–6582.
- [168] S. Pedragosa-Moreau, C. Morisseau, J. Zylber, A. Archelas, J. Baratti, R. Furstoss, Microbiological Transformations. 33. Fungal Epoxide Hydrolases Applied to the Synthesis of Enantiopure *Para*-Substituted Styrene Oxides. A Mechanistic Approach. *The Journal of Organic Chemistry* **1996**, *61*, 7402–7407.
- [169] B. L. Hodous, J. L. Kim, C. V. Miduturu, D. Wilson, Y. Zhang, COMPOSITIONS USEFUL FOR TREATING DISORDERS RELATED TO KIT. **2015**, US2015111857 (A1).

- [170] C. Houle, P. R. Savoie, C. Davies, D. Jardel, P. A. Champagne, B. Bibal, J. Paquin, Thiourea-Catalyzed C–F Bond Activation: Amination of Benzylic Fluorides. *Chem. Eur. J.* **2020**, *26*, 10620–10625.
- [171] P. S. Dragovich, F. Broccatelli, J. Chen, P. Fan, H. Le, W. Mao, T. H. Pillow, A. G. Polson, J. Wai, Z. Xu, H. Yao, D. Zhang, Design, synthesis, and biological evaluation of pyrrolobenzodiazepine-containing hypoxia-activated prodrugs. *Bioorganic & Medicinal Chemistry Letters* **2017**, *27*, 5300–5304.
- [172] C. Ge, F. Shen, Y. Yin, P. Zhou, C. Lu, A novel near-infrared and naked-eye fluorescence probe with a large Stokes shift for specific detection of cysteine and its application in living cells. *Tetrahedron Letters* **2020**, *61*, 151963.
- [173] F. de Nanteuil, J. Waser, Catalytic [3+2] Annulation of Aminocyclopropanes for the Enantiospecific Synthesis of Cyclopentylamines. *Angewandte Chemie International Edition* **2011**, *50*, 12075–12079.
- [174] J. M. Dener, L. H. Zhang, H. Rapoport, An effective chiroselective synthesis of (+)-pilocarpine from L-aspartic acid. *The Journal of Organic Chemistry* **1993**, *58*, 1159–1166.
- [175] J. P. Collman, M. Zhong, S. Costanzo, C. Zhang, New Imidazole-Based Tripodal Ligands as Cu_B Site Mimics of Cytochrome *c* Oxidase. *The Journal of Organic Chemistry* **2001**, *66*, 8252–8256.
- [176] D. Przybyla, U. Nubbemeyer, 4,5-Disubstituted *N*-Methylimidazoles as Versatile Building Blocks for Defined Side-Chain Introduction: 4,5-Disubstituted *N*-Methylimidazoles as Versatile Building Blocks for Defined Side-Chain Introduction. *European Journal of Organic Chemistry* **2017**, *2017*, 695–703.
- [177] R. M. de Figueiredo, L. Coudray, J. Dubois, Synthesis and biological evaluation of potential bisubstrate inhibitors of protein farnesyltransferase. Design and synthesis of functionalized imidazoles. *Organic & Biomolecular Chemistry* **2007**, *5*, 3299.
- [178] C. Jin, Q. Zhang, W. Lu, Synthesis and biological evaluation of hypoxia-activated prodrugs of SN-38. *European Journal of Medicinal Chemistry* **2017**, *132*, 135–141.
- [179] A. Singh, H.-J. Ha, J. Park, J. H. Kim, W. K. Lee, 3,4-Disubstituted oxazolidin-2-ones as constrained ceramide analogs with anticancer activities. *Bioorganic & Medicinal Chemistry* **2011**, *19*, 6174–6181.
- [180] A. P. Kostikov, N. Malashikhina, V. V. Popik, Caging of Carbonyl Compounds as Photolabile (2,5-Dihydroxyphenyl)ethylene Glycol Acetals. *The Journal of Organic Chemistry* **2009**, *74*, 1802–1804.

- [181] T. Tsunoda, M. Suzuki, R. Noyori, A facile procedure for acetalization under aprotic conditions. *Tetrahedron Letters* **1980**, *21*, 1357–1358.
- [182] M. Kurihara, W. Hakamata, Convenient Preparation of Cyclic Acetals, Using Diols, TMS-Source, and a Catalytic Amount of TMSOTf. *J. Org. Chem.* **2003**, *68*, 3413–3415.
- [183] R. L. Koder, A.-F. Miller, Steady-state kinetic mechanism, stereospecificity, substrate and inhibitor specificity of *Enterobacter cloacae* nitroreductase. *Biochimica et Biophysica Acta (BBA) - Protein Structure and Molecular Enzymology* **1998**, *1387*, 395–405.
- [184] D. Kessner, M. Chambers, R. Burke, D. Agus, P. Mallick, ProteoWizard: open source software for rapid proteomics tools development. *Bioinformatics* **2008**, *24*, 2534–2536.
- [185] The UniProt Consortium, A. Bateman, M.-J. Martin, S. Orchard, M. Magrane, S. Ahmad, E. Alpi, E. H. Bowler-Barnett, R. Britto, H. Bye-A-Jee, A. Cukura, P. Denny, T. Dogan, T. Ebenezer, J. Fan, et al., UniProt: the Universal Protein Knowledgebase in 2023. *Nucleic Acids Research* **2023**, *51*, D523–D531.
- [186] A. J. O'Neill, *Staphylococcus aureus* SH1000 and 8325-4: comparative genome sequences of key laboratory strains in staphylococcal research: Genomes of *Staph. aureus* SH1000 and 8325-4. *Letters in Applied Microbiology* **2010**, *51*, 358–361.
- [187] C. M. Verduin, C. Hol, A. Fleer, H. van Dijk, A. van Belkum, *Moraxella catarrhalis* : from Emerging to Established Pathogen. *Clin Microbiol Rev* **2002**, *15*, 125–144.
- [188] R. Karalus, A. Campagnari, *Moraxella catarrhalis*: a review of an important human mucosal pathogen. *Microbes and Infection* **2000**, *2*, 547–559.
- [189] T. F. Murphy, G. I. Parameswaran, *Moraxella catarrhalis*, a Human Respiratory Tract Pathogen. *CLIN INFECT DIS* **2009**, *49*, 124–131.
- [190] M. C. Enright, H. McKenzie, *Moraxella* (*Branhamella*) *catarrhalis* - clinical and molecular aspects of a rediscovered pathogen. *Journal of Medical Microbiology* **1997**, *46*, 360–371.
- [191] T. F. Murphy, A. L. Brauer, B. J. B. Grant, S. Sethi, *Moraxella catarrhalis* in Chronic Obstructive Pulmonary Disease: Burden of Disease and Immune Response. *Am J Respir Crit Care Med* **2005**, *172*, 195–199.
- [192] M. J. Brooks, J. L. Sedillo, N. Wagner, W. Wang, A. S. Attia, H. Wong, C. A. Laurence, E. J. Hansen, S. D. Gray-Owen, *Moraxella catarrhalis* Binding to Host Cellular Receptors Is Mediated by Sequence-Specific Determinants Not Conserved among All UspA1 Protein Variants. *Infect Immun* **2008**, *76*, 5322–5329.

- [193] S. P. W. de Vries, S. A. F. T. van Hijum, W. Schueler, K. Riesbeck, J. P. Hays, P. W. M. Hermans, H. J. Bootsma, Genome analysis of *Moraxella catarrhalis* strain BBH18, [corrected] a human respiratory tract pathogen. *J Bacteriol* **2010**, *192*, 3574–3583.
- [194] C.-P. Fung, S.-F. Yeo, D. M. Livermore, Susceptibility of *Moraxella catarrhalis* isolates to β -lactam antibiotics in relation to β -lactamase pattern. *J Antimicrob Chemother* **1994**, *33*, 215–222.
- [195] R. J. Wallace, V. A. Steingrube, D. R. Nash, D. G. Hollis, C. Flanagan, B. A. Brown, A. Labidi, R. E. Weaver, BRO beta-lactamases of *Branhamella catarrhalis* and *Moraxella* subgenus *Moraxella*, including evidence for chromosomal beta-lactamase transfer by conjugation in *B. catarrhalis*, *M. nonliquefaciens*, and *M. lacunata*. *Antimicrob Agents Chemother* **1989**, *33*, 1845–1854.
- [196] R. K. Budhani, J. K. Struthers, Interaction of *Streptococcus pneumoniae* and *Moraxella catarrhalis* : Investigation of the Indirect Pathogenic Role of β -Lactamase-Producing *Moraxellae* by Use of a Continuous-Culture Biofilm System. *Antimicrob Agents Chemother* **1998**, *42*, 2521–2526.
- [197] K. McGregor, B. J. Chang, B. J. Mee, T. V. Riley, *Moraxella catarrhalis*: Clinical significance, antimicrobial susceptibility and BRO beta-lactamases. *Eur. J. Clin. Microbiol. Infect. Dis.* **1998**, *17*, 219–234.
- [198] S. P. W. de Vries, P. Burghout, J. D. Langereis, A. Zomer, P. W. M. Hermans, H. J. Bootsma, Genetic requirements for *Moraxella catarrhalis* growth under iron-limiting conditions: *M. catarrhalis* gene essentiality under iron starvation. *Molecular Microbiology* **2013**, *87*, 14–29.
- [199] R. J. Melander, D. V. Zurawski, C. Melander, Narrow-spectrum antibacterial agents. *Med. Chem. Commun.* **2018**, *9*, 12–21.
- [200] T. Farmer, C. Reading, beta-Lactamases of *Branhamella catarrhalis* and their inhibition by clavulanic acid. *Antimicrob Agents Chemother* **1982**, *21*, 506–508.
- [201] F. M. Mobegi, S. A. van Hijum, P. Burghout, H. J. Bootsma, S. P. de Vries, C. E. van der Gaast-de Jongh, E. Simonetti, J. D. Langereis, P. W. Hermans, M. I. de Jonge, A. Zomer, From microbial gene essentiality to novel antimicrobial drug targets. *BMC Genomics* **2014**, *15*, 958.
- [202] I. Bludau, S. Willems, W.-F. Zeng, M. T. Strauss, F. M. Hansen, M. C. Tanzer, O. Karayel, B. A. Schulman, M. Mann, The structural context of posttranslational modifications at a proteome-wide scale. *PLoS Biol* **2022**, *20*, e3001636.

- [203] M. E. H. White, J. Gil, E. W. Tate, Proteome-wide structure-based accessibility analysis of ligandable and detectable cysteines in chemoproteomic datasets. **2022**, DOI 10.1101/2022.12.12.518491.
- [204] J. Jumper, R. Evans, A. Pritzel, T. Green, M. Figurnov, O. Ronneberger, K. Tunyasuvunakool, R. Bates, A. Žídek, A. Potapenko, A. Bridgland, C. Meyer, S. A. A. Kohl, A. J. Ballard, A. Cowie, et al., Highly accurate protein structure prediction with AlphaFold. *Nature* **2021**, *596*, 583–589.
- [205] M. Varadi, S. Anyango, M. Deshpande, S. Nair, C. Natassia, G. Yordanova, D. Yuan, O. Stroe, G. Wood, A. Laydon, A. Žídek, T. Green, K. Tunyasuvunakool, S. Petersen, J. Jumper, et al., AlphaFold Protein Structure Database: massively expanding the structural coverage of protein-sequence space with high-accuracy models. *Nucleic Acids Research* **2022**, *50*, D439–D444.
- [206] M. Ashburner, C. A. Ball, J. A. Blake, D. Botstein, H. Butler, J. M. Cherry, A. P. Davis, K. Dolinski, S. S. Dwight, J. T. Eppig, M. A. Harris, D. P. Hill, L. Issel-Tarver, A. Kasarskis, S. Lewis, et al., Gene Ontology: tool for the unification of biology. *Nat Genet* **2000**, *25*, 25–29.
- [207] The Gene Ontology Consortium, S. Carbon, E. Douglass, B. M. Good, D. R. Unni, N. L. Harris, C. J. Mungall, S. Basu, R. L. Chisholm, R. J. Dodson, E. Hartline, P. Fey, P. D. Thomas, L.-P. Albou, D. Ebert, et al., The Gene Ontology resource: enriching a GOld mine. *Nucleic Acids Research* **2021**, *49*, D325–D334.
- [208] R. P. Huntley, T. Sawford, P. Mutowo-Meullenet, A. Shypitsyna, C. Bonilla, M. J. Martin, C. O'Donovan, The GOA database: Gene Ontology annotation updates for 2015. *Nucleic Acids Research* **2015**, *43*, D1057–D1063.
- [209] D. Binns, E. Dimmer, R. Huntley, D. Barrell, C. O'Donovan, R. Apweiler, QuickGO: a web-based tool for Gene Ontology searching. *Bioinformatics* **2009**, *25*, 3045–3046.
- [210] K. F. Geoghegan, H. B. Dixon, P. J. Rosner, L. R. Hoth, A. J. Lanzetti, K. A. Borzilleri, E. S. Marr, L. H. Pezzullo, L. B. Martin, P. K. LeMotte, A. S. McColl, A. V. Kamath, J. G. Stroh, Spontaneous alpha-N-6-phosphogluconoylation of a “His tag” in *Escherichia coli*: the cause of extra mass of 258 or 178 Da in fusion proteins. *Anal Biochem* **1999**, *267*, 169–184.
- [211] M. C. Martos-Maldonado, C. T. Hjuler, K. K. Sørensen, M. B. Thygesen, J. E. Rasmussen, K. Villadsen, S. R. Midtgaard, S. Kol, S. Schoffelen, K. J. Jensen, Selective N-terminal acylation of peptides and proteins with a Gly-His tag sequence. *Nat Commun* **2018**, *9*, 3307.

- [212] Y. Ikeuchi, N. Shigi, J. Kato, A. Nishimura, T. Suzuki, Mechanistic Insights into Sulfur Relay by Multiple Sulfur Mediators Involved in Thiouridine Biosynthesis at tRNA Wobble Positions. *Molecular Cell* **2006**, *21*, 97–108.
- [213] J.-U. Dahl, C. Radon, M. Bühning, M. Nimtz, L. I. Leichert, Y. Denis, C. Jourlin-Castelli, C. Iobbi-Nivol, V. Méjean, S. Leimkühler, The Sulfur Carrier Protein TusA Has a Pleiotropic Role in Escherichia coli That Also Affects Molybdenum Cofactor Biosynthesis*. *Journal of Biological Chemistry* **2013**, *288*, 5426–5442.
- [214] R. Shi, A. Proteau, M. Villarroya, I. Moukadiri, L. Zhang, J.-F. Trempe, A. Matte, M. E. Armengod, M. Cygler, Structural Basis for Fe–S Cluster Assembly and tRNA Thiolation Mediated by IscS Protein–Protein Interactions. *PLoS Biol* **2010**, *8*, e1000354.
- [215] B. Selbach, E. Earles, P. C. Dos Santos, Kinetic Analysis of the Bisubstrate Cysteine Desulfurase SufS from *Bacillus subtilis*. *Biochemistry* **2010**, *49*, 8794–8802.
- [216] M. Pfanzelt, T. E. Maher, R. M. Absmeier, M. Schwarz, S. A. Sieber, Tailored Pyridoxal Probes Unravel Novel Cofactor-Dependent Targets and Antibiotic Hits in Critical Bacterial Pathogens. *Angew Chem Int Ed* **2022**, *61*, e202117724.
- [217] D. Szamosvári, T. Schuhmacher, C. R. Hauck, T. Böttcher, A thiochromenone antibiotic derived from the *Pseudomonas* quinolone signal selectively targets the Gram-negative pathogen *Moraxella catarrhalis*. *Chem. Sci.* **2019**, *10*, 6624–6628.
- [218] J. Cox, M. Mann, MaxQuant enables high peptide identification rates, individualized p.p.b.-range mass accuracies and proteome-wide protein quantification. *Nat Biotechnol* **2008**, *26*, 1367–1372.
- [219] S. Tyanova, T. Temu, P. Sinitcyn, A. Carlson, M. Y. Hein, T. Geiger, M. Mann, J. Cox, The Perseus computational platform for comprehensive analysis of (prote)omics data. *Nat Methods* **2016**, *13*, 731–740.

Abbreviations

λ	wavelength
δ	chemical shifts
Δm_{exp}	expected mass
A	alanine
ABP	activity-based probe
ABPP	activity-based protein profiling
ADEPT	antibody-directed enzyme prodrug therapy
AMR	antimicrobial resistance
B	biotin
BCA	bicinchoninic acid
BMK	bromomethyl ketone
br	broad signal
C	cysteine
CE	caged electrophile
conc.	concentrated
COPD	chronic obstructive pulmonary disease
CuAAC	copper (I)-catalyzed azide-alkyne cycloaddition
CYP450	cytochrome P450
d	day
d	doublet
dd	doublet of doublets
ddd	doublet of doublet of doublets
ddH ₂ O	double-distilled water

DMEM	Dulbecco's Modified Eagle's Medium
DMF	<i>N,N</i> -dimethylformamide
DMSO	dimethyl sulfoxide
DNA	deoxyribonucleic acid
dt	doublet of triplets
DTB	desthiobiotin
DTT	dithiothreitol
<i>e.g.</i>	<i>exempli gratia</i> – for example
eq	equivalent
ESI	electrospray ionization
<i>et al.</i>	et alii
Et ₂ O	diethyl ether
EtOAc	ethyl acetate
EU	European Union
FBS	fetal bovine serum
FDA	U.S. Food and Drug Administration
FMN	flavin mononucleotide
g	gravitational force equivalent
GDEPT	gene-directed enzyme prodrug therapy
GO	Gene Ontology
h	hour
HCD	higher-energy collisional dissociation
His	histidine
HPLC	high performance liquid chromatography
HRMS	high resolution mass spectrometry

Hz	Hertz
IA	iodoacetamide
IPMS	intact protein mass spectrometry
isoDTB	isotopically labelled desthiobiotin azide
isoDTB-ABPP	residue-specific activity-based protein profiling with isotopically labelled desthiobiotin azide tags
isoTOP-ABPP	isotopic tandem orthogonal proteolysis activity-based protein profiling
J	coupling constant
k_{-1} / k_{-2}	reverse rate constant
k_1 / k_2	forward rate constant
K_i	dissociation constant
LC-MS/MS	tandem mass spectrometry coupled to liquid chromatography
M	molar
m	multiplet
m/z	mass-to-charge ratio
MeCN	acetonitrile
MeOH	methanol
MIC	minimum inhibitory concentration
min	minute
MOPS	3-(morpholin-4-yl)propane-1-sulfonic acid
MRSA	methicillin-resistant <i>S. aureus</i>
MS	mass spectrometry
NADH	nicotinamide adenine dinucleotide
NADPH	nicotinamide adenine dinucleotide phosphate
NaOAc	sodium acetate

<i>n</i> -BuLi	<i>n</i> -butyllithium
NC	negative control
NMR	nuclear magnetic resonance
NP40	Nonidet P40
o/n	overnight
OD ₆₀₀	optical density at 600 nm
<i>p</i>	<i>para</i>
p	quintet
PBP	penicillin-binding protein
PBS	phosphate-buffered saline
PCR	polymerase chain reaction
pH	negative decadic logarithm of the hydrogen ion activity
p <i>K</i> _a	negative decadic logarithm of the acid dissociation constant
pLDDT	predicted local-distance difference test
POI	protein of interest
ppm	parts per million
pPSE	prediction-aware part-sphere exposure
PSM	peptide spectrum match
q	quartet
qd	quartet of doublets
<i>R</i>	competition ratio
r.t.	room temperature
<i>R</i> _f	retention factor
RG	reactive group
rpm	revolutions per minute

s	second
s	singlet
SDS	sodium dodecyl sulfate
SDS-PAGE	sodium dodecyl sulfate polyacrylamide gel electrophoresis
SOC	super optimal broth with catabolite repression
STP	sulfotetrafluorophenyl
t	time
t	triplet
TAMRA-azide	5-carboxytetramethylrhodamine-azide
TBAF	tetrabutylammonium fluoride
TBSCl	<i>tert</i> -butyldimethylsilyl chloride
TBTA	tris(benzyltriazolylmethyl)amine
^t BuOH	<i>tert</i> -butanol
TCEP	tris(2-carboxyethyl)phosphine
TCI	targeted covalent inhibitor
td	triplet of doublets
TEAB	triethylammonium bicarbonate
TEV	tobacco etch virus
TFA	trifluoroacetic acid
THF	tetrahydrofuran
TLC	thin layer chromatography
TMSOTf	trimethylsilyl trifluoromethanesulfonate
TOP-ABPP	tandem orthogonal proteolysis activity-based protein profiling
t_R	retention time
Tris	tris(hydroxymethyl)aminomethane

TsN ₃	tosyl azide
U.S.	United States
UK	United Kingdom
UV	ultraviolet
VDEPT	viral-directed enzyme prodrug therapy
WHO	World Health Organization
WT	wildtype
wt%	weight percentage

Appendix

1-bromohept-6-yn-2-one (BMK)

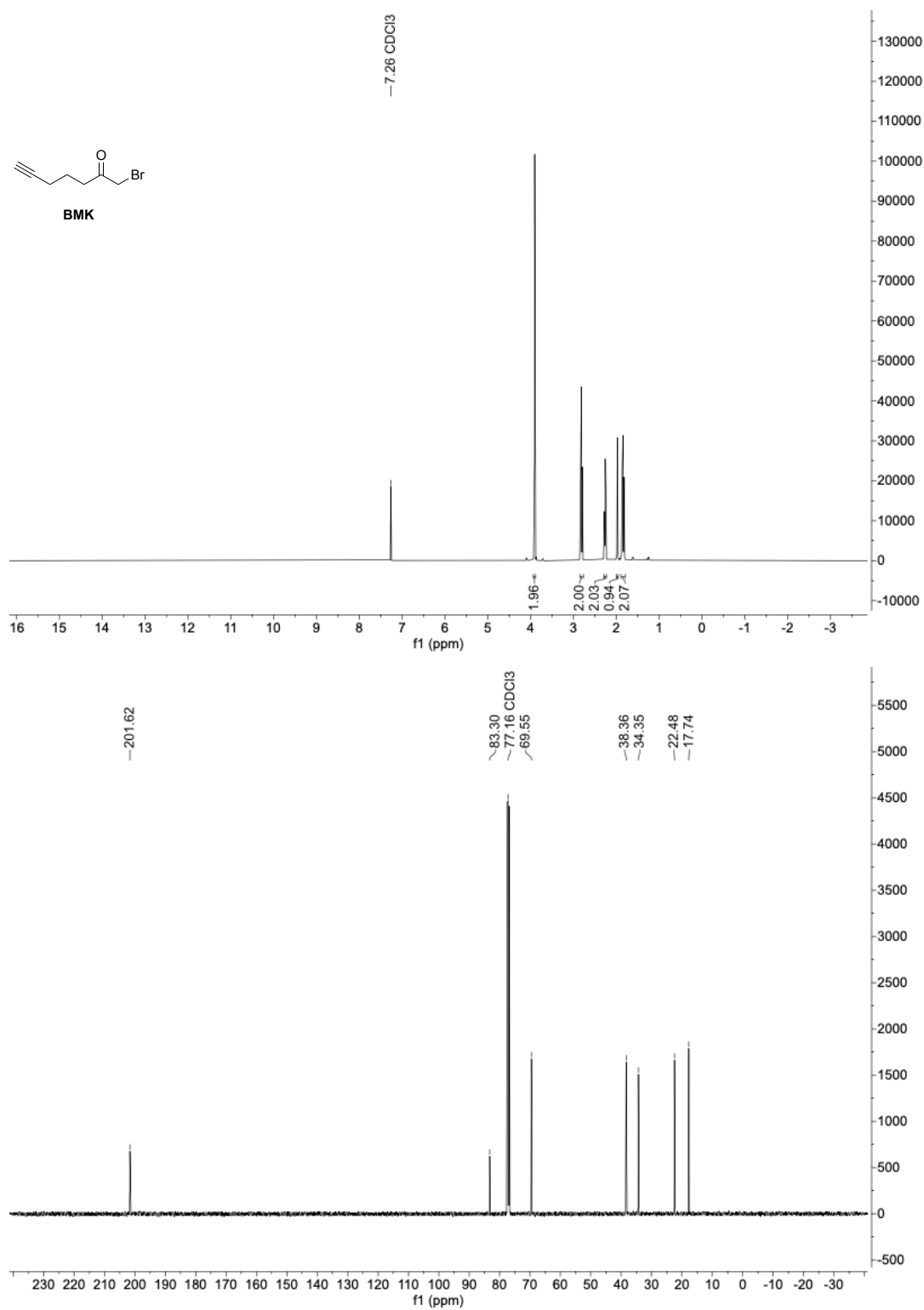


Figure 35: ¹H- and ¹³C-NMR spectra of 1-bromohept-6-yn-2-one (BMK).

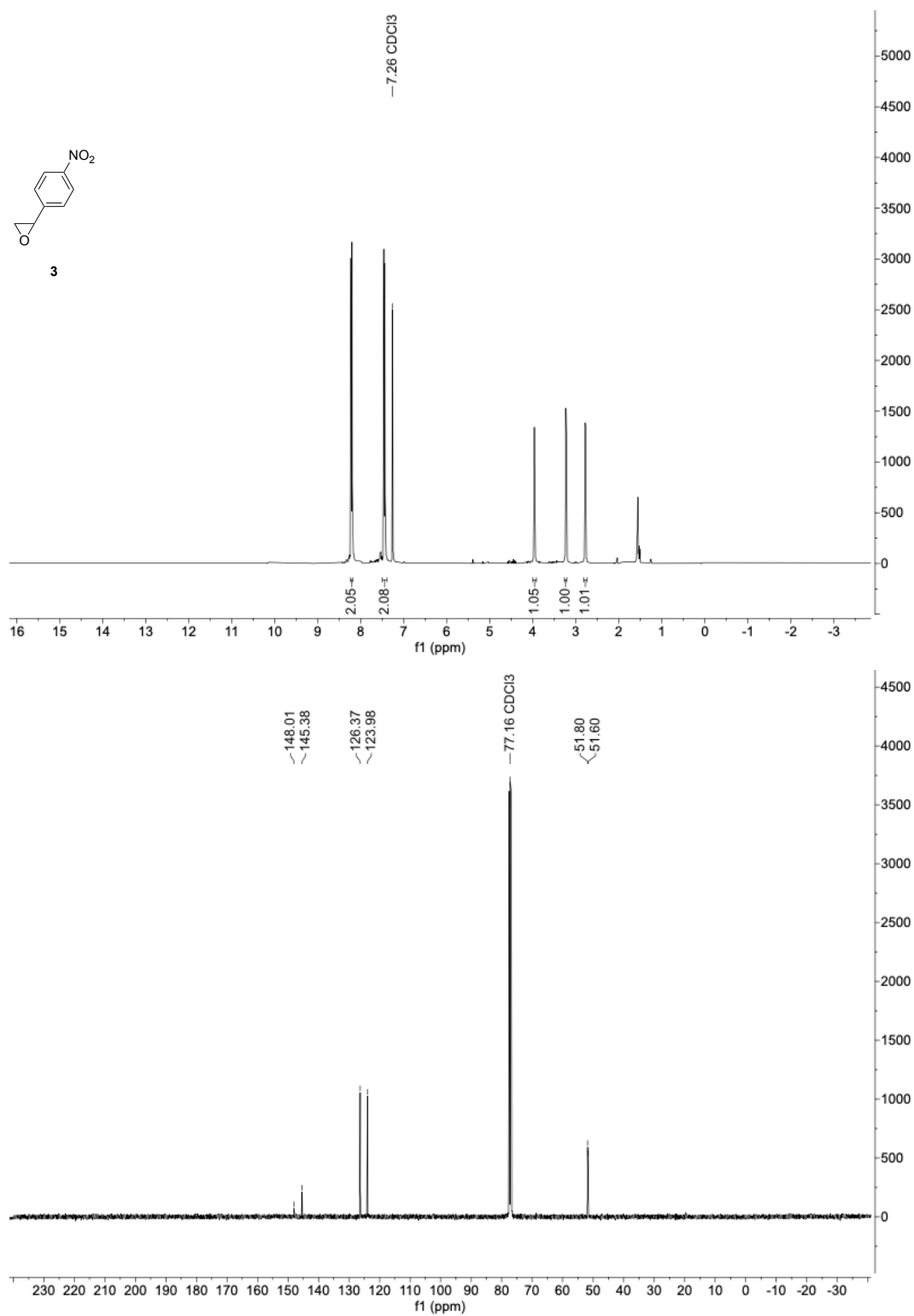
2-(4'-nitrophenyl)oxirane (**3**)

Figure 36: ¹H- and ¹³C-NMR spectra of 2-(4'-nitrophenyl)oxirane (**3**).

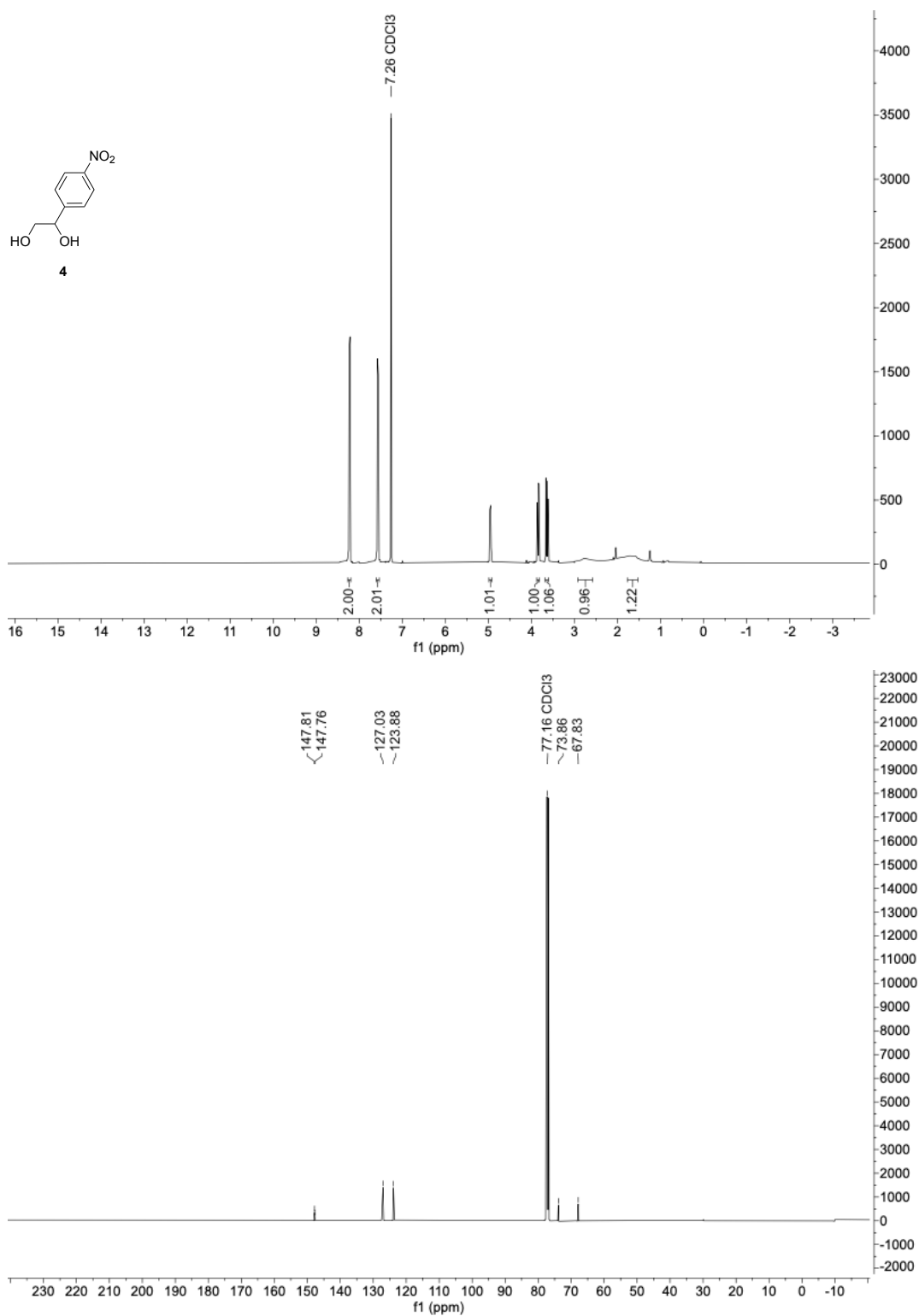
1-(4'-nitrophenyl)ethane-1,2-diol (**4**)

Figure 37: ¹H- and ¹³C-NMR spectra of 1-(4'-nitrophenyl)ethane-1,2-diol (**4**).

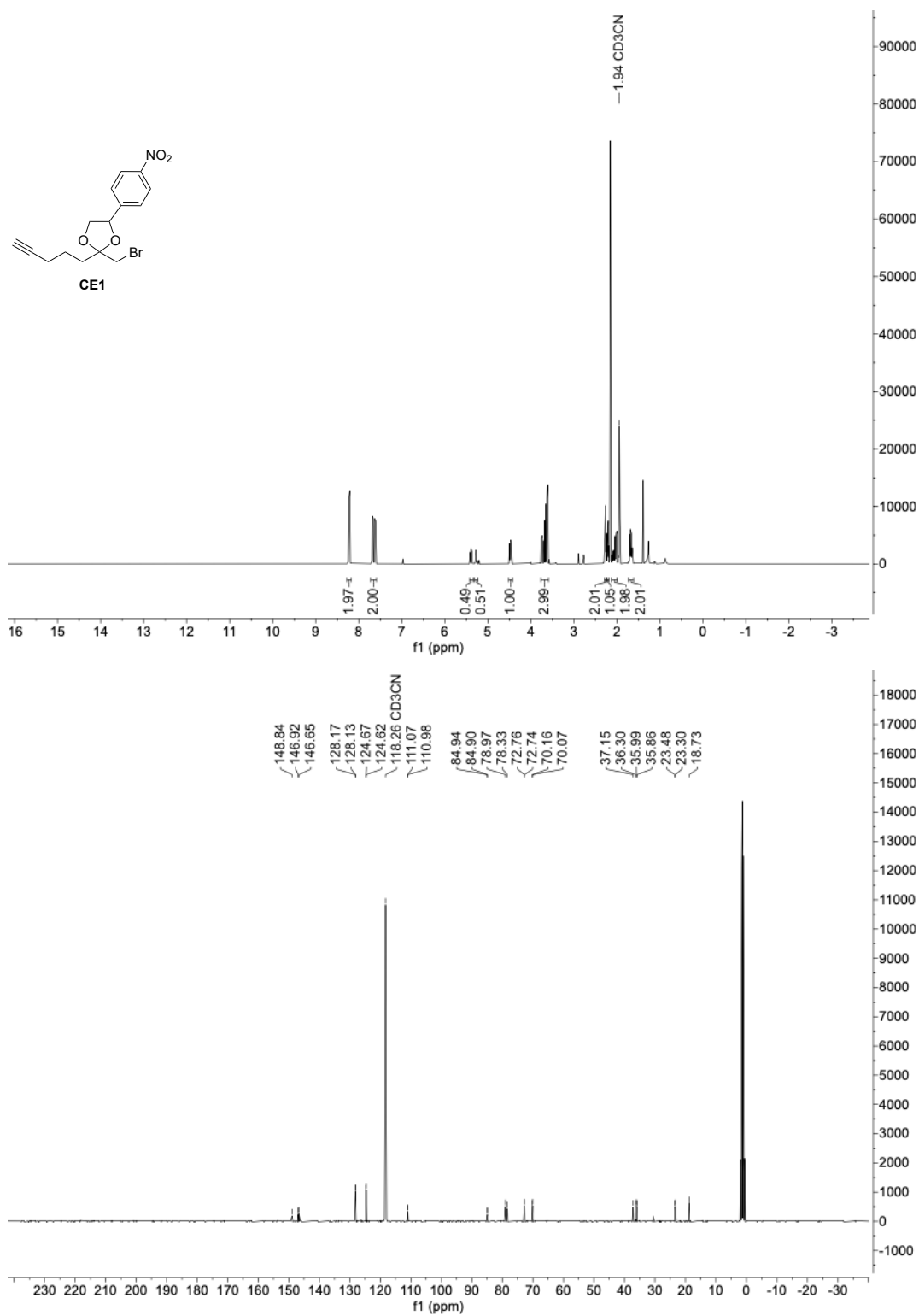
First-generation caged electrophile **CE1**

Figure 38: ¹H- and ¹³C-NMR spectra of first-generation caged electrophile **CE1**.

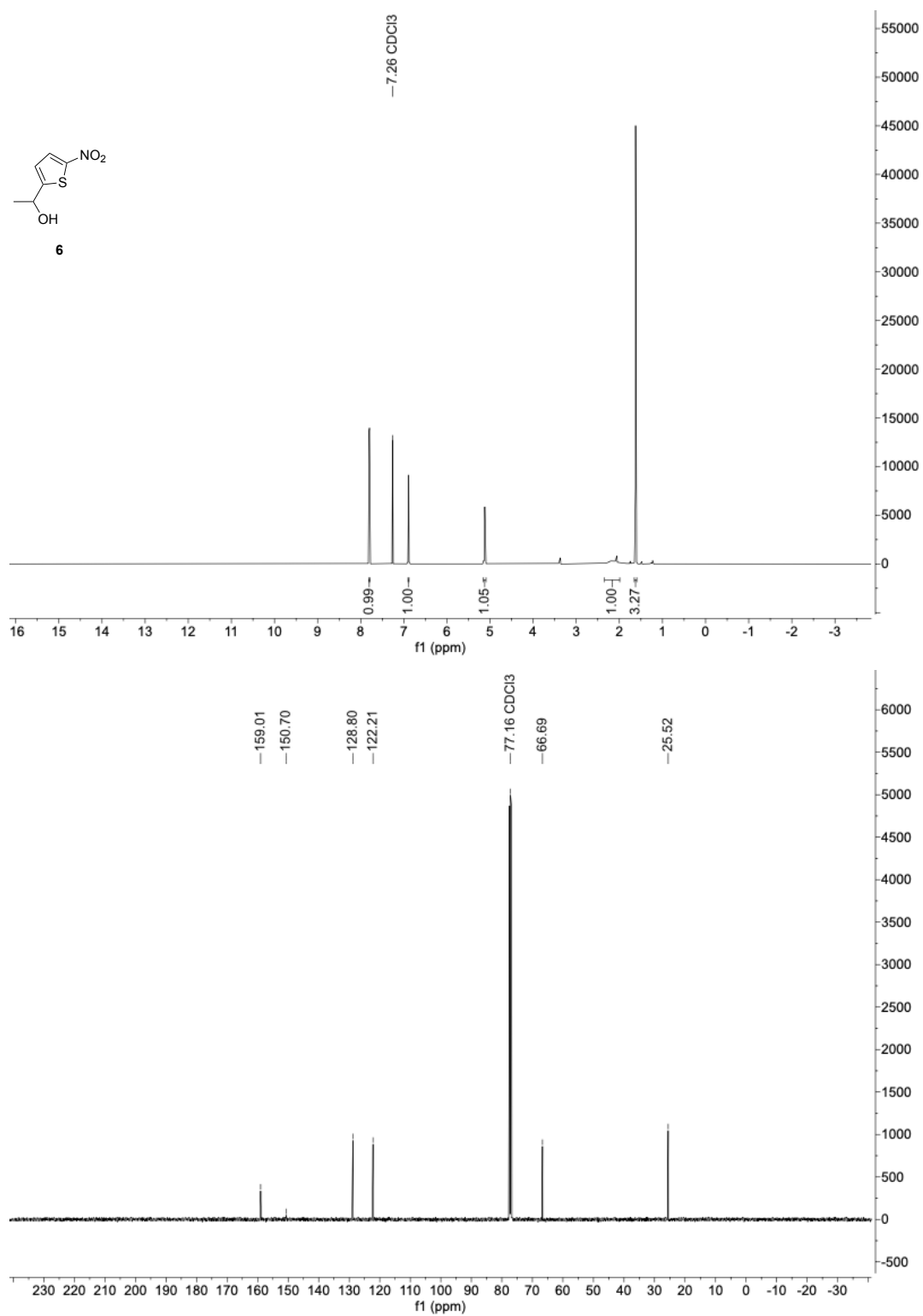
1-(5'-nitrothiophen-2'-yl)ethan-1-ol (**6**)

Figure 39: ¹H- and ¹³C-NMR spectra of 1-(5'-nitrothiophen-2'-yl)ethan-1-ol (**6**).

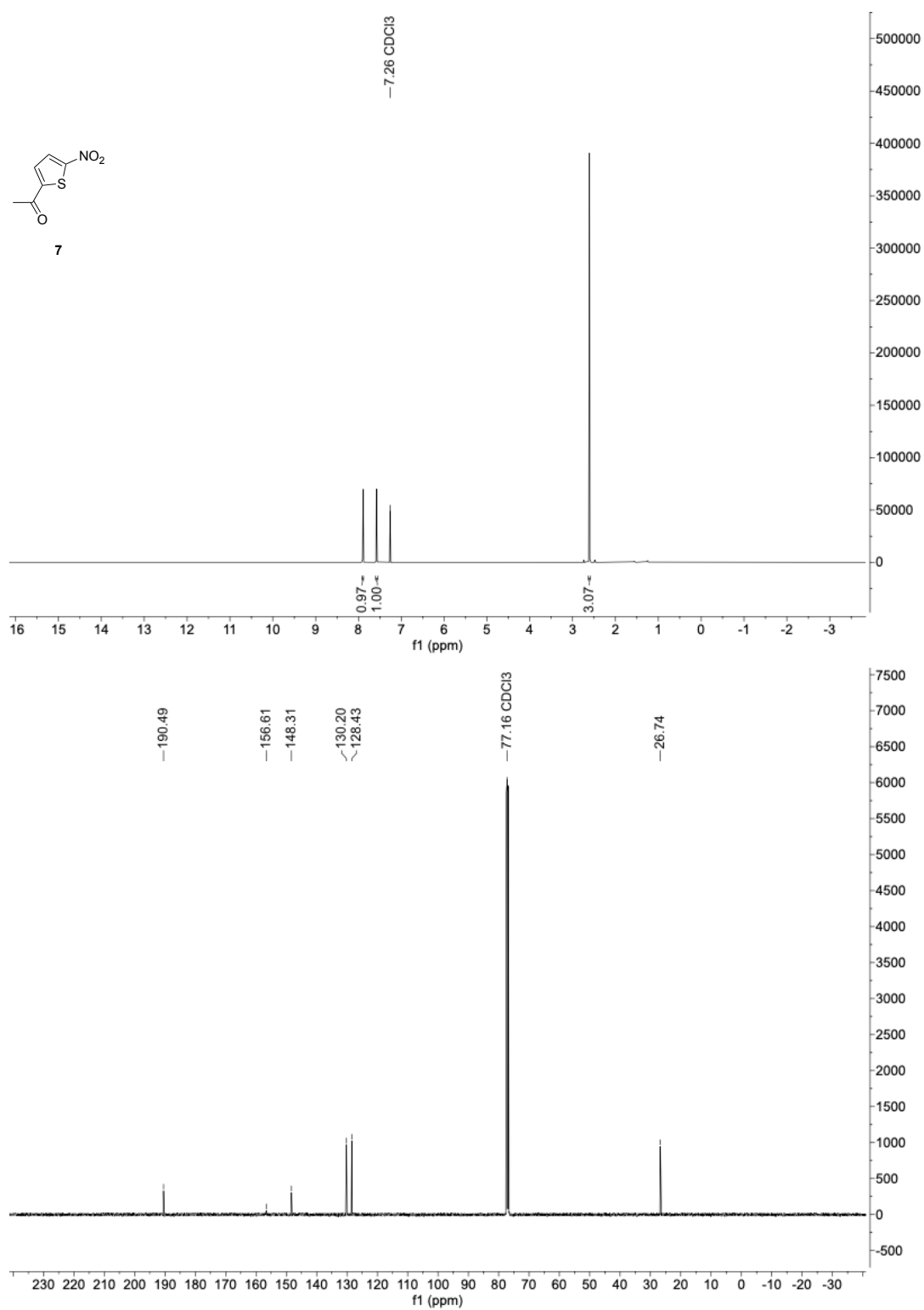
1-(5'-nitrothiophen-2'-yl)ethan-1-one (**7**)

Figure 40: ¹H- and ¹³C-NMR spectra of 1-(5'-nitrothiophen-2'-yl)ethan-1-one (**7**).

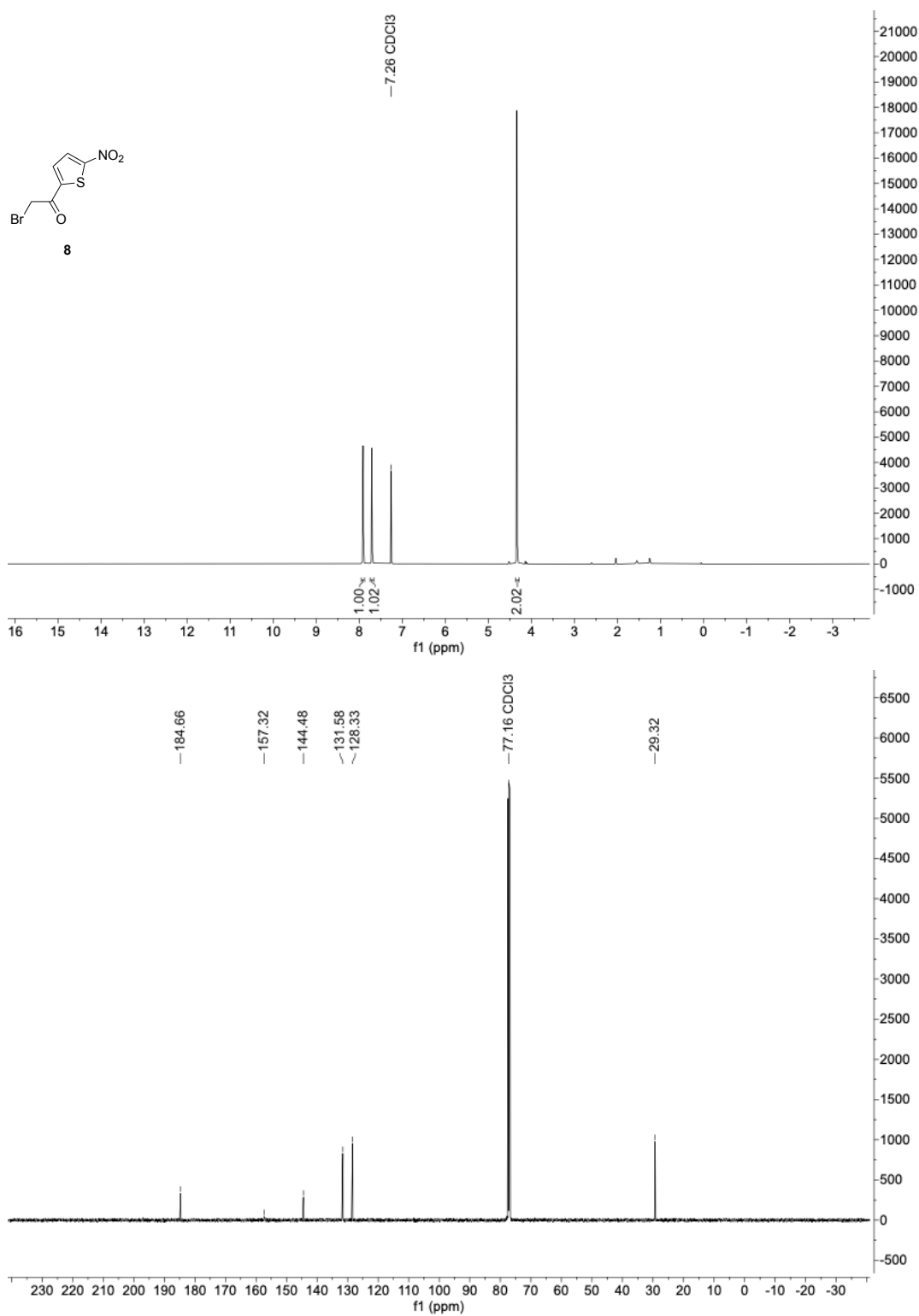
2-bromo-1-(5'-nitrothiophen-2'-yl)ethan-1-one (**8**)

Figure 41: ¹H- and ¹³C-NMR spectra of 2-bromo-1-(5'-nitrothiophen-2'-yl)ethan-1-one (**8**).

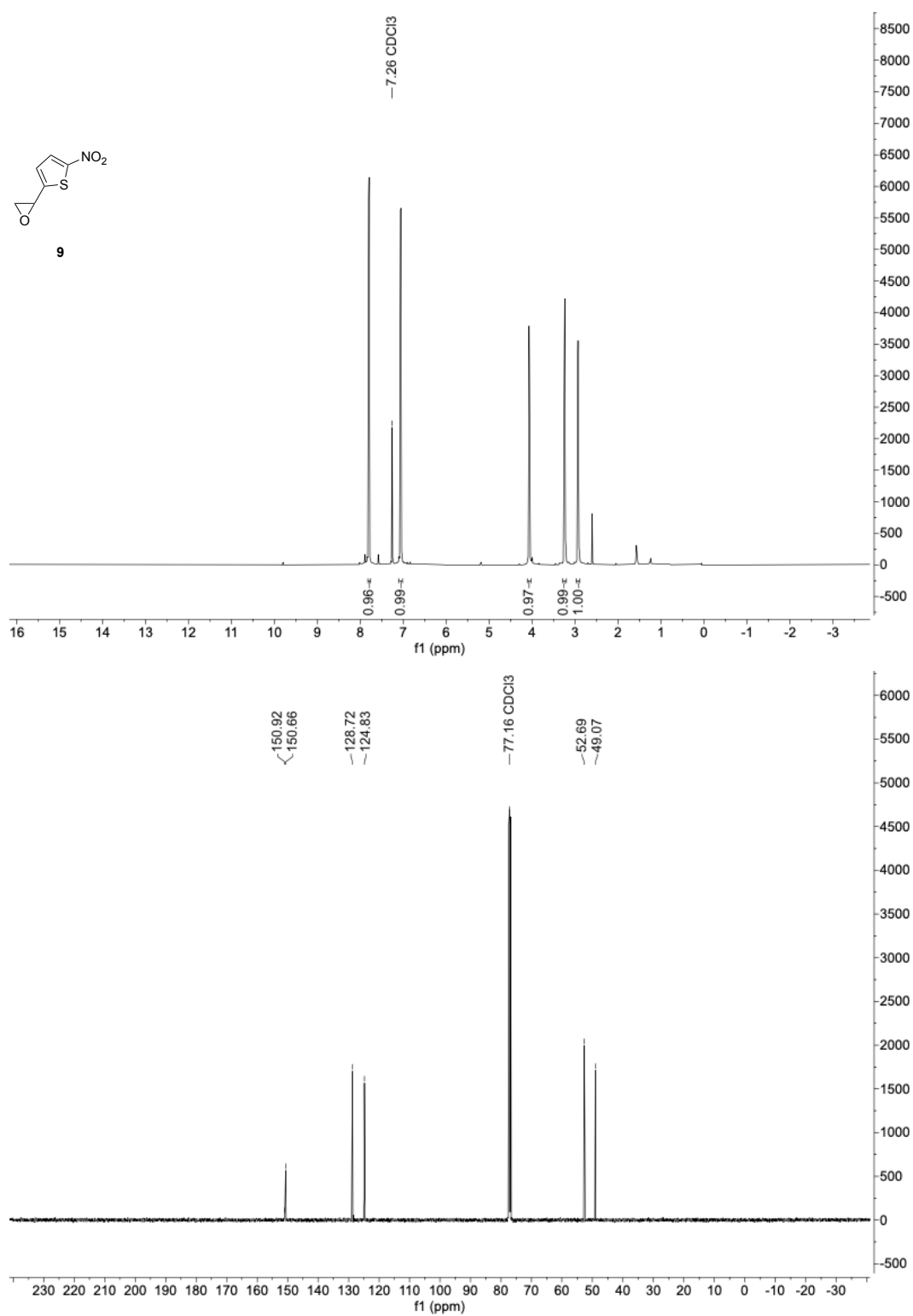
2-(5'-nitrothiophen-2'-yl)oxirane (**9**)

Figure 42: ¹H- and ¹³C-NMR spectra of 2-(5'-nitrothiophen-2'-yl)oxirane (**9**).

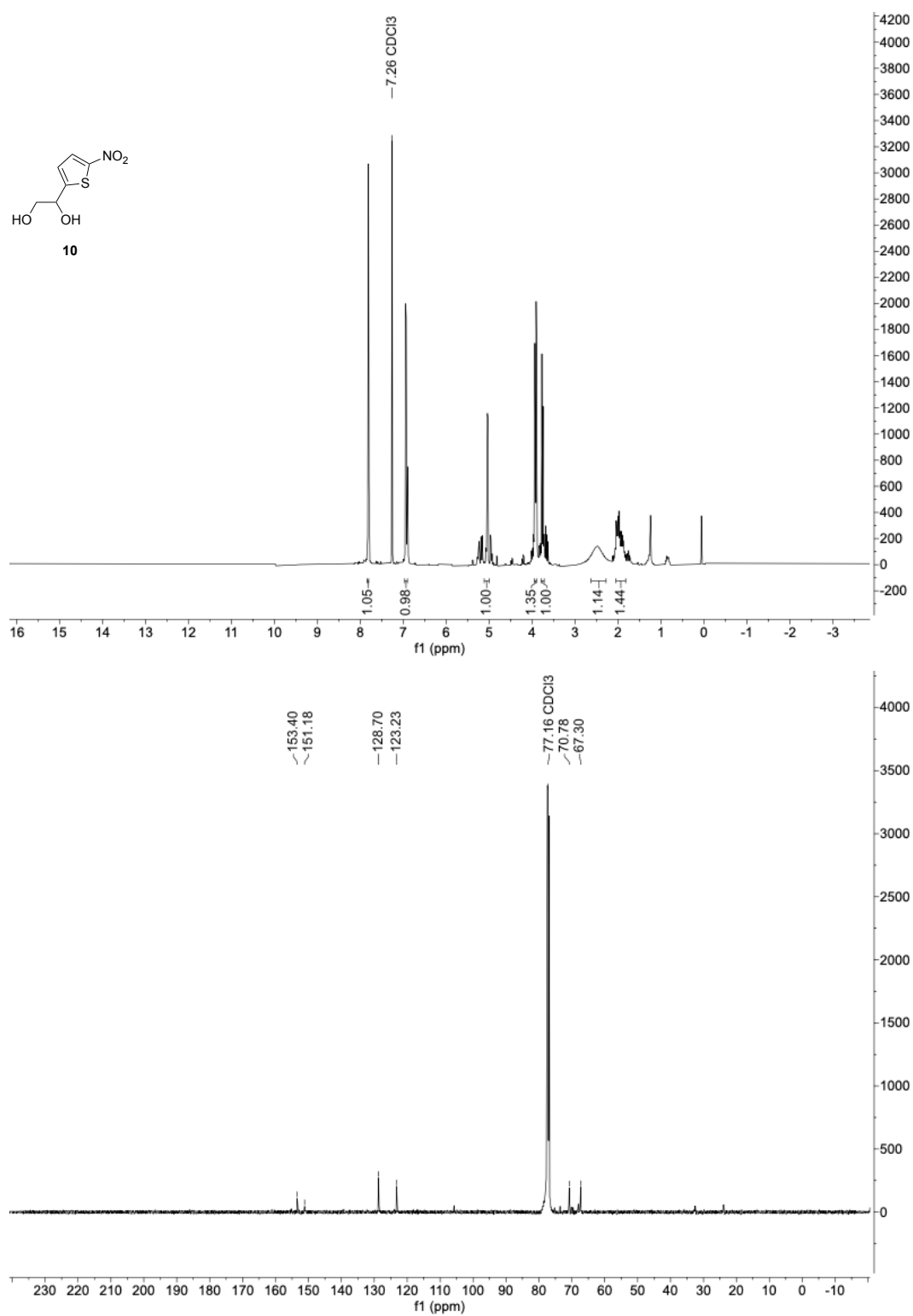
1-(5'-nitrothiophen-2'-yl)ethane-1,2-diol (**10**)

Figure 43: ¹H- and ¹³C-NMR spectra of 1-(5'-nitrothiophen-2'-yl)ethane-1,2-diol (**10**).

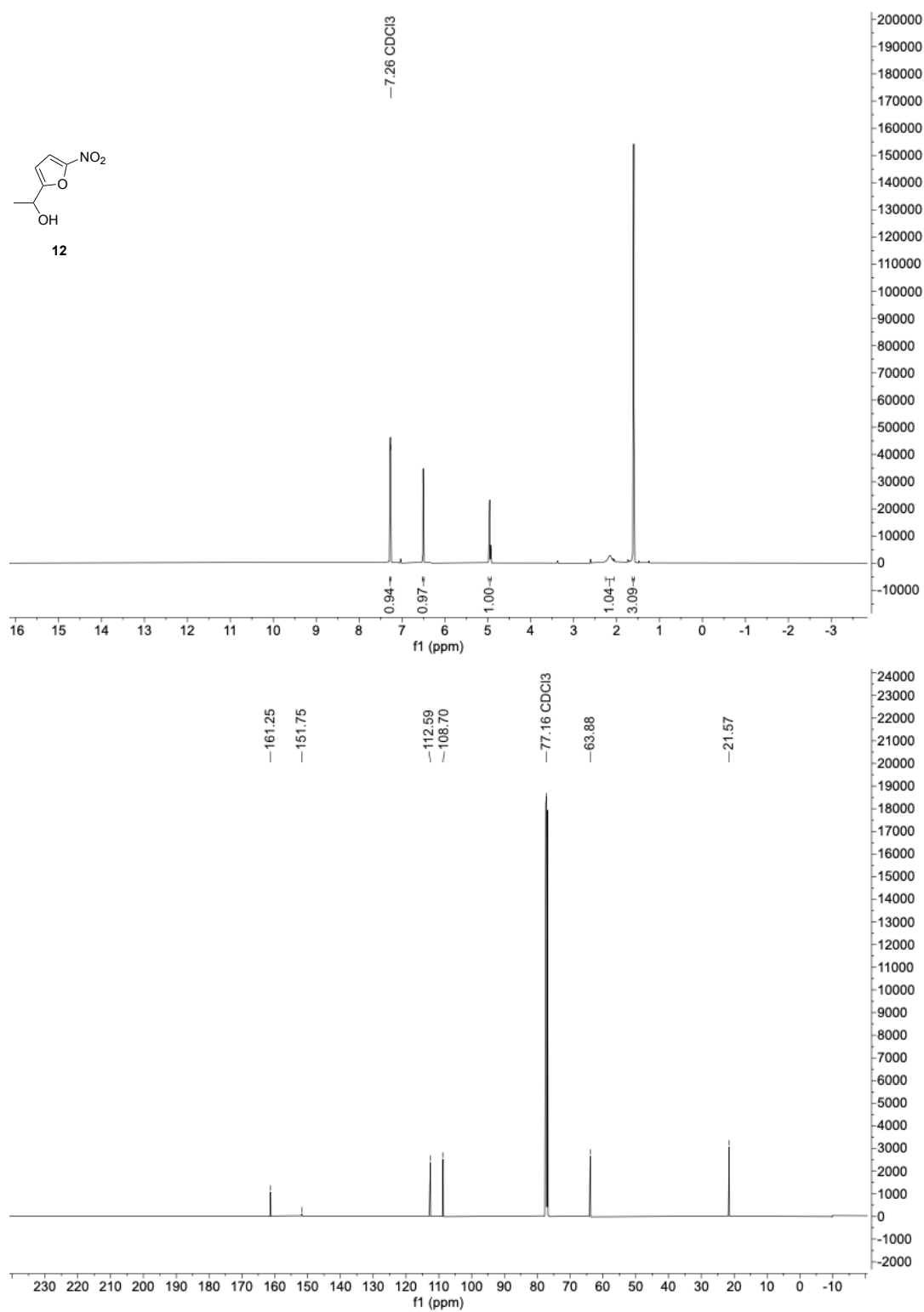
1-(5'-nitrofur-2'-yl)ethan-1-ol (**12**)

Figure 44: ¹H- and ¹³C-NMR spectra of 1-(5'-nitrofur-2'-yl)ethan-1-ol (**12**).

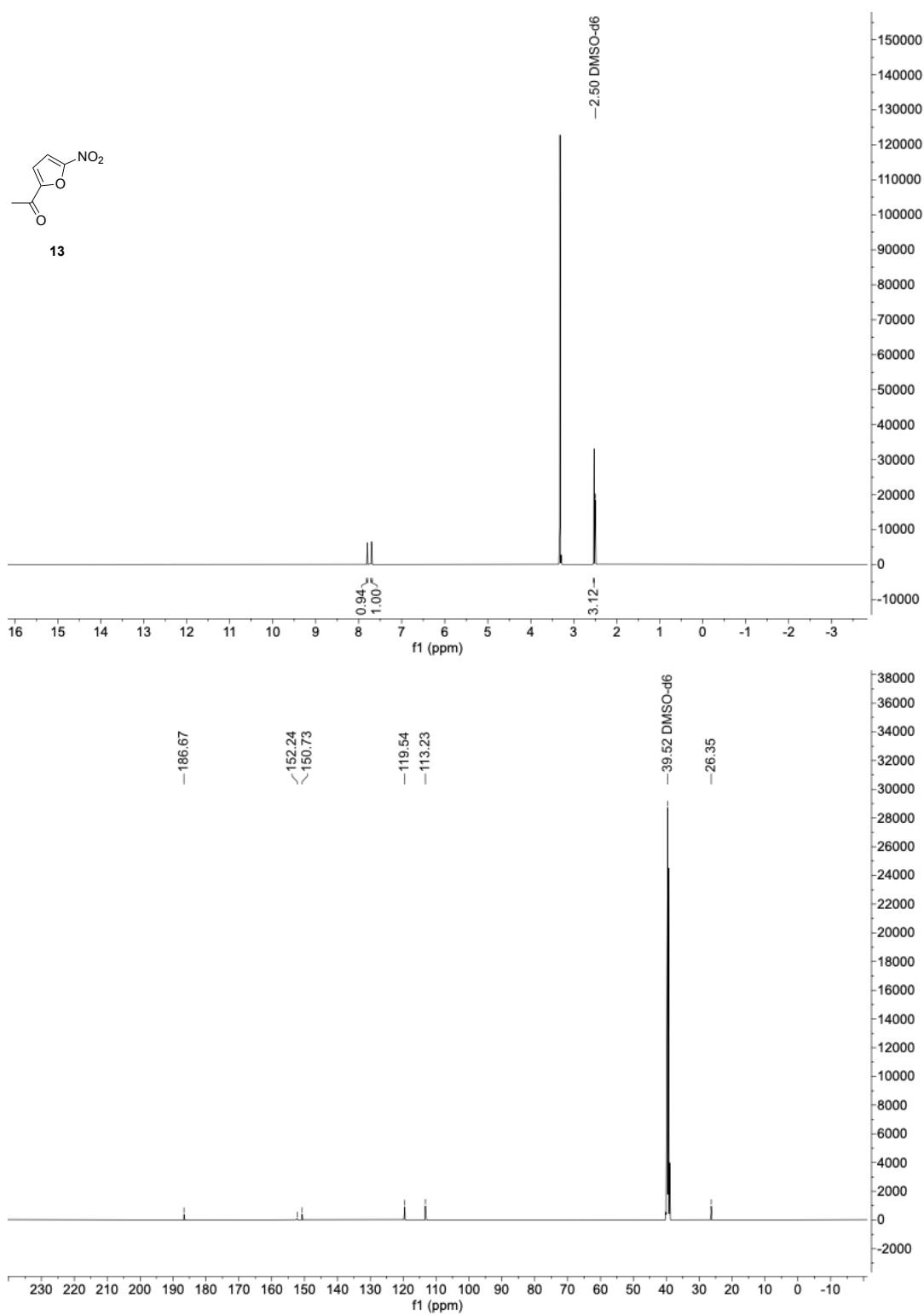
1-(5'-nitrofur-2'-yl)ethan-1-one (**13**)

Figure 45: ¹H- and ¹³C-NMR spectra of 1-(5'-nitrofur-2'-yl)ethan-1-one (**13**).

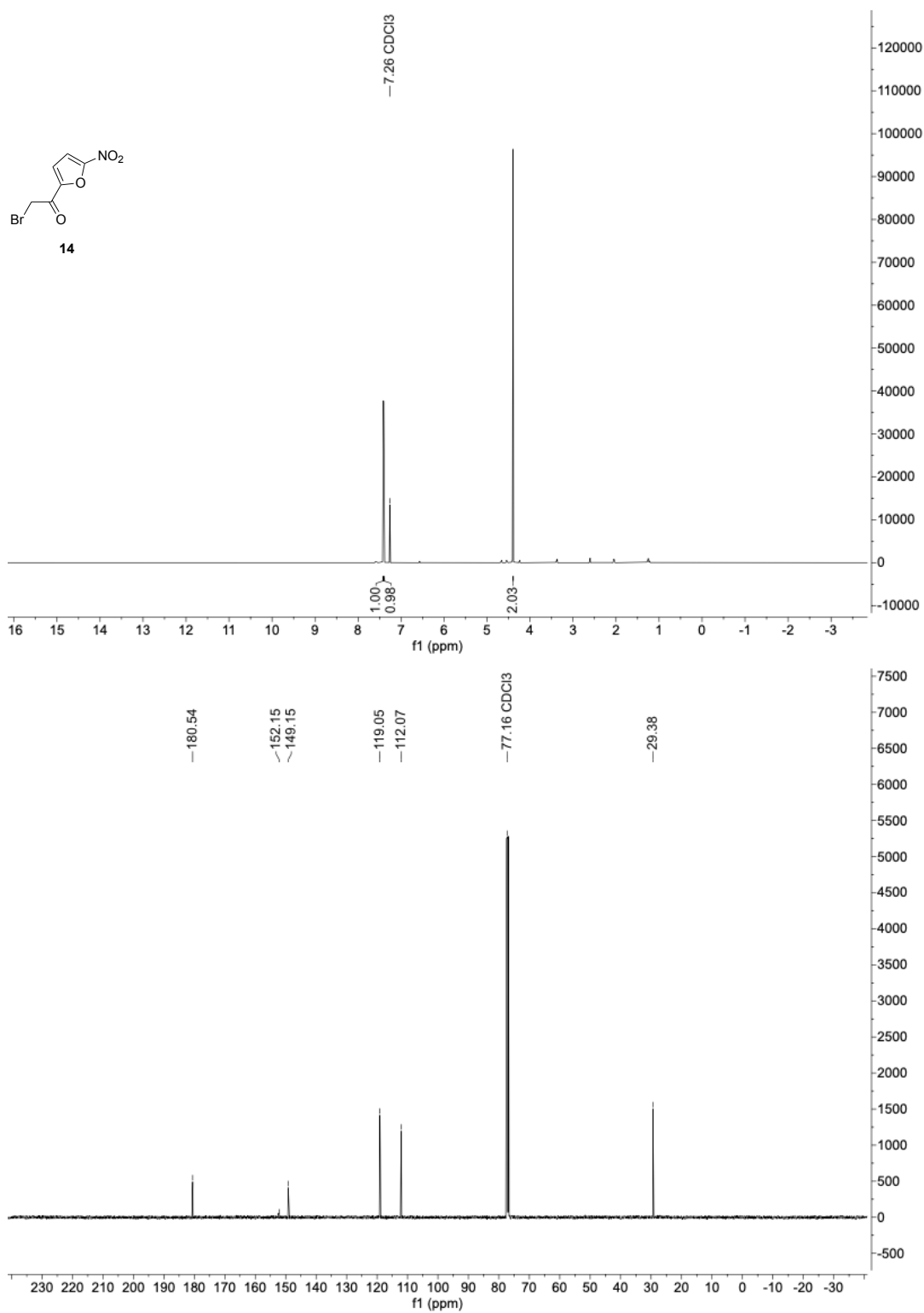
2-bromo-1-(5'-nitrofur-2'-yl)ethan-1-one (**14**)

Figure 46: ¹H- and ¹³C-NMR spectra of 2-bromo-1-(5'-nitrofur-2'-yl)ethan-1-one (**14**).

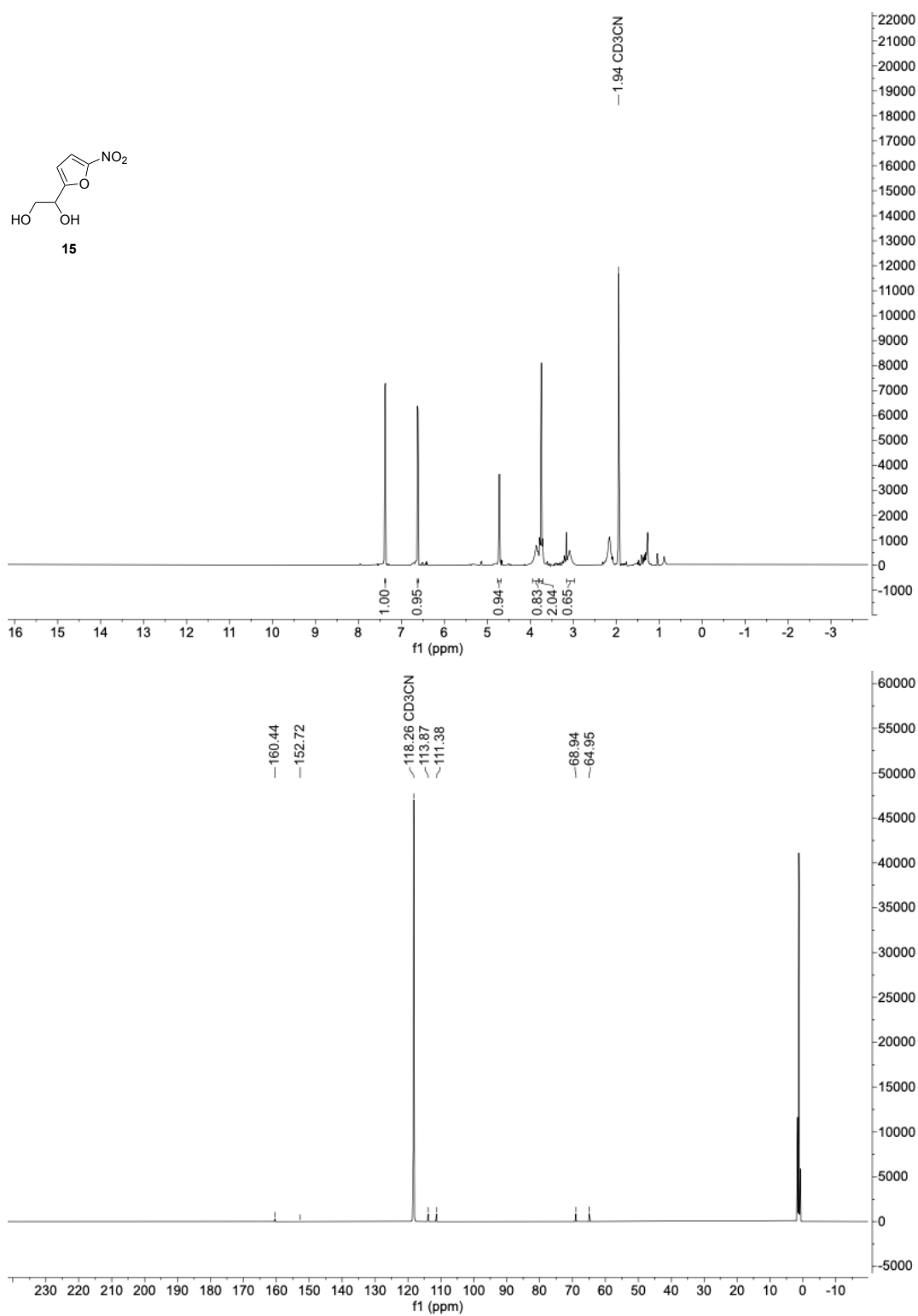
1-(5'-nitrofur-2'-yl)ethan-1,2-diol (**15**)

Figure 47: ¹H- and ¹³C-NMR spectra of 1-(5'-nitrofur-2'-yl)ethan-1,2-diol (**15**).

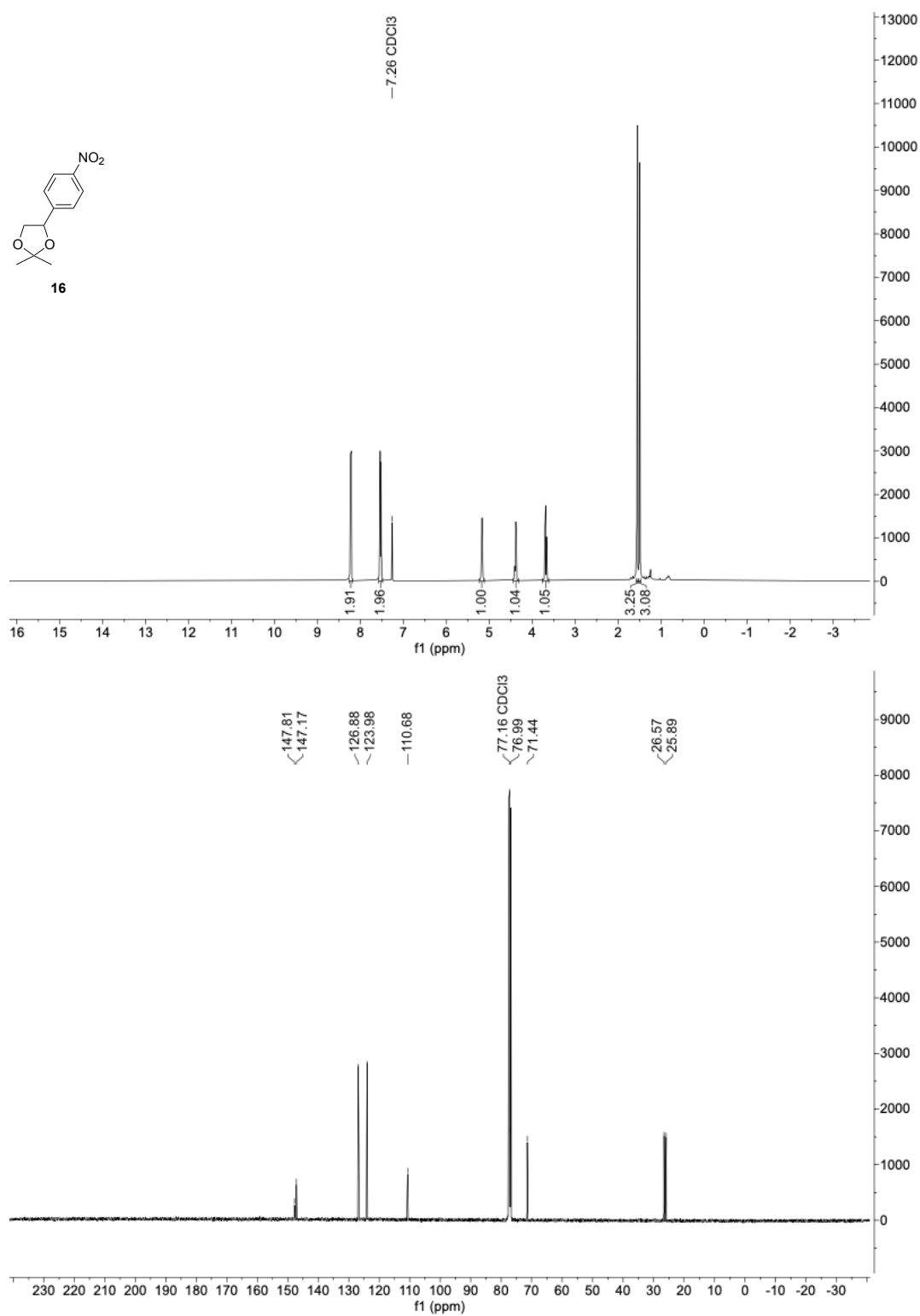
2,2-dimethyl-4-(4'-nitrophenyl)-1,3-dioxolane (**16**)

Figure 48: ¹H- and ¹³C-NMR spectra of 2,2-dimethyl-4-(4'-nitrophenyl)-1,3-dioxolane (**16**).

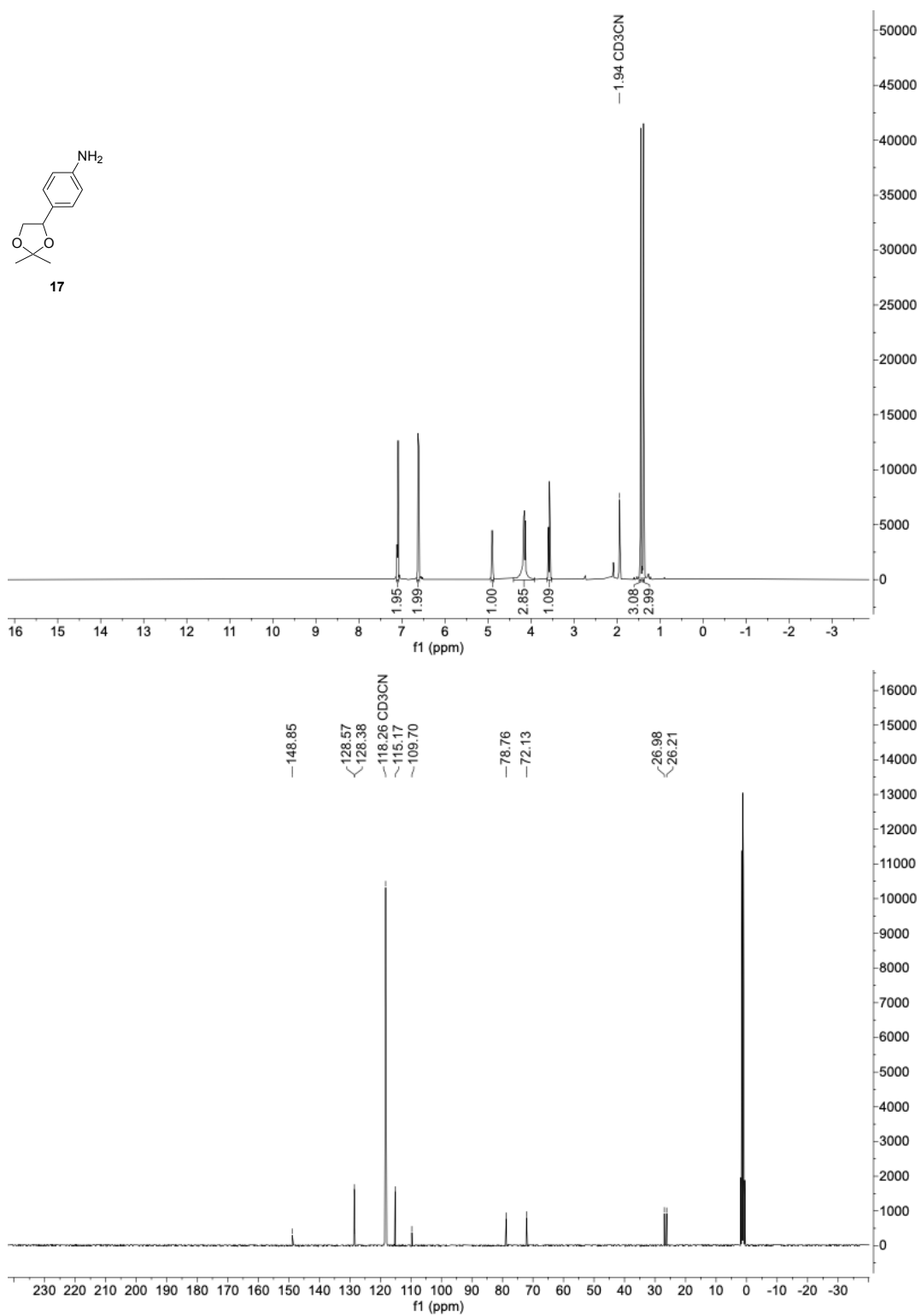
4-(2',2'-dimethyl-1',3'-dioxolan-4'-yl)aniline (**17**)

Figure 49: ¹H- and ¹³C-NMR spectra of 4-(2',2'-dimethyl-1',3'-dioxolan-4'-yl)aniline (**17**).

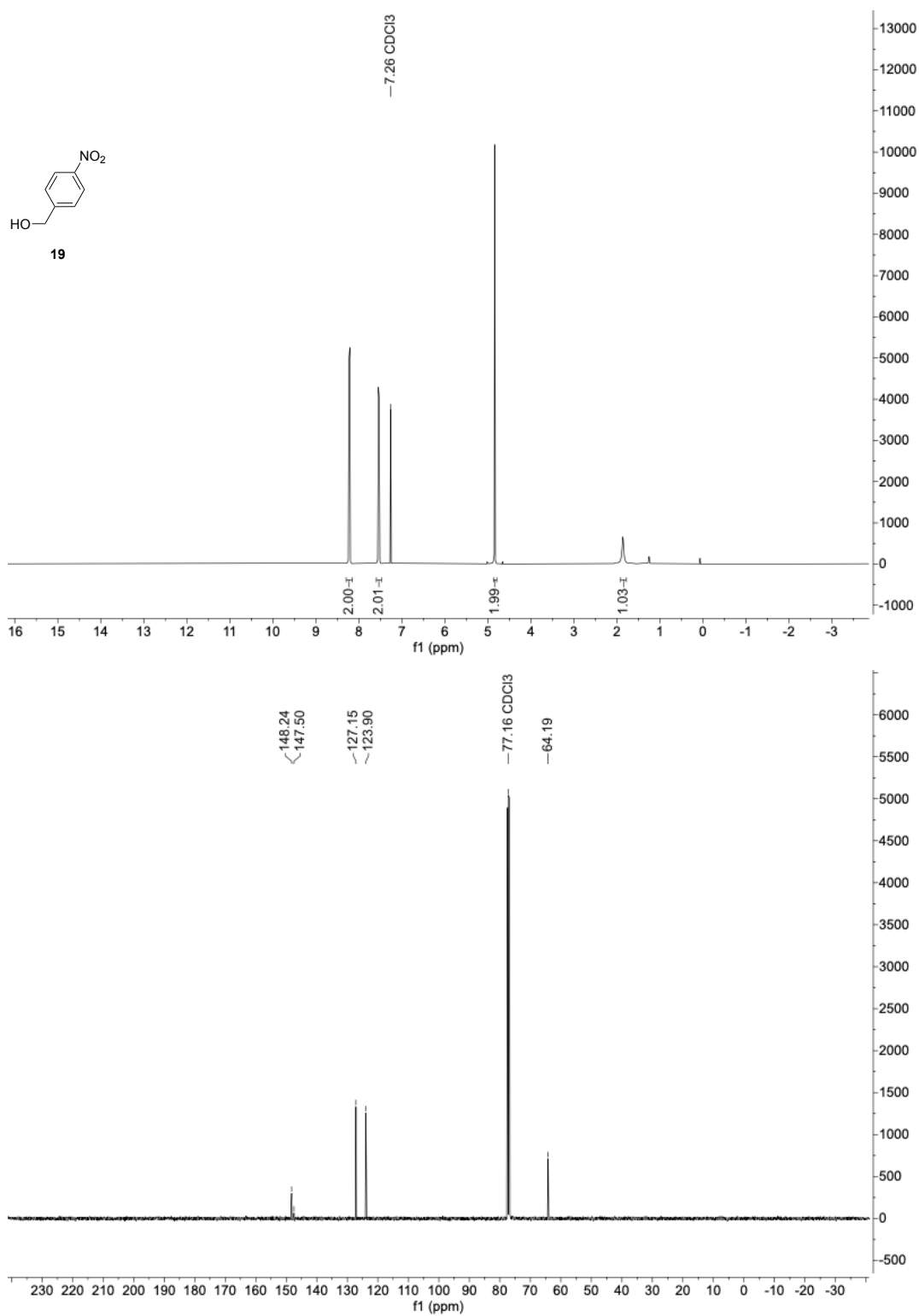
(4'-nitrophenyl)methanol (**19**)

Figure 50: ¹H- and ¹³C-NMR spectra of (4'-nitrophenyl)methanol (**19**).

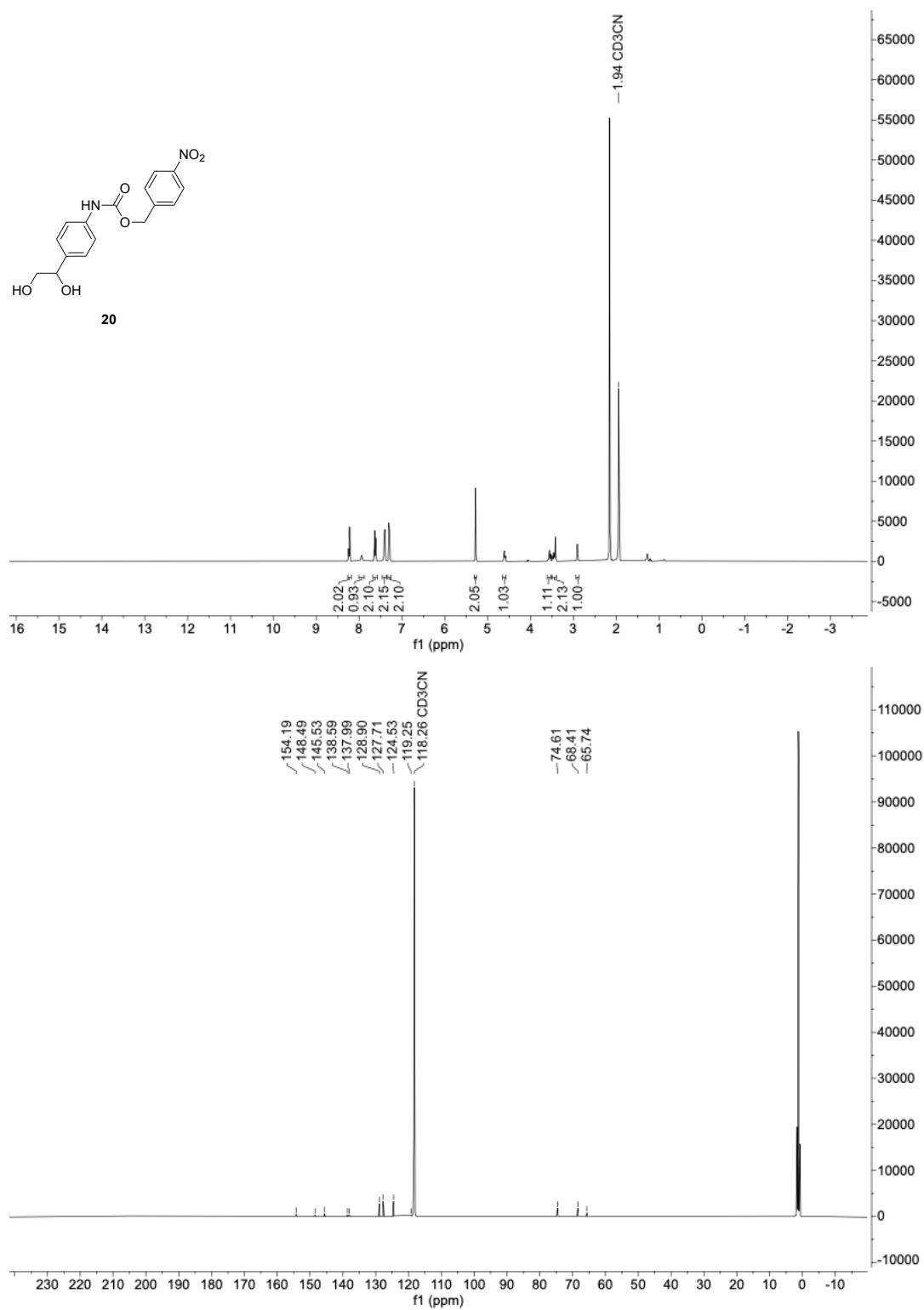
para-nitrophenyl-based caging group with a self-immolative linker **20**

Figure 51: ¹H- and ¹³C-NMR spectra of *para*-nitrophenyl-based caging group with a self-immolative linker **20**.

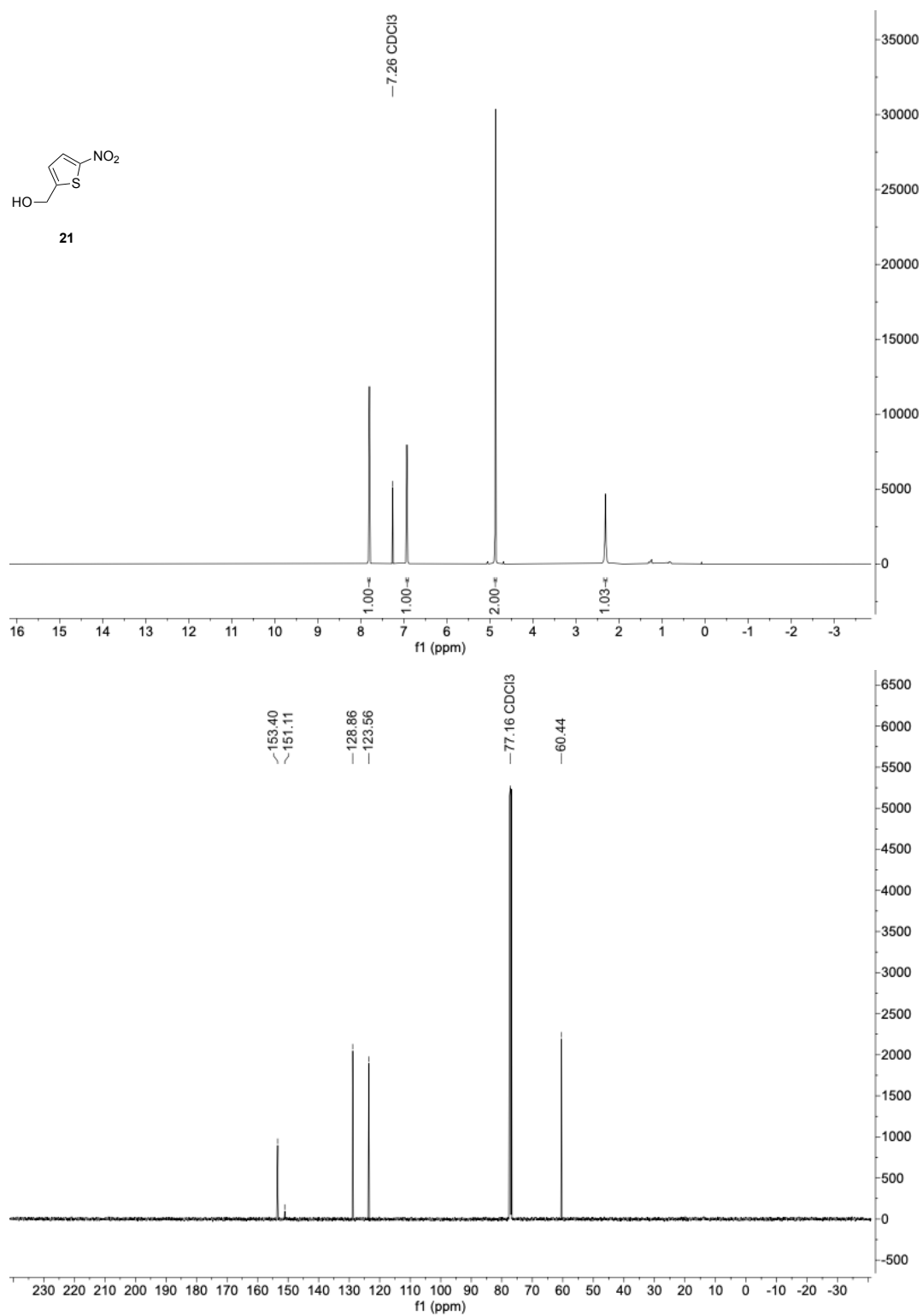
(5'-nitrothiophen-2'-yl)methanol (**21**)

Figure 52: ¹H- and ¹³C-NMR spectra of (5'-nitrothiophen-2'-yl)methanol (**21**).

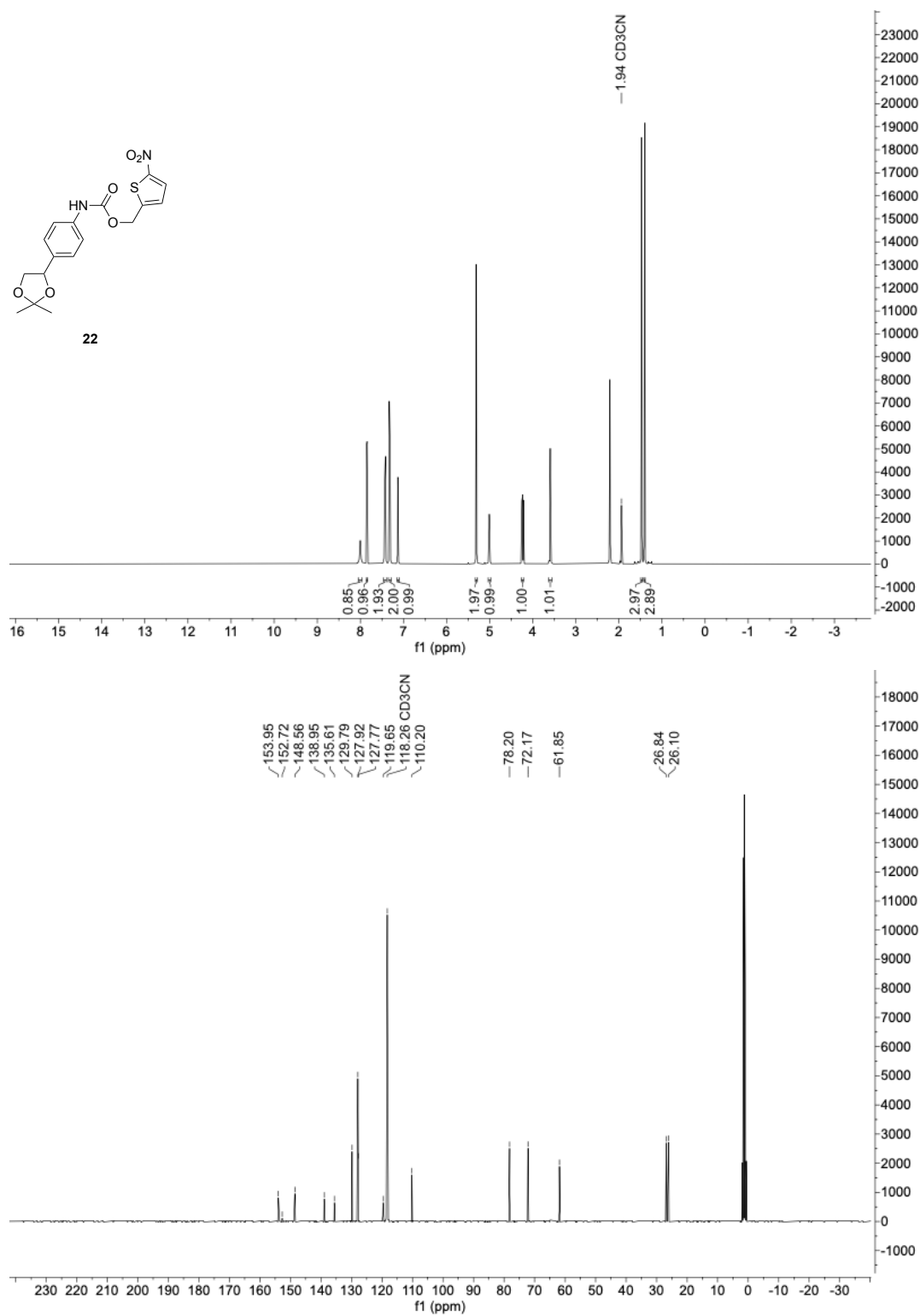
Protected thiophene-based caging group with a self-immolative linker **22**

Figure 53: ¹H- and ¹³C-NMR spectra of protected thiophene-based caging group with a self-immolative linker **22**.

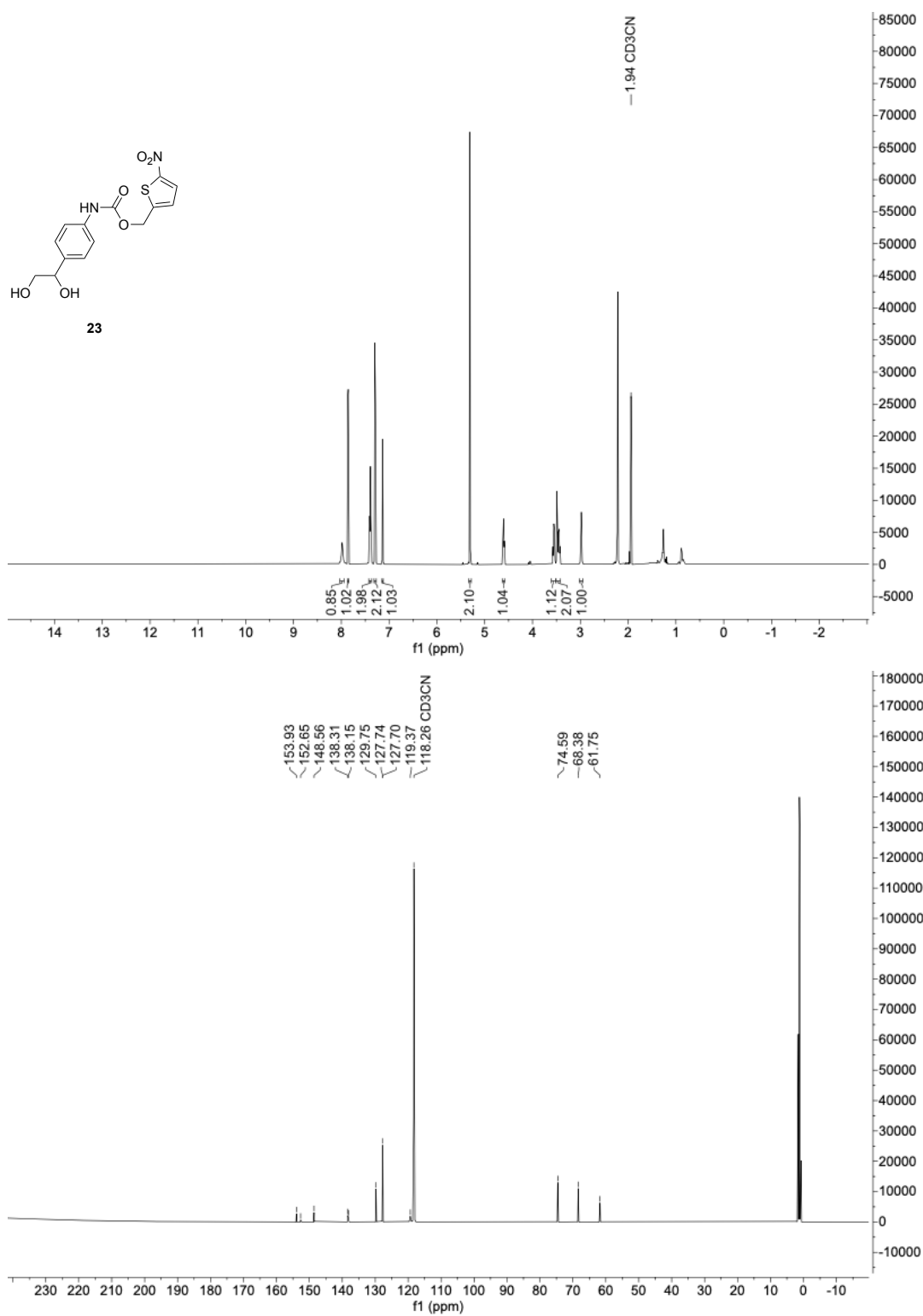
Thiophene-based caging group with a self-immolative linker **23**

Figure 54: ¹H- and ¹³C-NMR spectra of thiophene-based caging group with a self-immolative linker **23**.

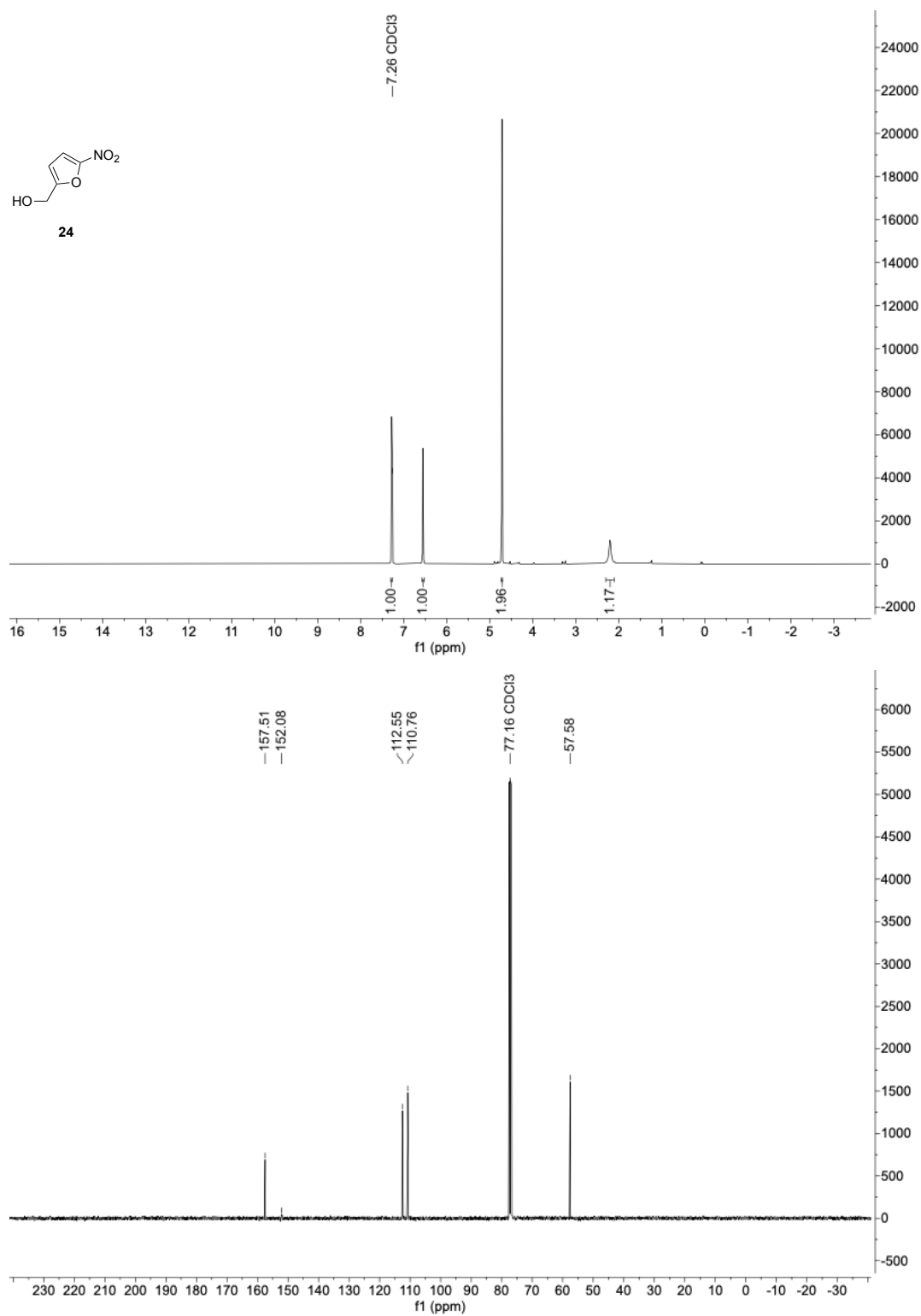
(5'-nitrofuran-2'-yl)methanol (**24**)

Figure 55: ¹H- and ¹³C-NMR spectra of (5'-nitrofuran-2'-yl)methanol (**24**).

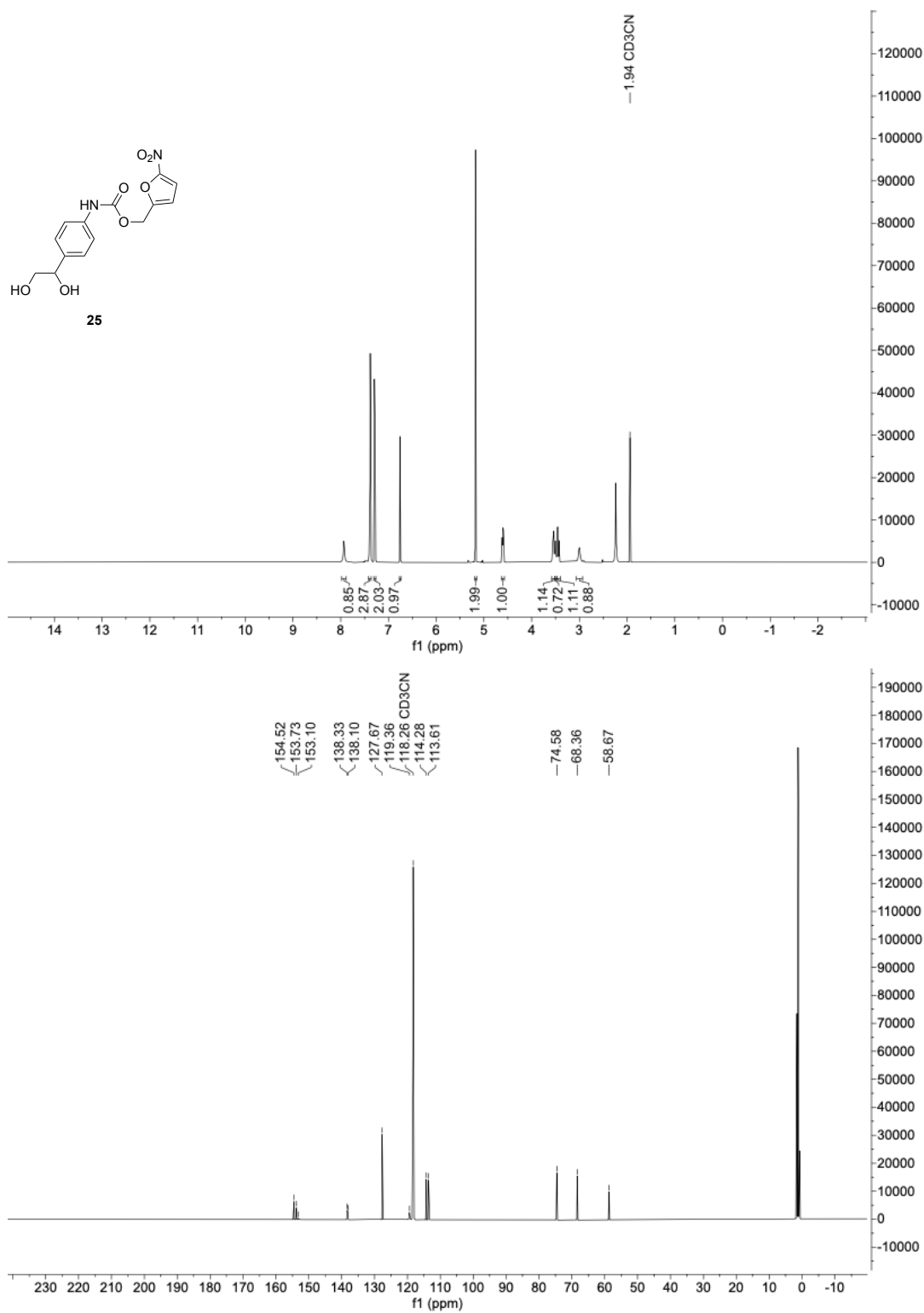
Furane-based caging group with a self-immolative linker **25**

Figure 56: ¹H- and ¹³C-NMR spectra of furane-based caging group with a self-immolative linker **25**.

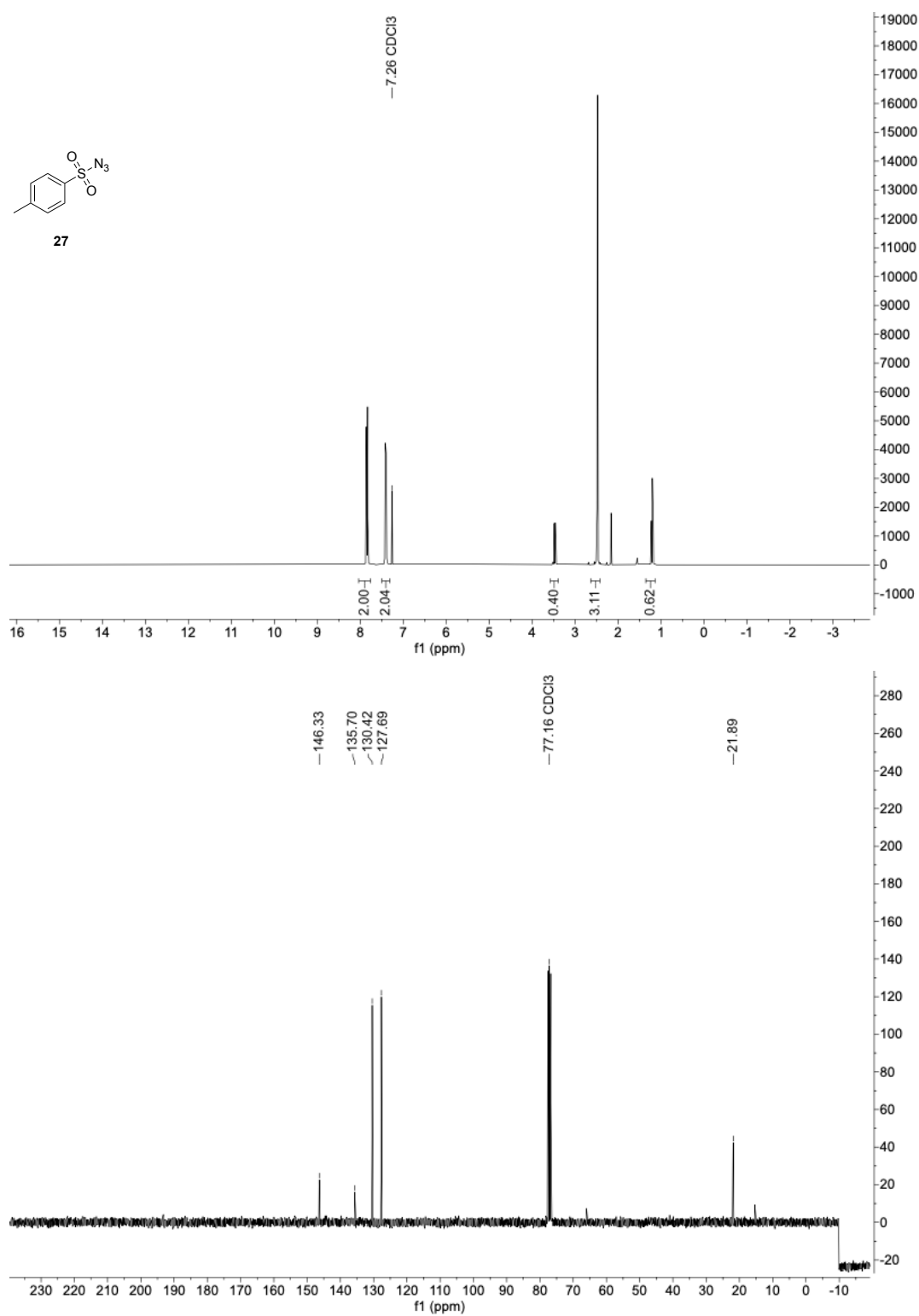
4-methylbenzenesulfonyl azide (**27**)

Figure 57: ¹H- and ¹³C-NMR spectra of 4-methylbenzenesulfonyl azide (**27**).

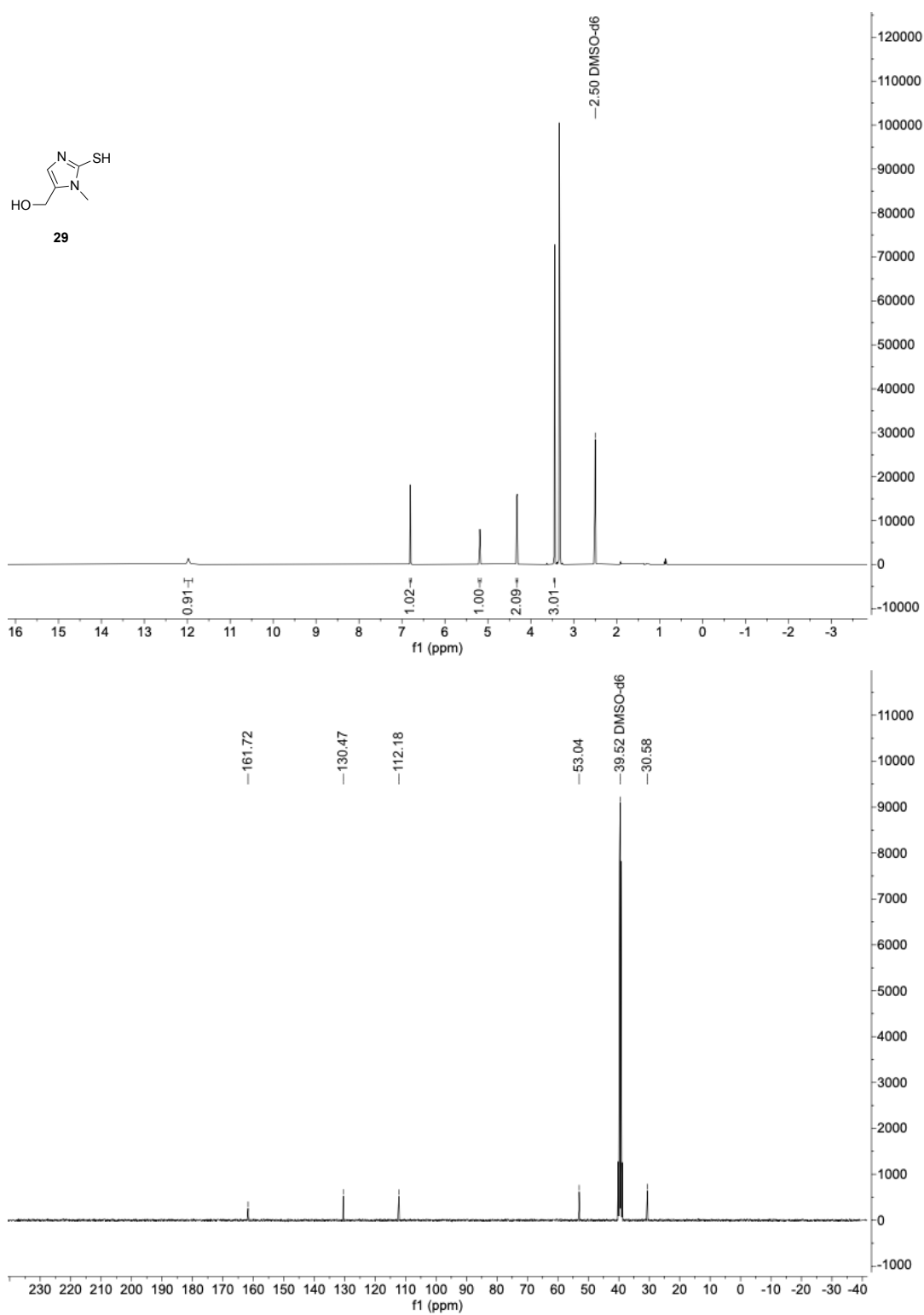
1-methyl-2-mercapto-5-hydroxymethyl-1*H*-imidazole (**29**)

Figure 58: ¹H- and ¹³C-NMR spectra of 1-methyl-2-mercapto-5-hydroxymethyl-1*H*-imidazole (**29**).

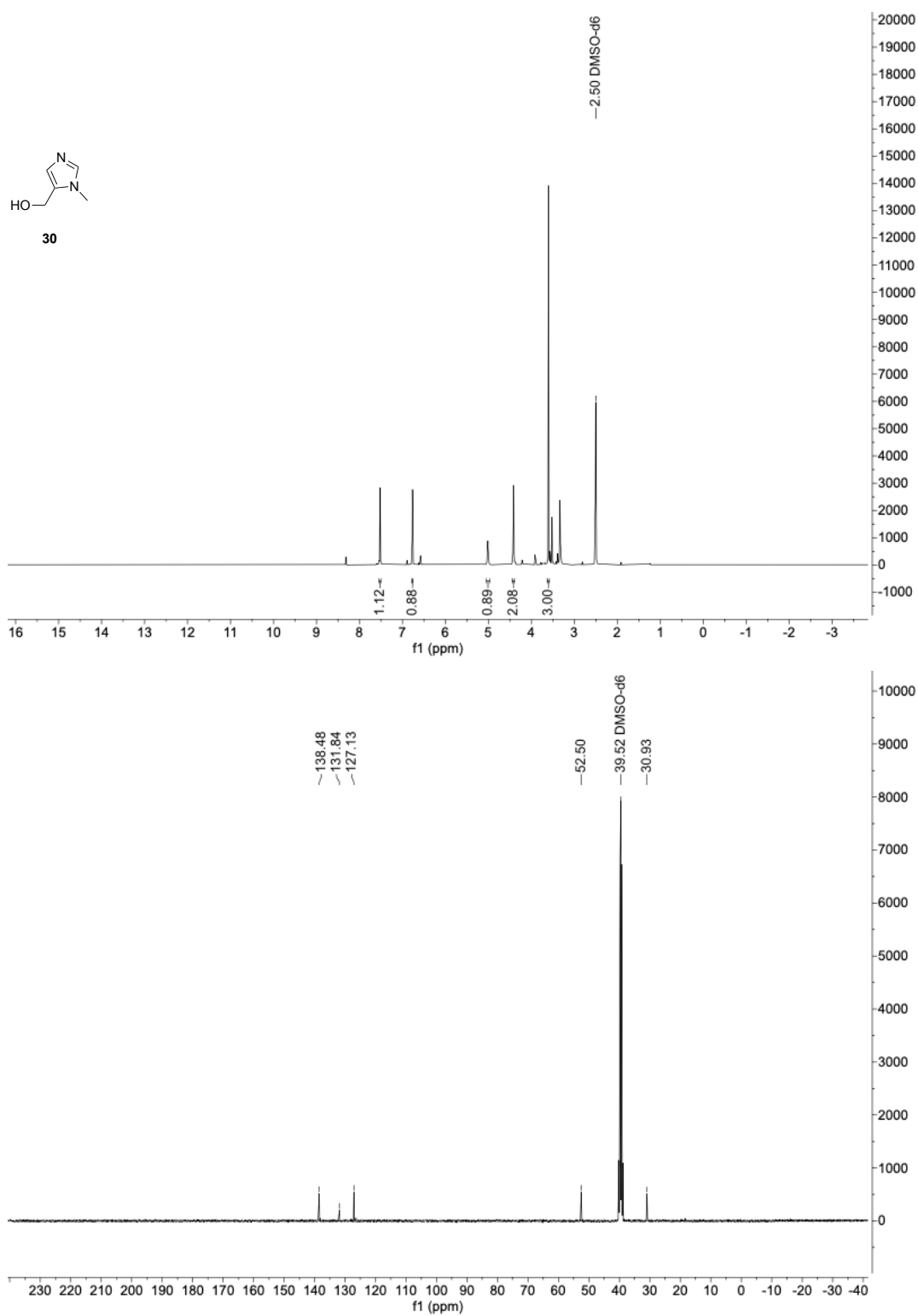
(1-methyl-1*H*-imidazol-5-yl)methanol (**30**)

Figure 59: ¹H- and ¹³C-NMR spectra of (1-methyl-1*H*-imidazol-5-yl)methanol (**30**).

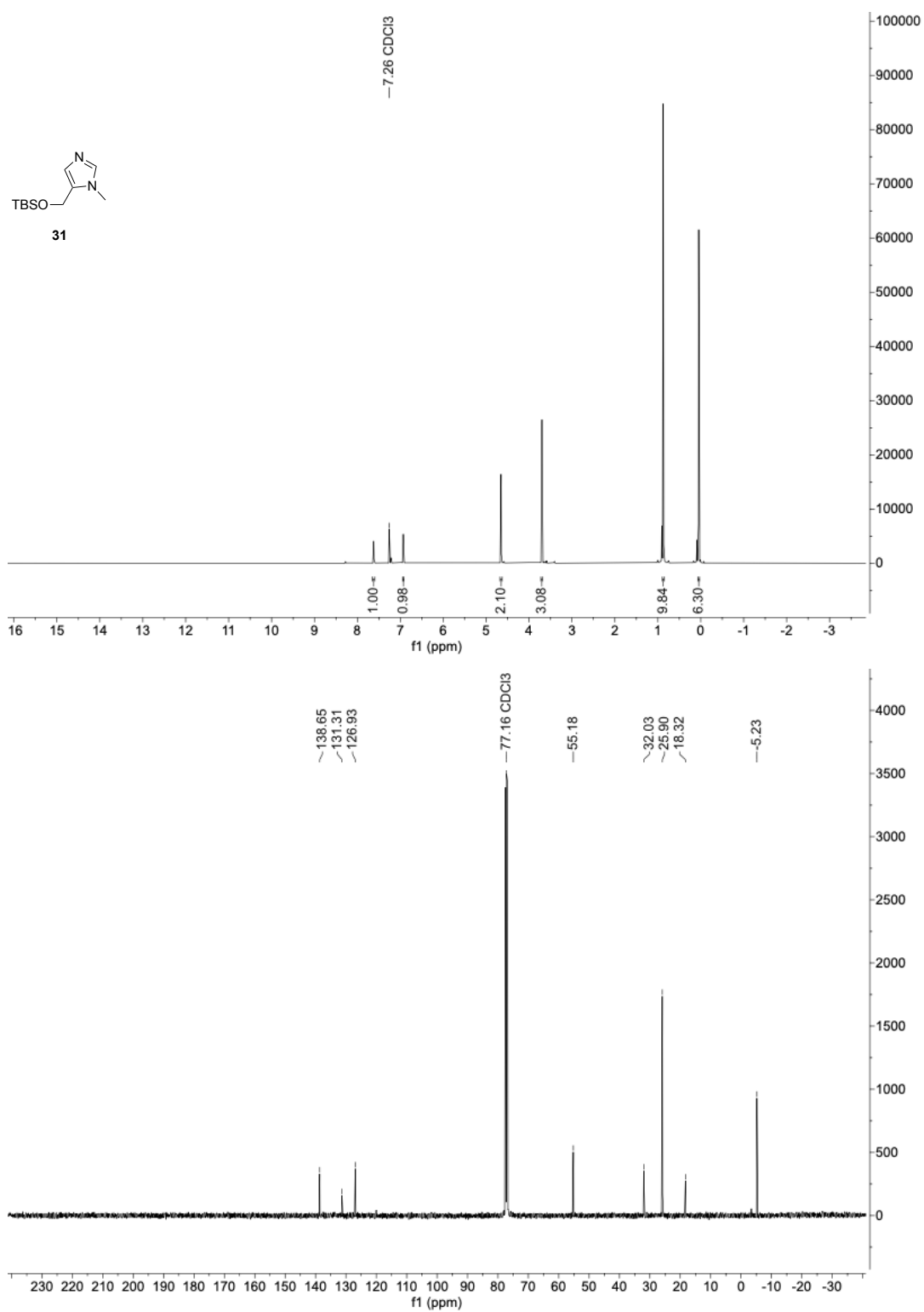
5-(((*tert*-butyldimethylsilyl)oxy)methyl)-1-methyl-1*H*-imidazole (**31**)

Figure 60: ¹H- and ¹³C-NMR spectra of 5-(((*tert*-butyldimethylsilyl)oxy)methyl)-1-methyl-1*H*-imidazole (**31**).

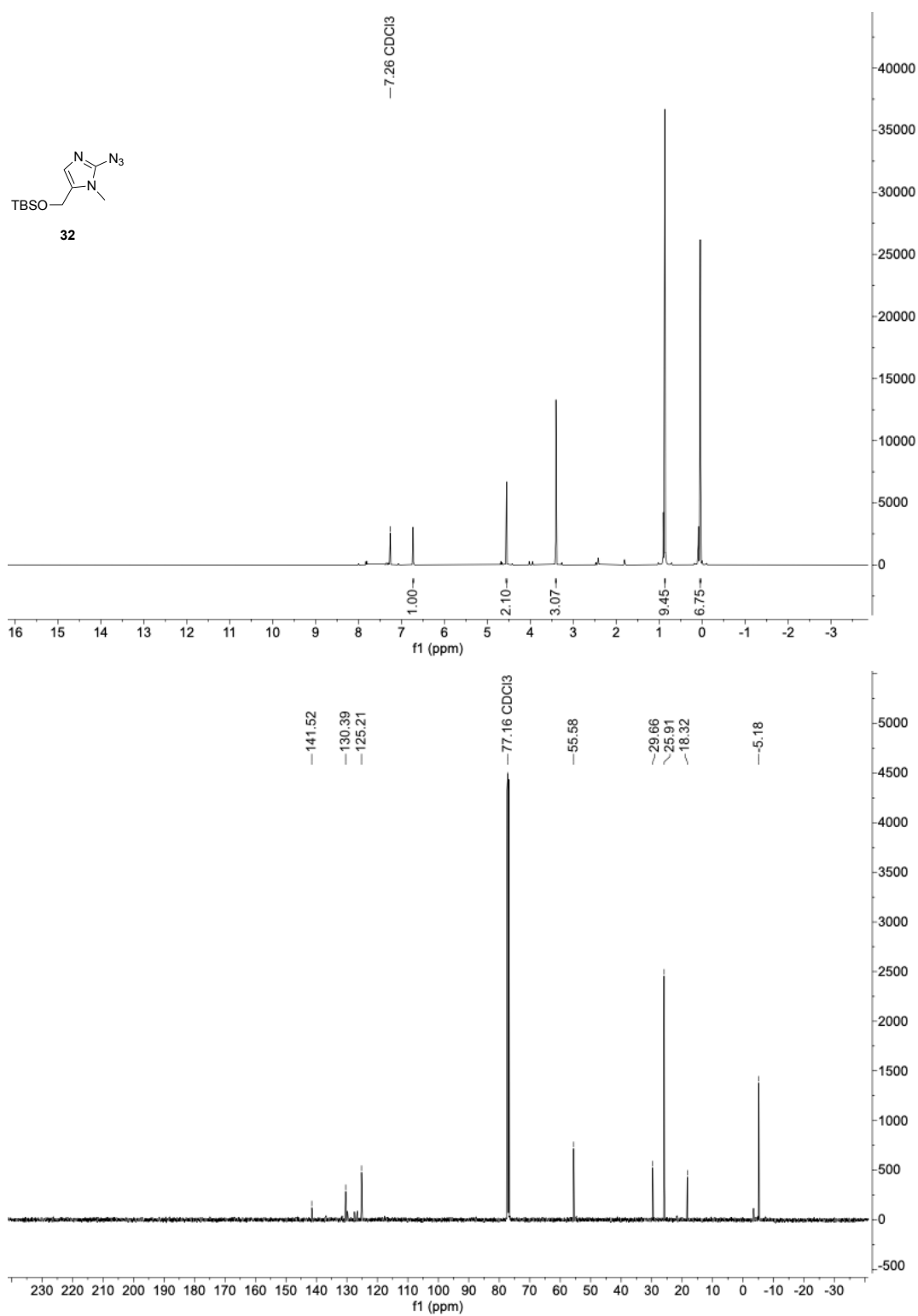
2-azido-5-(((*tert*-butyldimethylsilyl)oxy)methyl)-1-methyl-1*H*-imidazole (**32**)

Figure 61: ¹H- and ¹³C-NMR spectra of 2-azido-5-(((*tert*-butyldimethylsilyl)oxy)methyl)-1-methyl-1*H*-imidazole (**32**).

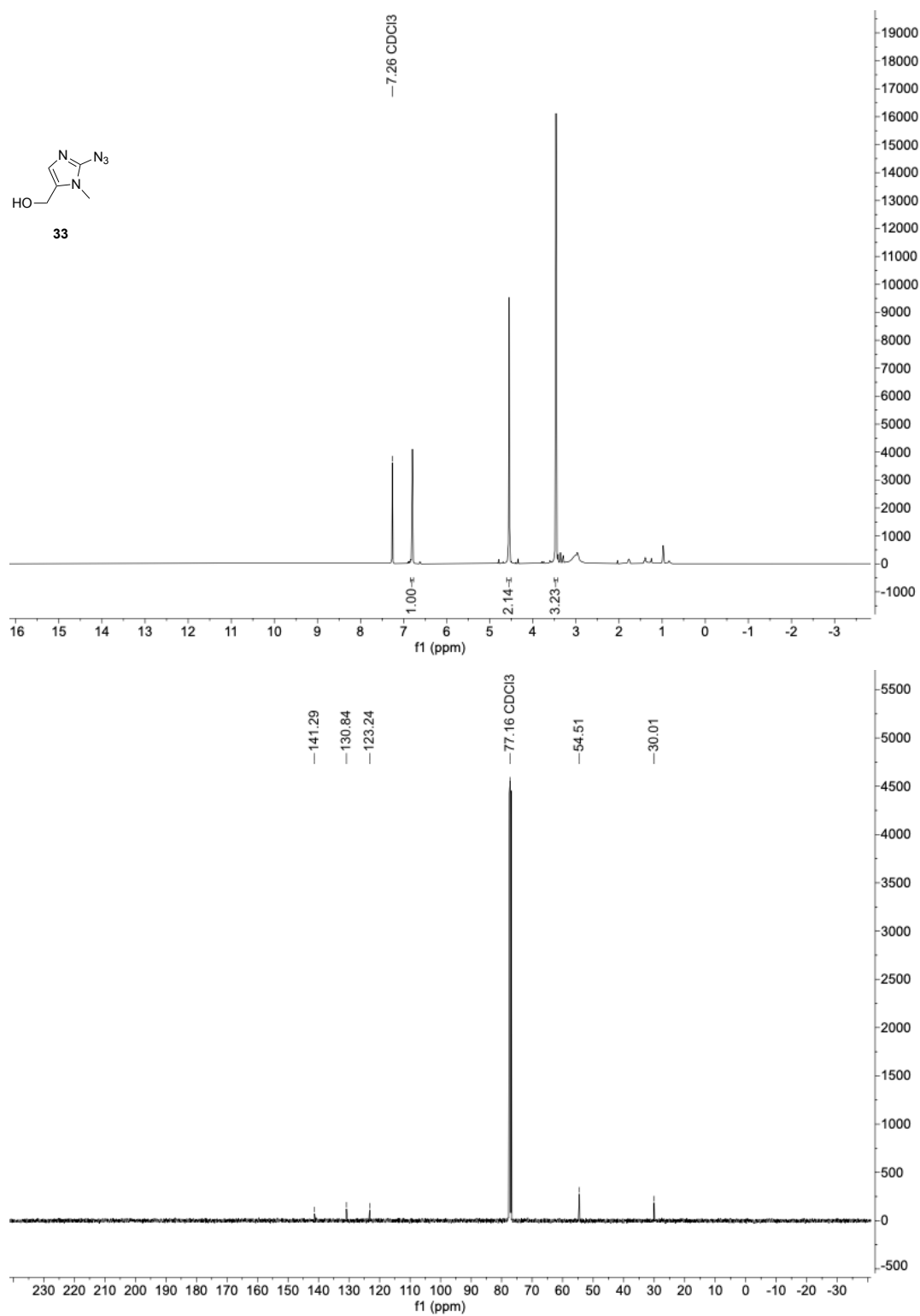
(2-azido-1-methyl-1*H*-imidazol-5-yl)methanol (**33**)

Figure 62: ¹H- and ¹³C-NMR spectra of (2-azido-1-methyl-1*H*-imidazol-5-yl)methanol (**33**).

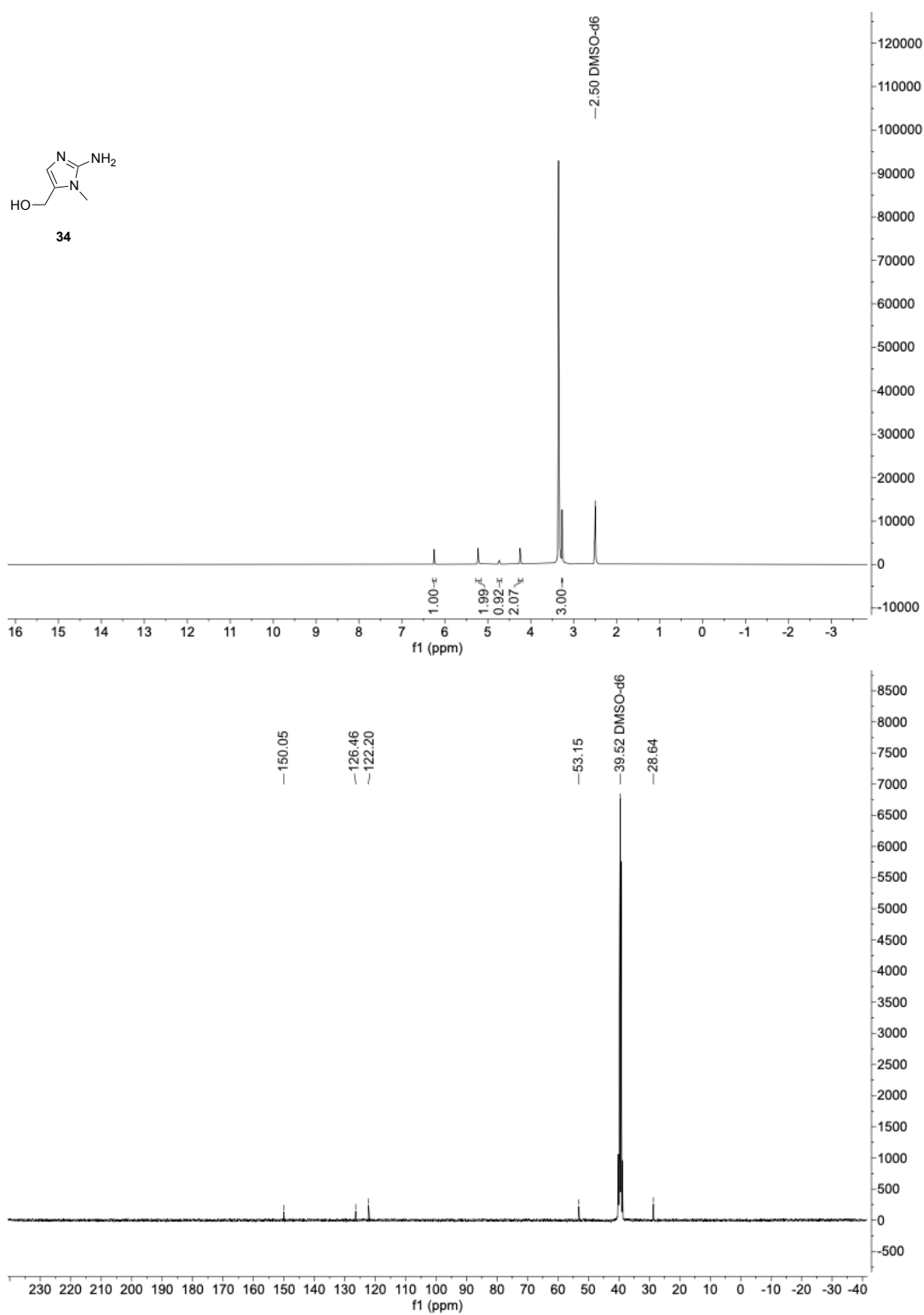
(2-amino-1-methyl-1*H*-imidazol-5-yl)methanol (**34**)

Figure 63: ¹H- and ¹³C-NMR spectra of (2-amino-1-methyl-1*H*-imidazol-5-yl)methanol (**34**).

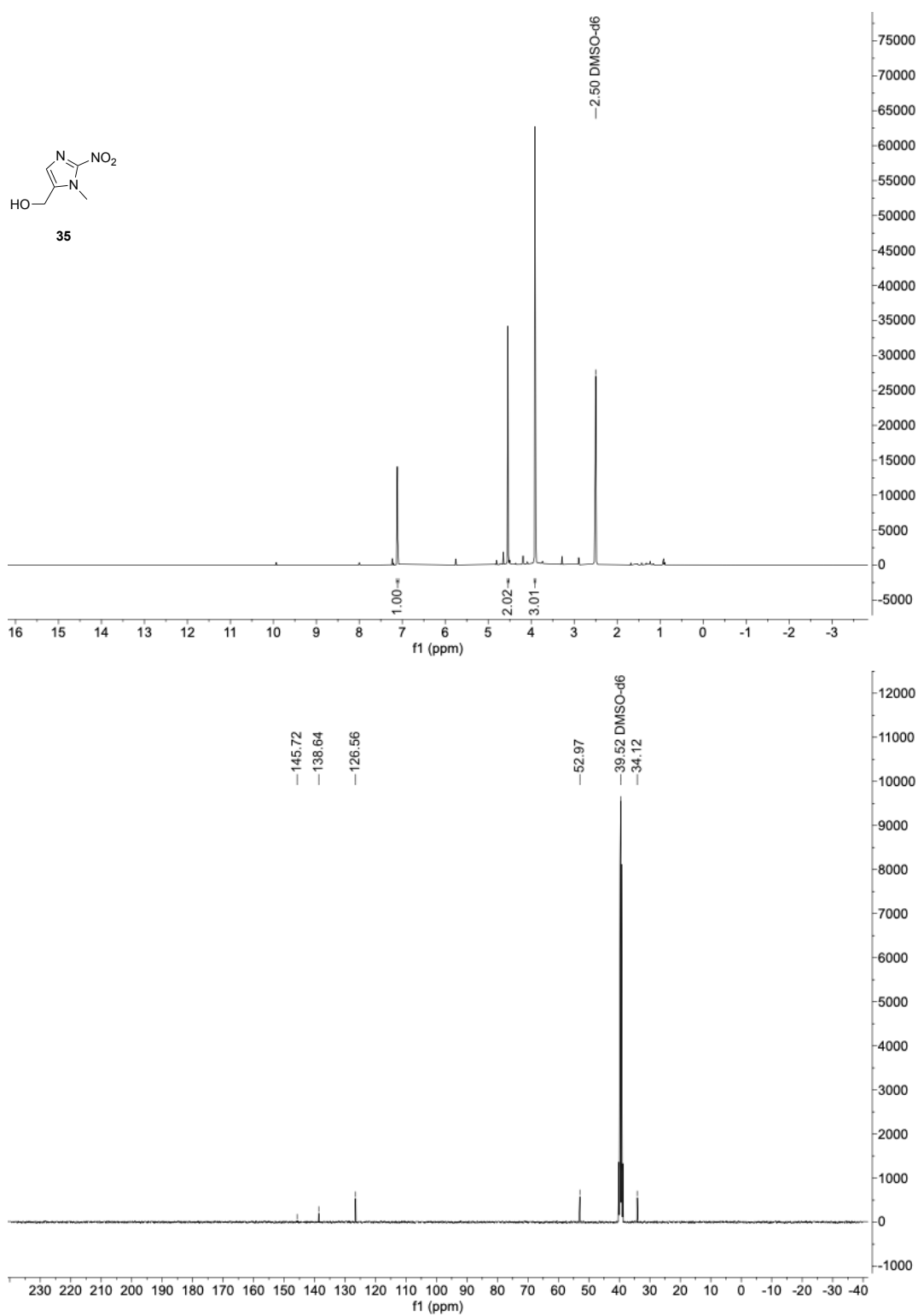
(1-methyl-2-nitro-1*H*-imidazol-5-yl)methanol (**35**)

Figure 64: ¹H- and ¹³C-NMR spectra of (1-methyl-2-nitro-1*H*-imidazol-5-yl)methanol (**35**).

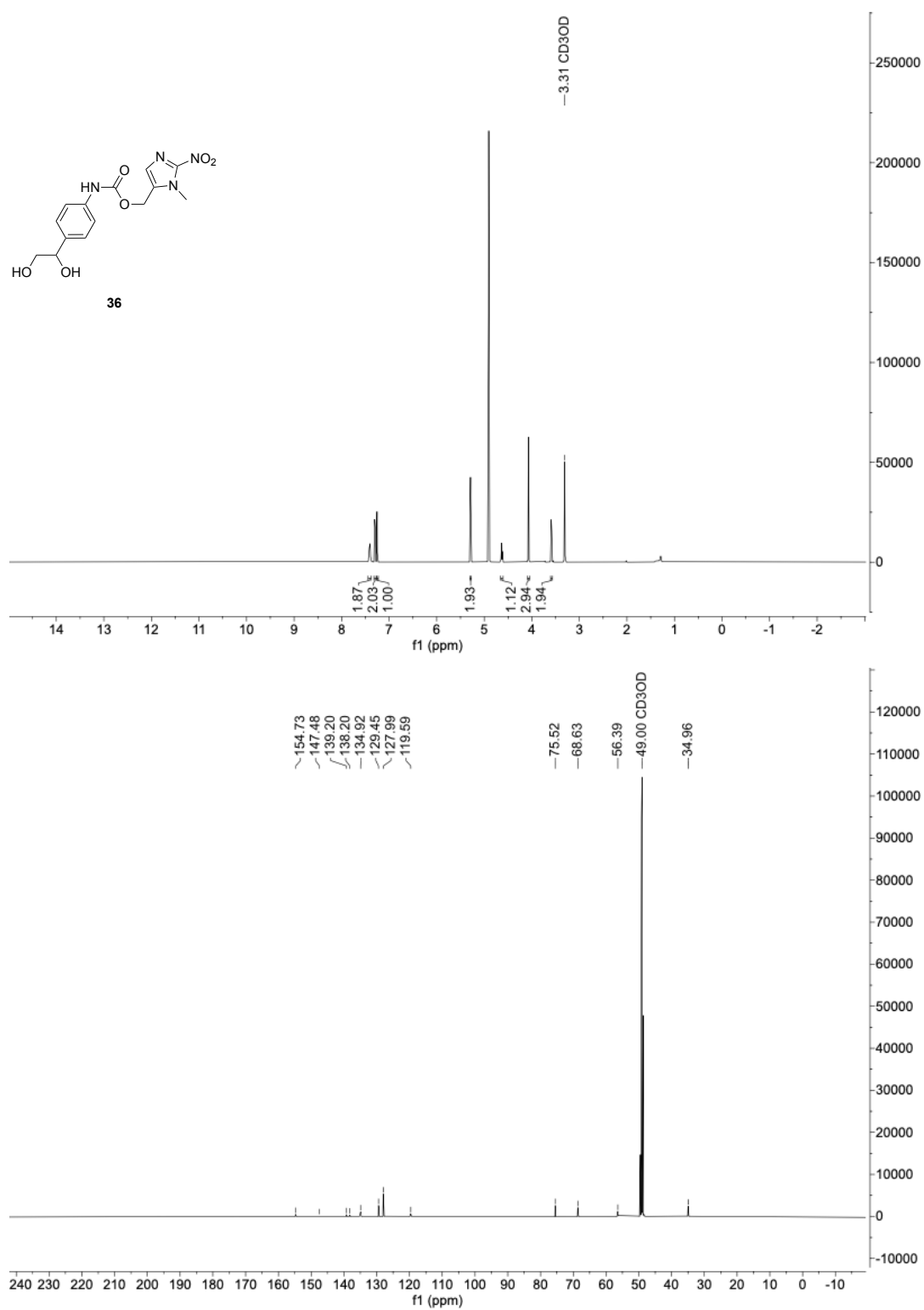
Imidazole-based caging group with a self-immolative linker **36**

Figure 65: ¹H- and ¹³C-NMR spectra of imidazole-based caging group with a self-immolative linker **36**.

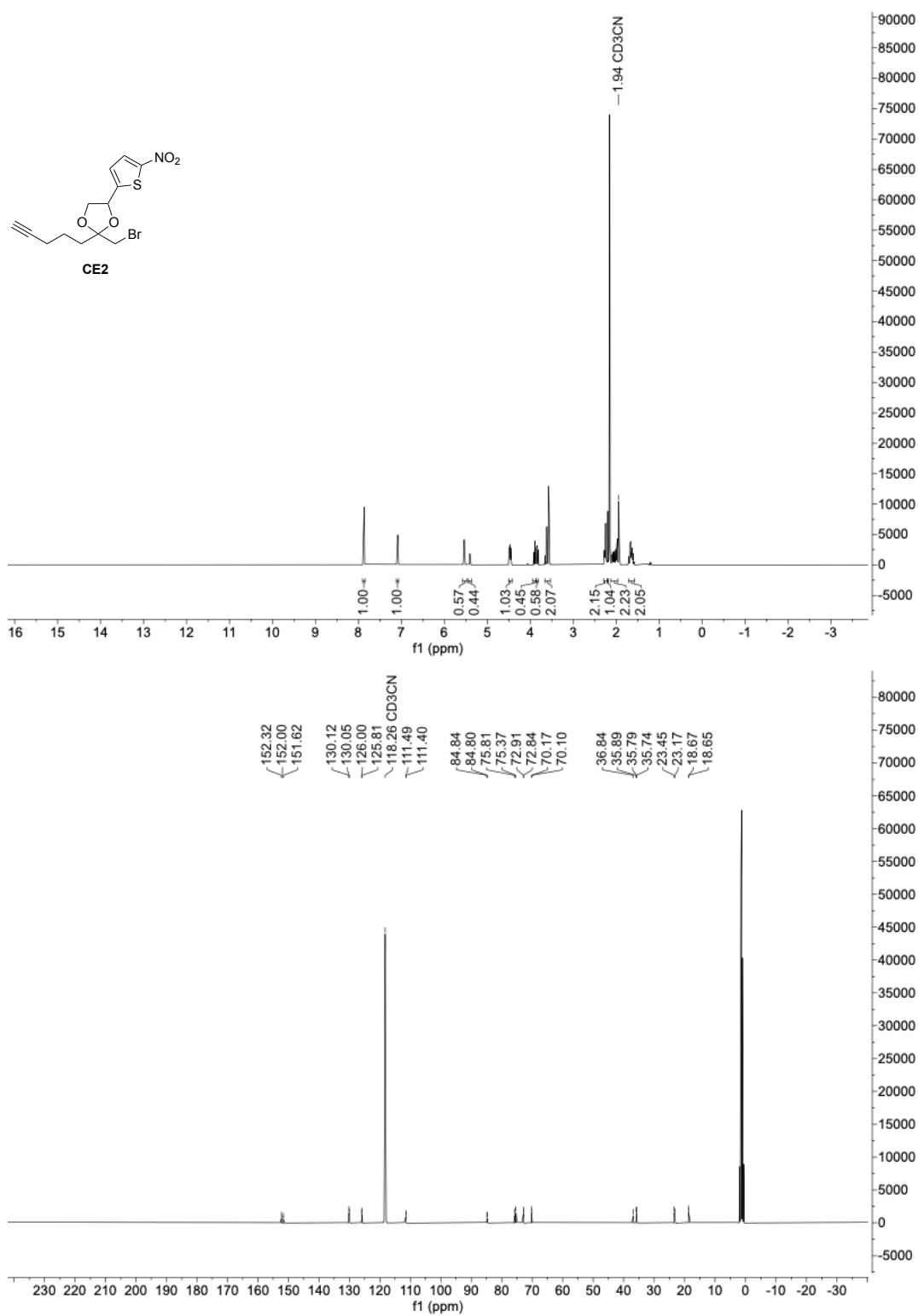
Thiophene-based caged electrophile **CE2**

Figure 66: ¹H- and ¹³C-NMR spectra of thiophene-based caged electrophile **CE2**.

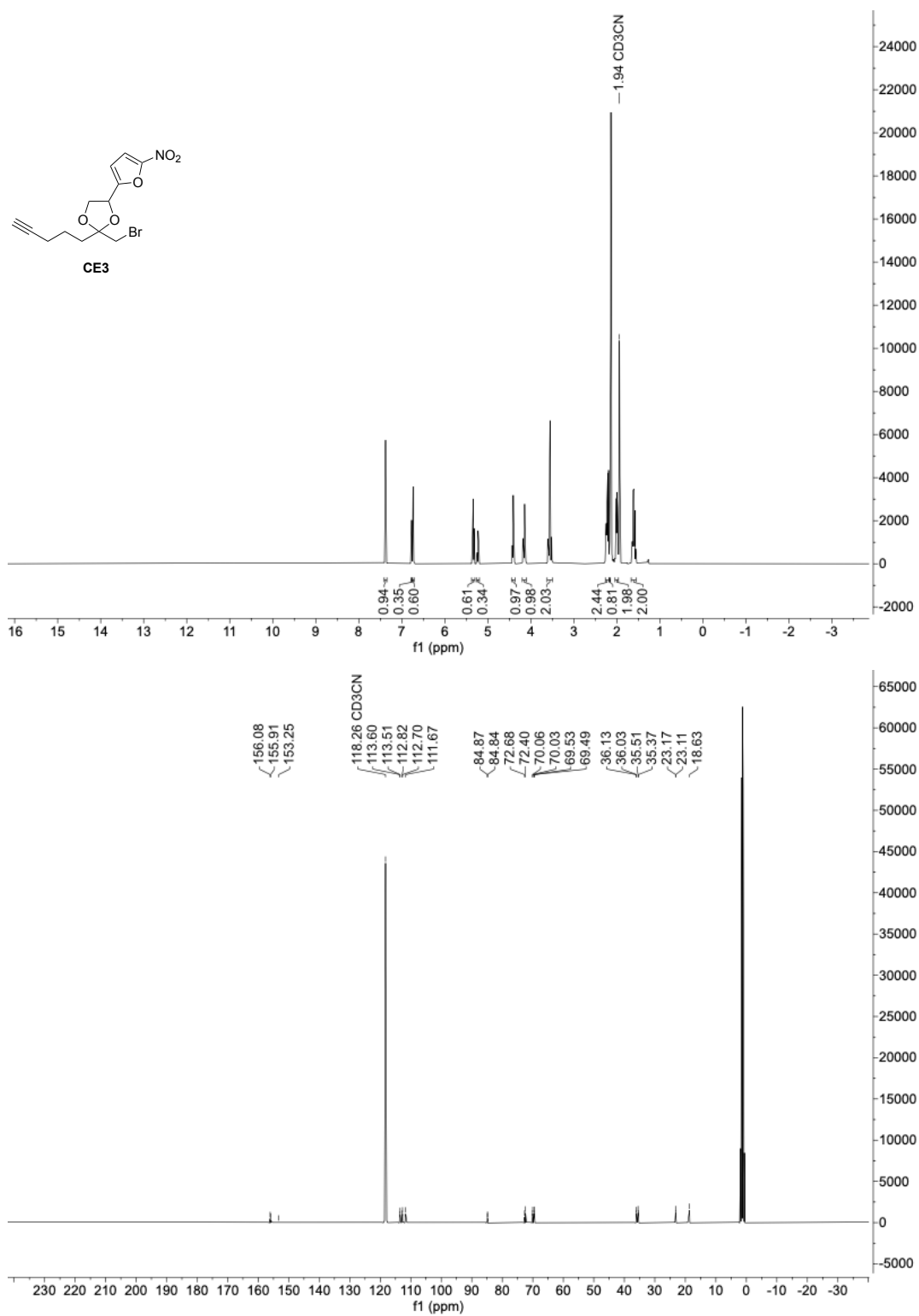
Furane-based caged electrophile **CE3**

Figure 67: ^1H - and ^{13}C -NMR spectra of furane-based caged electrophile **CE3**.

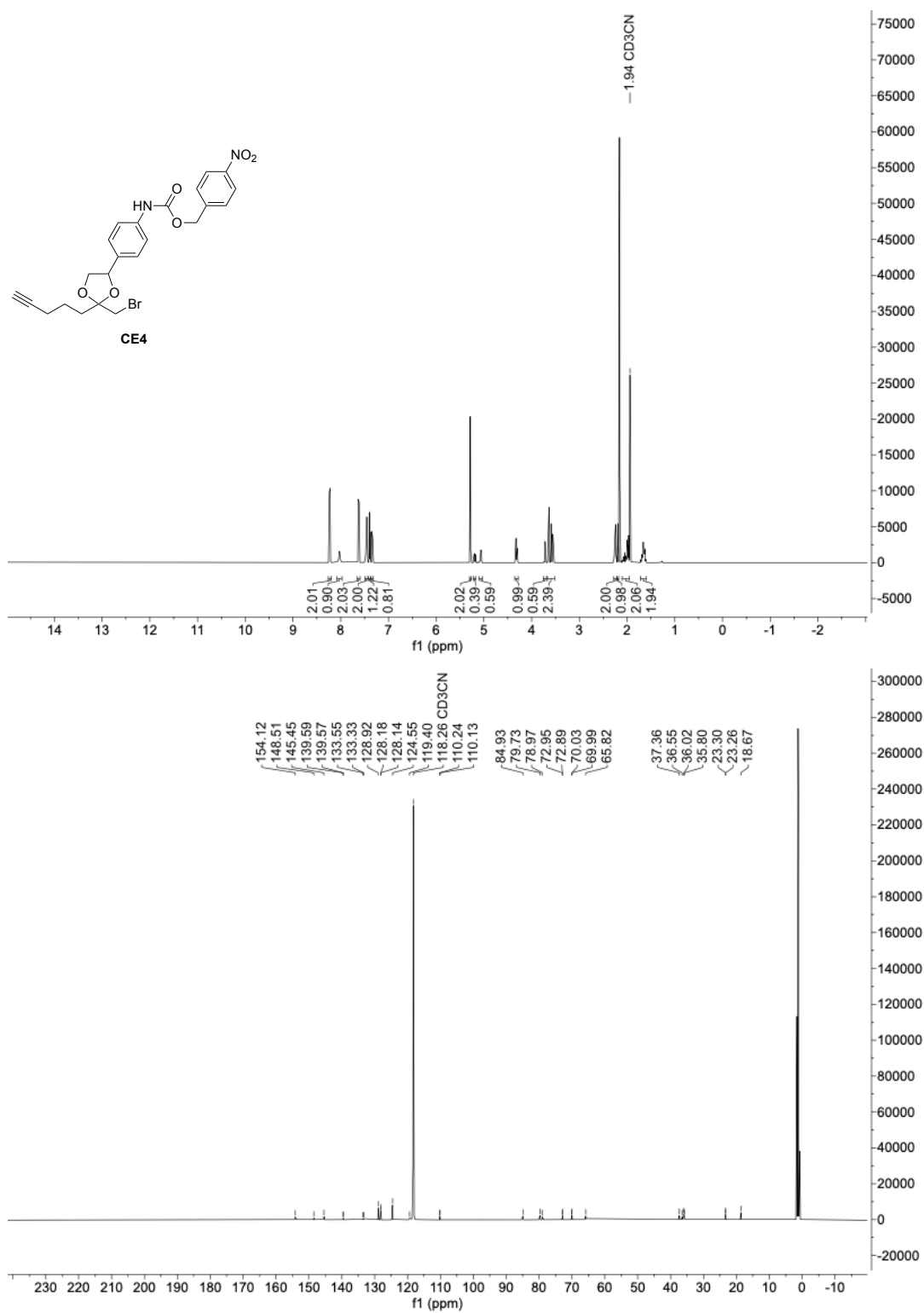
para-nitrophenyl-based caged electrophile with a self-immolative linker **CE4**

Figure 68: ¹H- and ¹³C-NMR spectra of *para*-nitrophenyl-based caged electrophile with a self-immolative linker **CE4**.

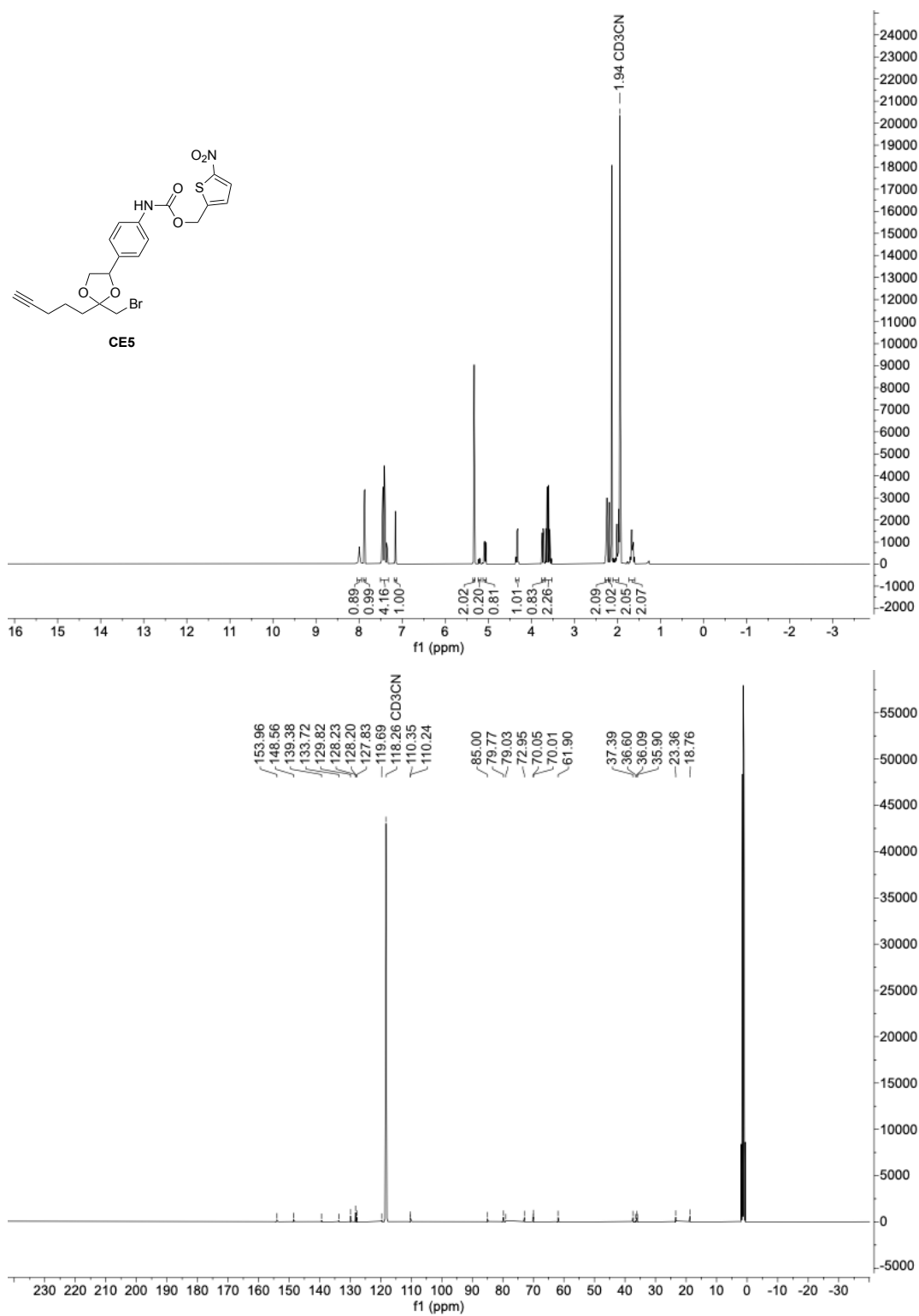
Thiophene-based caged electrophile with a self-immolative linker **CE5**

Figure 69: ¹H- and ¹³C-NMR spectra of thiophene-based caged electrophile with a self-immolative linker **CE5**.

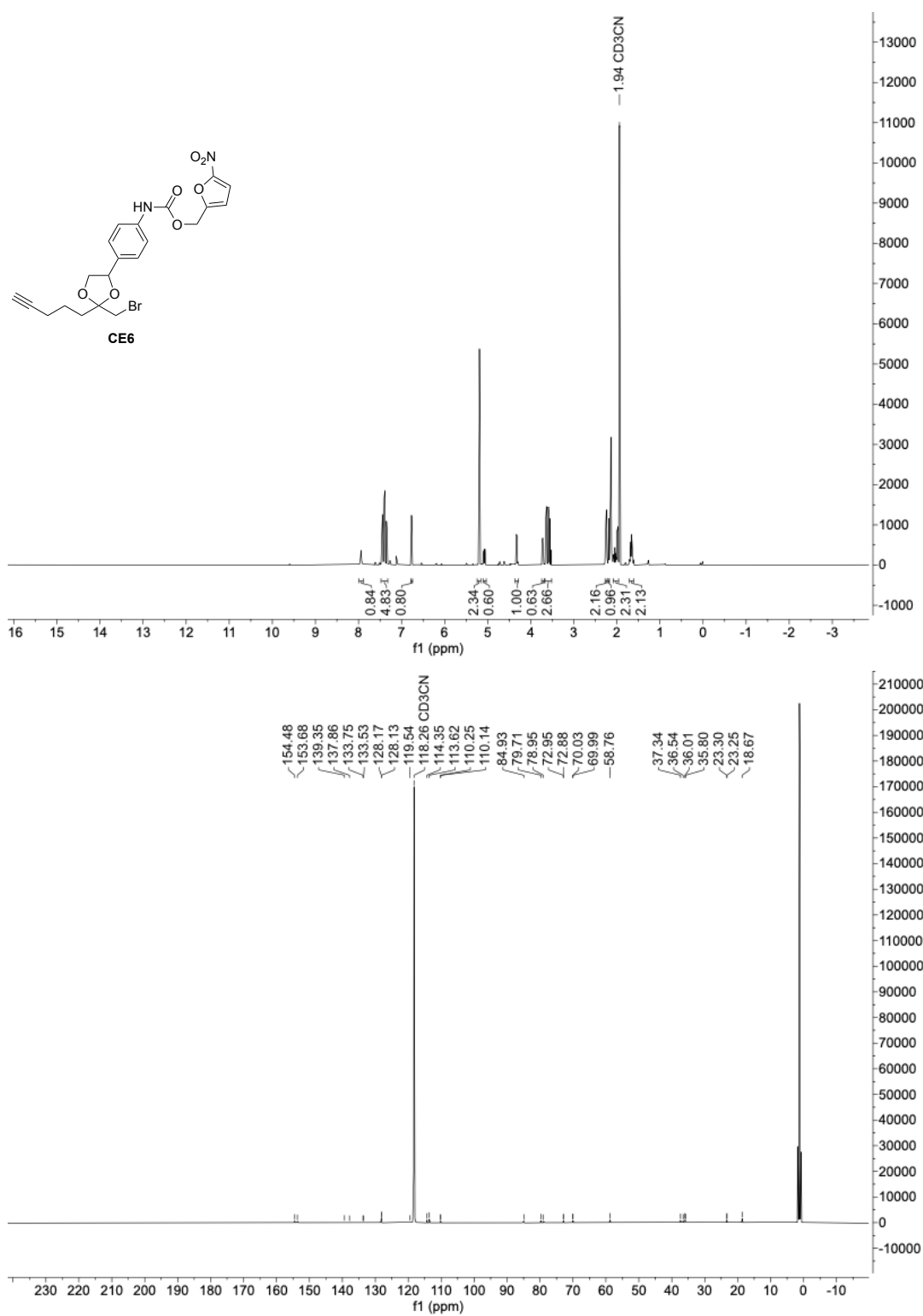
Furane-based caged electrophile with a self-immolative linker **CE6**

Figure 70: ^1H - and ^{13}C -NMR spectra of furane-based caged electrophile with a self-immolative linker **CE6**.

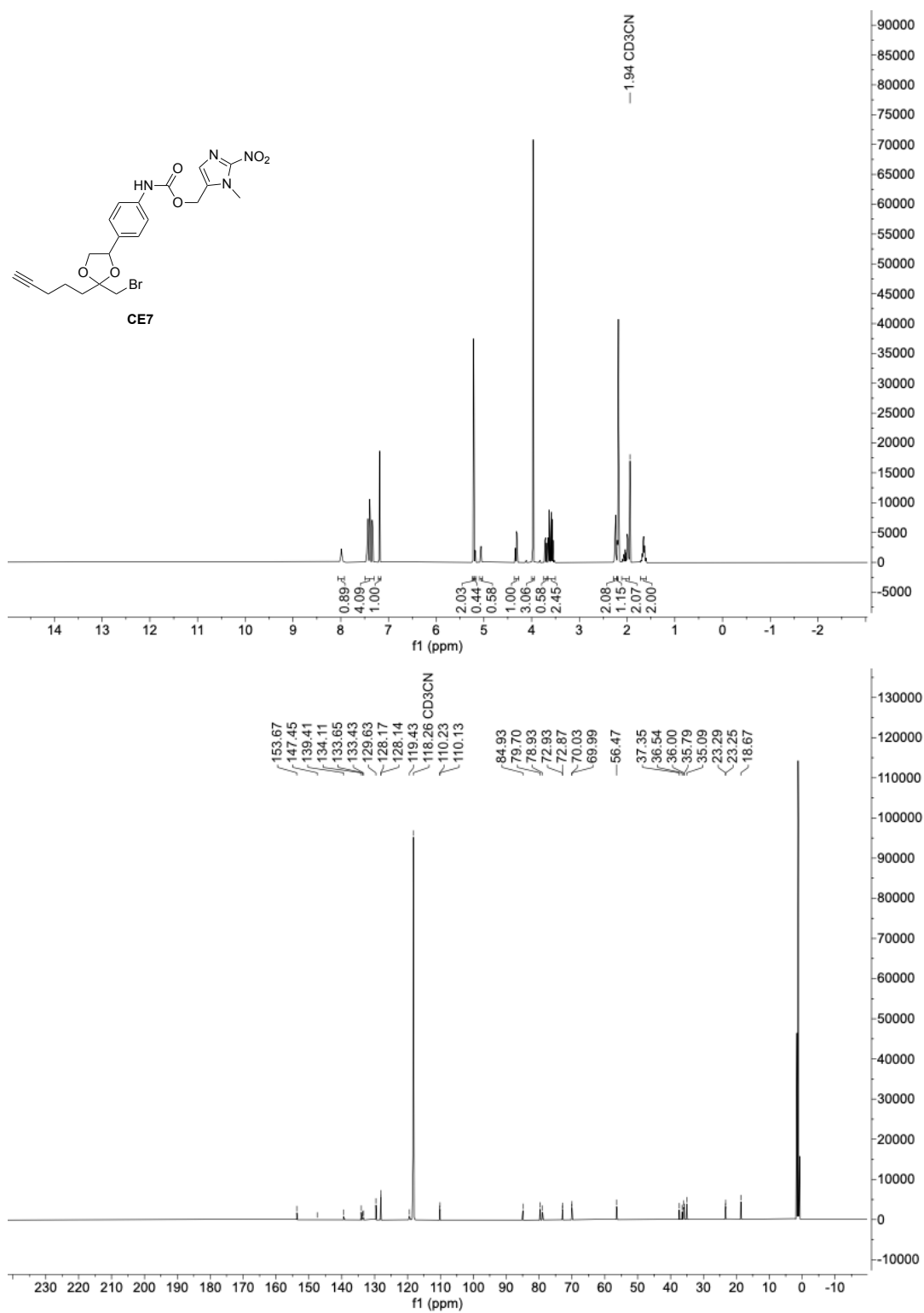
Imidazole-based caged electrophile with a self-immolative linker **CE7**

Figure 71: ^1H - and ^{13}C -NMR spectra of imidazole-based caged electrophile with a self-immolative linker **CE7**.

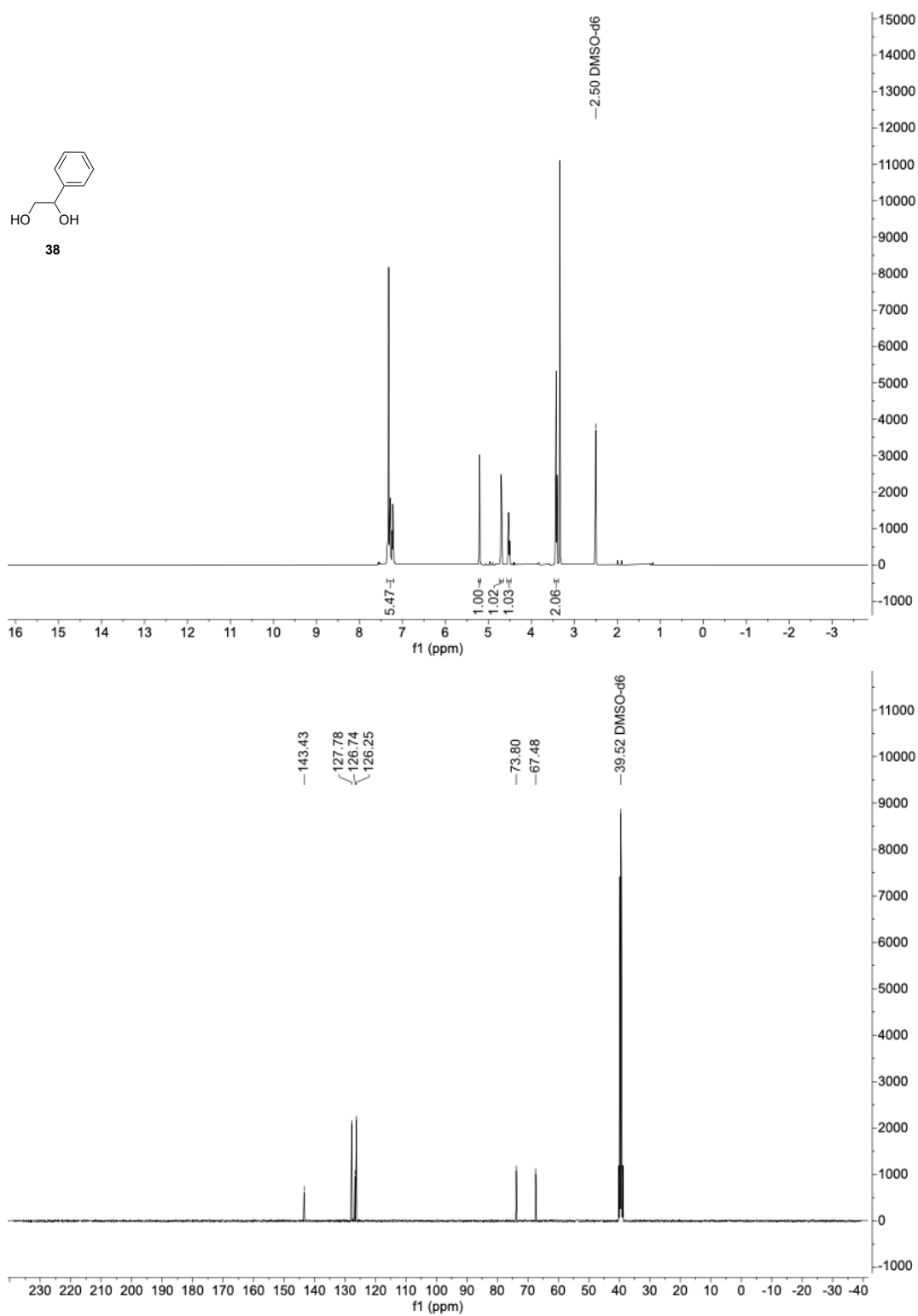
1-phenylethane-1,2-diol (**38**)

Figure 72: ¹H- and ¹³C-NMR spectra of 1-phenylethane-1,2-diol (**38**).

Negative control (NC)

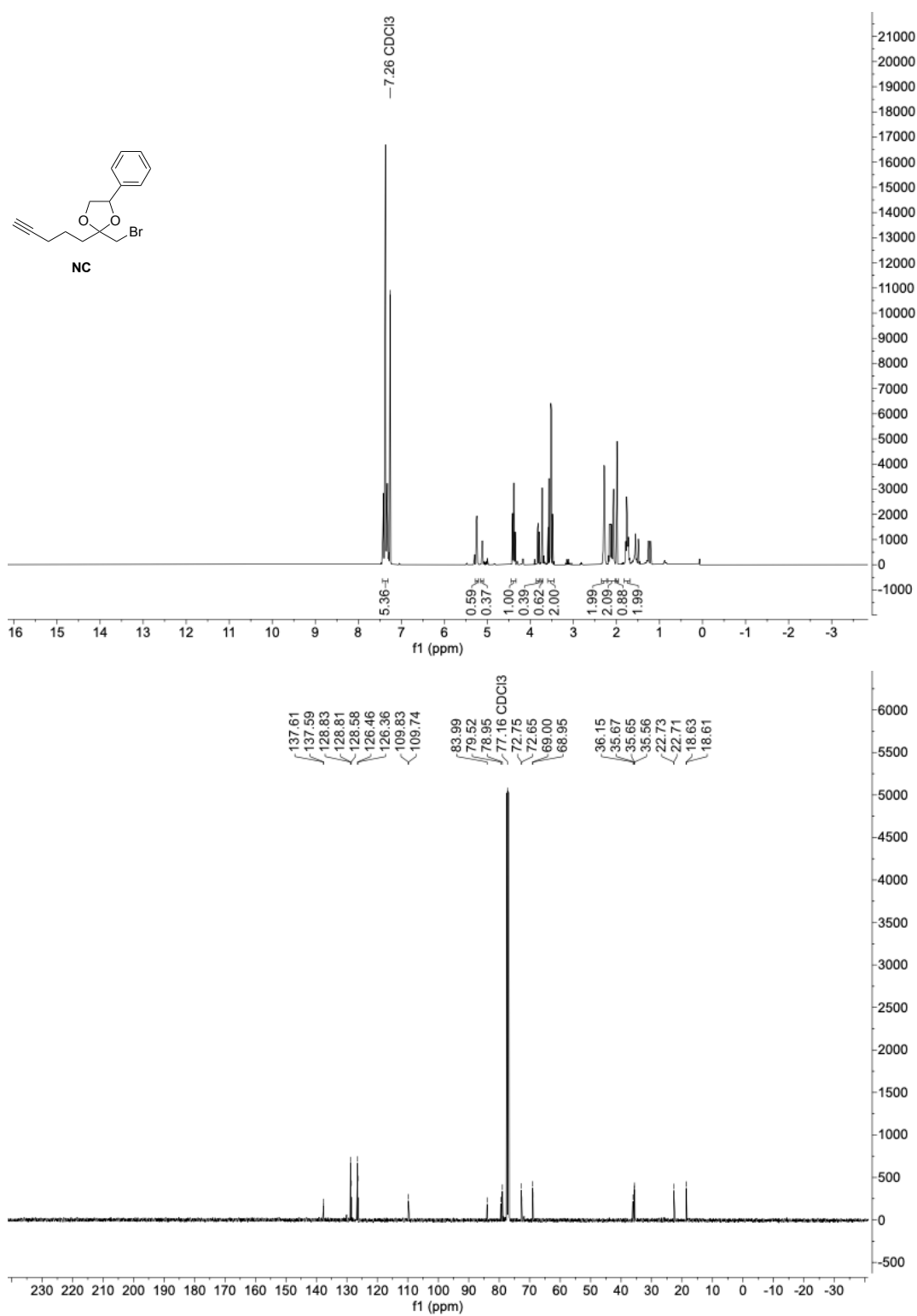


Figure 73: ¹H- and ¹³C-NMR spectra of Negative control (NC).